# DEVELOPMENT OF PROTEOMICS APPROACHES TOWARDS CHARACTERIZING OXIDATIVE MODIFICATIONS

BY

LIQING GU

BACHELOR OF SCIENCE, NANJING UNIVERSITY, 2009

SUBMITTED TO THE GRADUATE FACULTY OF

THE KENNETH P. DIETRICH SCHOOL OF ARTS AND SCIENCES IN PARTIAL FULFILLMENT

OF THE REQUIREMENTS FOR THE DEGREE OF

DOCTOR OF PHILOSOPHY

UNIVERSITY OF PITTSBURGH

2016

UNIVERSITY OF PITTSBURGH

The Kenneth P. Dietrich School of Arts and Sciences

This dissertation was presented

by

Liqing Gu

It was defended on

April 18th, 2016

and approved by

Dr. Renã A. S. Robinson, Assistant Professor, Department of Chemistry

Dr. Steve Weber, Professor, Department of Chemistry

Dr. Sunil Saxena, Professor, Department of Chemistry

Dr. Valerian Kagan, Professor, Department of Environmental and Occupational Health

Dissertation Advisor: Dr. Renã A. S. Robinson, Assistant Professor, Department of Chemistry

**Development of Proteomics Approaches towards Characterizing Oxidative Modifications**

Liqing Gu, Ph.D.

University of Pittsburgh, 2016

Mass spectrometry (MS) is an analytical technique allowing the investigation of a single protein or the entire complement of proteins from biomatrices for understanding attributes such as sequences, modifications, structures, abundances and interactions. Protein oxidative modifications, such as carbonylation and cysteine reversible oxidations, have important roles in physiological processes, including redox signaling, homeostasis, enzymatic catalysis and protein degradation. MS-based redox proteomics can identify and quantify oxidized protein modifications within the proteome. However it is challenging to globally investigate cysteine reversible modifications, due to the low abundance (~ < 1%) and diversity (e.g., S-nitrosylation, S-glutathionylation, sulfenic acid, disulfide bonds) of these modifications. Novel proteomics approaches are needed to better understand cysteine-related redox signaling and oxidative stress in disease.

This dissertation presents studies of protein oxidative modifications using MS-based approaches. First, proteomics methodologies to study protein carbonylation and cysteine reversible modifications are reviewed, including the relevant applications in neurodegenerative disease. Next, a MS-based characterization of a whole protein is described by studying oxidative modifications generated through treatment of a model protein with oxidants. Novel methods towards characterizing endogenous cysteine oxidations in disease are then presented, including inexpensive and high-throughput approaches. The first approach utilizes low-cost isotopic dimethyl peptide labeling for comparing two proteome samples. This methodology has the ability to isolate and quantify total cysteinyl peptides or oxidized cysteinyl peptides from complex samples, and is employed to characterize the liver proteome of an Alzheimer's disease (AD) mouse

model. The second approach is cysteine-selective combined precursor isotopic labeling and isobaric tagging (cysteine-selective cPILOT), which incorporates isobaric tags to achieve 12-plex multiplexing capability. Cysteine-selective cPILOT is used to isolate total cysteinyl peptides from liver proteins and S-nitrosylated peptides from brain proteins of an AD mouse model. Overall the novel proteomics approaches developed herein lower experimental costs and improve the throughput of cysteine redox proteomics studies.

**TABLE OF CONTENTS**

## LIST OF TABLES

## LIST OF FIGURES

## ACKNOWLEDGMENTS

It is a genuine pleasure to express my deep sense of thanks and gratitude to many people who have been assisting me throughout the process. First and foremost, I would like to thank my parents, Deyuan Gu and Meilang Tan, and parents-in-law, Wei Wang and Ying Yao. From the other side of the earth with limited family reunions, they have actively supported me in my determination to realize my potential and complete my degree in the past six years. In addition, I would like to thank my wife, Xi Wang, who continues to be a source of encouragement and inspiration to me throughout my journey towards the PhD degree. She has been studying and working in Chicago since I started my graduate study six years ago. In many weekends and holidays, she gave up vocations and accompanied me in Pittsburgh for my long working hours. I can't remember how many times we have embraced each other at the airport. Moreover, she has been incredibly supportive to me using her expertise in mathematics. Without her contributions, the data analysis in Chapters 5, 6 and 7 would have costed much more time. I would not have completed this without her support.

I would also like to thank my advisor, Dr. Renã A. S. Robinson, who has been a wonderful advisor and mentor in these past five years. As one of her earliest PhD students, I still remember the moment she gave me basic lab trainings five years ago. Starting that time, I learned how to be a researcher, a scientist and a person. She taught me how to make plans, to grasp the essentials and to see a bigger picture from multi-dimensional information. We enjoyed many scientific discussions and shared many novel ideas. Her scientific advice and emotional support is indispensable for me to overcome challenges and complete projects throughout my graduate life. I truly appreciate all her help for my PhD degree. In addition to my advisor, I want to thank my

committee members Dr. Steve Weber, Dr. Sunil Saxena and Dr. Valerian Kagan. They provided a lot of time, help and suggestions for my dissertation defense.

I would also like to thank current and former group members who have helped me in different ways. Dr. Zhiyun Cao and Dr. Adam Evans provided endless help in sample processing, instrument operation/maintenance and data analysis. In addition I would specially thank Dr. Adam Evans for his pioneering work in the cPILOT project, which inspired my work a lot. We worked closely together to test new workflows, conduct collaborative projects and share data analysis experiences. My sincere thanks also goes to Dr. Tasneem Howard for her early insight in the ubiquitin project, and Christina King for instrumental maintenance and laboratory housekeeping. I also thank Christopher Hughes and Veronica Lee for the protein oxidation work, and John Bambeck for the cysteine work. I also had the pleasure to work with Wentao Jiang, Ryan Dyer and Lucinda Boyd.

I would like to thank Dr. Huilin Shi and Dr. David Clemmer from Indiana University for conducting protein characterization using ion mobility mass spectrometry. This work was not incorporated into this dissertation, but went to publication as a follow-up work of Chapter 3. In addition, I acknowledge Dr. D. Allan Butterfield and Dr. Fabio Di Domenico for drafting a review paper of redox proteomics in Chapter 2. I also appreciate Dr. Getiria Onsongo and Dr. Timothy Griffin from University of Minnesota for providing the access to novel bioinformatics tools, GalaxyP.

In addition I appreciate Dr. Bhaskar Godugu's help for analyzing large proteins in my early project. I would also like to thank the Proteomics Core Facility at the University of Pittsburgh for hosting proteomics discussion meetings on campus, which benefited the scientific sharing across research groups. I would like to thank Dr. Michelle Ward, Stan Paul and Josh Jones who provided

me the chances of being a scientific educator in chemistry. I enjoyed the experience of not only helping others but also improving myself in different areas of chemistry.

# 1.0 INTRODUCTION

## 1.1 MASS SPECTROMETRY, PROTEIN ANALYSIS AND PROTEOMICS

Mass spectrometry (MS) is an analytical technique that measures the mass-to-charge (*m/z*) ratio of charged particles in the gas phase[1]. In the past several decades this technology has been widely applied to virtually all areas of life sciences[2]. One of the major reasons is the development of techniques that enable the transfer of large and polar molecules such as proteins from liquid and solid states to the gas phase through the process of ionization, such as electrospray ionization (ESI)[3] and matrix-assisted laser desorption/ionization (MALDI)[4]. In addition, the continuous development of biological sample preparations, multi-dimensional separations, bioinformatics tools, as well as the performance of mass analyzers such as the Orbitrap MS[5] with high resolution, sensitivity and accuracy, have facilitated the applications of MS in whole protein analysis[6]. Moreover, the use of MS for analyzing the entire complement of proteins within a given set of cells, tissues or whole organisms (i.e., proteomics) has led to the identification of new proteins, quantification of proteins and post-translational modifications (PTMs), discovery of biomarkers and therapeutic targets in diseases and elucidation of protein-protein interactions[7]. The following sections in **Chapter 1** will discuss the key techniques used in MS analysis of proteins with a focus on those employed in this dissertation.

### *1.1.1 Orbitrap Mass Spectrometry Instrumentation*

In order to combine different performance characteristics from various types of analyzers into one mass spectrometer, hybrid mass spectrometers have been developed. For example the ion trap-Orbitrap hybrid mass spectrometer (LTQ-Orbitrap Velos, marketed by Thermo Scientific)

possesses high resolution (up to 100,000), high mass accuracy (< 2 ppm) and fast tandem mass spectrometry (MS/MS) acquisition (~10 Hz)[8], making it an ideal MS platform for both whole protein analysis and large-scale proteomics experiments. The LTQ-Orbitrap Velos MS, which is used throughout this dissertation, is shown in Figure 1.1. An ESI source is equipped, where the analyte molecules from either liquid chromatography separation or direct infusion by a syringe pump are ionized and introduced into the MS by applying a high voltage (~1-5 kV). The accurate mass of the intact protein or peptide ions are first measured by the Orbitrap MS analyzer (MS scan) using high resolution (> 60,000). Simultaneously the peaks of interest are selected (automatically or manually) and fragmented in the dual ion trap to generate tandem mass spectra for sequence determination (MS/MS scan). MS/MS scans are much faster than MS scans (~0.1 s v.s. ~0.7 s), and these two types of scans are often executed simultaneously to maximize the instrument duty cycle.

Data dependent acquisition (DDA) (**Chapters 3**, **4** - **6**) is often employed in high throughput proteome analysis by liquid chromatography separation coupled with MS/MS (LC-MS/MS). DDA is automatic isolation and fragmentation of the top-*N* most intense ions detected from each precursor MS scan. Based on the user's setting, the *N* could be lower than 10 but may be up to 20, based on different experimental parameters and instrumental platforms. Different fragmentation techniques, such as collision induced dissociation (CID), higher energy collisional dissociation (HCD), electron transfer dissociation (ETD) and infrared multiphoton dissociation (IRMPD), have been developed[9,10]. CID is used throughout this dissertation for protein/peptide sequencing (**Chapter 3**, **4** - **6**). In a typical CID event, the isolated ions are trapped in the ion trap and excited by a radio frequency (RF) voltage. Ions with increased kinetic energy collide with helium gas and result in the cleaved peptide amide bonds. *B*-type fragment ions (containing N-

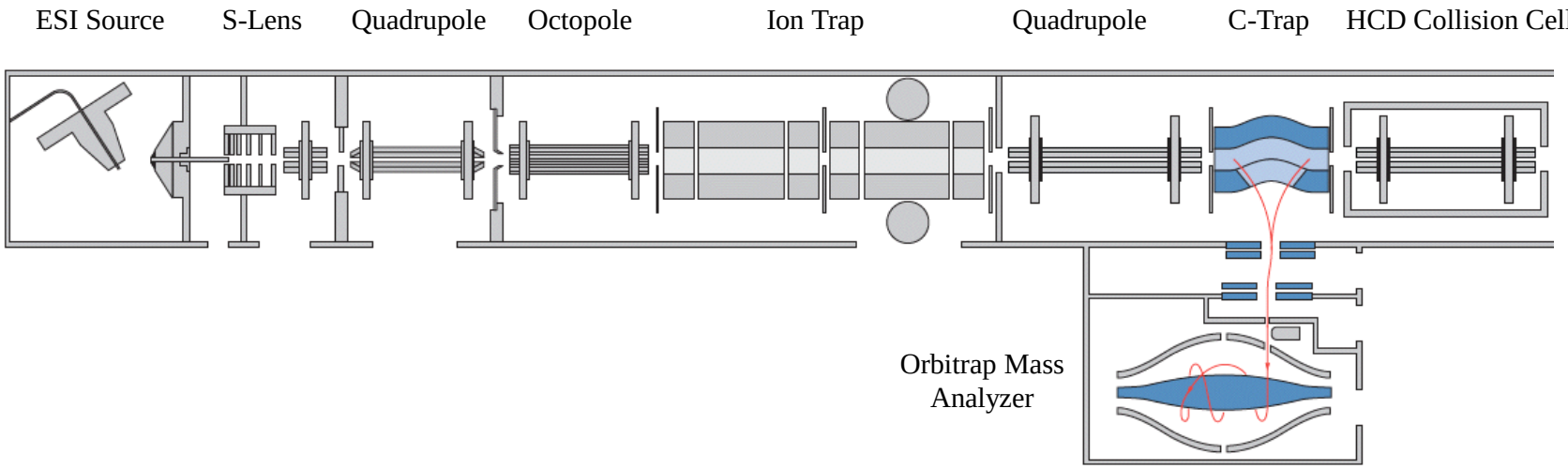


**Figure 1.1** Schematic of the LTQ-Orbitrap Velos (Thermo Scientific).

terminus) and *y*-type fragment ions (containing C-terminus) ions are detected by MS/MS scan and used as the peptide fingerprint for sequence determination by database search. CID is generally suitable for small to medium peptides (charge states < 6 and mass < 5 kDa) and can reach efficiency up to ~ 80% in ion trap[11,12]. One limitation of ion trap CID is the low-mass cutoff of MS/MS spectra, which is roughly 150 to 300 *m/z* for most peptide ions[13]. When it is necessary to detect mass tags at as low as 100 *m/z* in the MS/MS scan, HCD is often used, in which peptide ions are fragmented in an octopole HCD collision cell and detected in the Orbitrap[14]. HCD can also generate *b*- and *y*-type ions for peptide sequencing and is used exclusively for isobaric tag-based quantification in **Chapters 4** and **6**.

In a typical 3 hour LC-MS/MS run using DDA, more than 50,000 MS and MS/MS spectra can be acquired. Spectral interpretation in this dissertation is performed by database searching using the SEQUEST algorithm[15], which is integrated in the commercial software Proteome Discoverer (Thermo Scientific). SEQUEST compares every theoretical MS/MS spectra based on the input protein sequence information, calculates its correlation with the experimental MS/MS spectra and assigns the peptide sequence based on the highest correlation. One issue of SEQUEST search is the presence of false positive identification due to random matching, which can be evaluated and filtered by performing a decoy database search[16]. False discovery rates (FDR) are set to either 0.05 or 0.01 for 95% and 99% confidence, respectively in this dissertation.

### *1.1.2 Top-down and Bottom-up Mass Spectrometry*

Proteins can be analyzed as the intact molecules directly by MS (top-down MS)[17]. As shown in Figure 1.2a, the protein sample is directly infused into the MS and the MS scan is performed to record the precursor spectra. The peaks of interest are isolated and fragmented to

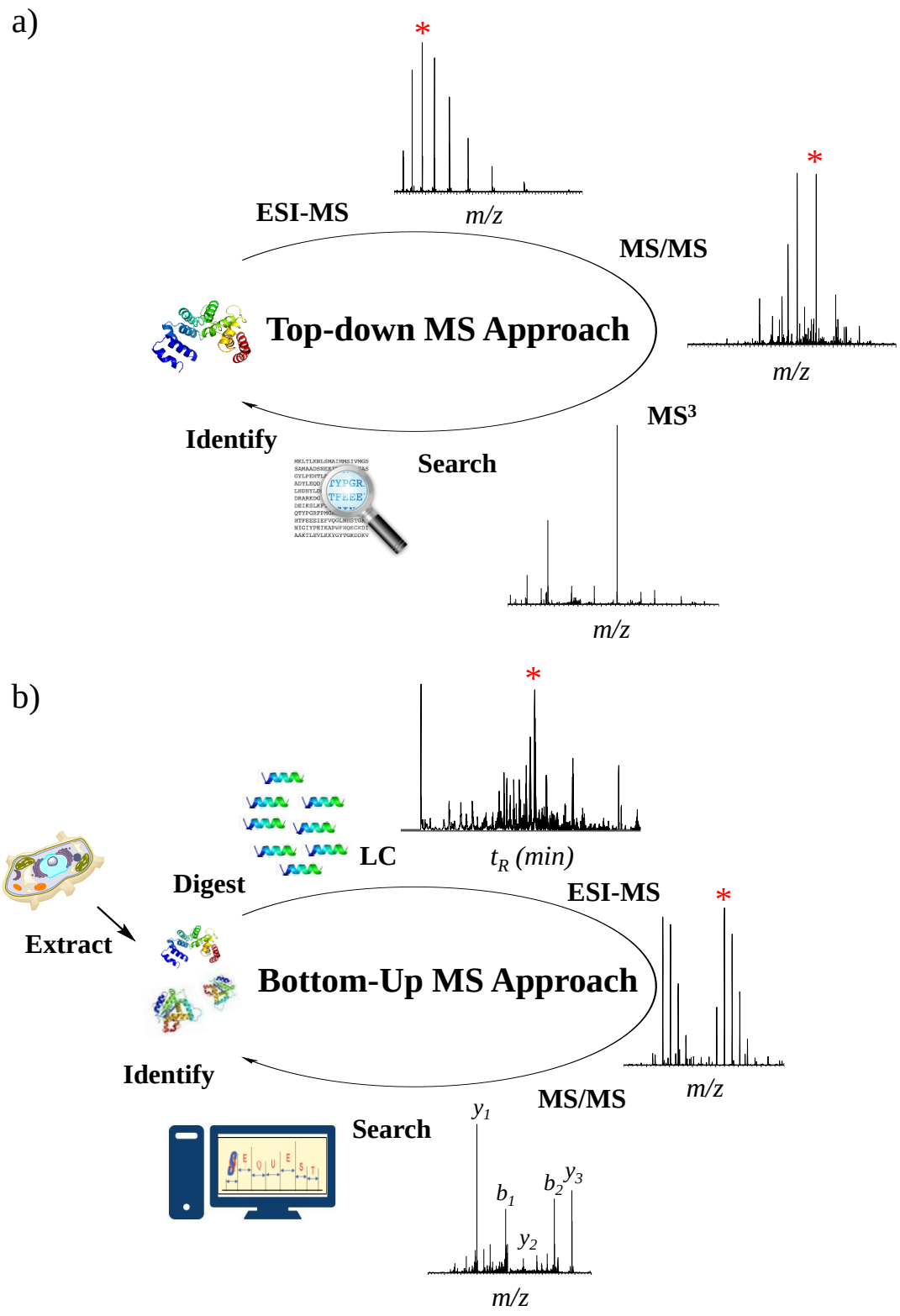


**Figure 1.2** General procedures for a) top-down and b) bottom-up MS proteomics analysis.

obtain MS/MS spectra for structural determination. An advantage of this approach is the ability to retain protein-level information, e.g., multiple proteoforms[18]. Top-down MS is utilized in **Chapter 3**, in which oxidized ubiquitin is directly sprayed and analyzed. Although top-down MS has been widely utilized in single protein characterization, including the therapeutic monoclonal antibody (~150 kDa), it is still challenging to characterize the whole cell/tissue context due to difficulties in protein separation, protein MS/MS fragmentation and MS resolution[19]; however current state-of-the-art top-down proteomics studies can achieve identification and quantification of more than 1,000 low molecular weight proteins (<80 kDa) from human cells[20,21]. An alternative approach is bottom-up MS, in which digests resulting from enzymatic protein digestion are analyzed by LC-MS/MS. Compared with top-down MS, bottom-up MS exhibits better separations, ionization efficiencies and peptide PTM localization, making it an ideal approach for complex sample analysis[22]. The general workflow for bottom-up MS is shown in Figure 1.2b. Proteins extracted from tissues or cells are digested by a protease. The most widely used protease is trypsin, which cleaves peptides at the carboxyl side of lysine or arginine. Other proteases such as Lys-C and Glu-C can also be used for generating different peptides and obtaining better sequence coverage (**Chapter 3**). Peptides are separated by LC, in which the reverse phase LC (RPLC) is mostly used due to its compatibility with ESI. For complex digest samples, an additional dimension of separation prior to RPLC can be used to simplify the MS spectra and improve the peptide identification[23]. For example, strong cation exchange (SCX) is coupled with RPLC to separate mouse tissue digests in **Chapters 4** and **6**. SCX separation is based on the differences of peptide charge states on a Polysulfethyl A column (**Chapter 4**) or a SCX spin tip (**Chapter 6**). An increasing salt gradient is used to elute peptides from the column and several fractions are collected. Each fraction is furthered separated by RPLC, which is based on the different hydrophobicities of

peptides. Eluted peptides are directly ionized by ESI and the *m/z* ratios as well as the relative intensities are measured and recorded by MS. MS/MS scans are triggered automatically by DDA to provide peptide sequence information throughout the RPLC separation period. Bottom-up MS is used in **Chapter 3** together with top-down MS to provide comprehensive mapping of ubiquitin oxidative modifications, and also used in **Chapters 4 - 6** for large-scale quantitative proteomics.

### *1.1.3 Quantitative Proteomics, Post-translational Modifications and Redox Proteomics*

MS-based quantitative proteomics can be used to understand global protein expression and modifications as well as the molecular mechanisms of biological processes in physiological and pathological conditions[24,25]. A number of methods use differential stable isotope labeling to create a specific mass tag that can be separated by a mass spectrometer and at the same time provide the basis for quantification[24,25]. These mass tags can be incorporated into proteins or peptides metabolically, chemically or enzymatically[26]. Quantification can also be achieved by label-free approaches, in which the spectral counts or peptide peak areas are directly compared among multiple sample runs[27]. The following discussion is focused on label-based quantitative proteomics methods employing stable isotopic mass tags, including precursor isotopic labels and isobaric tags. Some common techniques are listed in Table 1.1, and discussed below.

Precursor isotopic labeling acquires relative quantification information from MS scans. In a typical experiment, two peptides samples are modified so that the peptides in each sample have the same chemical structures but one contains heavy atoms (such as $^{13}C$, $^{2}H$ and $^{15}N$). Samples are pooled and analyzed by LC-MS/MS. The same peptide from two different samples co-elutes and can be discriminated by MS due to the mass difference between the light and heavy mass tags. The relative intensities of light and heavy peptide peaks are used for relative quantification. Stable

**Table 1.1** Representative stable isotope tags for relative quantitation.

| Category | Techniques | Multiplex[a] | Reactive Sites |
|---|---|---|---|
| Precursor isotopic labels | SILAC | 3 | Arg and Lys |
| | Acetylation | 2 | N-term and Lys |
| | mTRAQ | 3 | N-term and Lys |
| | Dimethylation | 5 | N-term and Lys |
| | Oxygen 18 | 2 | C-term |
| | ICAT | 2 | Cys |
| Isobaric tags | TMT | 10 | N-term and Lys |
| | iTRAQ | 8 | N-term and Lys |
| | DiLeu | 12 | N-term and Lys |
| | iodoTMT | 6 | Cys |

[a]Number of samples that can be compared in a single experiment.

isotope labeling with amino acids in cell culture (SILAC) grows cells in normal medium (light) or medium containing with stable-isotope-labeled amino acids (i.e., $^{13}C_6$-arginine and $^{13}C_6$-lysine)[28]. For tissue or bio-fluid samples, a good choice is performing precursor isotopic labeling by chemical reactions on the amino side chains such as the amine, sulfhydryl and carboxylic groups. Some representative techniques include dimethylation[29], acetylation[30], mass differential tags for relative and absolute quantification (mTRAQ)[31], isotope-coded affinity tags (ICAT)[32] and enzymatic $^{18}O$ labeling (Table 1.1)[33]. As shown in Figure 1.3, dimethylation uses formaldehyde and sodium cyanborohydride to label the peptide N-terminus and ε-amino group of Lys residues via reductive amination reaction[29]. Heavy labeling reagents can generate peptides with a mass shift of +8 Da or +16 Da compared with peptides labeled by light reagents. Moreover, the modified site can be limited to N-terminus and leave ε-amino of Lys intact if the dimethylation reaction is performed under acidic condition[34-36]. Due to its pH-based site selectivity, as well as other properties such as low cost[37], solid phase compatibility[38,39] and up to five sample multiplexing capability[40], dimethylation is attractive and is used in **Chapters 4 - 6**. However further increasing the sample multiplexing may complicate the MS spectra, and result in peak overlapping and inaccurate quantification.

An alternative way to multiplex samples is using isobaric tags, which enable comparison of up to twelve samples in a single run[41]. Some representative examples include tandem mass tag (TMT, used in **Chapter 6**)[42], iodoacetyl tandem mass tag (iodoTMT, used in **Chapter 4**)[43], carbonyl-reactive tandem mass tag (aminoxyTMT)[44], isobaric tag for relative and absolute quantitation (iTRAQ)[45], deuterium isobaric amine-reactive tag (DiART)[46] and dimethyl leucine tag (DiLeu) (Table 1.1)[41,47,48]. A typical isobaric tag consists of three portions (Figure 1.4): a reporter ion group, a mass balancer group, and a reactive site that targets a peptide functional group

a) pH = 8.5

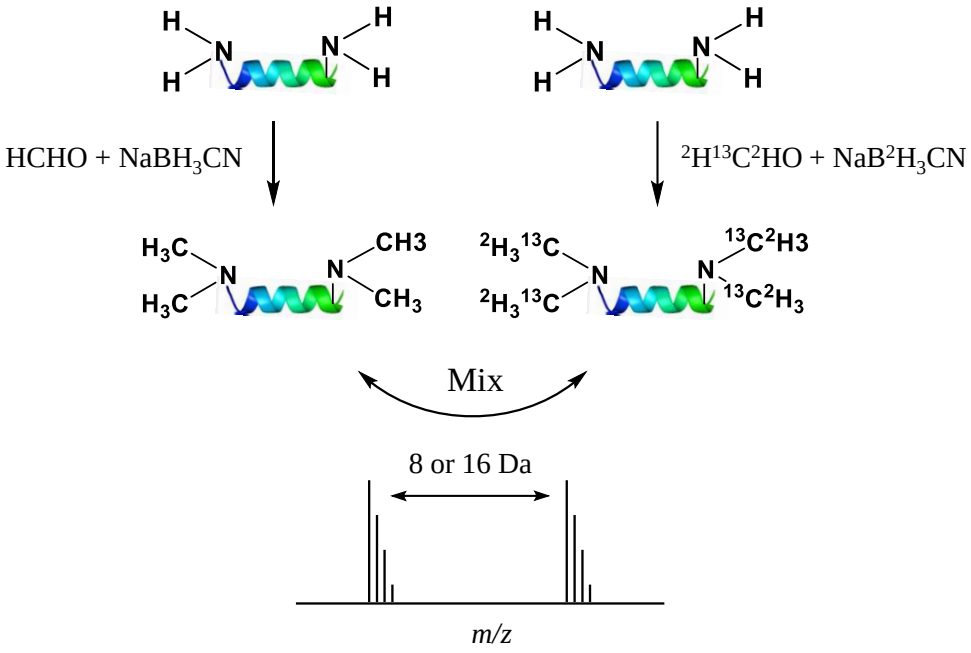


b) pH = 2.5

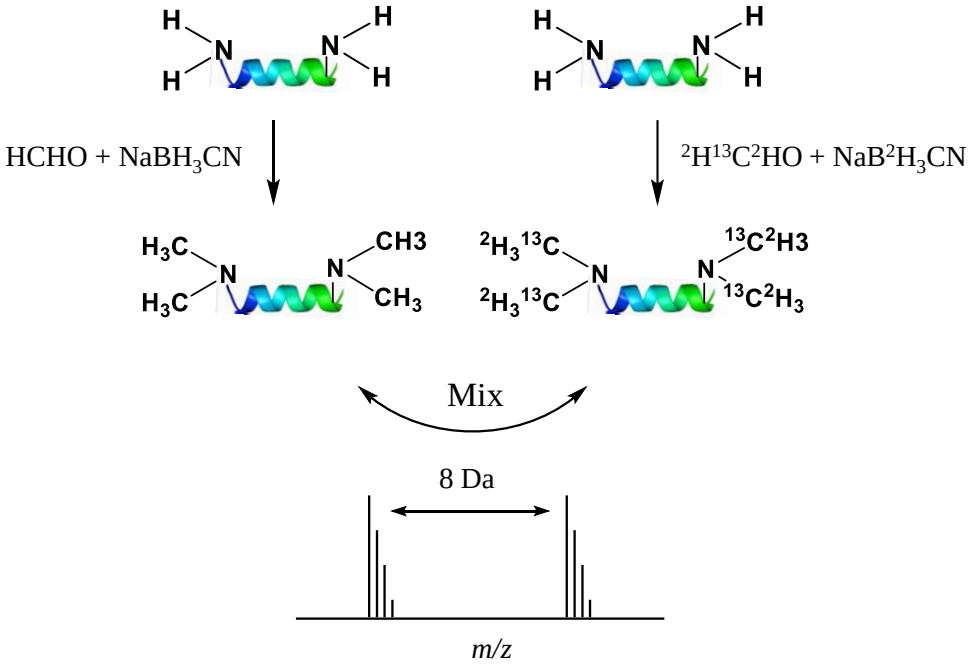


**Figure 1.3** Labeling schemes of duplex stable isotope dimethyl labeling at a) high and b) low pH.

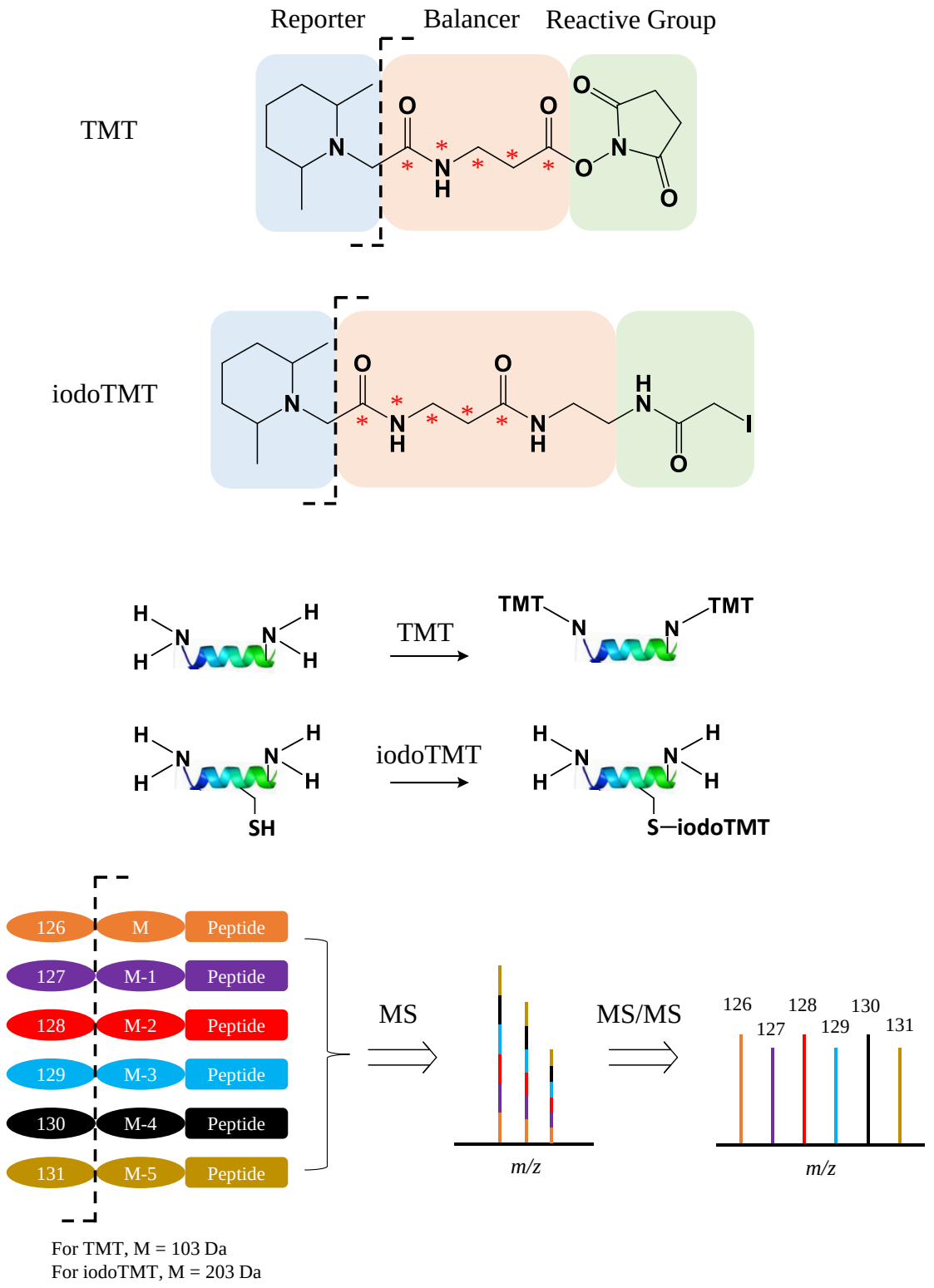


**Figure 1.4** Chemical structure for 6-plex TMT and iodoTMT tags and the modified peptide sites are shown. Samples are combined for LC-MS/MS analysis resulting in a single peak in MS scan. Isolation and fragmentation generates six reporter ion signals in the MS/MS scan.

such as amine, sulfhydryl or carbonyl. Each reagent has the same chemical structure, contains the same number of heavy atoms ($^{13}C$ and $^{15}N$) however these atoms are incorporated into different locations within the reporter ion and mass balancer regions. For TMT and iodoTMT tags, reporter ions are from *m/z* 126 through 131, while the respective balancer groups are from *m/z* 103 through 98 and 203 through 198. Each peptide from different sample origins co-elutes from the LC and is detected as a single peak in the MS scan. However, upon isolation and fragmentation of the peptide ion, the TMT and iodoTMT tags cleave between the mass balancer and reporter ion groups and result in six unique signals corresponding to the masses of the reporter ions (*m/z* 126-131 for TMT and iodoTMT tags). The intensities of reporter ions are compared for relative quantification. Isobaric tagging enables higher multiplexing capability without complicating the precursor spectra. However one issue of isobaric tagging-based quantitative proteomics is the ratio compression due to the co-isolation and co-fragmentation of target peaks with interfering ions[49]. Some strategies, such as simplifying MS spectra with ion mobility separation[50], reducing precursor ion charge state[51] and performing quantification at the $MS^3$ level[52], have been utilized for mitigating this issue. The last approach can be easily implemented using the LTQ-Orbitrap Velos MS and is employed in **Chapters 4** and **6** for quantification using iodoTMT and TMT.

Further increase of multiplexing ability in quantitative proteomics experiments can provide the ability to analyze many samples in one run, resulting in higher throughput, shorter instrument time and lower experimental variations. An effective strategy developed in our laboratory is combined precursor isotopic labeling and isobaric tagging (cPILOT) method[36], which labels multiple samples using combined precursor isotopic labeling and isobaric tagging. Briefly, peptides are modified with a precursor labeling reagent which generates a mass shift between light and heavy peaks in MS. Light and heavy peptides are further modified with isobaric tags.

Fragmentation of both light and heavy peptides separately can generate two sets of reporter ion spectra and double the original multiplexing capacity of the isobaric tag. This method was initially developed for 3-nitrotyrosine modified peptides[53], and further expanded for global proteome quantification[36,54]. This dissertation further expands this methodology to achieve enhanced quantification of cysteine-containing proteins (**Chapter 4)** and S-nitrosylation (SNO) PTMs (**Chapter 6)**. Other enhanced multiplexing techniques are also reported[55-58].

MS analysis of proteins can also characterize various PTMs on the amino acid side chains[59,60]. PTMs are the covalent modification of proteins during or after protein biosynthesis and have significant biological relevance. Oxidative PTMs, such as carbonylation and a variety of reversible modifications on cysteine sulfhydryl groups are of interest in this work[61]. Protein oxidative PTMs are formed through a variety of pathways but largely due to the attacks of radical oxygen and nitrogen species (ROS/RNS)[62], and closely related with diseases[61,63]. Characterization of oxidative PTMs on a single protein can be readily achieved using combined top-down and bottom-up MS (**Chapter 3**). However MS characterization of oxidative PTMs in tissues or cells are challenging mainly due to the low abundance and diverse structures[64,65]. **Chapter 2** reviews current proteomic techniques to investigate common oxidative PTMs such as cysteine reversible modifications and carbonylation. The relevant applications of these methods in aging and neurodegenerative diseases are also presented. **Chapters 4 - 6** discuss the development of novel redox proteomics methods to selectively identify and quantify cysteine reversible modifications from Alzheimer's disease (AD) mouse tissues.

### *1.1.4 Cysteine-selective Proteomics Approaches: Challenges and Strategies*

Cysteine is a rare amino acid but present in nearly all proteins, and widely involved in biological processes through the formation of a number of reversible modifications (reviewed in

**Chapter 2**). Cysteine-selective proteomics approaches can be used to study biological systems by targeting low abundant proteins and/or cysteine reversible PTMs. Existing tools, such as ICAT and iodoTMT, have been successfully applied in relevant studies (see **Chapter 2**). However a common challenge in discovery proteomic experiments is the large number of biological samples/replicates needed. For example, more than 1,000 plasma samples are used in a clinical study for biomarker discovery[66]. By using existing cysteine-selective tools, numerous experiments have to be performed to analyze all samples. As a result, increased tagging cost and instrumental time are expected. Towards this end, this dissertation presents two directions. One is developing inexpensive proteomic methods using isotopic dimethylation (**Chapters 4** and **5**), and the other is developing cPILOT approaches to compare many samples in a single instrumental run (**Chapters 4** and **6**). More importantly, these methods provide the flexibility of quantifying peptides containing cysteine, oxidized cysteine and a specific oxidized cysteine PTM. Researchers can choose the most appropriate method based on specific studies and laboratory conditions, such as the MS instrument, the budget and the time frame.

## 1.2 OVERVIEW OF DISSERTATION

This dissertation employs MS-based approaches to characterize proteins with a focus on development of novel strategies to study oxidative modifications in disease. Specifically, **Chapter 2** reviews proteomic approaches to identify and quantify protein oxidative modifications as well as relevant applications in neurodegenerative diseases. In **Chapter 3** a combined top-down and bottom-up MS method is developed to study protein oxidation and demonstrated on a model protein. **Chapter 4** introduces two cysteine-selective approaches enabling comparison of two or twelve proteome samples in a single run. In **Chapter 5** a simple method is developed to quantify reversible cysteine modification in AD. **Chapter 6** presents an optimized 12-plex approach to

study SNO in AD. **Chapter 7** summarizes the dissertation and discusses current challenges and future goals of MS-based oxidative PTM analysis.

# 2.0 REDOX PROTEOMIC APPROACHES TO STUDY OXIDATIVE MODIFICATIONS IN AGING AND NEURODEGENERATIVE DISEASES

(Note that information in this chapter is written based on two review papers[61,67]: 1) Gu, L.; Robinson, R. A. S. *Proteomics Clinical Applications* **2016**, *Manuscript in Preparation*; 2) Butterfield, D. A.; Gu, L.; Di Domenico, F.; Robinson, R. A. S. *Mass Spectrometry Reviews* **2014**, *33*, 277-301.)

## 2.1 INTRODUCTION

Radical oxygen/nitrogen species (ROS/RNS) can be generated endogenously (e.g., metabolism in mitochondria and peroxisomes) and exogenously (e.g., ultraviolet light and ionizing radiation) in biology[62]. Antioxidant defense systems (e.g., catalase and superoxide dismutase) are activated in the presence of ROS and work to maintain physiological homeostasis[62]. Many studies have indicated that the generation, reaction and disassembly of ROS/RNS are important regulatory mechanisms for many cellular activities[62]. However, an imbalance of ROS/RNS with the cellular antioxidant defense mechanism results in oxidative stress, and subsequent post-translational modifications (PTMs) on various biomolecules, including DNA, RNA and proteins[68].

One of the most susceptible amino acids to oxidative PTMs is cysteine. Cysteine is a rare amino acid with a natural occurrence of 2.26% among all amino acids in the mammalian proteome[65]. The percentage of cysteinyl peptides is only ~15% after *in silico* digestion of the whole human proteome[65]. Cysteine is highly nucleophilic and redox sensitive compared with other amino acid side chains. It is involved in redox homeostasis, enzymatic catalysis, signal conduction, metal binding and structural stabilization[69,70]. The pKa value of the cysteine thiol is ~ 8.0 but can be as low as 3.5 in some proteins due to electrostatic interactions and hydrogen bonding[71]. The low pKa results in spontaneous *in vivo* reactions of cysteine with electrophilic and/or oxidizing molecules[72].

Common reversible modifications of cysteine include formation of sulfenic acids (SOH), S-nitrosylation (SNO), S-glutathionylation (SSG), S-palmitoylation and disulfide bonds[73] (Figure 2.1). It is estimated that only 10% of all cysteine residues are reversibly oxidized *in vivo*[64]. These reversible PTMs have important biological roles and help maintain homeostasis by preventing the formation of irreversible oxidative modifications (e.g., sulfinic and sulfonic acid)[74]. Specifically, SOH is often the intermediate status of the active cysteine site during the catalytic process of redox enzymes such as peroxiredoxin[75]. SNO, resulting from the attack of endogenous NO to free cysteine, is often involved in cellular signal transduction pathways[76]. SSG is the reversible formation of protein disulfides with glutathione (GSH) and is found to modulate protein activities. In addition, the conversion of SOH and SNO derivatives to SSG followed by glutaredoxin reduction is an important mechanism to maintain protein-thiol homeostasis[77]. S-palmitoylation is the covalent lipid modification of cysteine with the 16-carbon fatty acid palmitate ($CH_3(CH_2)_{14}COOH$), and regulates protein trafficking and subcellular localization[78]. Disulfide bonds are important for maintaining the protein 3D structures, while recently it is found that disulfide bonds are involved in the regulation of protein functions[79]. Finally, modification of cysteine by lipid peroxidation products (e.g., HNE) is reported to inhibit protein disulfide isomerase in rat liver mitochondrial[80].

Thiol-based redox regulation is important in metabolism. Dysregulated redox homeostasis of thiols have been implicated in aging and diseases, such as cancer, diabetes, cardiovascular and neurodegenerative diseases[72]. Better understanding of thiol redox chemistry can give insight to biochemical events that occur in diseases, and may lead to potential biomarkers for disease diagnosis and therapy[81]. Redox proteomics can detect hundreds to thousands of oxidized proteins in a single experiment and this is attractive to study redox status of proteins[82]. Redox proteomics

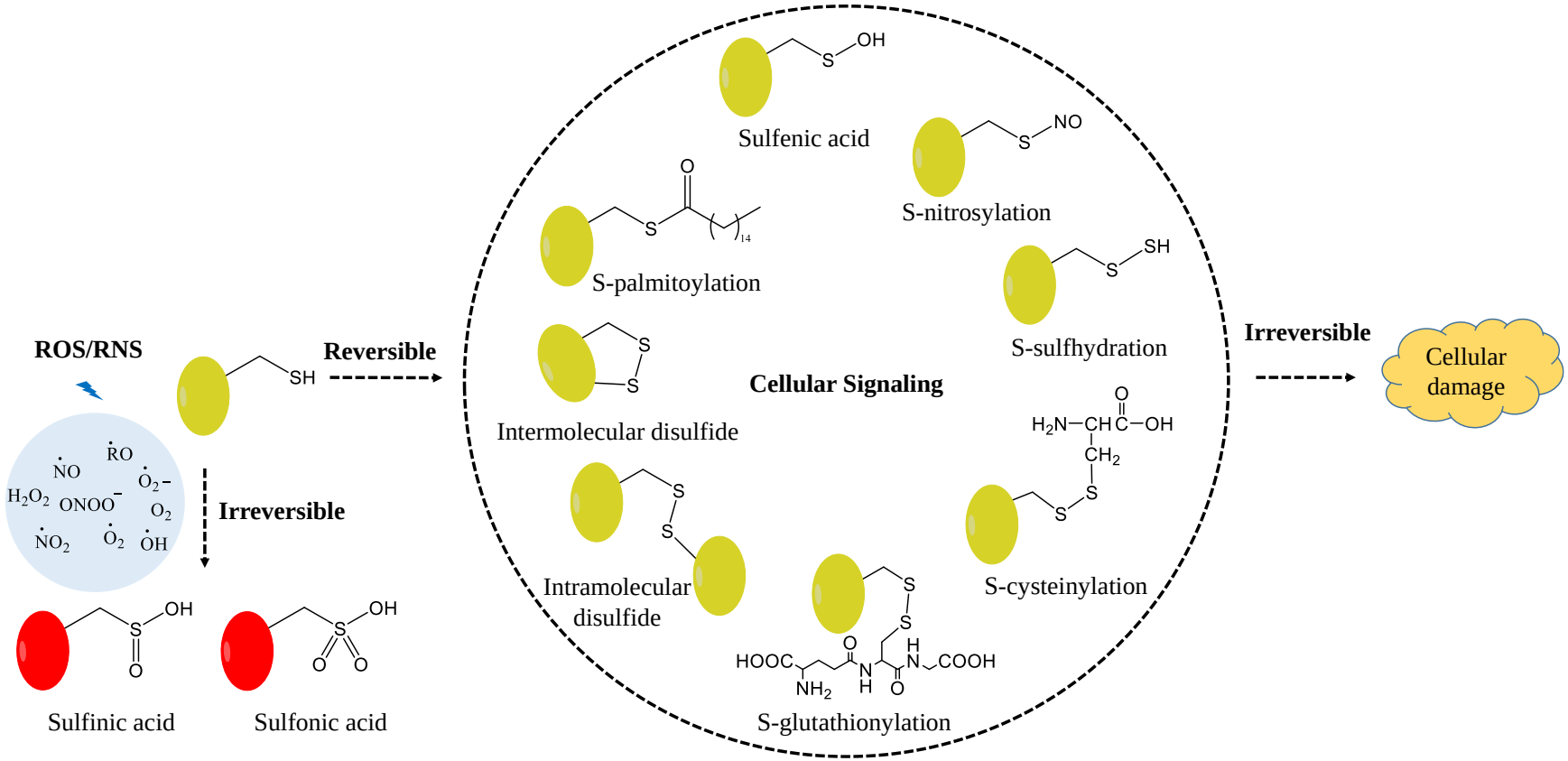


**Figure 2.1** Representative oxidative modifications of cysteine by ROS/RNS. Low levels of ROS/RNS lead to reversible cysteine modifications, including S-glutathionylation, S-nitrosylation, S-palmitoylation, sulfenic acid and disulfides. These modifications have important roles in various cellular activities. ROS/RNS can also oxidize cysteine irreversibly, and result in loss of protein function and cellular damage.

approaches have been developed to enrich, identify and quantify cysteine oxidative PTMs in complex biological samples and can be gel-based and nongel-based[83]. Gel-based methods offer direct detection of cysteine modifications via electrophoretic gel separation and immunoblotting[84]. In recent years, nongel methods have become more popular due to new technologies for PTM enrichment, multi-dimensional chromatographic separations and high-through protein quantification by mass spectrometry (MS)[24,25,85]. Redox proteomic workflows are limited by 1) the low abundance and high diversity of cysteine PTMs, 2) the labile and dynamic nature of modifications and 3) potentially the small changes in oxidative PTM levels that are not detectable between different biological conditions[83]. More effort is needed to overcome these challenges and to develop workflows that are efficient, straightforward, unbiased, high-through, sensitive and accurate.

Aging is a complex biological process accompanied by decline in biological and physiological functions of many organs[61]. Aging is also one of the significant risk factors for neurodegenerative diseases, including Alzheimer's disease (AD) and Parkinson's disease (PD)[86], in which the brain undergoes both morphological and functional modifications, accompanied by the alteration of motor and sensory systems, sleep, memory and learning[61]. Elevated oxidative stress is present in aging and neurodegenerative diseases and occurs in different organs[38,54], tissues and fluids[82,87]. Redox proteomic studies in aging and neurodegenerative diseases have been provided insights into the molecular consequences of oxidative stress. However, a detailed characterization of redox changes to the thiol proteome across tissues and disease stages does not exist.

In addition to oxidative cysteine modifications, oxidative stress can result in a variety of other oxidative PTMs (Figure 2.2). For example, carbonylation is generated by direct oxidation of

a) Methionine oxidation

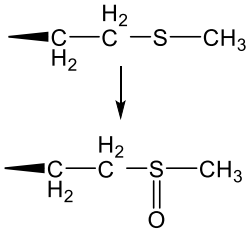

d) Carbonylation of lysine

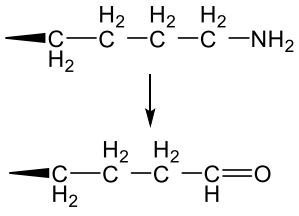

b) Hydroxylation of tyrosine

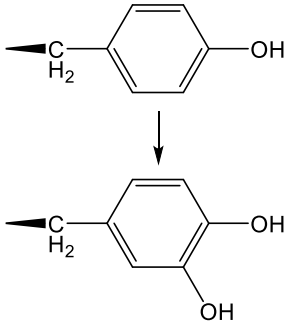

e) Carbonylation of threonine

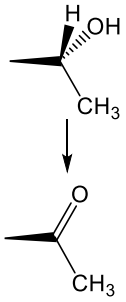

c) Deamidation of asparagine

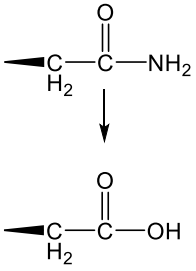

f) Histidine open ring reaction

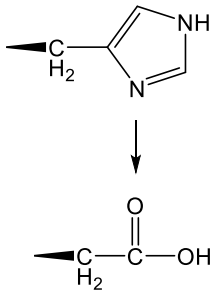

**Figure 2.2** Examples of oxidative modifications other than cysteine oxidation.

several amino acid side chains (i.e., Lys, Arg, Pro, Thr, His and others), backbone fragmentation, hydrogen atom abstraction at alpha carbons and Michael addition reactions of His, Lys, and Cys residues with products of lipid peroxidation causing inactivation, crosslinking or breakdown of proteins[88]. Carbonylation is generally considered as an irreversible modification, and can result in protein fragmentation, aggregation and increased susceptibility to proteolysis[89-91]. Protein carbonylation is accepted as a good indicator of the extent of oxidative damage of proteins associated with various conditions of oxidative stress, aging and physiological disorders[90]. Methionine residues can be readily oxidized to methionine sulfoxide by incorporating one oxygen atom, which is often observed even in physiological conditions. This modification is also a marker of oxidative stress and its repair by methionine sulfoxide reductases is related to diseases[92]. Other types of modifications by direct attack of hydroxyl radicals include hydroxylation, deamidation, decarboxylation, as well as histidine open ring reactions[89,93]. Most of these oxidative modifications can be identified by MS due to the distinct mass shift after oxidation. However some modifications have very small mass shifts, such as + 1 Da for deamidation, and -1 Da for carbonylation of Lys, and are challenging to characterize. Strict spectral validation is often required[68]. **Chapter 3** discusses a study of mapping various protein oxidations by using a model protein. Investigation of these modifications on the proteome level often requires affinity enrichment techniques due to the extremely low concentrations of these PTMs.

In this chapter, different quantitative proteomic methods to study cysteine modifications and protein carbonylation will be discussed. More emphasis will be focused on nongel-based approaches and MS-based quantitative profiling of cysteine PTMs, which is highly related to the work in **Chapters 4** - **6**. Finally, applications of different redox proteomic approaches in aging and neurodegenerative diseases will be described.

## 2.2 REDOX PROTEOMIC APPROACHES TO QUANTIFY CYSTEINE REVERSIBLE MODIFICATIONS

Proteomics is able to simultaneously identify and quantify nearly the whole proteome in a single experiment[94], making it a desirable technique to gain insights into the redox status of proteins. In addition, different chemical or biological probes can make the methods selective to cysteine oxidized PTMs[95]. Considering the diverse, labile and dynamic nature of cysteine PTMs, differential thiol blocking and selective reduction is frequently used[82,83,96,97].The primary steps of such workflows are summarized in Figure 2.3. This strategy was initially developed for gel-based SNO analysis[98], and later it was adapted to study a variety of cysteine reversible modifications in gel-based and nongel-based approaches. Regardless of the targeted cysteine modifications and the downstream processing, the general principles remain the same. First is the blocking of free thiols using N-ethylmaleimide (NEM), iodoacetamide (IAM) or methyl methanethiosulfonate (MMTS)[97] with typical concentrations from 10 mM to 200 mM[99-118]. In addition, cysteine-reactive mass tags can also be used, such as isotope-coded affinity tag (ICAT) and iodoacetyl tandem mass tag (iodoTMT). Thiol blocking is recommended at the earliest stage of sample processing such as cell lysis or tissue homogenization, in order to minimize artificial cysteine oxidation[83]. After removal of excess blocking reagents, substrate-specific reductants are added. Widely used reducing reagents, including ascorbate, arsenite, glutaredoxin, hydroxylamine and dithiothreitol (DTT) or tris(2-carboxyethyl)phosphine (TCEP), can reduce SNO, SOH, SSG, S-palmitoylation and all reversibly oxidative modifications, respectively[119]. Next, the nascent thiols react with cysteine-reactive isotopic or isobaric mass labels, affinity resins, biotin-based tags, fluorophores or radionucleotides. The following steps are highly diverse, and may include gel- or nongel-based separation, Western blot, proteolytic digestion, mass tagging, affinity purification and MS analysis.

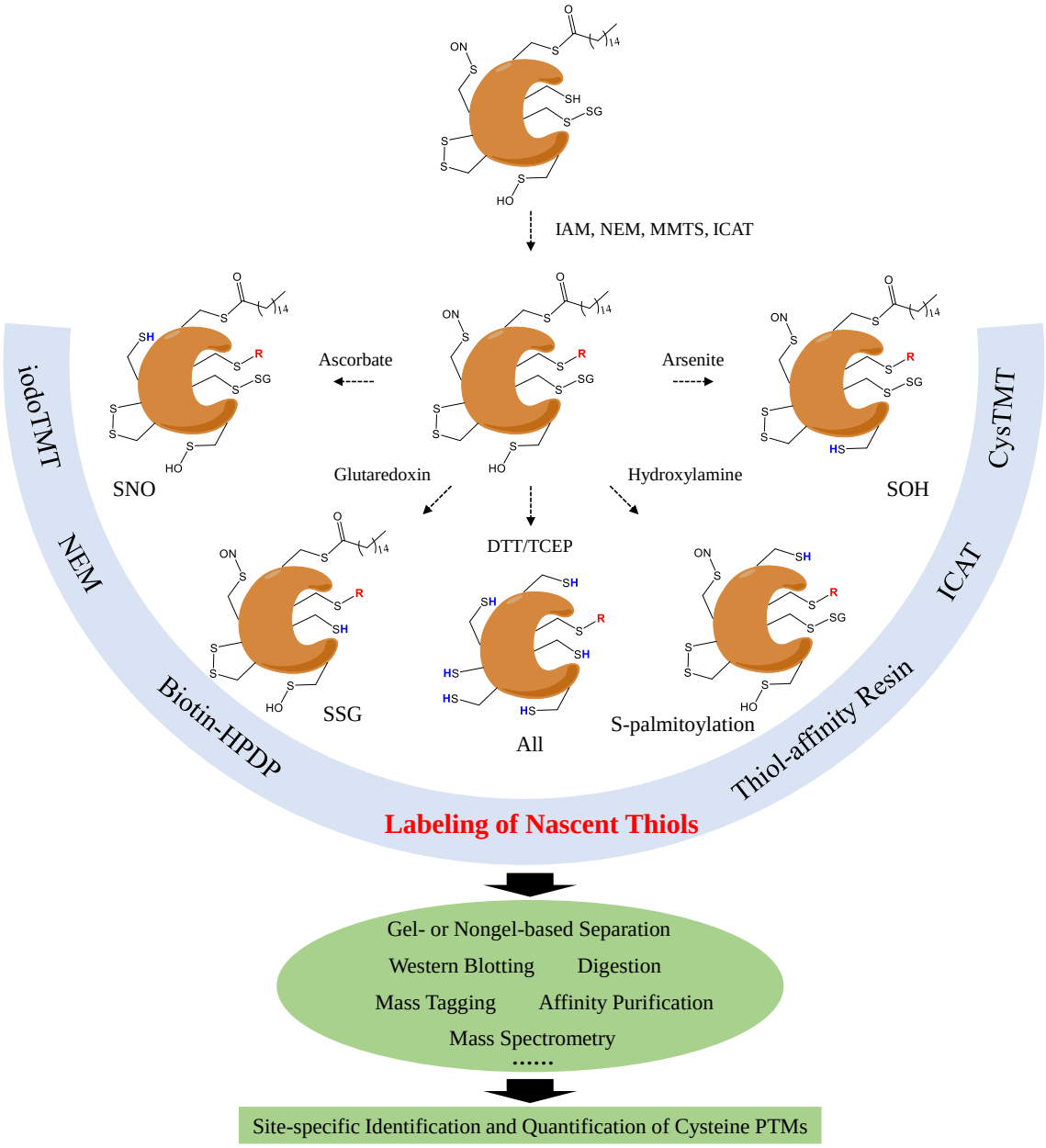


**Figure 2.3** Schematic summary of the principles of differential alkylation for identifying and quantifying cysteine reversible modifications in redox proteomics. Endogenously reduced cysteine thiols are first blocked by IAM, NEM, MMTS or ICAT (see text). Subsequently, different reducing reagents are used to selectively reduce targeted cysteine modifications. S-nitrosylation, S-glutathionylation, S-palmitoylation and sulfenic acid can be reduced by ascorbate, glutaredoxin, hydroxylamine and arsenite, respectively. A strong reductant such as DTT and TCEP (see text) reduces all reversible modifications. Next, nascent thiols are labeled with a variety of reagents for different purposes. Biotin-HPDP and thiol-affinity resin are widely used for isolating proteins and peptides containing reversible modifications. CysTMT/iodoTMT/NEM are cysteine-reactive mass tags and used for MS-based quantification. Finally, the procedures after labeling of nascent thiols are highly diverse. Samples may be separated by gel electrophoresis or chromatography, detected by Western blot, labeled by cysteine or amine-reactive mass tags, digested by proteases, purified by avidin resin or immunoaffinity, and analyzed by tandem MS. Not all of the steps are necessary, and the order of these steps may be switched. Sample mixing may also occur at different stages.

The overall objective is to discover redox-sensitive proteins and quantify the differences of site-specific cysteine modifications across different conditions/treatments.

Most of the quantitative redox proteomics approaches can be categorized into gel-based and nongel-based methods. In gel-based methods, an antibody towards specific cysteine PTM is utilized to detect and quantify redox-sensitive protein spots after gel separation. These gel spots are then digested and the protein is identified by MS[61]. Examples of gel-based redox proteomics approaches, such as 2D-Oxyblot, biotin-switch technique (BST) and redox difference gel electrophoresis (Redox-DIGE), are shown in Figure 2.4. 2D-Oxybot is a widely used gel-based technique to detect various types of modifications, e.g., protein carbonyls[120], 3-nitrotyrosine[121], 4-HNE[122], SNO[123], SSG[124], by using different primary antibodies. In this method, after 2D electrophoresis separation of lysates, immunoblotting analysis is performed to determine the protein spots with significant differences. The spots of interest are excised from the gel, in-gel digested and analyzed by MS (Figure 2.4a). This is a relatively low throughput technique, and may result in unambiguous identification due to the existence of multiple proteins in the same spot. Because all cysteine residues are in native states, 2D-Oxyblot is limited by artificial oxidation and thiol exchange reactions that occur during the sample processing[85]. To overcome these limitations, the biotin-switch technique (BST) was developed[98], in which free thiols are first blocked by MMTS, followed by selective reduction of oxidized cysteine modifications, e.g., SNO (Figure 2.4b). The newly-formed thiols are labeled with pyridyldithiol-biotin (biotin-HPDP), enriched by avidin affinity medium and analyzed by SDS-PAGE/immunoblotting or LC-MS/MS. Avidin conjugated horseradish peroxidase (Avidin-HRP) antibody can detect total SNO-modified proteins by Western blot, while a second antibody against a protein of interest can be used to detect an individual SNO-modified protein (Figure 2.4b). LC-MS/MS analysis of the avidin-enriched

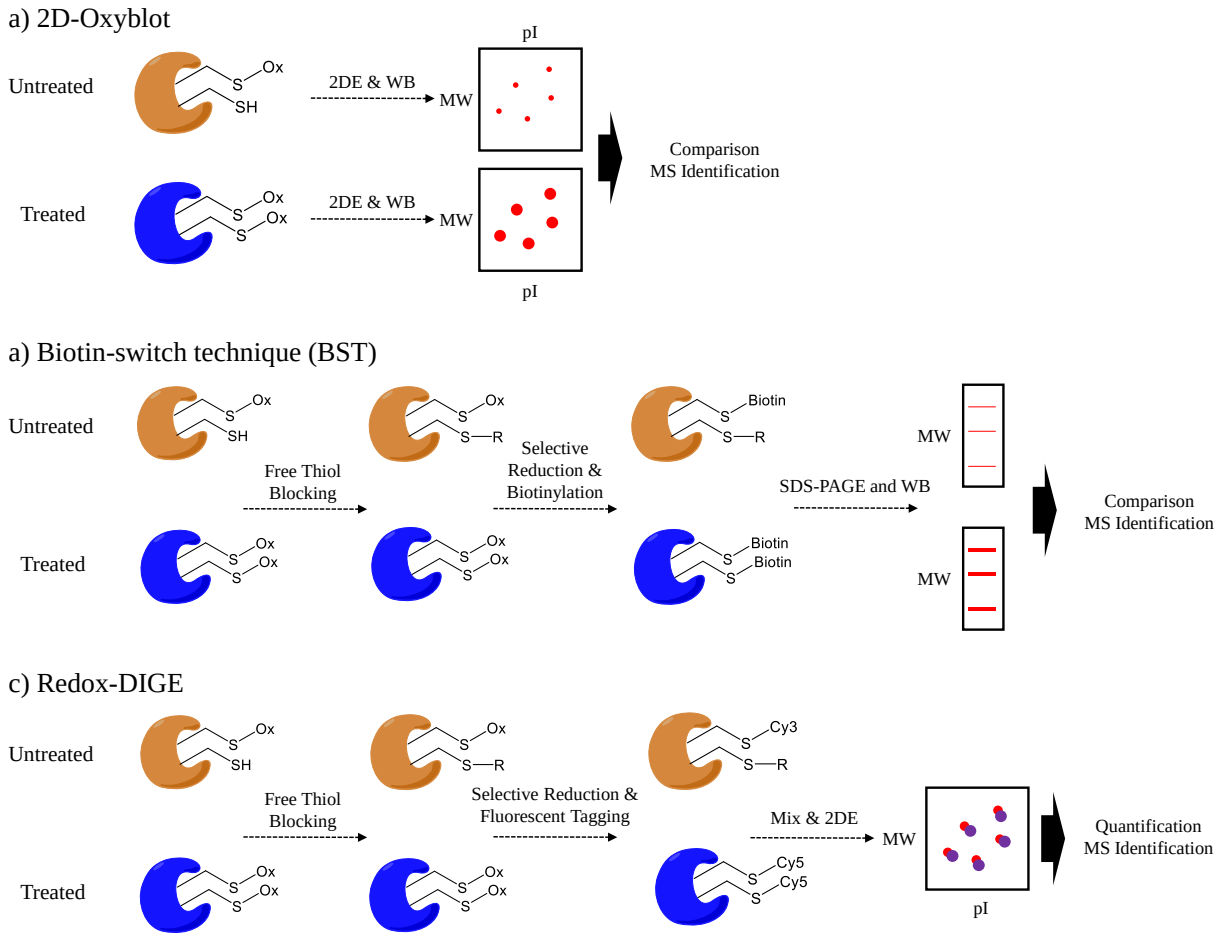


**Figure 2.4** Gel-based approaches for quantification of cysteine reversible modifications. a) In 2D-Oxyblot method first samples are separated by 2D SDS-PAGE separately. Gels are probed by Western blot using antibodies which recognize the particular cysteine PTM, such as S-nitrosylation and S-glutathionylation. Differentially-expressed protein spots are excised and identified by MS. b) Biotin-switch technique (BST) employs differential thiol blocking followed by selective reduction of the cysteine modification. The nascent thiols are labeled with biotin-HPDP. The oxidized proteins are then enriched by avidin affinity medium and analyzed by SDS-PAGE and Western blot. c) In Redox-DIGE method, different fluorescent tags are used to label samples after differential thiol blocking and selective reduction of cysteine modifications. Two samples are combined and analyzed on a single gel. The protein spots with differential fluorescent signals are excised and analyzed by MS.

mixtures allows the site specific identification of the oxidized cysteine without gel separation[103], which will be further discussed in below.

Both 2D-Oxyblot and BST approaches have limitations of poor gel reproducibility because samples are analyzed and quantified separately. An alternative strategy is redox difference gel electrophoresis (Redox-DIGE)[125]. This method employs a differential sample labeling step that uses two fluorescent dyes (e.g., Cy3 and Cy5) for untreated and treated samples. Both samples are mixed and separated on the same 2D gel (Figure 2.4c). Fluorescent scanning of the gel reveals the oxidized proteins with different levels between untreated and treated, which can be subsequently identified by MS. By using this approach, 13 mitochondrial SNO-proteins were identified upon treatment of rat mitochondrion with MitoSNO (mitochondria targeted S-nitrosothiol), and they were related with inhibition of energy-related metabolic enzymes[126].

Most of the gel-based quantitative approaches uses colorimetric or fluorescent detection to determine the protein spots with differential expression, followed by MS identification of the respective proteins. However there are other gel-based workflows using the stable isotopic labeling (SIL) technique for MS quantification of cysteine redox status. One method is called d-Switch [127,128], in which light and heavy NEM ($d_5$-NEM) are used to label endogenously reduced and oxidized cysteine, respectively. The sample is separated by gel electrophoresis, and the region containing the target protein is excised and analyzed by MS to obtain the quantitative information. Acrylamide matrix can also be used as the reaction chamber to lower sample loss, which is demonstrated in gel-based stable isotope labeling of oxidized cysteine (GELSILOX) approach[129]. In GELSILOX sample preparations can be simplified, which is beneficial for reliable quantification and better recovery. The differential $O^{16}/O^{18}$ labeling of control and treated samples allows the MS quantification of oxidized thiols in a duplex experiment.

The general limitations of the gel-based quantitative approaches include the lack of sensitivity when analyzing proteins with high or low molecular weight, with highly acidic or basic IP values, and with high hydrophobicity. Also the proteome coverage can be lower compared to full MS methods, and these approaches heavily rely on good and specific antibodies. Nevertheless, gel-based methods are very suitable to give a general visualization of oxidized proteins.

An effective strategy to overcome the limitations associated with gel-based methods and to probe deeper into the redox proteome is to employ nongel-based redox proteomics. Nongel-based approaches may identify and quantify hundreds to thousands of redox-sensitive cysteine residues from complex samples using an integrated shot-gun proteomic workflow. To date, numerous approaches have been developed and applied in biological studies, e.g., OxICAT (oxidized isotope-coded affinity tag)[101], OxiTRAQ (oxidized isobaric tag for relative and absolute quantitation)[109], SNO-RAC (SNO analysis by resin-assisted capture)[100], OxMRM (oxidized multiple reaction monitoring)[104], CysTMTRAQ (cysteine tandem mass tags and isobaric tag for relative and absolute quantification)[112] and OxcysDML (Oxidized cysteine-selective dimethylation), which was developed in this work (**Chapter 5**). Most of these methods have three distinct steps: 1) differential thiol alkylation and selective reduction (Figure 2.5), 2) affinity purification of nascent thiols, and 3) protein/peptide quantification using labeled or label-free approaches by MS.

Affinity purification plays an important role in nongel-based methods due to the low occurrence rate (~ 0.1%) of endogenously oxidized cysteine[64,65]. Enrichment methods reduce the complexity of the sample mixture, and can dramatically improve the signal to noise ratios of modified peptides in LC-MS/MS analysis. Affinity purification methods are: 1) high efficiency, 2) little to no non-specific binding, 3) simple workflow and 4) MS compatibility. Only a few

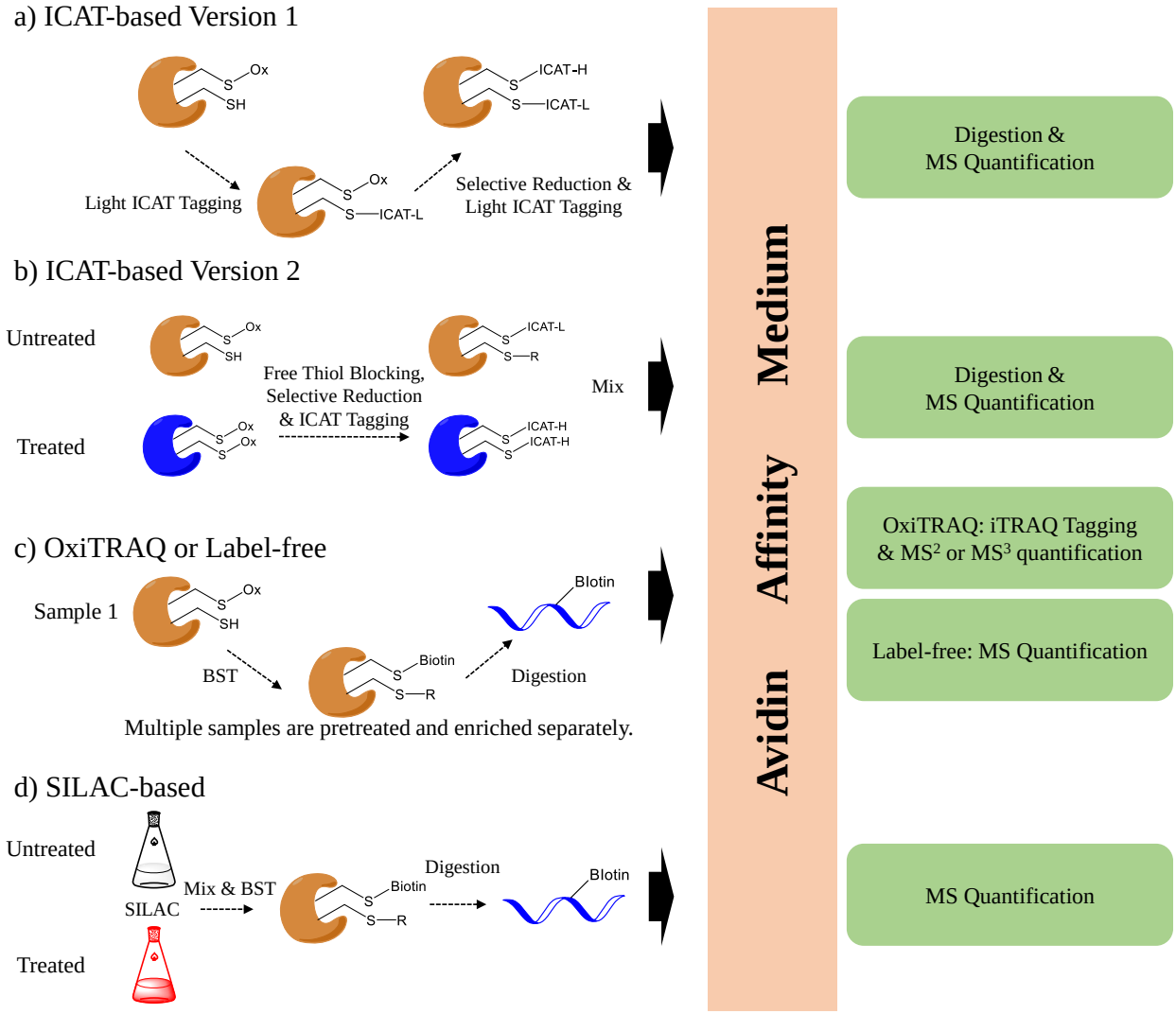


**Figure 2.5** Representative workflows using biotin as the purification technique. a) In an ICAT-based approach, only one sample is employed. The free thiols are blocked by light ICAT, and the nascent thiols after selective reduction are labeled with heavy ICAT. The sample is isolated by avidin affinity medium, digested and analyzed by MS. b) In another type of ICAT-based method, free thiol blocking, selective reduction and differential labeling of nascent thiols by light and heavy ICAT are performed for two different samples separately. After mixing, oxidized proteins are further processed, including enrichment, digestion and LC-MS/MS analysis. c) OxiTRAQ or label-free approaches use the biotin-switch technique (BST) to label oxidized cysteine sites followed by digestion and affinity purification for each sample. Enriched peptides are further tagged by iTRAQ and analyzed by MS, or analyzed by MS directly. d) In SILAC-based workflows, cells are grown in medium culture with light or heavy amino acids. Two samples are combined and processed using BST. Oxidized peptides are enriched and analyzed by MS.

enrichment approaches have been repeated to study oxidative cysteine PTMs: 1) biotin-avidin interaction, 2) thiol-affinity solid phase resin and 3) immunoaffinity capture.

Protein/peptide quantification involved in cysteine redox methods are similar to those techniques used in expression quantitative proteomics. For example, samples are differentially labeled with specific mass tags that can be recognized in MS analysis for relative quantification. These mass tags can be incorporated metabolically or chemically[24,25]. An alternative to labeling approaches is "label-free". Label-free approaches rely on ion intensity or spectrum counting to report on the abundance differences of redox-sensitive cysteine sites. Label-free can generally provide higher dynamic range compared to labeling methods, especially with multiple reaction monitoring (MRM) mode on a triple quadrupole MS analyzer[24].

Overall, differential thiol alkylation and selective reduction, as well as protein/peptide quantification using labeled or label-free methods, are readily transferable across different workflows. The following discussion gives more details of different enrichment techniques currently utilized.

### *2.2.1 Biotin-avidin Interaction*

The high affinity and specificity of interactions between biotin and avidin makes it an ideal technique to pulldown the target cysteine-containing peptides, which is mostly achieved by using isotope-coded affinity tag (ICAT). The first version of ICAT consisted of a thiol-reactive group (iodoacetyl), a deuterium-coded light or heavy linker, and an affinity group (biotin) for capturing tagged peptides[32]. ICAT was originally developed for quantifying protein expression in two different complex samples. Because only a small portion of the tryptic peptides have cysteine residues, ICAT technique can largely simplify the complex mixture, and enrich proteins with low abundance. Due to its inherent capability of cysteine tagging and purification, ICAT was readily

adapted into the characterization of reversibly oxidized thiol proteomes. Based on how the differential alkylation is performed, ICAT-based redox methods can either quantify the absolute oxidation status of each cysteine site in a single sample (termed OxICAT)[130-133], or quantify the relative abundance ratio of oxidized cysteine sites from two different samples[101,134-138].

OxICAT uses light ICAT as the blocking agent to label the reduced cysteine[130-133]. After reduction, the newly appearing cysteine with free thiol is labeled with heavy ICAT. After trypsinization, affinity purification and enrichment of cysteine-containing peptides is performed using streptavidin affinity column, followed by LC-MS/MS analysis (Figure 2.5a). The coeluted light and heavy-labeled peptides generate peaks in the precursor mass spectra, and the relative intensity of peak areas represent the abundances of the reduced and oxidized form for each cysteine residue.

In another ICAT-based approach, the ratio of oxidized cysteine from two samples can be compared in a single experiment[101,134-138]. The blocking step uses a generic thiol blocking reagent (e.g., NEM, IAM) for both samples. Upon reduction of reversibly oxidized thiols, nascent thiols are labeled with light ICAT for one sample and heavy ICAT for the second sample. The two samples are combined, digested, enriched and analyzed by LC-MS/MS (Figure 2.5b). Because peptides with reduced cysteine have been depleted, the parent mass spectrum is more simplified than the OxICAT method, and the light and heavy peaks in each pair have comparable intensities.

In addition to ICAT-based methods, biotin-based affinity purification has been coupled with other quantification methods, such as label-free, isobaric tag for relative and absolute quantitation (iTRAQ) and stable isotope labeling by amino acids in cell culture (SILAC). Palmitoylated proteins (S-acylated proteins) are isolated and quantified after free thiol blocking by NEM, selective reduction by hydroxylamine and label-free quantitation. This method is based on

the classic biotin-switch technique[105], and can be expanded to study other types of cysteine modifications (Figure 2.5c). ITRAQ has been utilized in biotin-based workflow (termed OxiTRAQ)[109] (Figure 2.5c), in which up to eight samples can be compared in a single experiment. In SILAC, cell samples are labeled by either light or heavy arginine and/or lysine in cell culture medium (Figure 2.5d)[107]. Tryptic peptides carry at least one labeled amino acid resulting in a mass increment over the non-labeled counterpart that is equivalent to the number of heavy isotope atoms incorporated. SILAC-based redox methods combine two different samples at the level of intact cells before affinity purification, resulting in lower sample error and higher accuracy compared with other quantitative methods.

### *2.2.2 Thiol-affinity Solid Phase Resin*

Thiol-affinity resin was initially used to enrich cysteine-containing peptides from complex mixture to improve identification of low abundant proteins[139,140]. The most widely used affinity resin is Thiopropyl sepharose® 6B, in which a reactive 2-thiopyridyl disulfide group is attached to sepharose through a chemically stable ether linkage. When mixing the affinity resin with peptide digests, cysteinyl peptides are covalently captured through the disulfide bond exchange reaction. The unbound, non-cysteinyl peptides and the released 2-thiopyridone are removed by washing. The captured peptides can be released by incubating the resin with a reducing reagent (e.g., DTT). This enrichment is quantitative and the specificity is ~98-99% based on studies in this thesis (**Chapters 4 - 6**)[38,39,141].

Recently thiol-affinity resin has gained popularity for isolating and quantifying cysteine reversible modifications in complex mixtures. Different quantitative MS methods, e.g., isotopic labels[100,141], isobaric tags[99,115,116,119,142], label-free methods[143-145], have been coupled with resin-based enrichment, to quantify SNO[100,116,142-144], SSG[115,119], S-palmitoylation[99,119], and all oxidative

cysteine[119,135,142,145] (Figure 2.6). Resin-assisted approaches have several advantages. First, it is a simple workflow in which peptides are directly captured on the thiol-affinity resin without pre-derivatization. Second, enriched peptides do not have fragmentable tags that will be generated in MS/MS, and no side reaction is expected in the reversible capture and release reaction. Third, enriched peptides are linked to the resin through stable covalent bonding, so stringent washing steps can be applied to remove non-specific binders. Fourth, resin matrix can serve as a sample sorbent to facilitate the on-resin peptide labeling reaction by using different amine-reactive tags, e.g., acetylation[100], dimethylation[39], TMT[119,142] and iTRAQ[99,115,116]. This is very attractive, as no more sample cleanup is needed between steps, which is beneficial for minimizing sample loss. The cost of this workflow can become high, especially if isobaric tags are employed.

An alternative way to lower the cost is using inexpensive stable-isotope dimethyl labeling on solid phase resin, termed OxcysDML (**Chapter 5**)[39]. This technique can achieve peptide on-resin dimethylation using different isotopomers of formaldehyde and cyanoborohydride. The average tagging cost of each sample is ~$1. This inexpensive, efficient and accurate method has been applied to study the redox proteome of liver tissues from an AD mouse model (**Chapter 5**). Inspired by our previous cPILOT methodologies[36,38,54], our laboratory recently further expanded the multiplexing capacity of OxcysDML by employing on-resin cPILOT tagging of cysteinyl peptides. This approach, termed oxidized cysteine-selective cPILOT (OxcyscPILOT)[141], enabled sample multiplexing up to twelve samples in a single run, and has been demonstrated in the study of endogenous SNO of brain proteins in an AD mouse model (**Chapter 6**).

### *2.2.3 Immunoaffinity Capture*

Immunoaffinity capture is not widely reported until recent years, and most of these studies use cysteine-reactive tandem mass tag (cysTMT) or iodoacetyl tandem mass tag (iodoTMT) as the

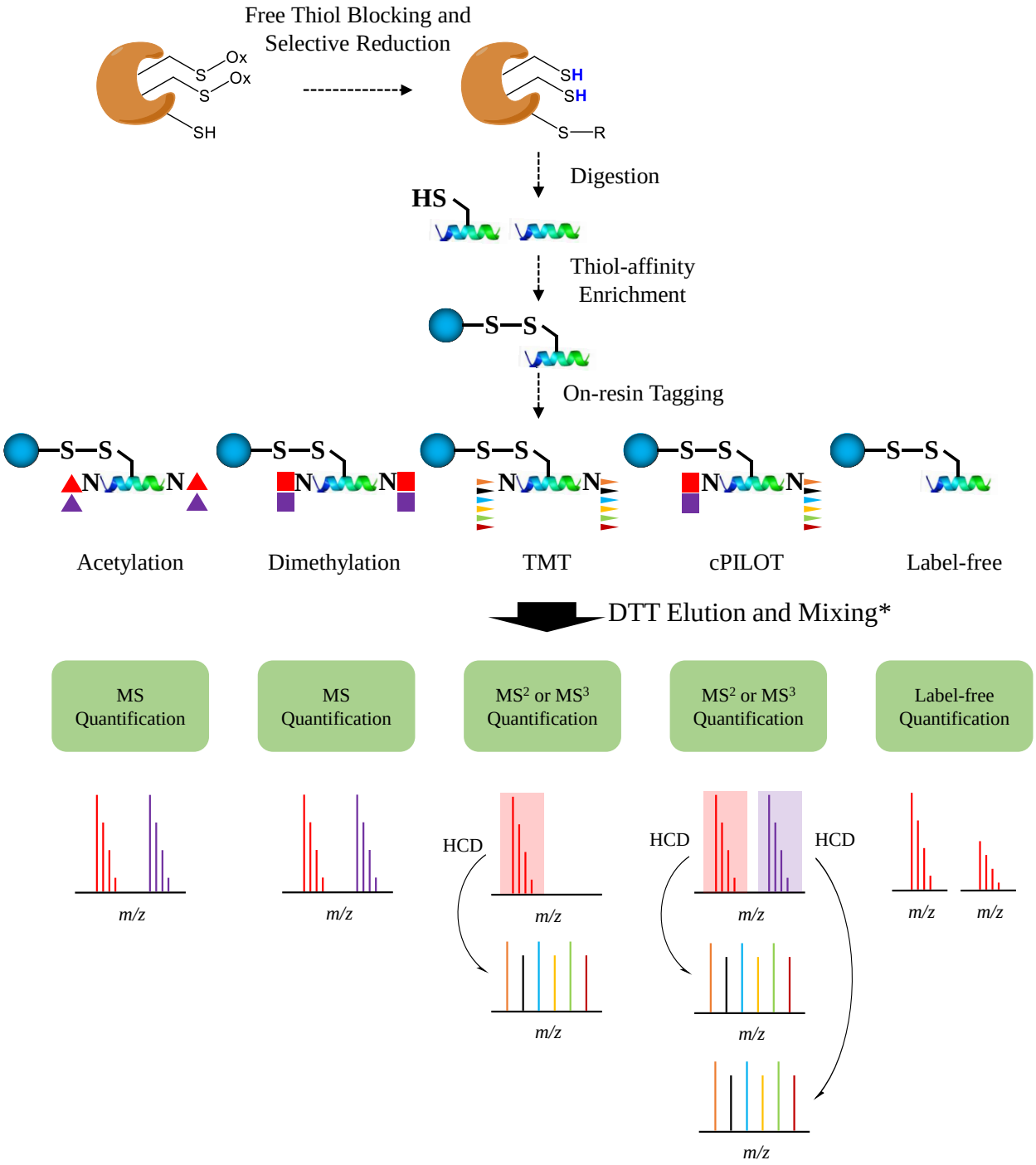


**Figure 2.6** Typical workflows using thiol-affinity resin for purification. Free thiols in each protein sample are blocked followed by selective reduction of cysteine modifications. After proteolytic digestion, peptides containing nascent thiols are enriched by thiol-affinity solid phase resin. Different amine-reactive tagging methods can be performed to label peptides on the resin, including acetylation, dimethylation, TMT and cPILOT. Finally enriched peptides are eluted, combined and analyzed by MS. Typical spectra obtained by each method is provided.*In the label-free approach, peptides are not tagged on the resin so sample mixing is not needed.

quantitative mass tag. CysTMT contains a mass reporter group, a mass normalizer moiety and a pyridyldithiol cysteine-reactive group. CysTMT-tagged peptides are enriched by anti-TMT resin immobilized with an antibody recognizing the mass reporter structure of the mass tag. During the LC-MS/MS step, cysTMT-tagged peptides can generate up to six reporter ions between 126 and 131 Da, the intensities of which are used for relative quantification. IodoTMT works similar to CysTMT, except its irreversible reaction with sulfhydryl groups. CysTMT and iodoTMT-based approaches have been successfully applied in studying the redox proteome alteration of human pulmonary arterial endothelial cells treated with S-nitrosoglutathione[111], the NO-mediated cardioprotection processes[43], and the SNO sites responding to lipopolysaccharide (LPS) stimulation in microglial cells[113]. Recently, a novel iodoTMT-based workflow, termed SNO/SOH TMT strategy, has been developed to provide quantitative profiling of SNO and SOH changes simultaneously[118]. Compared with other methods, SNO/SOH TMT strategy uses two channels to isolate total cysteinyl peptides for correcting protein abundance changes during sample treatment and preparation.

Although not frequently reported, conventional protein immunoaffinity purification - using an immobilized antibody to pull down the targeted protein - can also be coupled with differential thiol blocking to quantify the redox status of cysteine residues in specific proteins[104]. In one study, diamide treated human breast cancer cells are differentially alkylated with $d_0$ and $d_5$ NEM for reduced and oxidized cysteine, respectively. The target protein p53 and protein tyrosine phosphatase-1B (PTP1B) are then serially immunoaffinity-purified and analyzed by MRM. This method, termed OxMRM, indicated that Cys182 and Cys215 are the redox-sensitive sites in p53 and PTP1B, respectively.

### *2.2.4 Non-enrichment Approaches*

When comparing the reversibly oxidized cysteine across multiple samples in one experiment, one has to consider the effects of total protein-level changes to the cysteine PTM changes. Generally a separate experiment is involved to address the protein turnover issue in the course of experiments[138]. In order to obtain the protein expression and cysteine redox information by using a single run, a possible strategy, although not widely used, is to retain the non-redox portion of the sample. Cysteinyl peptides help determine the redox changes, while the non-cysteinyl peptides are responsible for quantifying protein-level changes. In these cases, affinity purifications are normally not involved. The previously discussed GELSILOX approach is one of the relevant examples[129]. Another good example is cysTMTRAQ (cysTMT and iTRAQ) method[112], which uses cysTMT to label protein thiols responsive to a treatment, and uses iTRAQ to label peptide amines for analysis of protein-levels changes between different treatments. In tandem MS spectra, reporter ions generated by cysTMT tags (*m/z* 126, 127, 128, 129, 130, 131 for six samples) and iTRAQ tags (*m/z* 114, 115, 116, 117, 119, and 121 for six samples) enable the quantification of protein redox and total levels simultaneously.

## 2.3 REDOX PROTEOMIC APPROACHES TO STUDY PROTEIN CARBONYLATION

2D-gel based redox proteomics can also be used to study protein carbonylation[146,147]. After treatment with 2, 4-dinitrophenylhydrazine (DNPH) to form a DNP hydrazone adduct, protein samples can be resolved by 2D gel and recognized by anti-DNP antibodies. Derivatization can occur before or after the gel separation[148]. Individual carbonylation signals from the blot are normalized to the total protein level present on the gel and compared across different

conditions[149,150]. Despite the extensive usage of DNPH for derivatizing carbonylation it should be noted that DNPH is not exclusive for carbonyl groups, as it also reacts with sulfenic acids-oxidized thiol groups-under acid catalysis conditions[151]. Biotin-hydrazide may be used to label carbonyl groups with fluorescein or peroxidase linked avidin[152,153]. A protein carbonyl enzyme immuno-assay kit has recently become available[154].

Non-gel redox proteomics have been widely applied in the study of protein carbonylation and have been reviewed recently[146,155,156]. A key step in these approaches is the incorporation of enrichment procedures for carbonylation which is necessary since the average abundance of carbonylated proteins has been reported as ~0.2% in human plasma[157]. One of the most common methods uses avidin affinity chromatography to enrich biotin-hydrazide derivatized carbonylated peptides. Derivatization with biotin hydrazide also results in the formation of a Schiff base that can be reduced to a more stable C-N bond. Label-free or isobaric tagging strategies (e.g., iTRAQ) can be used for quantifying carbonylation level across different samples[158,159]. Regnier and coworkers have successfully applied biotin/avidin affinity chromatography proteomics to study carbonylation in *in vitro* metal-catalyzed oxidation models, yeast, rat and human plasma tissues, and diabetic rats[156-161]. A similar tag based on biotin/avidin is N'-aminooxymethylcarbonylhydrazino D-biotin (aldehyde reactive probe, ARP), the hydroxylamine moiety of which can form a stable C=N bond, thus further reduction is not necessary[162-164]. This ARP however undergoes substantial fragmentation in MS/MS experiments which decreases peptide confidence after database searching due to complex spectra. The development of an algorithm which incorporates ARP fragment ions and neutral loss into the database searching has enhanced identification of protein carbonylation with ARPs[165].

However MS-based identification of protein carbonylation is still challenging due to the complexity and diversity of modifications as carbonyl groups occur many amino acid side chains and the range in mass shifts. In **Chapter 3** we demonstrate how iterative database searching and manual spectral validation can help solve this problem.

## 2.4 APPLICATIONS OF CYSTEINE-SELECTIVE REDOX PROTEOMICS IN AGING AND NEURODEGENERATIVE DISEASES

In aging part of the brain shrink, communication between neurons are reduced, and tiny plaques and tangles develop outside or inside neurons[166]. Neurodegenerative diseases including AD, PD and human prion diseases are a group of diseases affecting the central nervous system (CNS) with different etiologies. It is accepted that aging is an important risk factor for age-related neurodegenerative diseases, and many efforts are filling the gaps in our knowledge about the earliest stage of AD[61]. Studies have shown that the imbalanced defense mechanism of antioxidants and oxidative damage to cellular macromolecules such as proteins, peptides and DNA accumulates with aging and neurodegenerative diseases[167]. In the past two decades much effort has been made to better elucidate the mechanism of oxidative damage in aging and neurodegenerative diseases, including using cysteine-selective redox proteomics. These studies gained quantitative insights into the redox-sensitive proteins and specific cysteine residues from human tissues and model animals. To date, quantitative studies of aging and neurodegenerative diseases using redox proteomics are reported in Table 2.1.

Surprisingly, most of the aging-related redox proteomics are focused on total cysteine oxidations (i.e., the specific PTM is not identified). For example, an analysis of liver cytosolic proteins from young (4-6 months) and old mice (26-28 months) revealed 11 proteins (such as GAPDH, regucalcin and peroxiredoxin 1) showing a more than two-fold increase in cysteine

**Table 2.1** Representative redox proteomics approaches to quantify various types of cysteine modifications in aging and neurodegenerative diseases.

| Year | Sample | Disease | Method | Cysteine Modification | Results |
|---|---|---|---|---|---|
| 2004 | Human brain tissues | AD & PD | 2D gel, immunostaining and MS | Sulfonic acid | Cys220 of UCH-L1 is oxidized to cysteic acid[168]. |
| 2007 | Inferior parietal lobule from patients | AD | 2D-Oxyblots and MS | SSG | Deoxyhemoglobin, α-crystallin B, glyceraldehyde phosphate dehydrogenase (GAPDH), and α-enolase were significantly S-glutathionylated in AD[169]. |
| 2008 | Foetal, aged normal and advanced nuclear cataract lenses from human | Aging | Gel-free switch assay, label-free quantification, no enrichment | Total oxidized cysteine | Quantified relative amount of reduced form and oxidized form of each cysteine site within the same biological condition. αA, Cys 142; βA1/3, Cys 52; βB3, Cys 39 and Cys 45 had higher oxidized form in nuclear cataract and aged normal lenses compared with foetal[170]. |
| 2009 | Entorhinal cortex from patients | Aging | 2D Western blots and MS | SNO | Glial fibrillary proteins were nitrosylated in a brain tissue from a 78-year-old female, 13 h postmortem delay without neurological disease[171]. |
| 2010 | Liver tissues from mouse at 4-6 and 26-28 months | Aging | Fluorescence-based 2D gel and MS | Total oxidized cysteine | Global protein disulfide levels increased significantly with age in liver cytosolic proteins, an 11 proteins showed a more than twofold increase in disulfide content with age[172]. |
| 2011 | Brain cerebrum tissue from 5-month old transgenic mice (B6Cg-Tg) and WT controls | AD | CE-Laser induced fluorescence, switch assay | SNO | Transgenic mice brain had higher SNO than control[173] . |

*Continued on Page 39*

**Table 2.1** Representative redox proteomics approaches to quantify various types of cysteine modifications in aging and neurodegenerative diseases.

| Year | Sample | Disease | Method | Cysteine Modification | Results |
|---|---|---|---|---|---|
| 2012 | Brain from 11-month old transgenic mice (B6Cg-Tg) and WT controls | AD | 2D micro-electrophoresis | SNO | 2D profiling of nitrosylated proteins in AD and WT brains. AD brain proteins with a MW between 35 kDa and 65 kDa were most susceptible to SNO[174]. |
| 2012 | Brain tissues and blood samples from 1-mon, 5-mon and 11-mon TG mice and controls | AD | CE-Laser induced fluorescence, switch assay, PCA analysis | SSG | AD and controls could be differentiated (> 90% sensitivity and specificity) based on SSG electrophoretic profiling[175]. |
| 2014 | Autopsied brain specimens | AD | 2D-Oxyblot and MS | SNO | Superoxide dismutase (SOD2) [Mn], fructose-bisphosphate aldolase C (ALDOC) and voltage-dependent anion-selective channel protein 2 (VDAC2) showed differential S-nitrosylation signal[123]. |
| 2014 | Synaptosome of transgenic mouse (14-15 mon) | AD | BST, avidin enrichment, label-free quantification, gel-free | SNO | 138 S-nitrosylated proteins were involved in various cellular pathways, including: glycolysis, gluconeogenesis, calcium homeostasis, ion and vesicle transport[176]. |
| 2014 | Mouse skeletal muscles | Aging | Labeling reduced and oxidized cysteine using light and heavy NEM, respectively. Gel-free, non-enriched | Total oxidized cysteine | The reversible redox state of specific cysteine residues within individual muscle samples was obtained[177]. |
| 2015 | Hippocampus from patients | AD | 2D-Oxyblots and MS | Sulfenic acid, sulfinic acid and sulfonic acid | Pin1 was identified to be oxidized on Cys113. This modification was elevated in human AD brain[178,179]. |

*Continued on Page 40*

**Table 2.1** Representative redox proteomics approaches to quantify various types of cysteine modifications in aging and neurodegenerative diseases.

| Year | Sample | Disease | Method | Cysteine Modification | Results |
|---|---|---|---|---|---|
| 2015 | Human cortex and cerebellum samples | Human prion diseases (neurodeg enerative disorders) | BST, avidin enrichment, iTRAQ, gel-free | SNO | 1509 S-nitrosylated proteins (SNO-proteins) were identified with differential expressions in many pathways[180]. |
| 2015 | Amyloid-activated BV2 cells | AD | BST, avidin enrichment, gel-free | Total oxidized cysteine | 60 proteins changed the redox status of their selective cysteine residues upon treatment with the amyloidogenic Aβ25-35 peptide[181]. |
| 2015 | Drosophila melanogaster (heads and thoraces) | Aging and fasting | OxICAT, gel-free | Total oxidized cysteine | Aging had no impact on cysteine-residue redox state. In contrast, fasting dramatically affected cysteine redox status[182]. |
| 2015 | Old and young Human eye tissues, glutathione depleted LEGSKO mouse lens | Aging | 2D gel and OxICAT | Total oxidized cysteine | Shift of intramolecular disulfides to intermolecular disulfides during aging process was observed. Several disulfide formation sites necessitated prior conformational changes in γ-crystallin[183]. |
| 2016 | Liver tissue from AD model mouse | AD | Gel-free, dimethylation | Total oxidized cysteine | More than 1000 oxidized cysteine were identified. The most dysregulated pathway was metabolism. The over oxidized proteins involved in lipid metabolism could be linked with oxidative stress in AD liver[141]. |
| 2016 | Brain tissue from AD model mouse | AD | Gel-free, cPILOT | SNO | 135 SNO-modified proteins were identified, and the majority of them were involved in metabolism and signal transduction. Statistical analysis indicated 12 SNO-modified peptides had differential levels in AD compared with WT[141]. |

oxidation content with aging[172]. In another study using young adult (12 months) and old (25 months) mouse skeletal muscle, the absolute redox status of each cysteine site could be measured[177]. LC-MS/MS identified 50 and 24 redox cysteine proteins in young adult and old samples, respectively. Metabolic proteins (e.g., phosphofructokinase, glucose 6-phosphate isomerase, glycogen phosphorylase, phophoglycerate mutase 1, and phosphoglucomutase 2) containing oxidized cysteine were only identified in young adult samples, which suggests that muscle from adult mice has greater flexibility in the metabolic redox response. However different biological models may lead to inconsistent conclusions when using redox proteomics to study aging. For example, aging was found to have no impact on cysteine-residue redox status in *Drosophila melanogaster*[182]. However after 24-hour fasting significant oxidation of cysteine residues was observed[182]. Aging is not always accompanied with elevated oxidative stress, but fasting is able to induce major metabolic changes and cysteine oxidation, and serve as the organism's response to fasting. Age-related nuclear cataract (ARNC) is a human eye disease with covalent crosslinking of polypeptides and loss of protein thiols[184]. In order to better understand the change of site-specific oxidation of cysteine residues in aging and ARNC, three different types of human lenses, including foetal lenses, order normal lenses and nuclear cataract lenses, were compared[170]. Ten cysteine residues were found not sensitive to aging, but they were largely oxidized in ARNC. Two cysteine residues in γC-crystallin were not oxidized in ARNC due to insufficient exposure to the oxidative environment. Another similar study revealed the shift of intramolecular disulfides to intermolecular disulfides during aging[183]. Redox proteomics using ICAT determined several disulfide formation sites necessitating prior conformational changes in γ-crystallin, which is consistent with the previous study[170].

AD is a neurodegenerative disorder characterized by neurofibrillary tangles, senile plaques, and loss of synapses[185]. AD is also the main cause of senile dementia (approximately 75%). Oxidative stress has been reported in AD brain[186], plasma[187], heart[188], spleen[189] and liver[141]. These studies support the notion that oxidative stress plays a major role in the pathogenesis of AD.

Cysteine can be oxidized into a variety of PTMs, among them SNO is the most frequently investigated in AD. SNO originates from the modification of free cysteine by nitric oxide (NO), a signaling molecule mainly formed by NO synthase in the CNS[190]. Protein nitrosylation and denitrosylation controls the activities of proteins and pathways in physiological conditions. For example, SNO of N-methyl-D-aspartate receptor (NMDAR) can decrease its enzyme activity to facilitate neuroprotection[191]. Also SNO modification has been linked with protein misfolding, mitochondrial fragmentation and subsequent neuronal loss[63], and has been considered as a therapeutic target for neurodegenerative diseases[192]. In a study of entorhinal cortex from AD patients, although a variety of SNO-modified proteins in human brain tissue were identified, no significantly changed proteins in AD were observed[171]. However glial fibrillary proteins were found to be nitrosylated in a brain tissue from a 78-year-old female without neurological disease, which may suggest the involvement of SNO in aging process. In another study SNO-modified proteins of autopsied brain specimens, including hippocampus, substantia nigra and cortex from AD patients were investigated[123]. A total of 45 proteins were identified with endogenous nitrosocysteines. These proteins are involved in metabolism, signaling pathways, apoptosis and redox regulation. Three proteins, superoxide dismutase [Mn], fructose-bisphosphate aldolase C and voltage-dependent anion-selective channel protein 2, had enhanced SNO in AD compared with healthy controls. Elevated SNO of these proteins may result in altered detoxification, glycolysis and ion transportation in AD brain. SNO of brain synaptosomal proteins were quantified

using wild type and transgenic mice overexpressing mutated human amyloid precursor protein (hAPP) at 14 month old, a widely used animal model for AD[176]. One hundred and thirty-eight synaptic proteins were SNO-modified, and 38 of those were differentially SNO-modified in hAPP mice. SNO-modified proteins were involved in glycolysis, gluconeogenesis, calcium homeostasis, ion and vesicle transport, indicating the wide involvement of SNO in basic cellular pathways. Brain tissues from APP/PS1 AD mouse model was also investigated using OxcyscPILOT, in which 135 SNO-modified proteins were identified, and the majority of which participated in pathways of metabolism and signal conductions (**Chapter 6**)[141]. The identified proteins containing SNO modification, as well as the quantitative information obtained by this study, had considerable agreement with previous studies[123,176].

In addition to SNO, SSG is also an important cysteine reversible PTM with biological relevance in neurodegenerative diseases[193]. SSG was probed in inferior parietal lobule (IPL) and hippocampus from AD patients[169]. This work found deoxyhemoglobin, a-crystallin B, glyceraldehyde phosphate dehydrogenase (GAPDH), and a-enolase were significantly modified by SSG in AD. More interestingly, GAPDH and α-enolase had reduced activity in the AD IPL.

Our knowledge of redox-modified proteins involved in the pathogenesis and progression of AD is consistently being updated. Proline isomerase Pin1 was significantly carbonylated in AD hippocampus with decreased activity both *in vivo* and in *vitro*[194]. Recent studies showed the oxidation of Pin1 Cys113 was significantly elevated in human AD brains and AD mouse models[178]. Pin1 oxidation on Cys113 inactivated its activity, but the oxidative inhibition of Pin1 could be partially reversed by treatment with dithiothreitol[179]. Cys113 of Pin1 in AD brain tissue was probably oxidized into sulfenic acid, sulinic acid or sulfonic acid. It is challenging to determine

the relative abundances of the three PTMs *in vivo*, which may be solved by using chemical derivatization coupled with MS[195].

A new method, which couples capillary gel electrophoresis with laser induced fluorescence detection and fluorescence switch assay, is able to differentiate the cysteine-modified proteins between different complex samples. This method was applied to differentiate the SNO and SSG proteins in AD transgenic mice and age matched WT controls[173].

In addition to SNO and SSG, the total cysteine reversible modifications were also examined in AD related studies. For example, the reversibly modified microglial proteome of BV2 cells after treatment of $A\beta_{25-35}$, a short peptide known to be able to induce the inflammatory and oxidative status on microglia without affecting cell viability, was quantified[181]. This study identified 60 proteins with changed redox status. In another report the redox-regulated liver proteins from transgenic AD mouse were examined[39]. This work identified 1129 reversibly-oxidized cysteine sites, among which 19 showed significant differences between AD and controls (**Chapter 5**). Proteins involved in lipid metabolism were found in more oxidized form, and is correlated with the overwhelmed oxidative stress in AD liver tissue.

PD is the second most prevalent degenerative disease of the nervous system with the accumulation of insoluble proteinaceous deposits such as Lewy bodies[61]. Ubiquitin carboxyl-terminal hydrolase L1 (UCH-L1) is associated with familial forms of PD[196], and oxidized of Cys220, as well as Met124 and Met179 in both AD and PD[168]. In addition to AD and PD, human prion diseases, fatal neurodegenerative disorders characterized by neuronal damage in brain and accumulation of misfolded protein deposits in the CNS[197], have also been investigated by redox proteomics. SNO-modified proteins of human cortex and cerebellum tissues from normal controls, sporadic Creutzfeldt-Jakob disease (sCJD), fatal familial insomnia (FFI), and genetic CJD with a

substitution of valine for glycine at codon 114 of the prion protein gene (G114V gCJD) were compared[180]. A total of 1509 endogenous SNO-proteins were identified, making it one of the relevant studies with the highest proteome coverage. Differentially expressed SNO-proteins were mainly involved in metabolism, cell cytoskeleton/structure, immune system, cell-cell communication and miscellaneous function protein.

## 2.5 APPLICATIONS OF REDOX PROTEOMICS TO STUDY PROTEIN CARBONYLATION IN ALZHEIMER'S DISEASE

Redox proteomics studies can directly identify, from brain, fluids or other biological sample, a large number of carbonylation modified proteins potentially involved in the pathogenesis and/or progression of AD characterized by increased oxidative stress[198,199]. Some representative studies are listed in Table 2.2.

Increased carbonylation levels exist in AD inferior parietal lobule (IPL) compared to age-matched controls[200,201]. Following studies performed on hippocampal region of AD subject compared to CTR demonstrated specific carbonylation of Pin1, phosphoglycerate mutase 1, UCH L-1, DRP-2, carbonic anhydrase II, triose phosphate isomerase, α-enolase, and γ-SNAP[202]. The impairment of the functionality of the proteins found oxidized in these studies correlates features of AD pathology such as the inhibition of cellular degradation machinery and synaptic failure[203]. Korolainen et al. applied a similar redox proteomics approach to frontal cortex samples of AD patients compared to healthy subjects showing a decrease of carbonyls in malate dehydrogenase 1, glutamate dehydrogenase, 14-3-3 protein ς/δ, aldolases A and C, and increased oxidation of carbonic anhydrase[204].

**Table 2.2** Redox proteomics studies of neurodegenerative diseases[61].

| Pathology | Sample | Oxidative modification | Oxidatively modified proteins | Altered biological functions |
|---|---|---|---|---|
| AD | Human brain (hippocampus, IPL and cortex) | Carbonylation | CKBB, GS, UCH-L1, DRP-2, ENO1, HSC71, Pin1, PGM1, TPI, γ-SNAP, CA, MDH, GDH, 14-3-3 ς/δ, FBA A/C | energy metabolism, protein degradation, neuron outgrow, cell signaling, cell cycle, neurotransmission, protein transport, molecular chaperone[194,200-202,204] |
| | Human body (CSF and plasma) | Carbonylation | λ-chain precursor, hemopexin, transferrin, fibrinogen λ chain precursor, α1 antitrypsin precursor, Hp β chain, α2 macroglobulin | heme transport, iron transport, blood coagulation, extracellular chaperone[205-208] |
| | Synaptosomes with Aβ (1-42) | Carbonylation | β- and γ- chain, GFAP, ATP synthase, SNBP1, GDH, GS, EAAT2, DRP-2, EF-Tu | cell structure, energy metabolism, neurotransmission, neuron outgrow, protein biosynthesis[209] |
| | Rat brain with Aβ (1-42) | Carbonylation | GS, tubulin β chain 15/α, 14-3-3 ς, HSP60, β-synuclein, PDH, GAPDH, PGM1 | neurotransmission, cell structure, cell signaling, molecular chaperone, energy metabolism[210] |
| | C. elegans with Aβ (1-42) | Carbonylation | medium and short-chain acyl-CoA DH, EF-1 γ, MDH, AK, RACK1, mlc-1 and 2, actin, ADK, nematode specific protein, lbp-6, TKT, α and β proteasome subunit, GST | energy metabolism, protein biosynthesis, protein degradation, axon extension, cell structure, cell cycle, antioxidant[211] |

In addition to human brain tissues, other models have been used to study protein carbonylation in AD. For example, the SAMP8 model (the senescence-accelerated prone mouse) exhibits age-dependent learning and memory deficits[212], making it a model for studying age-related cognitive impairments that might lead to AD onset and progression[213]. Analysis of protein carbonylation by redox proteomics show increased levels for LDH-2, DRP2, α-spectrin and CK in the brain of 12-month-old SAMP8 mice when compared with the 4-month-old SAMP8 brain. Other relevant studies include *in vitro* treatment of synaptosomes with Aβ (1-42)[209] and *in vivo* injection of rat brain with Aβ (1-42)[210]. Proteins such as actin, GFAP, 14-3-3 ζ and HSP60 were significantly oxidized, suggesting the mechanism of neurodegeneration driven by Aβ deposition. It is noteworthy to highlight that there are no models which contain all of the characteristics and behaviors of AD. When designing new experiments and comparing results from different sources, one must be careful of the models as well as potential limitations of their use in studying AD.

## 2.6 CONCLUSIONS

Oxidative protein modifications (including cysteine oxidation and protein carbonylation) have been shown to be ubiquitously and dynamically involved in aging and aging-related neurodegenerative diseases. The growth of MS-based proteomics, including gel-based and nongel-based approaches, has led to discovery of new PTMs and their identification and quantification. For example in **Chapter 3**, a MS method was developed to characterize a model protein carrying various types of oxidative modifications. We believe that the key for future improvements of redox proteomics is development of novel methods with higher sensitivity, accuracy, simplicity and throughput, for example, the OxcysDML and OxcyscPILOT approaches that will be discussed in **Chapters 5** and **6**. Continued advances in redox proteomics will further the understanding of aging

and aging-related neurodegenerative diseases, especially the redox molecular mechanism, the roles of oxidative stress and redox signaling in cellular processing.

# 3.0 MULTIPLE PROTEASES TO LOCALIZE OXIDATION SITES

(Note that information in this chapter is written based on a published research paper[214], Gu, L.; Robinson, R. A. S. *PloS one* **2015**, *10*, e0116606.)

## 3.1 INTRODUCTION

Reactive oxygen and nitrogen species (ROS/RNS) in cellular environments can result in macromolecular oxidative damage[215] and lead to loss of protein function[62], which have been reviewed in **Chapter 2**[93,156,216]. Key to understanding the events that affect protein function is the ability to characterize the distribution of oxidized proteoforms.

Techniques for the identification of proteoforms have been recently discussed[18,217-220]. Proteoforms can include molecules that arise due to the same post-translational modification (PTM) occurring at different amino acid residue positions in the protein. For example, a protein that incorporates a single oxygen atom during a free radical attack from hydrogen peroxide ($H_2O_2$) or superoxide anion, may exist in multiple locations. One population of the protein molecules can incorporate the oxygen at residue "A", others incorporate at residue "B", while the remaining molecules incorporate at both "A" and "B". For the molecules with only a single oxygen addition, mass spectrometry (MS) measurements of intact protein would only detect a single M+16 Da species. Liquid chromatography (LC) or electrophoresis separations may be able to resolve the two proteoforms (i.e., A and B), however multiple dissociation methods such as collisional activation dissociation (CAD)[221], infrared multiphoton dissociation[222], electron capture dissociation (ECD)[223], or electron transfer dissocation (ETD)[224] are necessary to localize the modification site.

Top-down and bottom-up protein analysis provides complementary information regarding protein sequence and PTMs[218,225-228], especially for identification of oxidation sites[229-231]. Top-

down MS has been employed to characterize four oxidation sites in viral prolyl-r-hydroxylase[230] and for the identification of 250 isoforms of oxidized calmodulin[231]. Bottom-up proteomics is very useful for the verification of PTM types and sites although it can be challenging to identify the specific proteoform from which peptides originated. This is because shotgun analysis of all proteins extracted will lead to many similar peptides produced from various proteoforms. Because fragmentation of peptides is very accessible with CID and other dissociation methods, as compared to intact proteins, it is very practical to use bottom-up analyses to localize sites of oxidative modification. However, for complex biological samples the number of modification sites that can be characterized without extensive enrichment or separation strategies is generally low[232,233]. Therefore, it will be necessary to incorporate enrichment with our strategy of multiple proteases and iterative database searching to gain localize oxidative modification sites and obtain insight to the complexity of oxidized proteoforms present in complex mixtures.

Ubiquitin is a low molecular weight protein which has significant roles in protein turnover and degradation through its molecular chaperoning activity in the proteasome[234]. Ubiquitin is implicated in oxidative stress and disease[235,236]. The 76 amino acid sequence of this protein is highly conserved amongst eukaryotes, such as bovine and human[237]. Herein, we aimed to characterize the heterogeneity of proteoforms of ubiquitin using moderate oxidizing conditions[238] and bottom-up MS with multiple proteases. Chemical oxidizing conditions using Fenton chemistry [$Fe(II)/H_2O_2$][238] rely on the metal serving as an electron donor to catalyze the formation of highly reactive hydroxyl radical (·OH) which can result in modification of amino acid side chains[216,239]. Previous studies have investigated oxidized forms of ubiquitin after exposure to peroxynitrite[240], electrochemical oxidation[241,242], and photochemical reactions[243] for the purpose of structural footprinting. The influence of N-terminal oxidation of Methionine (hereafter referred to as Met1-

Ox) on protein structures and stabilities were examined by ion mobility spectrometry-mass spectrometry (IMS-MS)[244] and indicate that oxidation of Met1 can lead to destabilization of the native state and result in unfolded structures. Thus simple oxidized proteoforms can have a huge influence on protein structure.

Bottom-up LC-MS/MS of peptides generated from multiple proteases[245] allows multiple oxidation products of ubiquitin to be identified, including several proteoforms of the M+16 Da peak. Under Fe(II)/$H_2O_2$ conditions, numerous amino acid modifications are possible[246] and include side chain hydroxylation, carbonylation and backbone cleavage. The variety of these modifications requires multiple database searches to be performed[157]. Sample integrity was confirmed by using high resolution ESI-MS on an Orbitrap Velos of intact oxidized protein mixtures.

## 3.2 EXPERIMENTAL METHODS

### *3.2.1 In Vitro Oxidation of Ubiquitin*

Bovine ubiquitin was purchased from Sigma-Aldrich (St. Louis, MO). Protein (10 mg·mL$^{-1}$) was dissolved in 10 mM sodium phosphate buffer solution (pH 7.4) and 10 mM $H_2O_2$ and 1 mM $FeCl_2$ were added and allowed to react at 37 °C for 2 hours. The reaction was quenched by flash freezing with liquid nitrogen. Protein sample was desalted on an HLB cartridge (Waters; Milford, MA) according to manufacturer's instructions. Solvent was removed by centrifugal evaporation and dried protein stored at -80 °C until further analysis.

### *3.2.2 Top-down ESI-MS and $MS^n$ Analysis*

Intact oxidized ubiquitin (~30 μM) was solubilized in 49:49:2 water:methanol:acetic acid. ESI-MS analysis was performed on a LTQ-Orbitrap Velos mass spectrometer (Thermo-Fisher Scientific, Waltham, MA) with direct infusion by a syringe pump. The following electrospray ionization parameters were used: spray voltage 4.25 kV; capillary temperature 200.00 °C and flow rate 3 $\mu L \cdot min^{-1}$. Orbitrap detector settings included resolving power of 100 k, parent *m/z* scan range 600-2000, 3 μscans, and 30 and 100 scans for parent and fragmentation spectra, respectively. MS/MS data were recorded in the FT. MS/MS and $MS^3$ settings used an isolation width of 1 *m/z* and normalized collision energy of 35%.

### *3.2.3 Protein Digestion*

Purified oxidized ubiquitin (1 $\mu g \cdot \mu L^{-1}$) was solubilized in a denaturing buffer (0.2 M Tris, 8 M urea, 10 mM $CaCl_2$, pH 8.0). Tris buffer (0.2 M Tris, 10 mM $CaCl_2$, pH = 8.0) was added to dilute urea to 2 M. The solution was separated into three equal volume aliquots and each incubated with TPCK-treated trypsin (Sigma), glutamic acid-C [(Glu-C); Princeton Separation, Inc, Adelphia, NJ] or lysine-C [(Lys-C); Princeton Separation, Inc] proteases at a 1:50 protein:enzyme mass ratio for 24 h at 37 °C. Liquid nitrogen was used to quench digestions and samples were acidified by adding formic acid, desalted with HLB cartridges and the eluent dried by centrifugal evaporation.

### *3.2.4 Nanoflow LC-MS/MS*

Online desalting and reversed-phase chromatography was performed with a nanoLC system equipped with an autosampler (Eksigent; Dublin, CA). Mobile phases A and B for these

analyses were 96.95:2.95:0.1 water:acetonitrile:formic acid and 99.9:0.1 acetonitrile:formic acid, respectively. Five μL of each peptide sample (1 $\mu g \cdot \mu L^{-1}$ in 0.1% formic acid) was loaded on to a trapping column [100 μm i.d. × 2 cm; 3 μm $C_{18}$ 200 Å stationary phase material (Michrom Bioresource Inc.;Auburn, CA)] at 3 $\mu L \cdot min^{-1}$ in 3% mobile phase B for 3 min. After desalting, the sample was loaded onto a pulled-tip (using a $CO_2$ laser) analytical column (75 μm i.d. × 13.2 cm), packed in-house with 3 μm $C_{18}$ 100 Å stationary phase material (Michrom Bioresource Inc.). The following gradient was delivered at a flow rate of 300 $nL \cdot min^{-1}$: 0-5 min, 10% mobile phase B; 5-15 min, 10-30% B; 15-45 min, 30-45% B; 45-50 min, 45-60% B; 50-55 min, 60-80% B; 55-65 min, 80% B; 65-75 min, 10% B. The LC eluent was introduced into the ESI source with ~1.5-2.0 kV. Data-dependent acquisition parameters were: parent Orbitrap MS resolving power 60 k; *m/z* scan range 300-1800; the top eight most intense ions were selected and activated using CID; isolation width 3 *m/z*; normalized collision energy 35%; dynamic exclusion was enabled with a repeat count of two for a duration of 60 sec; and, a minimum of 5000 ion counts for MS/MS. Samples were analyzed in triplicate.

### *3.2.5 Data Analysis*

Top-down spectra were viewed and analyzed by Xcalibur 2.1 software (Thermo). The Xtract program (Xcalibur) was used to deconvolute the spectra and calculate protein masses. Spectra were manually inspected and the *m/z* values matched to theoretical *b*- and *y*-type ions generated by ProteinProspector v5.9.4[247]. For peptide data, .RAW files were analyzed with Proteome Discoverer 1.3 software (Thermo) and MS/MS spectra searched against a .fasta file containing the ubiquitin sequence (truncated from the N-terminal region of Uniprot ID P0CH28). Sequest search parameters included two maximum enzyme miscleavages; precursor mass

tolerance of 10 ppm; fragment mass tolerance of 0.8 Da; dynamic modifications (see Table 3.1) of mono oxidation to Lys, Arg, Pro, Thr, Met, His, Tyr, Ala, Asn, Asp, Glu, Gln, Ile, Leu, Phe, Ser and Val (Ox, +15.995 Da), dioxidation to Lys, Arg, Pro, His, Tyr, Asn, Asp, Phe and Met (DiOx, + 31.990 Da), carbonylation to Lys, Arg, Pro, Glu, Gln, Leu, Ser, Val and Ile (+13.979 Da), deamidation to Gln, Arg and Asn (0.984 Da), decarboxylation to Asp and Glu (-30.010 Da), oxidation of His to Asn (-23.0159 Da) or Asp (-22.032 Da) or aspartylurea (-10.032 Da) or ring open (4.979 Da), carbonylation of Arg to glutamic semialdehyde (GluSA, -43.053 Da), Lys to aminoadipic semialdehyde (AminoAdSA, -1.032 Da) or aminoadipic acid (14.963 Da), Pro to pyrrolidinone (-30.010 Da), and Thr to 2-amino-3-oxo-butanoic acid (Oxd'n, -2.016 Da). Only peptides with medium ( $p < 0.05$) and high confidence ($p < 0.01$) as determined from a reverse decoy database search (which in Proteome Discoverer sets appropriate thresholds for XCorr values as a function of charge state) were used for initial filtering of the data[53,248,249]. For final inclusion of peptide hits and localization of modification sites, all MS/MS spectra were manually validated.

## 3.3 RESULTS AND DISCUSSION

### *3.3.1 MS Analysis of Intact Oxidized Ubiquitin*

High-resolution ESI-MS analysis of a solution containing only untreated ubiquitin shows an M+16 Da peak that represents < 2% of the total unmodified peak intensity in a deconvoluted spectrum (*data not shown*). Because the untreated sample has very limited sample handling, the M+16 Da species could be from the manufacturing and storage of the protein product, or from the electrospray ionization, (e.g. solution contact with metal needle or the electrolysis of water under high spray voltage. However, utilizing Fenton chemistry, several peaks belonging to oxidized ubiquitin are observed (Figure 3.1). The most intense oxidized peak belongs to an M+16 Da

**Table 3.1** List of all oxidative modifications searched.

| | Modification | Mass Change | Residues |
|---|---|---|---|
| | Mono Oxidation | 15.99491 Da | Lys, Arg, Pro, Thr, Met, His, Tyr, Ala, Asn, Asp, Glu, Gln, Ile, Leu, Phe, Ser, Val |
| | Dioxidation | 31.98982 Da | Lys, Arg, Pro, His, Tyr, Asn, Asp, Phe, Met |
| | Carbonylation | 13.97926 Da | Lys, Arg, Pro, Glu, Gln, Leu, Ser, Val, Ile |
| | Deamidation | 0.98402 Da | Gln, Arg, Asn |
| | Decarboxylation | -30.01056 Da | Asp, Glu |
| Special oxidations of histidine | His-Asn | -23.0159 Da | His |
| | His-Asp | -22.0319 Da | His |
| | His-Aspartylurea | -10.03198 Da | His |
| | His - Formy Asn | 4.97892 Da | His |
| Special carbonylation | Lys-AminoAdSA | -1.0316 Da | Lys |
| | Lys-Aminoadipic acid | 14.9632 Da | Lys |
| | Arg-GluSA | -43.0534 Da | Arg |
| | Pro-Pyrrolidinone | -30.0105 Da | Pro |
| | Thr-Oxd'n | -2.01565 Da | Thr |

species at each charge state measured (i.e., +5 - +13). The inset of Figure 3.1 shows a zoom-in of the +12 charge state, whereby two protein isotopic distributions are measured for unmodified and oxidized ubiquitin ions. Upon deconvolution of the spectrum it is noted that the M+16 Da species constitutes ~20% of the unmodified abundance. This is a factor of ten increase in M+16 Da ions in comparison to solutions containing only untreated ubiquitin. The masses of the deconvoluted native and M+16 Da peaks are 8564.601 and 8580.592 Da. These values are < 5 ppm of the theoretically derived mass values and indicate a mass shift of 15.991 Da. Notably, this shift corresponds to the predominance of monooxygenated proteoforms in the Fe(II)/$H_2O_2$-ubiquitin mixture. The incorporation of an oxygen atom does not appear to influence the ionization efficiencies and hence observed signal intensity of ubiquitin in ESI[250], and is directly related to the relative abundance of each proteoform. Other proteoforms are observed in the spectrum: M-114 Da, M-57 Da, M-44 Da, M-16 Da, M+32 Da species, M+48 Da and M+96 Da. However, these peaks are low intensity and its possible many proteoforms are not observed in this direct infusion experiment.

### *3.3.2 Characterizing Methionine Oxidation Proteoform*

Based on the sequence of ubiquitin, we anticipated methionine oxidation. The $[M+O+12H]^{12+}$ protein peak was isolated and fragmented in the linear ion trap with CID. As shown in Figure 3.2 many of the *b*- type fragment ion peaks are shifted in mass from expected fragments of unmodified ubiquitin ions by 16 Da. Moderate sequence coverage of the intact protein (Figure 3.2) was obtained with CID and could be increased using dissociation methods such as ECD and ETD[251-254]. Inspection of the lower mass region (*m/z* 260-410) of the spectrum in Figure 3.2 revealed the detection of $[b_2+O+H]^+$ and $[b_3+O+H]^+$ ions, indicating the oxygen atom addition on

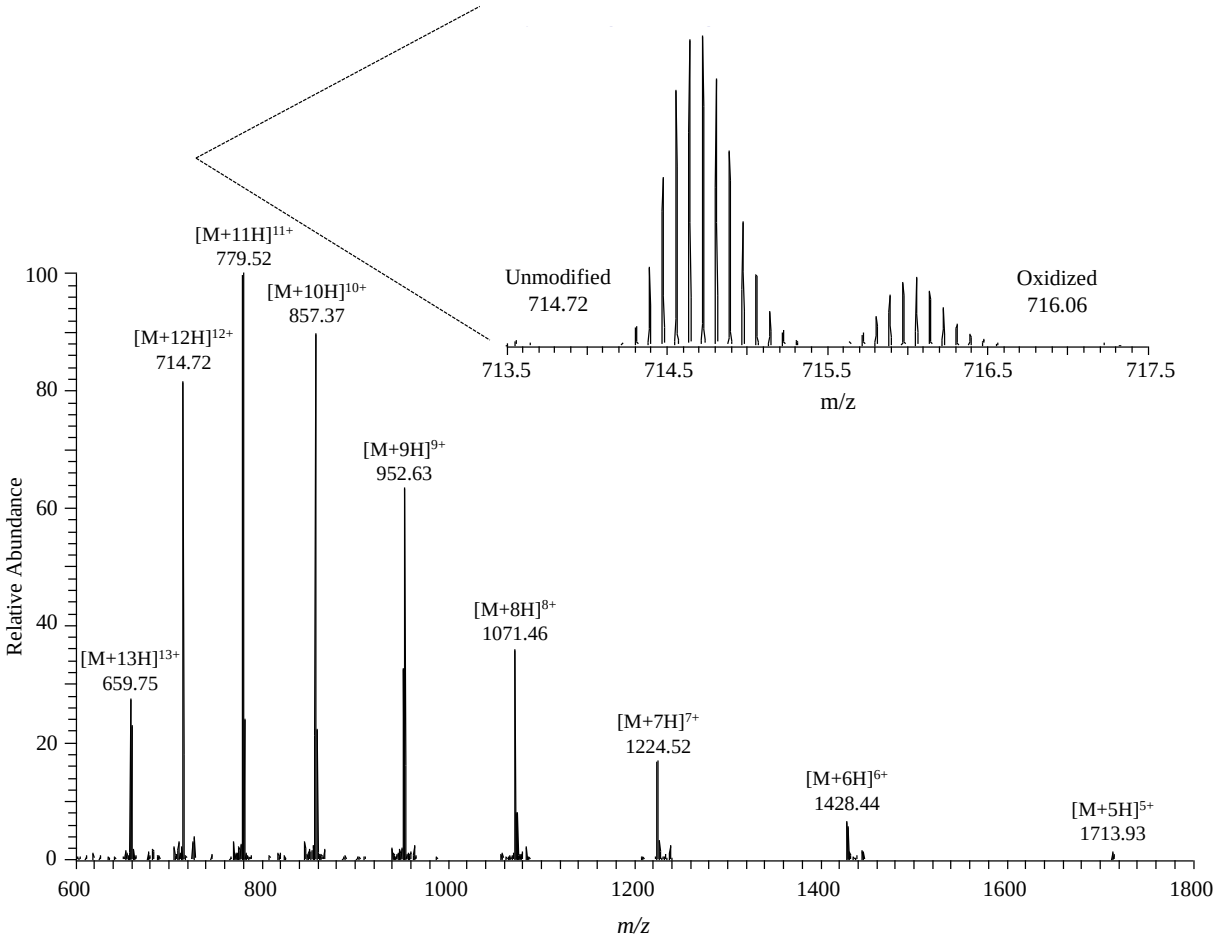


**Figure 3.1** Precursor ion mass spectra of oxidized ubiquitin. In the inset is a zoom-in of the +12 charge state that shows unmodified and oxidized ubiquitin species. The observed mass shift between native and oxidized ubiquitin is indicated in the figure.

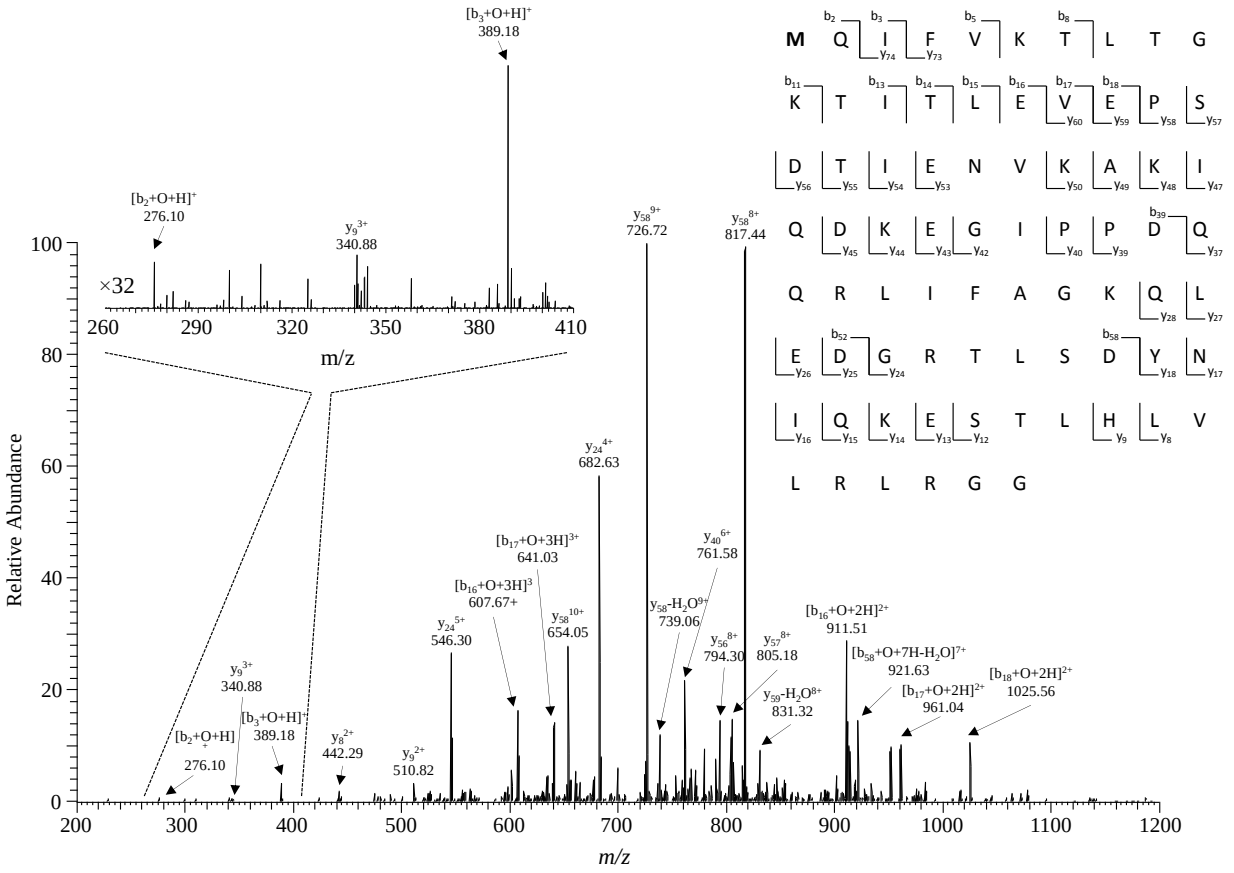


**Figure 3.2** CID MS/MS spectra obtained upon isolation of +12 charge state oxidized ubiquitin species (*m/z* 716.06, isolation window 1 *m/z*). Zoom-in CID MS/MS spectra of the *m/z* range 260-410. To the right top is the sequence of ubiquitin with observed fragment ions across all *z* labeled.

residue Met-1 or Gln-2. Based on the higher sensitivity of methionine to oxidation[89], it is very probable that the conversion of the single methionine residue to methionine sulfoxide occurred.

Multiple proteases allow for enhanced sequence coverage in proteomics as some cleavage sites are inaccessible with common enzymes[245] and oxidative modification may also hinder enzymatic cleavage for some residues (e.g., Lys and Arg)[161]. Peptide analysis of oxidized ubiquitin digests using trypsin, Lys-C, and Glu-C proteases is consistent with an M+16 Da methionine sulfoxide proteoform (see Table 3.2). Several oxidized methionine-containing peptides were identified in nanoLC-MS/MS analyses including doubly-charged mQIFVKTLTGK, mQIFVK, and mQIFVKTLTGKTITLE peptides derived from trypsin, Lys-C, and Glu-C proteases, respectively (Figure 3.3). The most predominant peak in the MS/MS spectra of each of these peptides is the doubly-charged precursor ion with the loss of methyl sulfoxide $[M+2H-CH_3SOH]^{2+}$. This precursor ion is consistent with the presence of an oxidized methionine residue and has been observed by others[255,256]. For the spectra in Figure 3.3, observed *b*-ions (including $b_2$ fragments) are shifted by 16 Da which localizes the modification site to Met1. While not performed in these studies, methionine oxidation can also be tested through enzymatic action with peptidyl methionine sulfoxide reductase or by treatment with dithiothreitol[257,258].

### *3.3.3 Mapping Other M+16 Da Proteoforms*

Figures 3.4a and 3.4b show MS/MS spectra of the tryptic peptide $[LIfAGK+H]^+$ and the Lys-C peptide $[EGIPPDQQRLIfAGK+2H]^{2+}$, respectively. Each of these spectra contains fragment ions that localize an oxidative modification to a phenylalanine residue (i.e., Phe45). Phenylalanine contains an aromatic ring which upon oxidation can be modified by hydroxyl radicals at the *para*-, *ortho*-, or *meta*- positions as shown in Figure 3.4a[259,260]. Similarly, MS/MS

**Table 3.2** List of oxidative modifications identified from multiple proteases.

| Sequence[a] | Modifications[b] | XCorr | Charge | *m/z* | MH+ (Da) | Δm (ppm) | $t_r$ (min) | Protease |
|---|---|---|---|---|---|---|---|---|
| EGIPpDQQR[c] | $P^{38}$-Oxidation | 2.15 | 2 | 528.2591 | 1055.5109 | -0.71 | 16.88 | Trypsin |
| EGIPpDQQR[c] | $P^{38}$-Carbonylation | 2.39 | 2 | 527.2507 | 1053.4942 | -1.73 | 15.8 | Trypsin |
| EGIpPDQQR[c] | $P^{37}$-Carbonylation | 1.73 | 2 | 527.2507 | 1053.4941 | -1.85 | 18.43 | Trypsin |
| EGiPPDQQR[c] | $I^{36}$-Carbonylation | 2.18 | 2 | 527.2531 | 1053.499 | 2.79 | 13.43 | Trypsin |
| EGIPPDQQRLIfAGK | $F^{45}$-Oxidation | 3.03 | 2 | 842.9547 | 1684.9022 | 0.21 | 22.71 | LysC |
| ESTLhLVLR[c] | $H^{68}$-Oxidation | 1.77 | 2 | 542.3115 | 1083.6158 | 0.04 | 24.09 | Trypsin |
| ESTLHlVLR[c] | $L^{69}$-Carbonylation | 2.57 | 2 | 541.3021 | 1081.5969 | -2.98 | 21.07 | Trypsin |
| EStLHLVLR[c] | $T^{66}$-Oxd'n | 2.75 | 2 | 533.3046 | 1065.6019 | -3.1 | 20.55 | Trypsin |
| ESTLhLVLR[c] | $H^{68}$-Asp | 2.17 | 2 | 523.2972 | 1045.5872 | -1.57 | 20.72 | Trypsin |
| ESTLHlVlR[c] | $L^{69}$-Oxidation, L71-Oxidation | 2.14 | 2 | 550.3061 | 1099.6049 | -5.22 | 22.16 | Trypsin |
| ESTLhLVLR[c] | $H^{68}$-Dioxidation | 1.79 | 2 | 550.3055 | 1099.6037 | -6.33 | 20.42 | Trypsin |
| ESTLhLVLR[c] | $H^{68}$-Histidine ring open (+5) | 2.00 | 2 | 536.801 | 1072.5947 | -4.74 | 22.56 | Trypsin |
| EstLHLVLRLRGG[c] | $S^{65}$-Oxidation,T66-Oxd'n | 2.32 | 3 | 488.949 | 1464.8325 | 2.91 | 28.46 | LysC |
| EVEPSDTIeNVKAKIQ[c] | $E^{24}$-Decarboxylation | 2.63 | 2 | 885.465 | 1769.9227 | -3.05 | 28.22 | LysC |
| GkQLEDGR[c] | $K^{48}$-Carbonylation | 1.98 | 2 | 458.7275 | 916.4476 | -0.78 | 14.51 | Trypsin |
| IQDKEGIPpDQQR[c] | $P^{38}$-Dioxidation | 3.67 | 2 | 778.389 | 1555.7707 | -0.3 | 19.16 | Trypsin |
| IQDKEGiPPDQQR[c] | $I^{36}$-Carbonylation | 2.55 | 3 | 513.2579 | 1537.7591 | -0.98 | 14.3 | Trypsin |
| LIfAGK | $F^{45}$-Oxidation | 1.79 | 1 | 664.4038 | 664.4038 | 1.31 | 22.16 | Trypsin |
| LIfAGKQLEDGR[c] | $F^{45}$-Oxidation | 2.29 | 3 | 454.9167 | 1362.7355 | -1.58 | 16.12 | Trypsin |
| mQIfVK[c] | $M^{1}$-Oxidation, F4-Oxidation | 2.16 | 2 | 399.2154 | 797.4235 | 1.1 | 21.18 | LysC |
| MQIfVK[c] | $F^{4}$-Oxidation | 1.97 | 2 | 391.2171 | 781.4269 | -1.09 | 22.53 | LysC |
| mQIFVK[c] | $M^{1}$-Oxidation | 1.77 | 1 | 781.4302 | 781.4302 | 3.23 | 22.04 | GluC |

*Continued on Page 61*

**Table 3.2** List of oxidative modifications identified from multiple proteases.

| Sequence[a] | Modifications[b] | XCorr | Charge | *m/z* | MH+ (Da) | Δm (ppm) | $t_r$ (min) | Protease |
|---|---|---|---|---|---|---|---|---|
| mQIfVK[c] | $M^1$-Oxidation,F4-Oxidation | 2.13 | 2 | 399.215 | 797.4228 | 0.18 | 21.01 | Trypsin |
| MQIfVK[c] | $F^4$-Oxidation | 1.79 | 2 | 391.2177 | 781.4282 | 0.63 | 22.09 | Trypsin |
| mQIFVK[c] | $M^1$-Oxidation | 1.72 | 1 | 781.4271 | 781.4271 | -0.84 | 12.65 | Trypsin |
| mQIFVK[c] | $M^1$-Oxidation | 1.96 | 2 | 391.2167 | 781.4261 | -2.1 | 13.6 | Trypsin |
| mQIFVK | $M^1$-Oxidation | 1.95 | 2 | 391.2177 | 781.4282 | 0.55 | 21.27 | LysC |
| mQIFVK[c] | $M^1$-Oxidation | 1.76 | 1 | 781.4271 | 781.4271 | -0.84 | 21.33 | LysC |
| mQIFVKTL[c] | $M^1$-Oxidation | 2.84 | 2 | 498.2857 | 995.5641 | 4.63 | 25.08 | GluC |
| MQIFVkTLTGK | $K^6$-AminoAdSA | 3.09 | 2 | 632.8536 | 1264.7 | 2.35 | 26.95 | LysC |
| mQIFVKTLTGK[c] | $M^1$-Oxidation | 3.05 | 3 | 427.9143 | 1281.7283 | 3.66 | 23.55 | GluC |
| mQIFVKTLTGK | $M^1$-Oxidation | 3.52 | 2 | 641.3641 | 1281.7209 | -2.12 | 18.11 | Trypsin |
| mQIFVKTLTGK[c] | $M^1$-Oxidation | 2.8 | 3 | 427.9117 | 1281.7207 | -2.27 | 18.12 | Trypsin |
| mQIFVKTLTGKTITLE | $M^1$-Oxidation | 4.79 | 2 | 920.0217 | 1839.0362 | 3.53 | 26.58 | GluC |
| mQIFVKTLTGKTITLE VEPSDTIENVKAK[c] | $M^1$-Oxidation | 5.18 | 4 | 813.1945 | 3249.756 | -2.84 | 22.06 | Trypsin |
| NVKAKIQDkeG[c] | $K^{33}$-Oxidation; E34-Decarboxylation | 3.1 | 2 | 608.3413 | 1215.6752 | 4.92 | 18.97 | GluC |
| NVKAKIQDKEGIPp[c] | $P^{38}$-Dioxidation | 2.54 | 3 | 523.6282 | 1568.8702 | 3.71 | 20.44 | GluC |
| QLEDGRTLSDyNIQK | $Y^{59}$-Oxidation | 3.68 | 2 | 898.4461 | 1795.8849 | 1.55 | 22.14 | LysC |
| QLEDGrTLSDYNIQK[c] | $R^{54}$-GluSA | 2.34 | 2 | 868.9171 | 1736.827 | -3.94 | 19.35 | Trypsin |
| tITLEVEPSDTIENVK[c] | $T^{12}$-Oxd'n | 3.14 | 2 | 893.4609 | 1785.9145 | 1.54 | 25.96 | LysC |
| TITlEVEPSDTIENVK[c] | $L^{15}$-Oxidation | 3.44 | 2 | 902.4661 | 1803.9249 | 1.42 | 24.32 | Trypsin |
| TITLEVEPsDTIENVK[c] | $S^{20}$-Carbonylation | 2.83 | 2 | 901.4577 | 1801.9081 | 0.83 | 24.64 | Trypsin |
| TITLEVePSDTIENVK[c] | $E^{18}$-Decarboxylation | 2.03 | 2 | 879.4589 | 1757.9105 | -3.62 | 22.07 | Trypsin |
| TLSDYNIQk[c] | $K^{63}$-Oxidation | 2.56 | 2 | 549.2772 | 1097.5472 | -0.17 | 21.3 | Trypsin |

*Continued on Page 62*

**Table 3.2** List of oxidative modifications identified from multiple proteases.

| Sequence[a] | Modifications[b] | XCorr | Charge | *m/z* | MH+ (Da) | Δm (ppm) | $t_r$ (min) | Protease |
|---|---|---|---|---|---|---|---|---|
| TLSDYNIqK[c] | $Q^{62}$-Deamidation | 2.17 | 2 | 541.7697 | 1082.532 | -4.09 | 14.47 | Trypsin |
| TLSDyNIQK | $Y^{59}$-Oxidation | 2.61 | 2 | 549.2759 | 1097.5446 | -2.51 | 14.33 | Trypsin |
| tLSDYNIQK[c] | $T^{55}$-Oxd'n | 2.13 | 1 | 1079.5325 | 1079.5325 | -4 | 19.29 | Trypsin |
| tLSDYNIQK | $T^{55}$-Oxd'n | 1.74 | 2 | 540.269 | 1079.5307 | -5.65 | 20.28 | Trypsin |

[a]Lowercase letters represent the amino acid residues that have oxidative modifications. [b]Positions of modified residues in the entire ubiquitin sequence are shown and are abbreviated as follows: Oxidation indicates an oxygen addition to the amino acid residue, Dioxidation indicated two oxygens addition to the amino acid residue, carbonylation indicates formaton of carbonyl group with a mass increase of 14 Da, GluSA indicates the carbonylation of arginine to glutamic semialdehyde, AminoAdSA indicates the carbonlyation of lysine to aminoadipic semialdehyde, Oxd'n indicates the carbonlyation of threonine to 2-amino-3-oxo-butanoic acid, Asp indicates the oxidation of histidine to aspartic acid, Deamidation indicates the conversion of $-NH_2$ to -OH and Decarbonylation indicates the loss of carboxyl group .[c]MS/MS spectra of each peptide is provided in Appendix A Figure 3.1.

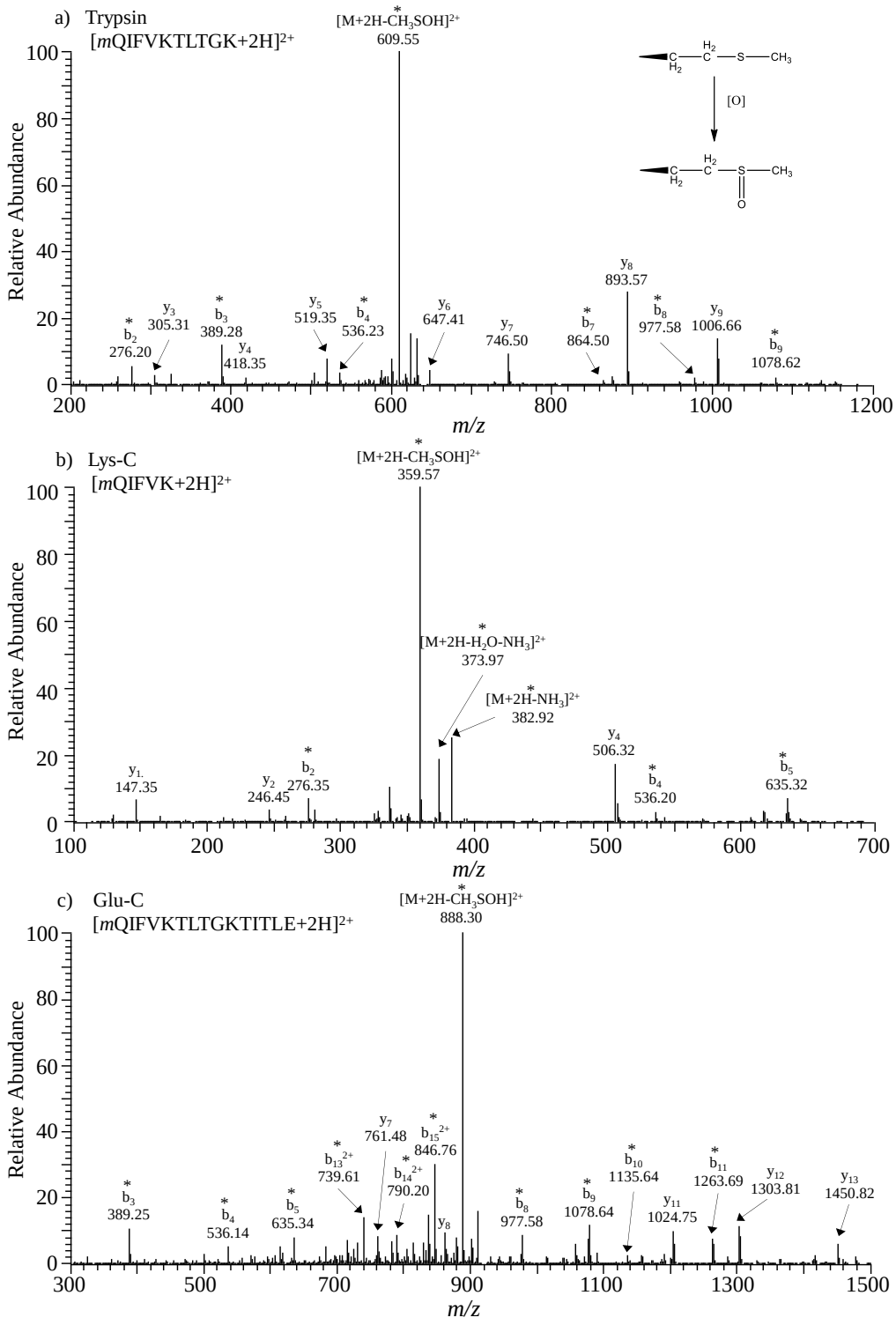


**Figure 3.3** CID MS/MS spectra of a) [mQIFVKTLTGK+2H]$^{2+}$ with Met1-Ox as observed by trypsin proteolysis , $t_r$=18.11 min, *m/z*=641.36; b) [mQIFVK+H]$^{2+}$ with Met1-Ox as observed by Lys-C proteolysis, $t_r$=21.27 min, *m/z*=391.22 and c) [mQIFVKTLTGKTITLE+2H]$^{2+}$ with Met1-Ox as observed by Glu-C proteolysis, $t_r$ =26.58 min, *m/z*=920.02. Note that lowercase letters represent the oxidation of methionine to methionine sulfoxide. Ions labeled with asterisks (*) contain modifications.

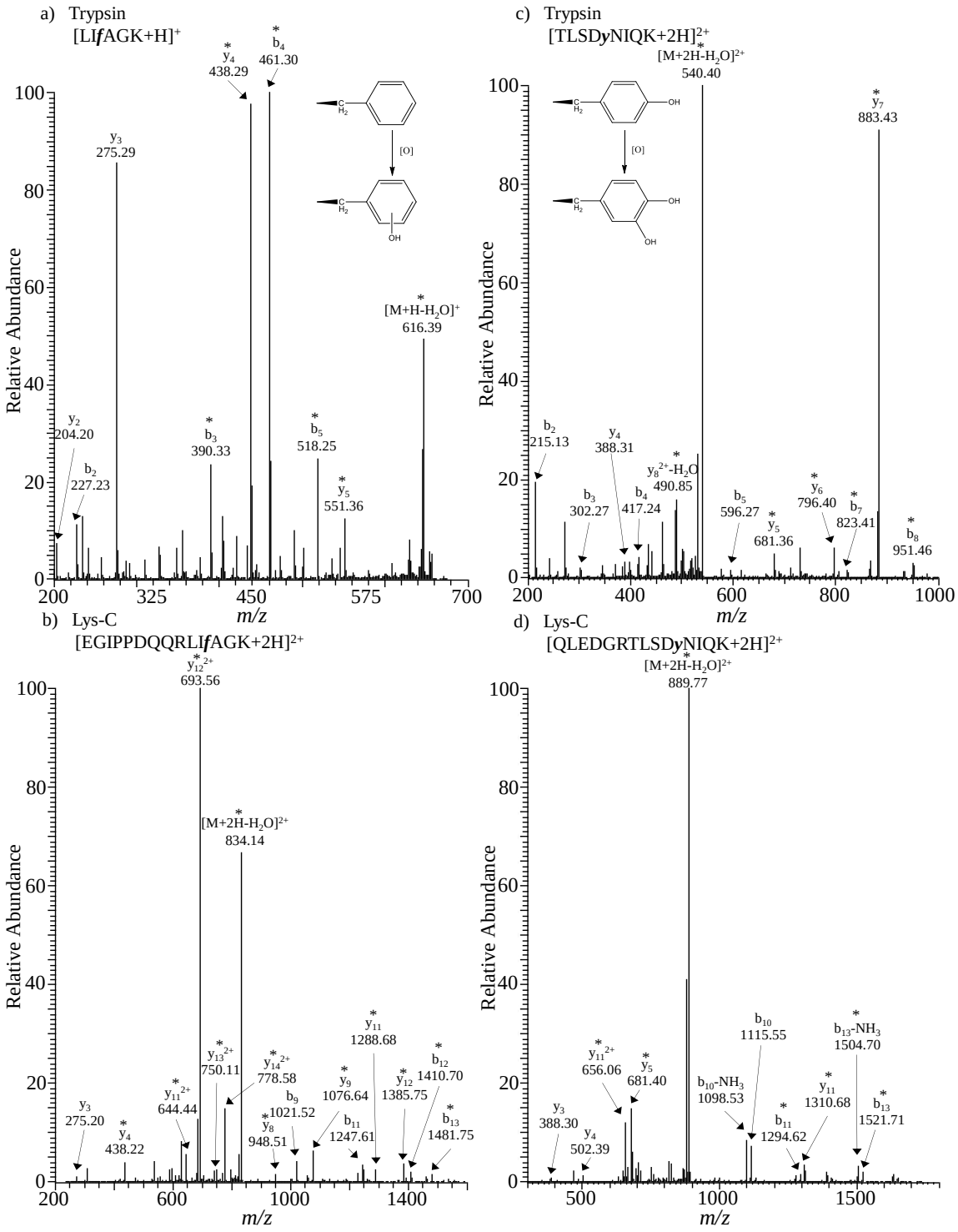


**Figure 3.4** CID MS/MS spectra of a) $[LIfAGK+H]^+$ with Phe45-Ox as observed by trypsin proteolysis, $t_r$=22.16 min, *m/z*=664.40; b) $[EGIPPDQQRLIfAGK+2H]^{2+}$ with Phe45-Ox as observed by Lys-C proteolysis, $t_r$=22.71, *m/z*=842.95; c) $[TLSDyNIQK+2H]^{2+}$ with Tyr59-Ox as observed by trypsin proteolysis, $t_r$=14.33 min, *m/z*=549.28 and d) $[QLEDGRTLSDyNIQK+2H]^{2+}$ with Tyr59-Ox as observed by Lys-C proteolysis, $t_r$=22.14 min, *m/z*=898.45. Note that lowercase letters represent the oxidation of phenylalanine and tyrosine. Ions labeled with asterisks (*) contain modifications.

spectra of the tryptic peptide $[TLSDyNIQK+2H]^{2+}$ and Lys-C peptide $[QLEDGRTLSDyNIQK+2H]^{2+}$ tentatively assign oxidation of the Tyr59 residue (Figures 3.4c and 3.4d, respectively).

Overall we observe several peptides which contain a monoxygenated residue (Table 3.2). Positions of these modifications are: Met1, Phe4, Leu15, Lys33, Phe45, Ser55, Tyr59, Lys63, His68, Leu69, and Leu71. It is possible that each of these peptides arise from different molecules of intact M+16 Da proteoforms. However, it is also likely that they arise from lower intensity M+32 Da or other oxidized proteoforms. Ambiguous identifications include Pro37 which is shifted by 16 Da and could correspond to oxygen incorporation or a carbonyl shift to glutamic semialdehyde.

### *3.3.4 Identification of Other Oxidative Proteoforms*

The most abundant oxidized species that exist in these data arise from the incorporation of oxygen to amino acid side chains however other proteoforms are present. Figures 3.5a and 3.5b are example MS/MS spectra from trypsin and Lys-C peptides $[tLSDYNIQK+2H]^{2+}$ and $[MQIFVkTLTGK+2H]^{2+}$, respectively. Fragment ions are present (Figure 3.5a) which locate an oxidation site to Thr55. Threonine oxidation results in carbonylation to 2-amino-3-oxo-butanoic acid represented by a mass loss of -2.016 Da. Figure 3.5b provides MS/MS fragments which identify Lys6 oxidation represented by a mass loss of 1.032 Da. It is noted that this N-terminal peptide contains an unmodified methionine residue and thus originates from other oxidized proteoforms. Other modifications observed with multiple proteases are provided in Table 3.2 (and Appendix A Figure 3.1). It is possible that oxidative modifications present can influence MS/MS fragmentation patterns and this is dependent on particular amino acid and modification type.

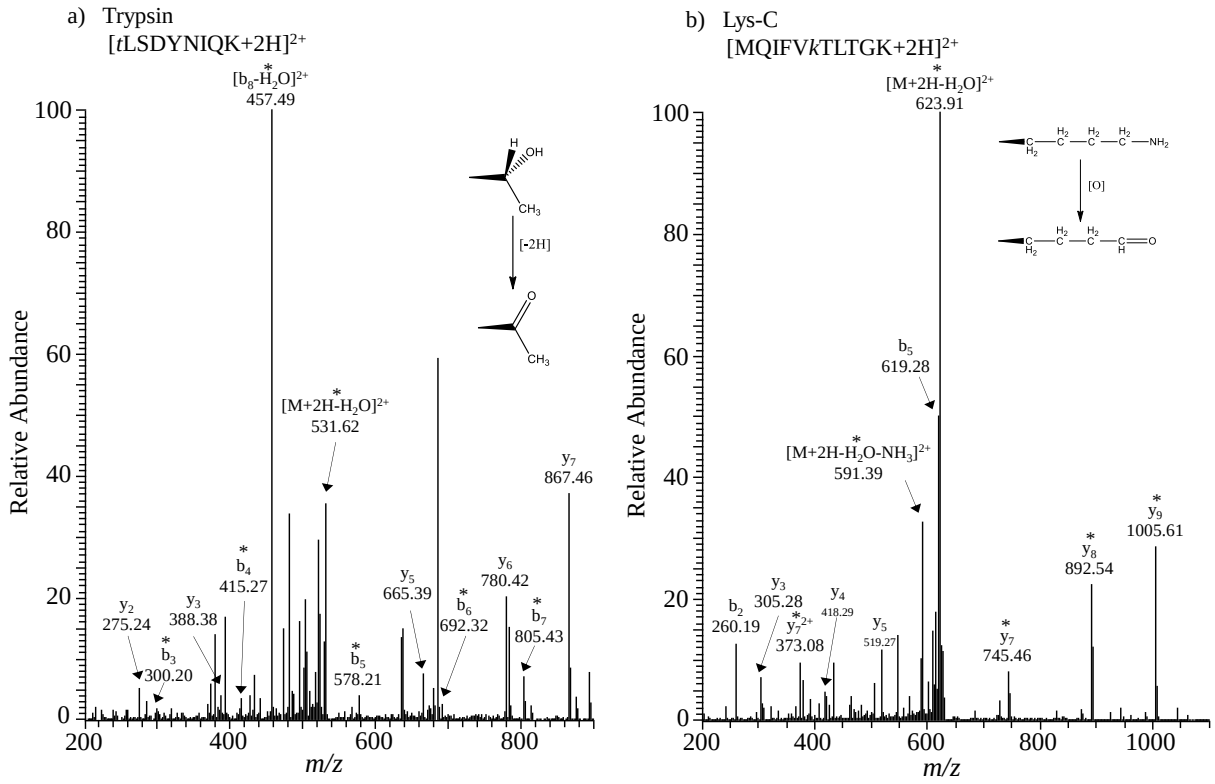


**Figure 3.5** CID MS/MS spectra of a) $[tLSDYNIQK+2H]^{2+}$ with Thr55-Oxd'n as observed by trypsin proteolysis, $t_r$=20.28min, *m/z*=540.27 and b) $[MQIFVkTLTGK+2H]^{2+}$ with Lys6-AminoAdSA as observed by Lys-C proteolysis, $t_r$=26.95, *m/z*=632.85. Note that lowercase letters represent the carbonylation of threonine to 2-amino-3-oxo-butanoic acid and lysine to aminoadipic semialdehyde. Ions labeled with asterisks (*) contain modifications.

MS/MS spectra were manually inspected to eliminate ambiguous and low confidence assignments.

Extensive database searches were performed in order to search for many potential oxidative modifications that may occur using metal-catalyzed oxidation. In addition to searching for hydroxylation and carbonylation of Lys, Arg, Thr and Pro residues, our searches also included dioxidation, carbonylation on other amino acids, deamidation, decarboxylation, as well as different oxidative products of His (Table 3.1). Examples of new modifications, e.g. ring opening of His68, carbonylation of Ser20, Ile36, Leu69, were successfully identified through these additional database searches (Table 3.2).

Fe(II)/$H_2O_2$ oxidation of ubiquitin leads to multiple M+16 Da and other proteoforms. The most abundant M+16 Da species contains Met1-Ox and is consistent with high oxidation reactivity[261]. M+16 Da and M+32 Da proteoforms were distinguishable using top-down $MS^n$ however, CID MS/MS – $MS^n$ only provided a limited amount of information about modification sites. Other dissociation methods such as ECD and ETD may provide more extensive sequence coverage and directly localize oxidative modification sites. On the other hand, bottom-up data only provide information about peptides that are observed in solution and do not completely reflect the specific oxidized proteoforms from which they originate. For example, the tryptic peptide mQIFVK could have arisen from an intact M+16 Da ubiquitin molecule or from other oxidized proteoforms. The observation of the tryptic peptide mQIfVK with two oxidized residues and the variety of modified residues listed in Table 3.2, clearly indicates that many oxidized proteoforms are present.

Thus use of multiple proteases greatly improved our ability to localize oxidative modification sites of oxidized ubiquitin. Specifically, six out of 24 modified sites identified by trypsin are validated by Lys-C and Glu-C experiments (e.g. Met1 is identified by all three

proteases). Modifications to residues such as Lys6, Thr12, Glu24 and Ser65 were only identified with Lys-C and Lys33, Glu34 were only identified by Glu-C (See Table 3.2). We note that incorporation of an enrichment or tagging step may improve the detection of other oxidized proteoforms[231-233]. The combination of multiple proteases with iterative database searching was key to identification of so many oxidized sites and proteoforms of ubiquitin. Due to limitations with the number of modifications that can be simultaneously searched with SEQUEST (in Proteome Discoverer), we performed iterative database searches by classifying the modifications into seven groups (methionine oxidation, non-methionine oxidation, carbonylation (+14 Da), deamidation, decarboxylation, histidine oxidation and special carbonylation)[157]. This resulted in each RAW file being searched 22 times. For simple protein mixtures in which one seeks to gain knowledge about the complexity of oxidized proteoforms we present this strategy (combination of top-down mapping, multiple proteases, and iterative database searching) as an alternative to targeted chemistries or enrichment steps.

## 3.4 CONCLUSIONS

This work reports on the detection of oxidized species of Fe(II)/$H_2O_2$ oxidized ubiquitin molecules using multiple proteases and iterative database searching of oxidative modifications. Multiple proteases allowed numerous modification sites to be identified and increased confidence in each oxidative site. Multiple proteases also allowed inaccessible sites by trypsin digestion to be available with other proteases. Iterative database searching allowed different types of oxidative modifications to be identified, however this also required manual validation of MS/MS spectra and extended computing times. Under the mM concentrations of oxidizing reagent used, oxidative modifications to ubiquitin included protein carbonylation. The ability to identify distributions of proteoforms for simple systems, such as ubiquitin, using multiple proteases in shotgun proteomics

can be extended to larger and more complex protein samples. Complex protein samples will benefit from additional enrichment steps. The utility of multiple proteases combined with iterative database searching of oxidative modifications can be extended to other types of PTMs such as glycosylation, cysteine oxidations, and deamidation and has promising applications in pharmaceutical industries for the analysis of intact antibodies. In this work only one protein is present in the sample, making it possible to characterize oxidations of various amino acid acids by MS directly. For complex sample analysis, e.g., cell lysates or tissue homogenates, affinity purification is often required to simplify complex matrices and target a specific residue or modification. In **Chapters 4 - 6**, novel workflows were developed to enrich cysteine-containing peptides using the solid phase capture technique and study oxidative modifications to cysteine.

# 4.0 SAMPLE MULTIPLEXING WITH CYSTEINE-SELECTIVE APPROACHES: CYSDML AND CPILOT

(Note that information in this chapter is written based on a published research paper[38], Gu, L.; Evans, A. R.; Robinson, R. A. S. *Journal of the American Society for Mass Spectrometry* **2015**, *26*, 615-630.)

## 4.1 INTRODUCTION

Mass spectrometry (MS) - based quantitative proteomics is an important tool to measure relative and absolute protein abundances in order to discover disease biomarkers and to provide insight into biological processes. Comprehensive proteome analysis still remains challenging however, partially due to heterogeneity associated with biological samples, the wide dynamic range of protein concentrations, the presence of protein post-translational modifications (PTMs) and proteoforms[262]. Furthermore, even with considerable advances in MS technology there is still a demand for proteomics workflows which are all-inclusive and offer high-throughput, high efficiency, and deep proteome coverage. A widely-used strategy to reduce sample complexity and improve detection of low-abundance proteins is to isolate cysteinyl-peptides[65]. Cysteine occurs ~2.3% among the twenty amino acids in mammals[65]. According to our in-house calculations ~14% of peptides contain cysteine which corresponds to ~96% of proteins in the mouse proteome (Uniprot database, 05/21/2014 release, 51344 sequences). This trend is similar for human, yeast, and other species[65] and suggests that cysteinyl-enrichment can greatly reduce sample complexity while affording high proteome coverage. Cysteine is a highly reactive nucleophilic amino acid and is implicated in biological processes, such as cell recognition and apoptotic signaling[65], cellular homeostasis, immune signaling, and redox chemistry[263]. Cysteine can be subject to a variety of covalent oxidative PTMs (e.g. sulfinic acid, disulfide formation, S-nitrosylation, and S-

glutathionylation) as described in **Chapter 2**[85,263] and the study of these oxidation states gives insight to cellular redox status.

Cysteinyl-peptides can be enriched directly via the reactions of sulfhydryl groups, such as: solid phase thiopropyl resin[99,140,145,264,265], superparamagnetic[266] and gold nanoparticles[267], organomercurial beads[268], and aldehyde resin[269]. Alternatively, cysteine residues may be captured indirectly[270], through derivatization[271], biotin/avidin affinity chromatography[272,273], or with chemical tagging and antibody enrichment[43,113]. After the enrichment of cysteinyl-peptides, the incorporation of chemical tagging steps with stable-isotopes can be used to design cysteine-selective quantitative proteomics approaches. The most widely used techniques including precursor isotopic labeling such as diemthylation[24,25] and isobaric tags such as TMT, iTRAQ and DiLeu[274], which were introduced in **Chapter 1**.

One of the first and most-widely used cysteine-selective quantitative proteomics approaches is isotope-coded affinity tag (ICAT)[32,275-281], which was reviewed in **Chapter 2**. In addition, enriching techniques such thiol-affinity resin and biotin/avidin can couple with various isotope-coded mass tags[100,109,116,119,139,282-285] for either cysteine subproteome characterization or cysteine redox quantification (**Chapter 2**). Recently, iodoTMT - a cysteine-reactive TMT reagent - was applied to map and quantify nitrosylation[43,111,113]. While there are attractive features to many of these approaches, few cysteinyl-based quantitative proteomics workflows provide all the following features: 1) effective cysteinyl-peptide enrichment; 2) simple and straightforward sample processing; 3) moderate sample multiplexing (at least > 2-plex and up to 8-plex or higher); and 4) cost-effective reagents.

Herein we developed two novel cysteine-based quantitative proteomics workflows. The first method is cysteine-selective precursor dimethyl labeling (CysDML). In this workflow,

cysteinyl-peptides are captured on a commercially available Thiopropyl Sepharose 6B resin and captured peptides are labeled on resin with either light (-$C_2H_6$) or heavy (-$^{13}C_2{}^2H_6$) dimethyl tags[29]. CysDML appears to be a convenient, efficient, accurate, and affordable cysteine-selective quantitative proteomic technique. However, this approach is limited to a maximum of two samples in this report thus we sought to develop another approach which could significantly improve on sample multiplexing capabilities. Higher multiplexing capacity is useful for reducing sample preparation and analysis time, minimizing errors, and allowing a readout of differences in relative protein abundances from a variety of sample types, conditions, time points, etc. Recently, our laboratory developed combined precursor isotopic labeling and isobaric tagging (cPILOT), a method that increases multiplexing capabilities of isobaric tags to 12 and 16 samples for TMT and iTRAQ, respectively. We[36,53] and others[55,56] have used enhanced multiplexing to study global and PTM specific protein abundances in complex mixtures. To-date, there is no report of a cysteine-selective enhanced multiplexing method. The second approach that we present is a cysteine-selective cPILOT approach using a 12-plex experiment. This novel technique relies on cysteinyl-peptide enrichment and on-resin isotopic dimethyl labeling, in combination with iodoTMT[6] reagent tagging. The combination of duplex dimethyl labeling and 6-plex iodoTMT[6] tagging results in twelve channels available for sample multiplexing in a single experiment. We note that this method could be extended to 16 or 20 samples if cysteine-reactive iTRAQ or TMT[10 286] reagents were available. Both CysDML and cysteine-selective cPILOT workflows were benchmarked relative to each other and applied to liver tissues from an Alzheimer's disease (AD) mouse model. The performance of these methods and results from the application are discussed.

## 4.2 EXPERIMENTAL

### *4.2.1 Animal Husbandry*

Fourteen-month old APP/PS-1 male mice [B6.Cg-Tg(APPswe,PSEN1dE9)85Dbo/Mmjax, stock number 005864, genetic background C57BL/6J express the chimeric mouse/human (Mo/Hu) APP695swe (i.e., K595N and M596L) and a mutant human PS1-dE9] and the genetically heterogeneous wild type (WT) (stock number 000664, genetic background C57BL/6J) were purchased from Jackson Laboratory. Mice were housed in the Division of Laboratory Animal Resources at the University of Pittsburgh and fed standard Purina rodent laboratory chow *ad libitum* on a 12 hour light/dark cycle. APP/PS-1 (hereafter referred to as AD) and WT mice ($N$ = 6 for each genotype) were euthanized using $CO_2$. Liver tissues were harvested immediately and stored at -80°C until further experiments. Animal protocols were approved by the Institutional Animal Care and Use Committee at the University of Pittsburgh.

### *4.2.2 Liver Homogenization and Protein Digestion*

Liver tissues were homogenized in an ice-cold phosphate buffer saline (PBS) solution containing 8 M urea with 100 passes of a Wheaton homogenizer. Homogenate solution was collected, sonicated, and centrifuged at 13000 rpm for 10 minutes (4°C). Supernatants were collected, aliquoted into ~50 µL portions, and stored at -80°C. Protein concentrations were determined using the BCA assay according to the manufacturer's instructions (Pierce Thermo; Rockford, IL). Liver proteins (100 µg and 75 µg) were digested for each sample in CysDML and cPILOT experiments, respectively. After dilution to 1 µg/µL, the liver proteins were denatured and reduced in 50 mM Tris buffer (pH = 8.2), 8 M urea, 10 mM dithiothreitol (DTT) for 1 hour at 37°C. The resulting protein mixture was diluted 10-fold with 20 mM Tris buffer (pH = 8.2). TPCK-

treated trypsin from bovine pancreas (Sigma; St. Louis, MO) was added to each sample in a 4% w/w enzyme/protein ratio and incubated at 37°C for 18 hours. Samples were acidified with 0.5% formic acid, cleaned using Waters Oasis HLB $C_{18}$ cartridges, and lyophilized.

### *4.2.3 Cysteinyl-Peptide Enrichment*

All solutions used in the following steps were degassed to prevent oxidation of thiols. Tryptic digests were reduced with 5 mM DTT in 20 µL of 50 mM Tris buffer (pH = 7.5) with 1 mM EDTA (coupling buffer) for 1 hour at 37°C, after which the samples were diluted to 100 µL by adding coupling buffer. Thiopropyl Sepharose 6B thiol-affinity resin (35 mg each) was prepared from dried powder per the manufacturer's instruction (Sigma, St. Louis, MO). Briefly, the dried powder was rehydrated in 1 mL water for 15 minutes, suspended and transferred to spin columns (Pierce Thermo; Rockford, IL), and washed with 0.5 mL water six times. Next, the slurry was washed with 0.5 mL coupling buffer ten times. Reduced peptide samples were incubated with the resin for 1.5 hours at room temperature with a shaking speed of ~800 rpm, and the unbound portion (non-cysteinyl peptides) was removed by centrifugation. The resin was washed in the spin column sequentially with the following solutions: 0.5 mL of 50 mM Tris buffer (pH = 8.0) with 1 mM EDTA (washing buffer), 2 M NaCl, 80% acetonitrile/0.1% TFA, and 100 mM tetraethylammonium bromide (TEAB). Each wash was repeated six times.

### *4.2.4 On-Resin Stable-Isotope Dimethyl Labeling*

Washed samples were contained in spin columns and 100 µL of 100 mM TEAB was added. Then, 11.2 µL of 4% $CH_2O/^{13}C^2H_2O$ (98% $^2H$ and 99% $^{13}C$) and 11.2 µL of 0.6 M $NaBH_3CN/NaB^2H_3CN$ (96% $^2H$) were added to the sample for light and heavy labeling, respectively. In the CysDML experiments, WT samples were labeled with light ($-C_2H_6$) dimethyl

tag and AD samples were labeled with heavy (-$^{13}C_2{}^2H_6$) dimethyl tag. In the cPILOT experiment, randomly selected WT and AD samples ($N$ = 3 each) were labeled with the light dimethyl tag and heavy dimethyl tags ($N$ = 3 each). Samples were incubated for 1 hour at room temperature while mixing at a speed of ~800 rpm. The reaction was terminated by adding ammonia to a final 0.2% (v/v) concentration and after, formic acid to a final 0.3% (v/v) concentration. Buffer and reagents were removed by centrifugation, and the resin was washed with 0.5 mL 100 mM TEAB (three times) and 0.5 mL washing buffer (six times). The captured and labeled cysteinyl-peptides were released by incubating the resin with 100 µL of washing buffer with freshly prepared 20 mM DTT at room temperature for 30 minutes while shaking. The above step was repeated two more times with shorter 10 minute incubations followed by a final incubation with 80% acetonitrile. Flow-through fractions were collected and combined. In CysDML experiments, the released peptides were further alkylated with 80 mM of iodoacetamide (IAM) for 1 hour at room temperature in the dark. AD and WT samples were pooled, concentrated, acidified, desalted using $C_{18}$ cartridges, and lyophilized. CysDML samples were stored at -80°C for LC-MS/MS. In the cPILOT experiment, the released peptides were concentrated, acidified, desalted using $C_{18}$ tips (Pierce Thermo; Rockford, IL), and lyophilized.

### *4.2.5 IodoTMT Tagging*

In cPILOT experiments, light and heavy labeled AD and WT samples were labeled with iodoTMT$^6$ reagents according to the manufacturer's protocol (Pierce Thermo; Rockford, IL) with modifications. Briefly, each peptide sample was dissolved in 10 µL of degassed washing buffer containing 5 mM DTT, reduced for 1 hour at 37°C, and diluted by adding 65 µL washing buffer. Each iodoTMT$^6$ reagent was solubilized with 10 µL of MS-grade methanol and transferred to the peptide mixture. After 1 hour incubation at 37°C in the dark, the reaction was quenched by adding

20 mM DTT. All tagged samples were pooled into a single cPILOT sample, concentrated, acidified, desalted using $C_{18}$ cartridges, and lyophilized.

### *4.2.6 Offline SCX Fractionation*

SCX fractionation of the cPILOT sample was carried out on a PolySulfoethyl A 100 mm × 2.1 mm, 5 µm, 200 Å column (The Nest Group, Inc.; Southborough, MA) with buffers as follows: mobile phase A was 5 mM monopotassium phosphate (25% v/v acetonitrile, pH 3.0), and mobile phase B was 5 mM monopotassium phosphate, 350 mM potassium chloride (25% v/v acetonitrile, pH 3.0). Dried sample was resuspended in 300 µL of mobile phase A and injected onto the SCX column. The gradient for SCX was 0-5 min, 0% B; 5-45 min, 0-40% B; 45-90 min, 40-80% B; 90-100 min, 80-100% B; 100-110 min, 100% B; 110-121 min, 0% B. One-minute fractions were collected into a 96-well-plate and pooled into a final eight fractions which were desalted using a $C_{18}$ tip.

### *4.2.7 LC-MS/MS Analysis*

Online desalting and reversed-phase chromatography was performed with a Nano-LC system equipped with an autosampler (Eksigent; Dublin, CA). Mobile phases A and B were 3% (v/v) acetonitrile with 0.1% formic acid and 100% (v/v) acetonitrile with 0.1% formic acid, respectively. Sample (5 µL) was loaded onto a trapping column (100 µm i.d. × 2 cm), which was packed in-house with $C_{18}$ 200 Å 5 µm stationary phase material (Michrom Bioresource Inc.; Auburn, CA) at 3 µL/min in 3% mobile phase B for 3 min. The sample was loaded onto an analytical column (75 µm i.d. × 13.2 cm), which was packed in-house with $C_{18}$ 100 Å 5 µm stationary phase material (Michrom Bioresource Inc.; Auburn, CA). The following gradient was used for both CysDML and cPILOT experiments: 0-5 min, 10% mobile phase B; 5-40 min, 10-

15% B; 40-90 min, 15-25% B; 90-115 min, 25-30% B; 115-130 min, 30-60% B; 130-135 min, 60-80% B; 135-145 min, 80% B; 145-150 min, 80-10%B; 150-180 min, 10%B. The LC eluent was analyzed with positive ion nanoflow electrospray using a LTQ-Orbitrap Velos mass spectrometer (Thermo-Fisher Scientific; Waltham, MA).

CysDML samples were analyzed by employing three gas phase fractionations (GPF). Specifically, each sample was injected seven times and subject to different MS scans: $1^{st}$ injection) precursor scan over the *m/z* range 350-1700, $2^{nd}$ – $4^{th}$ injections) *m/z* 350-800, *m/z* 785-975 and *m/z* 960-1700, respectively, and the $5^{th}$ – $7^{th}$ injections were repeats of the $2^{nd}$ – $4^{th}$ injections. GPF mass ranges were determined from a preliminary analysis of the full *m/z* range scan and optimized to generate similar numbers of PSMs in each GPF. The following data-dependent acquisition (DDA) parameters were used in each injection: the MS survey scan in the Orbitrap was 60,000 resolution; the top 15 most intense peaks in the MS survey scan were isolated and fragmented with CID at an isolation width of 3 *m/z*; CID was performed in the ion trap with normalized collision energy 35%. The maximum fill time for MS and MS/MS is 500 ms and 50 ms, respectively. A complete duty cycle timing is ~3 sec.

SCX fractions of the cPILOT sample were injected three times and subject to various top ion acquisitions. The MS survey scan in the Orbitrap was 60 000 resolution over *m/z* 350-1700. The first injection included the top five ions for DDA. The second and third injections included the $6^{th}$ to $10^{th}$ and $11^{th}$ to $15^{th}$ most intense peaks in the MS survey scan for DDA, respectively. DDA parameters were as follows: precursor ions were isolated with a width of 3 *m/z* and normalized collision energy of 35%, the most intense CID fragment ion over the *m/z* range 400-1300 was selected for HCD-$MS^3$. The HCD fragment-ion isolation width was set to 4 *m/z*, the normalized collision energy was 60%, and HCD resolution was 7500 in the Orbitrap. The

maximum fill time for MS, MS/MS and MS3 is 500 ms, 50 ms and 250 ms, respectively. The total duty cycle timing is ~2.4 sec.

### *4.2.8 Database Searching and Data Analysis*

RAW files were analyzed using the SEQUEST HT search engine with Proteome Discoverer 1.4 software (Thermo-Fisher Scientific; Waltham, MA) and searched against the Uniprot mouse database (05/21/2014, 51344 sequences). SEQUEST HT search parameters of CysDML data are as follows: precursor mass tolerance 15 ppm; fragment mass tolerance 1 Da; static modifications light dimethyl/+28.031 Da (Lys) or heavy dimethyl/+36.076 Da (Lys), carbamidomethyl modification/+57.021 Da (Cys); dynamic modifications light dimethyl/+28.031 Da (N-terminal) or heavy dimethyl/+36.076 Da (N-terminal), oxidation/+15.995 Da (Met). Decoy database searching was employed to calculate false discovery rate (FDR). Only peptides with medium confidence (<5% FDR) were used further analysis[287]. Proteome Discoverer 1.4 provided peak area information for light and heavy labeled peptides and protein ratio calculations. Protein ratios were normalized based on the protein median ratio in each biological replicate experiment for CysDML. SEQUEST HT search parameters of cPILOT data are the same as CysDML data except the static modification on cysteine is iodoTMT$^6$/+329.226 Da. The reporter ions (i.e., m/z 126-131) were identified with the following parameters: centroid with smallest delta mass, 30 ppm for reporter ion mass tolerance. The isotope correction was employed according to the manufacturer's data sheet (Pierce Thermo; Rockford, IL). The median reporter ion intensity of each channel was calculated across all peptide spectral matches (PSMs). The median of all reporter ion channels (from light and heavy) was used to normalize reporter ion intensities. Peptide ratios were calculated and finally, protein ratios were determined from peptide median ratios. Noncysteinyl-peptides were excluded from quantification.

### *4.2.9 Statistics*

Normalized AD/WT ratios were transformed to $\log_2$ scale and subject to permutation. Permutation testing calculates *p*-values by randomly enumerating all possible permutations. The null hypothesis is $H_{0:}\mu = 0$ with alternative of $H_{1:}\mu \neq 0$. The *p*-value was calculated as $p = (1 + b)/(1 + m)$, where *b* is the number of times in the 10,000 permuting counts, *m*, that $t_{permuted}$ (test statistics in permutation test) is larger than $t_{observed}$ (observed test statistic)[288-290]. Calculations were performed in MATLAB R2014a. A $p < 0.05$ was considered statistically significant. Stringent filter criteria were applied to generate a list of statistically significant differentially expressed proteins as follows: 1) protein must be quantified in $N = 6$ biological replicates; 2) for CysDML, AD/WT ratios < 0.78 or > 1.20 and for cPILOT, AD/WT ratios < 0.72 or > 1.40[54] and 4) standard deviation < 0.5 for protein AD/WT ratios across all biological replicates.

## 4.3 RESULTS AND DISCUSSION

Here we present two novel multiplexing approaches based on the enrichment of cysteinyl-peptides termed: CysDML and cPILOT. Both strategies are depicted in Figure 4.1 and were used to compare differences in the liver proteomes of AD and WT mice. First, twelve liver protein samples (i.e., six WT and six AD) were serially digested by trypsin. Next, cysteinyl-peptides were enriched using a Thiopropyl Sepharose 6B resin. On resin, captured peptides were labeled with either light (-$C_2H_6$) or heavy (-$^{13}C_2{}^2H_6$) dimethyl tags on primary amines such as the N-termini and Lysine residues. The CysDML approach relies on precursor labeling to quantify relative protein abundances between WT and AD samples. Because CysDML is a duplex experiment it was necessary to repeat six independent times to accommodate all biological replicates. On the other hand, the cPILOT approach is a 12-plex experiment and dimethylation is used to double the

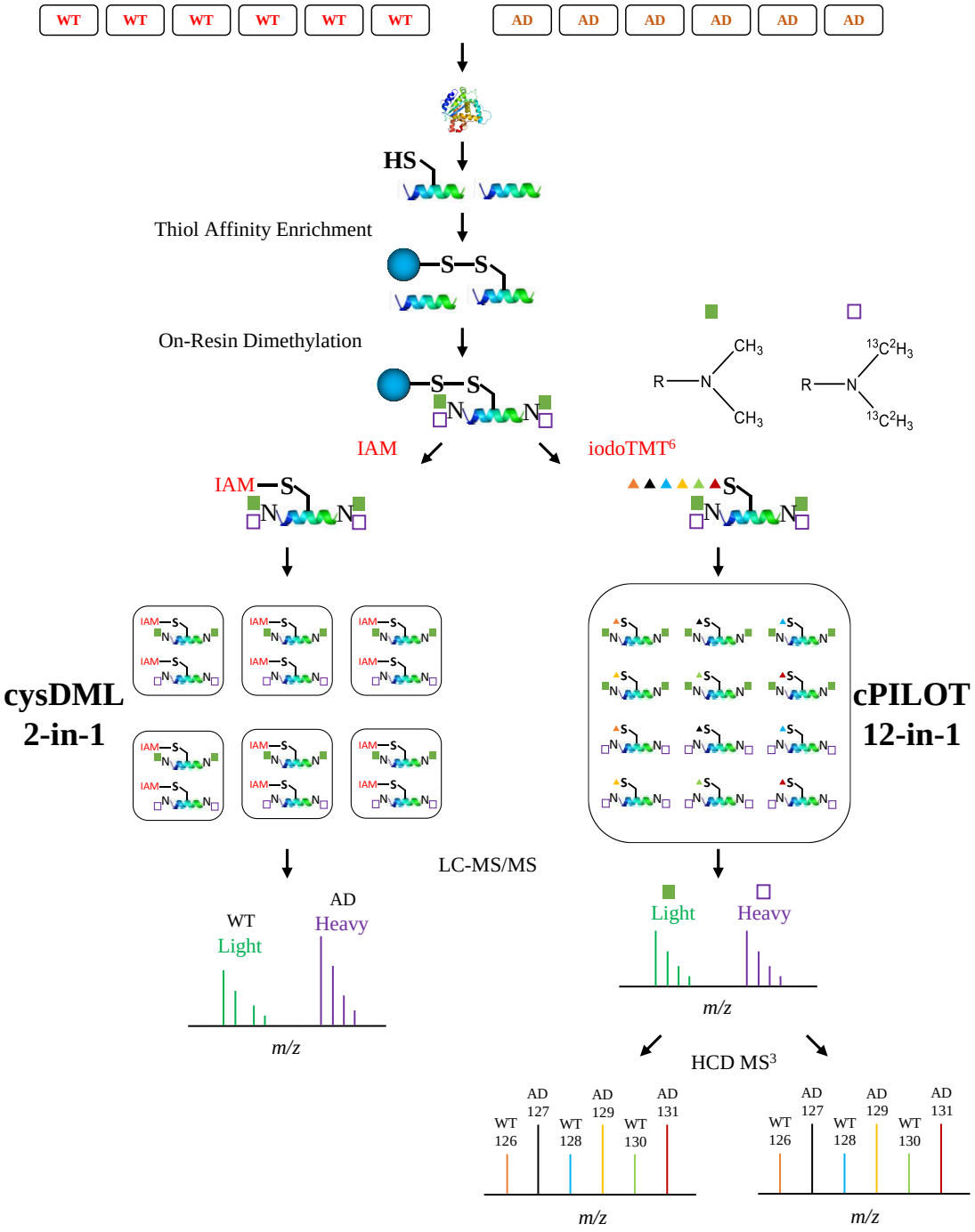


**Figure 4.1** Schematic representation of cysteine-selective proteomics workflow. Mouse liver peptides are enriched by a thiol-affinity resin. Samples are labeled with either light (-$C_2H_6$) or heavy dimethyl (-$^{13}C_2{}^2H_6$) tags on resin. In the CysDML experiment: a) WT and AD samples are tagged with light and heavy dimethyl groups, respectively; b) peptides are eluted from the resin with 20 mM dithiothreitol (DTT); c) iodoacetamide is used to alkylate free cysteines; and d) WT and AD samples are combined, desalted and analyzed by LC-MS/MS. In the cPILOT experiment: a) WT and AD samples are tagged with light or heavy dimethyl groups on resin; b) after elution with DTT, iodoTMT$^6$ reagents are added to each sample; c) all 12 samples are combined, cleaned, fractionated and analyzed by LC-MS$^3$.

number of channels accessible with the TMT isobaric tagging method. Here, three WT and three AD samples were labeled with the light dimethyl group whereas the remaining samples in each group were labeled with the heavy dimethyl group. After precursor labeling steps, peptides were released from the resin using DTT. CysDML samples were alkylated, six WT and AD pairs were pooled independently, and analyzed using gas-phase fractionation (GPF)[291] and LC-MS/MS. CPILOT samples were cleaned, tagged with iodoTMT[6] reagents, and the twelve samples were pooled into a single mixture that was analyzed using LC-MS/MS and HCD-MS[3].

### *4.3.1 Optimization of On-Resin Dimethylation Reaction Conditions*

Stable-isotope dimethylation is an attractive precursor isotopic labeling technique because (1) the tag is inexpensive[25], (2) it offers up to five sample channels[40], (3) the reaction is versatile and can be performed in solution or on resin[292], and (4) the reaction is pH-dependent and site-selective[34]. In order to minimize sample loss we performed dimethylation on the Thiolpropyl Sepharose 6B resin. Initially, we achieved an ~90% labeling efficiency (Figure 4.2a) using starting conditions that mimicked in-solution labeling conditions (i.e., 25 mM $NaBH_3CN$, 55 mM $CH_2O$, and one hour incubation). Significant improvement of the labeling efficiency to >98% was achieved with a longer incubation time (i.e., 24 hours). Because we are interested in maximizing the overall throughput of multiplexing experiments we sought to reduce the reaction time while maintaining high efficiency. This was made possible by increasing the reagent concentrations ~2.5 fold (60 mM $NaBH_3CN$, 145 mM $CH_2O$) with a one hour incubation period (Figure 4.2b). These conditions are consistent with dimethyl labeling performance on solid phase hydrazide beads[293] and were used for remaining CysDML and cPILOT experiments. Because $NaBH_3CN$ is a much weaker reducing regent than $NaBH_4$, it will not affect aldehydes, ketones as well as disulfide

a)

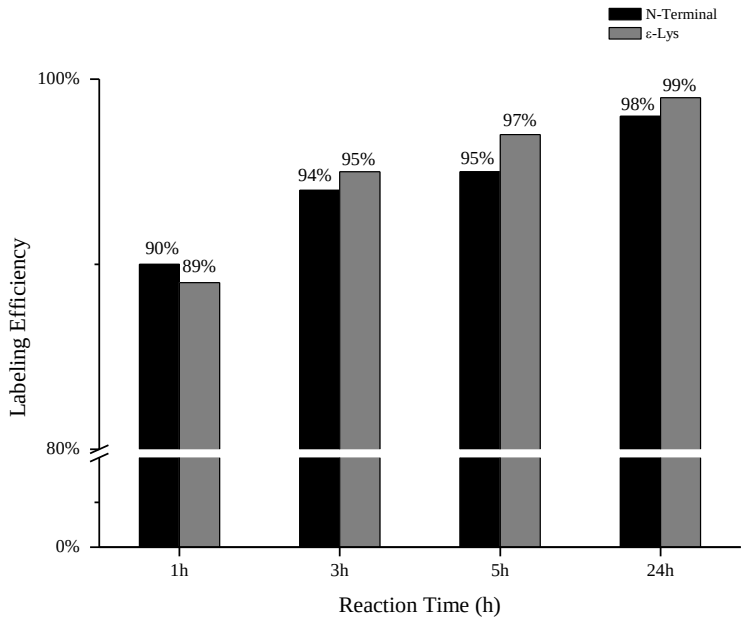


b)

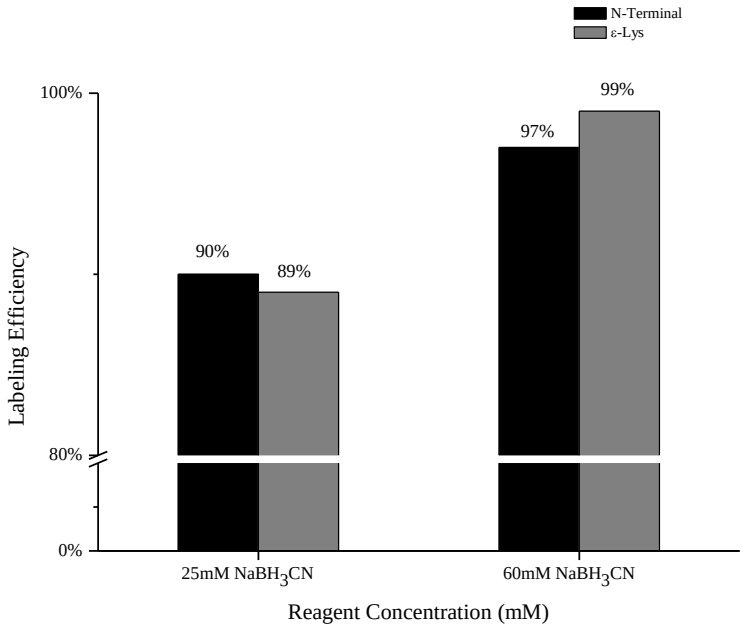


**Figure 4.2** Optimization of on-resin dimethylation. a) Plot of on-resin dimethylation labeling efficiency (calculated based on spectral counts) of N-terminal and Lys residues using various reaction times; b) labeling efficiency of N-terminal and Lys residues using 25 mM $NaBH_3CN$ and 60 mM $NaBH_3CN$ with a one-hour incubation time.

between peptides and resin[294]. We also did not observe any change to the physical property of the resin after dimethyl labeling, indicating the presence of intact disulfide bonds[295].

### *4.3.2 Evaluation of Quantification Accuracy and Resin Loading Range for CysDML*

CysDML is a novel precursor dimethylation technique. Thus we assessed the quantitative accuracy and linear dynamic range using tryptic peptides from WT mouse liver. The first experiment evaluated quantitative accuracy of a mixture of 1:1 light:heavy labeled tryptic peptides that were separated using a three hour LC gradient. A total of 689 proteins were identified and 424 of these were quantified (i.e., proteins had reported ratios for light and heavy peptides from Proteome Discoverer report). The average heavy/light ratio for the quantified proteins is 0.98±0.21 (mean±standard deviation) as shown in Figure 4.3a; this error is consistent with other reports[296]. More than 95% of the proteins have ratios falling within two standard deviations of the mean and thus fits a normal distribution. To understand the effects of resin loading amount on quantitative accuracy, we varied the sample loading on resin as follows: six CysDML samples contained a fixed amount (100 µg) of peptides prior to resin loading, while the heavy channel varied from 12.5 µg, 25 µg, 50 µg, 100 µg, 200 µg to 400 µg. When the sample loading amount was between 25 µg to 200 µg, accurate heavy/light ratios were obtained (Figure 4.3b). However, on the low and high ends the ratios were skewed. We attribute this to dilute samples on the low end that result in an overall minimal capture of cysteinyl-peptides. On the high end, inefficient capture on the resin occurred as the amount of DTT concentration was not increased to accommodate higher concentrations of peptide thiols. Excessive DTT concentrations are damaging to the Thiolpropyl Sepharose 6B resin. The measured dynamic range is 8-fold which is comparable to other reports[145,297], and the maximum standard deviation was ~0.5. Results of these experiments were used to establish appropriate criteria for determining differential expression of proteins.

a)

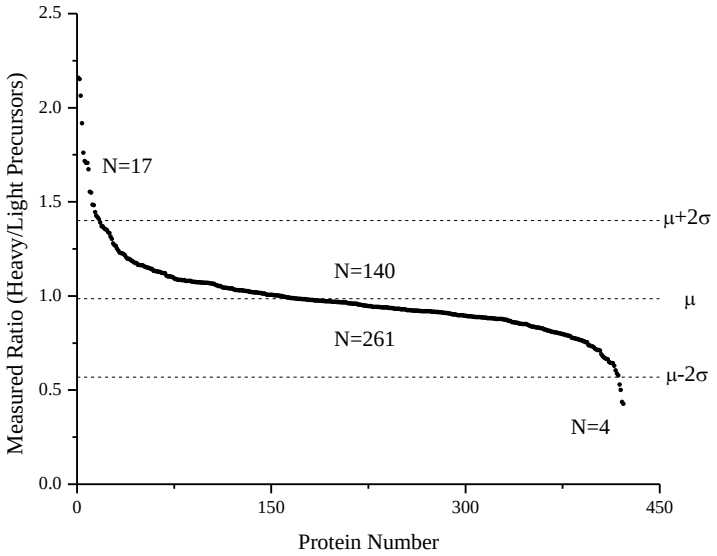


b)

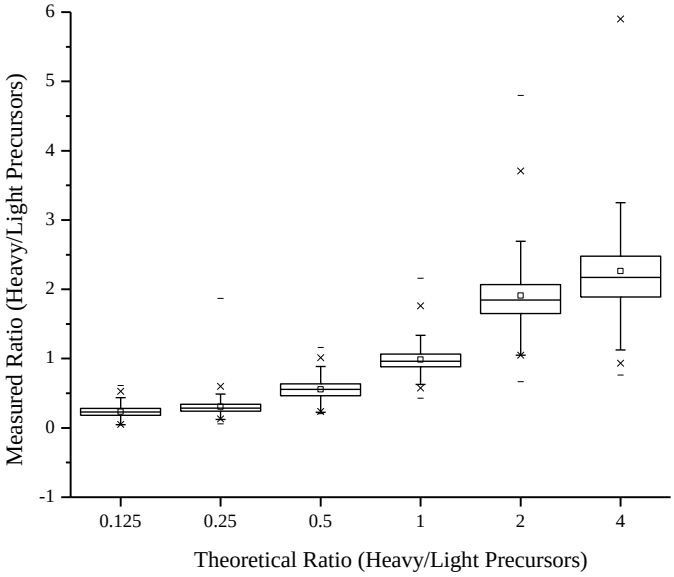


**Figure 4.3** On-resin loading capacity of CysDML experiment. a) Scatter plot of protein ratios measured in CysDML experiment designed to have theoretical ratios of 1:1 for light and heavy labeled peaks. Horizontal lines represent average±2×standard deviation (μ±2σ) and the numbers of quantified proteins within each region are labeled. b) Box plot of measured ratios in CysDML dynamic range experiment. The amount of peptide labeled with the light tag is fixed at 100 μg, while the amount of peptide labeled with the heavy tag varies as follows: 12.5 μg, 25 μg, 50 μg, 100 μg, 200 μg and 400 μg. The theoretical ratios of light and heavy labeled peaks are designed to 0.125, 0.25, 0.5, 1, 2 and 4.

### *4.3.3 Application of CysDML to the Liver Proteome of an AD Mouse Model*

A tradeoff that must be considered in any proteomics experiment is proteome depth or coverage versus sample preparation, acquisition, and analysis time. We wanted to minimize the number of sample handling steps (and potential sample loss) while maintaining adequate proteome coverage, because each CysDML sample is only ~40 µg. Thus GPF was used as a fractionation step for CysDML samples[291]. Figure 4.4 provides example base peak chromatograms of seven GPFs for one of the pooled AD/WT sample pairs. The first injection was analyzed with a full *m/z* range of 350-1700. Six subsequent injections were collected over the *m/z* ranges of 350-800, 785-975 and 960-1700 such that each fraction was not analyzed back-to-back. An overlapping window of 15 *m/z* was used between adjacent GPFs to ensure that light and heavy pairs were detected within the same spectrum. Comparisons of GPF to a single LC-MS/MS analysis over the full *m/z* range of 350-1700, indicate that GPF increases protein and peptide identifications by 79% and 75%, respectively (*data not shown*). Furthermore, the replicate injections are highly reproducible. Figure 4.5a displays several example spectra containing light (*m/z* = 974.03) and heavy (*m/z* = 982.07) pairs of the doubly charged peptide [V(dimethyl)AVVAGYGDVGK (dimethyl)GC (IAM)AQALR+2H]$^{2+}$ from protein adenosylhomocysteinase. The observed spacing (Δm = 16 Da) between the peaks is consistent with two dimethyl groups being present on the peptide. Also, the diversity in peptide levels across the six biological replicates is apparent. An M+7 Da species, which has a relative abundance of ~10%, is observed for heavy dimethylated peaks consistent with other reports[37,292]. The presence of this peak could be from use of isotopically pure reducing reagent however does not have significantly influence on quantitative accuracy and precision (Figure 4.3a and 4.3b). Overall, the average number of spectral counts, peptides, proteins identified, and proteins quantified across the replicates is 14005±2125, 1823±238, 850±92, and

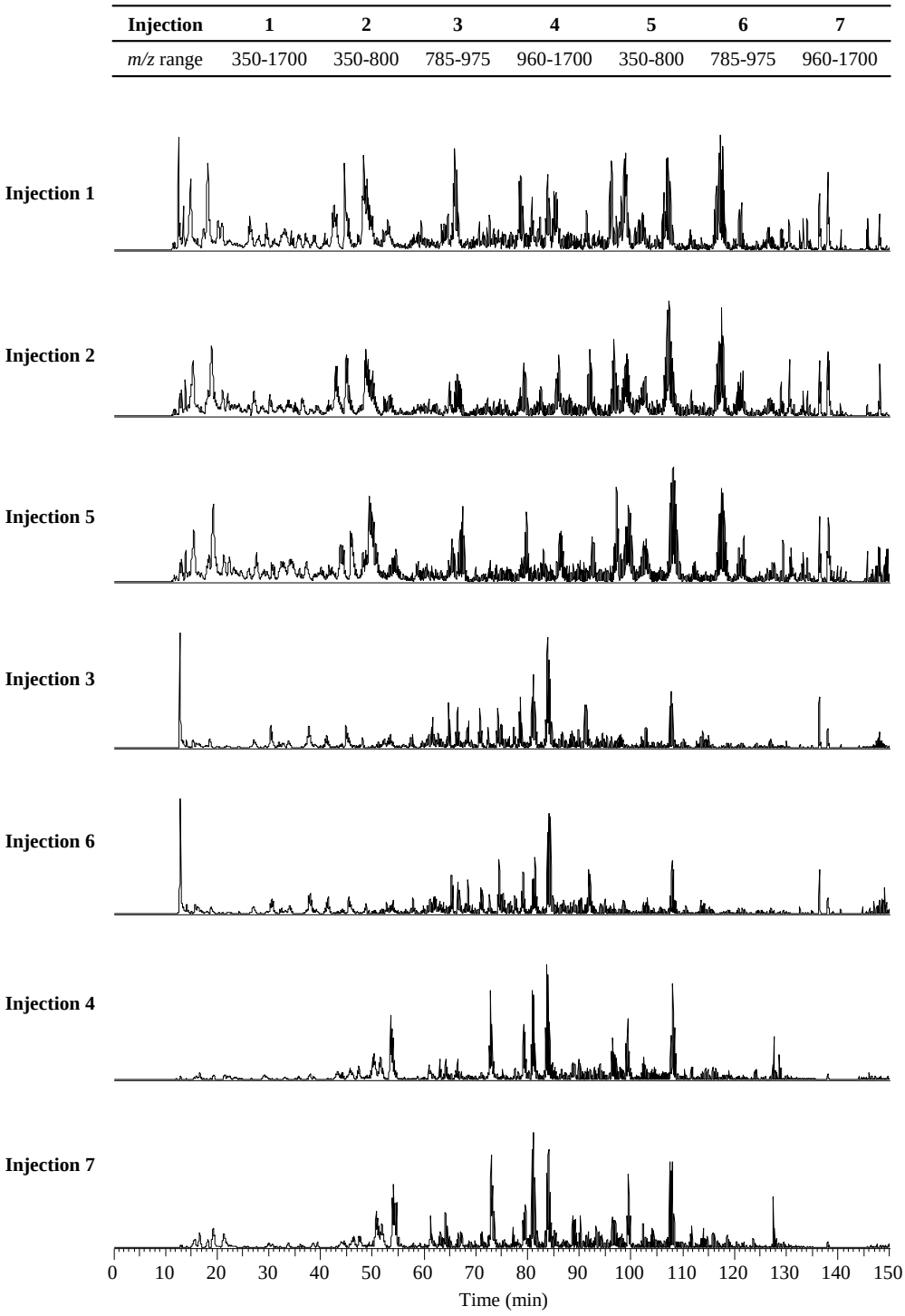


**Figure 4.4** Base peak chromatograms for an example CysDML experiment (one biological replicate). Samples are injected a total of seven times. The first injection is analyzed with a full *m/z* range of 350-1700. The subsequent injections use gas phase fractionation (GPF) such that data are acquired over the *m/z* ranges of 350-800, 785-975 and 960-1700, and repeated twice. The top 15 most intense ions are selected and fragmented in each run.

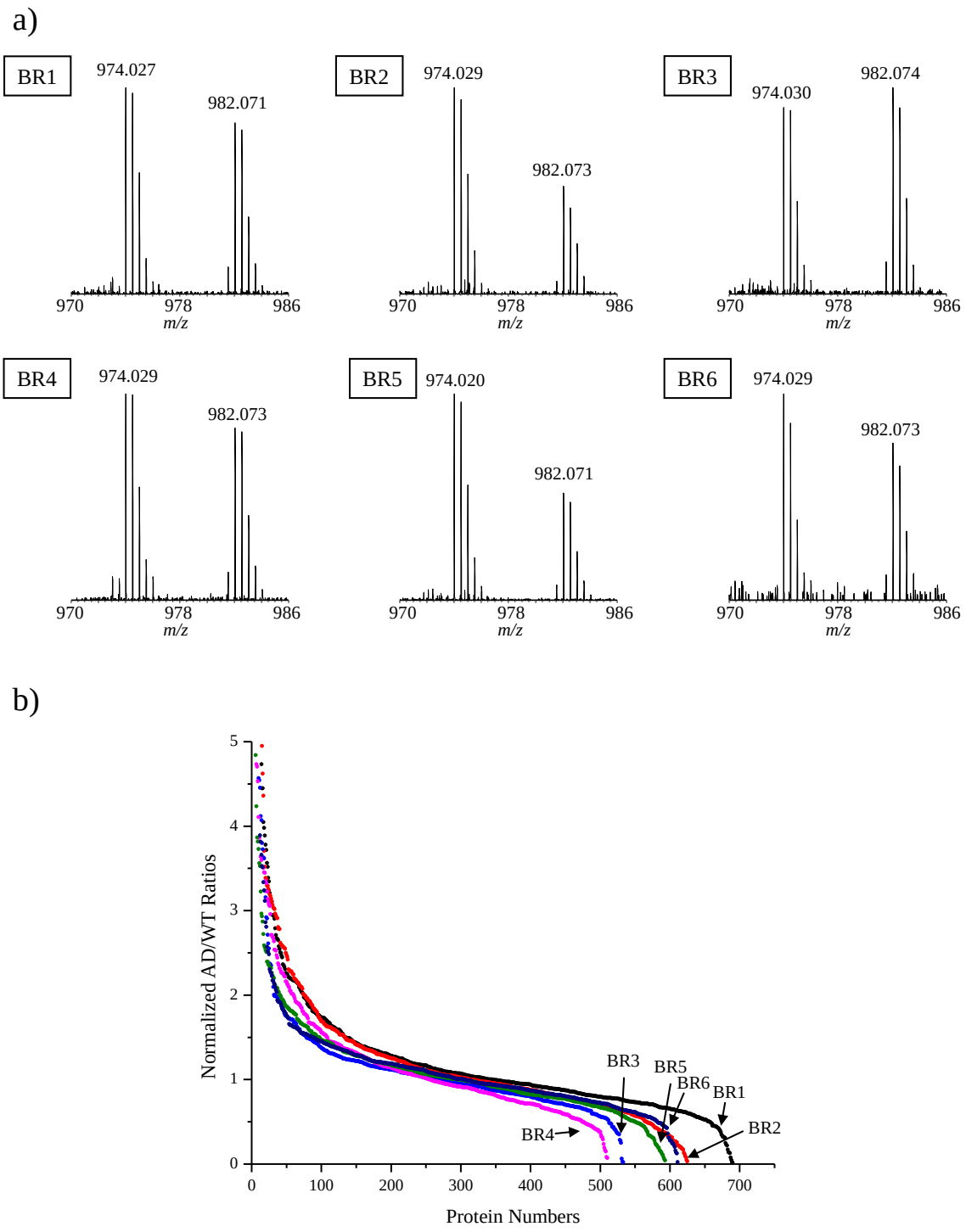


**Figure 4.5** Example CysDML MS spectra for: a) pair of light (*m/z* = 974.03) and heavy (*m/z* = 982.07) peaks assigned to the doubly charged peptide V(dimethyl)AVVAGYGDVGK(dimethyl)GC(IAM)AQALR of adenosylhomocysteinase in each biological replicate (BR); b) scatter plot of normalized protein ratios (AD/WT) measured in CysDML experiment for each BR.

594±65, respectively (Table 4.1). In total, 2085 unique proteins were identified from CysDML experiments. A large number of the spectral counts (~98%) and peptides (~91%) identified in each CysDML experiment can be attributed to cysteinyl-peptides. Thus, the CysDML approach is very efficient at enrichment and detection of cysteinyl-peptides. When assessing the AD/WT ratios for proteins quantified in each of the six CysDML experiments, we find that they are very similar across biological replicates (Figure 4.5b). Many proteins have ratios that fall outside of an AD/WT ratio of one. We used permutation testing and conservative filtering criteria (see Experimental) and identified 54 proteins that are differentially-expressed in the AD mice from CysDML experiments (Table 4.2). Twenty-three of these proteins have higher levels in AD mice, whereas 31 proteins have lower levels in AD mice relative to WT. Differentially-expressed proteins are involved in various biological processes which will be briefly discussed below.

### *4.3.4 Application of cPILOT to the Liver Proteome of an AD Mouse Model*

Previously our laboratory has demonstrated enhanced multiplexing using global[36] and 3-nitrotyrosine[53] specific cPILOT approaches. The combination of precursor isotopic labeling with isobaric tagging methods can increase the number of sample multiplexing channels by a factor of two to three times. Capabilities afforded by enhanced sample multiplexing include increasing biological replication, the ability to examine many tissues, sample types, environmental stimuli, longitudinal studies, etc. in a single analysis, and minimizing biases caused by multiple sample preparation steps and LC and MS acquisitions. We note that because cPILOT involves post-digestion chemical labeling, errors introduced prior to sample pooling are still inherent in the final ratios reported. In order to increase sample multiplexing capabilities, simplify the protein mixture, assay (Figure 4.1) and benchmarked its performance against the CysDML method. Compared with

**Table 4.1** Summary of CysDML and cPILOT experiments.

| | CysDML | | | | | | | | cPILOT |
|---|---|---|---|---|---|---|---|---|---|
| | BR1 | BR2 | BR3 | BR4 | BR5 | BR6 | Average | $S_d$[c] | |
| Total PSMs | 16800 | 15513 | 12627 | 10766 | 13991 | 14334 | 14005 | 2125 | 3748 |
| Total Peptides | 2175 | 1963 | 1649 | 1499 | 1783 | 1867 | 1823 | 238 | 414 |
| Cysteine PSMs | 16469 | 15238 | 12412 | 10574 | 13778 | 14125 | 13766 | 2080 | 3318 |
| Cysteine Peptides | 1972 | 1772 | 1492 | 1354 | 1624 | 1716 | 1655 | 217 | 245 |
| %Enrichment[a] | 98.0 | 98.2 | 98.3 | 98.2 | 98.5 | 98.5 | 98.3 | 0.2 | 88.5 |
| %Enrichment[b] | 90.7 | 90.3 | 90.5 | 90.3 | 91.1 | 91.9 | 90.8 | 0.6 | 59.2 |
| Proteins Identified | 982 | 908 | 769 | 728 | 840 | 871 | 850 | 92 | 330 |
| Proteins Quantified | 690 | 625 | 533 | 510 | 593 | 611 | 594 | 65 | 151 |

[a]Enrichment efficiency is calculated by PSMs (cysteine PSMs count/total PSMs count) [b]Enrichment efficiency is calculated by unique peptides (unique cysteine peptide count/total unique peptide count).
[c]Standard deviation across six biological replicates.

**Table 4.2** Differentially expressed proteins quantified from CysDML experiment.

| Acc.no.[a] | Protein name | AD/WT[b] | $S_d$[c] | *p*-value[d] |
|---|---|---|---|---|
| Q61838 | Alpha-2-macroglobulin | 1.64 | 0.28 | 0.0001 |
| Q3UEJ6 | Phosphorylase | 1.58 | 0.45 | 0.0138 |
| P54869 | Hydroxymethylglutaryl-CoA synthase, mitochondrial | 1.54 | 0.38 | 0.0001 |
| Q7TMF3 | NADH dehydrogenase [ubiquinone] 1 alpha subcomplex subunit 12 | 1.52 | 0.46 | 0.0006 |
| Q9CQC9 | GTP-binding protein SAR1b | 1.45 | 0.45 | 0.0130 |
| P20918 | Plasminogen | 1.41 | 0.48 | 0.0008 |
| P16332 | Methylmalonyl-CoA mutase, mitochondrial | 1.40 | 0.21 | 0.0002 |
| P80313 | T-complex protein 1 subunit eta | 1.37 | 0.31 | 0.0120 |
| Q9D0S9 | Histidine triad nucleotide-binding protein 2, mitochondrial | 1.36 | 0.46 | 0.0011 |
| Q571F8 | Glutaminase liver isoform, mitochondrial | 1.31 | 0.36 | 0.0127 |
| Q8BWT1 | 3-Ketoacyl-CoA thiolase, mitochondrial | 1.29 | 0.36 | 0.0476 |
| O35718 | Suppressor of cytokine signaling 3 | 1.28 | 0.27 | 0.0001 |
| Q3UT49 | Cytochrome P450 2C29 | 1.28 | 0.30 | 0.0408 |
| Q9QZD8 | Mitochondrial dicarboxylate carrier | 1.27 | 0.26 | 0.0456 |
| P97742 | Carnitine O-palmitoyltransferase 1, liver isoform | 1.26 | 0.19 | 0.0125 |
| Q8VDN2 | Sodium/potassium-transporting ATPase subunit alpha-1 | 1.26 | 0.38 | 0.0454 |
| Q9QXD6 | Fructose-1,6-bisphosphatase 1 | 1.26 | 0.17 | 0.0001 |
| P68040 | Guanine nucleotide-binding protein subunit beta-2-like 1 | 1.23 | 0.22 | 0.0004 |
| F2Z459 | Protein Acat3 | 1.22 | 0.14 | 0.0004 |
| P51881 | ADP/ATP translocase 2 | 1.22 | 0.13 | 0.0001 |
| Q4LDG0 | Bile acyl-CoA synthetase | 1.22 | 0.22 | 0.0460 |
| J3QNG0 | MCG15755 | 1.22 | 0.11 | 0.0008 |
| Q3UXD9 | Peroxisomal trans-2-enoyl-CoA reductase | 1.21 | 0.21 | 0.0001 |
| F6T930 | Enoyl-CoA hydratase, mitochondrial (Fragment) | 0.77 | 0.09 | 0.0001 |
| Q8BWF0 | Succinate-semialdehyde dehydrogenase, mitochondrial | 0.75 | 0.15 | 0.0006 |
| P60335 | Poly(rC)-binding protein 1 | 0.75 | 0.18 | 0.0001 |
| D3YXF4 | 14-3-3 protein zeta/delta (Fragment) | 0.75 | 0.24 | 0.0480 |
| P14094 | Sodium/potassium-transporting ATPase subunit beta-1 | 0.74 | 0.07 | 0.0008 |
| A2A815 | Protein DJ-1 (Fragment) | 0.73 | 0.07 | 0.0015 |
| P27659 | 60S ribosomal protein L3 | 0.73 | 0.07 | 0.0002 |
| A2AD25 | MCG49690 | 0.73 | 0.12 | 0.0001 |
| P08228 | Superoxide dismutase [Cu-Zn] | 0.72 | 0.18 | 0.0120 |
| Q8BGD8 | Cytochrome c oxidase assembly factor 6 homolog | 0.72 | 0.14 | 0.0003 |
| Q99PG0 | Arylacetamide deacetylase | 0.72 | 0.25 | 0.0124 |
| Q9DBW0 | Cytochrome P450 4V2 | 0.71 | 0.25 | 0.0134 |
| F8WIT2 | Annexin | 0.71 | 0.13 | 0.0001 |
| Q8BP47 | Asparagine--tRNA ligase, cytoplasmic | 0.69 | 0.08 | 0.0008 |
| A2AVJ7 | Ribosome-binding protein 1 | 0.69 | 0.28 | 0.0138 |
| Q9CXS4-2 | Isoform 2 of centromere protein V | 0.69 | 0.20 | 0.0008 |
| A2AKV0 | ATP synthase subunit gamma, mitochondrial (Fragment) | 0.68 | 0.11 | 0.0001 |

*Continued on Page 91*

**Table 4.2** Differentially expressed proteins quantified from CysDML experiment.

| Acc.no.[a] | Protein name | AD/WT[b] | $S_d$[c] | *p*-value[d] |
|---|---|---|---|---|
| B1AXY0 | DnaJ homolog subfamily A member 1 (Fragment) | 0.68 | 0.18 | 0.0005 |
| Q91ZA3 | Propionyl-CoA carboxylase alpha chain, mitochondrial | 0.68 | 0.33 | 0.0128 |
| B1ASE2 | ATP synthase subunit d, mitochondrial (Fragment) | 0.67 | 0.08 | 0.0001 |
| P63276 | 40S ribosomal protein S17 | 0.67 | 0.21 | 0.0001 |
| E9Q2H8 | Hydroxyacylglutathione hydrolase, mitochondrial (Fragment) | 0.65 | 0.16 | 0.0001 |
| Q99P30-5 | Isoform 5 of Peroxisomal coenzyme A diphosphatase NUDT7 | 0.65 | 0.28 | 0.0005 |
| D3Z5M2 | Protein gm10110 | 0.64 | 0.14 | 0.0001 |
| D3Z6C3 | 40S ribosomal protein S3a | 0.62 | 0.33 | 0.0468 |
| Q9D0E1-2 | Isoform 2 of heterogeneous nuclear ribonucleoprotein M | 0.60 | 0.25 | 0.0002 |
| Q8BGY2 | Eukaryotic translation initiation factor 5A-2 | 0.59 | 0.09 | 0.0001 |
| D3Z0E6 | 3'(2'),5'-bisphosphate nucleotidase 1 | 0.56 | 0.19 | 0.0010 |
| Q60991 | 25-hydroxycholesterol 7-alpha-hydroxylase | 0.55 | 0.44 | 0.0165 |
| Q8R164 | Valacyclovir hydrolase | 0.49 | 0.14 | 0.0002 |
| E9Q1R2 | 4-hydroxy-2-oxoglutarate aldolase, mitochondrial | 0.45 | 0.23 | 0.0006 |

[a]Accession number provided from the Uniprot mouse database (05/21/2014, 51344 sequences). [b]Average ratio of AD/WT. [c]Standard deviation. [d]*p*-value calculated from permutation test.

CysDML, cPILOT used iodoTMT to replace iodoacetamide at the last step. Before iodoTMT tagging, excess DTT (~20 mM) was depleted by C18 cleanup according a relevant report [298]. In order to reduce any possible oxidized thiols, right before using iodoTMT tag, a low level of DTT (5 mM) was applied. After dilution and adding iodoTMT tag, our calculation indicated that the remaining DTT will not quench all iodoTMT, and the active tag amount (~4 mM) was sufficient for reaction according to manufacturer's protocol (Pierce Thermo; Rockford, IL). We tested this process by using iodoacetamide and iodoTMT$^0$ before applying to WT/AD samples. We believe Tris(2-carboxyethyl)phosphine (TCEP) can be used as a substitute for DTT.

Data-dependent acquisition was employed on a LTQ-Orbitrap Velos MS such that the top five most intense ions were subject to CID MS/MS and the most intense fragment ion (over the *m/z* range 400-1300) was further subjected to HCD-MS$^3$. MS$^3$ has been demonstrated to address co-isolation and ratio suppression issues of isobarically-tagged peptides[52]. Figure 4.6 provides example MS spectra for a tryptic peptide detected in the cysteine-specific cPILOT experiment. The precursor MS scan (Figure 4.6a) displays a light (*m/z* = 693.02) and heavy (*m/z* = 698.39) pair of peaks that arise from a triply-charged ion. In independent CID MS/MS scans, both the light and heavy peaks were isolated and fragmented to provide the MS/MS spectra shown in Figure 4.6b. The fragmentation patterns for the light and heavy labeled precursor ions are very similar and the fragment peaks only differ by the masses of the heavy isotope atoms from the dimethyl tag. Based on the MS/MS spectral information, the peptide sequence has been assigned to the peptide [T(dimethyl)SAC(iodoTMT$^6$)FEPSLDYMVTK(dimethyl)+3H]$^{3+}$ that belongs to the protein carbamoyl-phosphate synthase. We applied a relatively large isolation width (3 m/z) in precursor selection for better sensitivity in MS$^3$ quantification. We also analyzed the distribution of charge state and *m/z* spaces between light and heavy species across all PSMs. Although 35.4% of PSMs

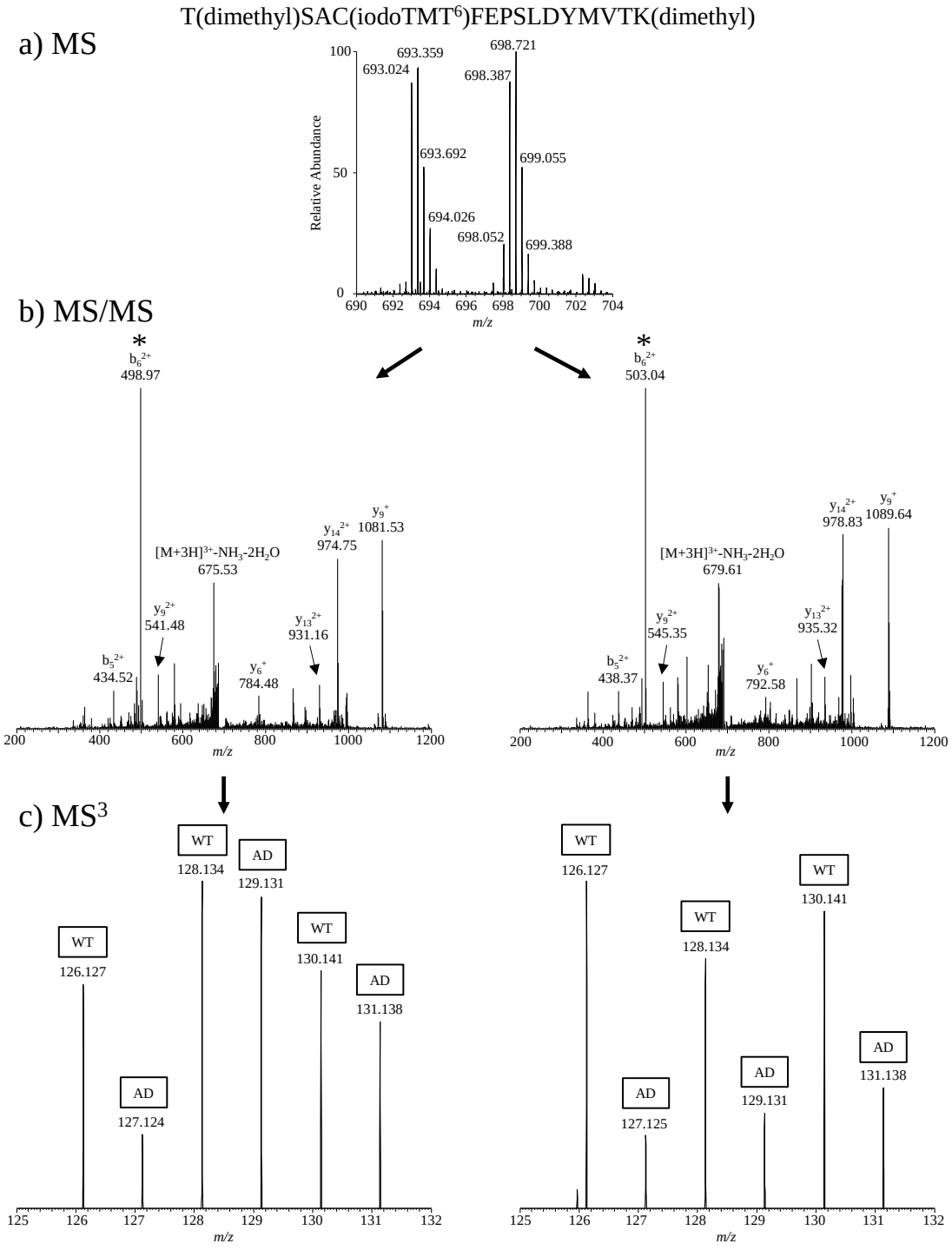


**Figure 4.6** Example cPILOT MS spectra for: a) pair of peaks assigned to the peptide T(dimethyl)SAC(iodoTMT$^6$)FEPSLDYMVTK(dimethyl) of carbamoyl-phosphate synthase; b) CID MS/MS spectra of the peaks with *m/z* = 693.024 and *m/z* = 698.387 from a). The most intense peaks (*) within the *m/z* range of 400-1300 were further selected and fragmented to give the HCD MS$^3$ spectra shown in c**)**, which are zoomed-in over the reporter ion region.

have charge states more than three, only 5.5% of PSMs have *m/z* gap less than 2.7, and these PSMs may have co-isolation issue (see Figure 4.7). However, the following $MS^3$ isolation and fragmentation could alleviate it. Isolation and HCD fragmentation of the most intense peaks in the CID spectra (i.e., the $b_6^{2+}$ ion at *m/z* = 498.97 for light and *m/z* = 503.04 for heavy), result in the $MS^3$ spectra shown in Figure 4.6c. The low *m/z* region of the spectra are shown and two sets of reporter ions (*m/z* 126-131) are detected for the light and heavy labelled fragment ions. Relative abundances of the reporter ion peaks for WT and AD samples indicate that this peptide has an overall lower level in AD liver relative to WT. When considering the average reporter ion AD/WT ratio (i.e., AD/WT=0.81, $p$=0.015) for this protein, it is excluded according to filter criteria (see Experimental) for differential expression.

There was a total of 3318 spectral counts and 245 peptides that are specific to cysteinyl peptides in the cPILOT experiment. Overall, this total number results in 330 identified proteins in which 151 proteins were quantified. It is clear that the performance of the 12-plex experiment compared to the CysDML duplex experiment is lower with regards to total proteins identified and quantified. A very possible reason for this difference is that cPILOT analysis employed slower HCD $MS^3$ data acquisition. Using the same DDA duty cycle timing (~3 sec), the number of isolated and fragmented parent ions for CysDML and cPILOT is 15 and 7, respectively. Another major reason is the sample loss arising from multistep sample handling and cleanup in the cPILOT experiment. In lieu of GPF with the cPILOT experiment, we performed offline SCX separations. We believe that with the additional condensed phase separation sample loss occurred as another sample clean-up step is necessary between SCX fractionation and final LC-MS3 analysis. Furthermore, the detection of reporter ions relies on the generation of intense fragments that contain the iodoTMT tag. Based on the location of the cysteine residue relative to the N-terminus,

a)

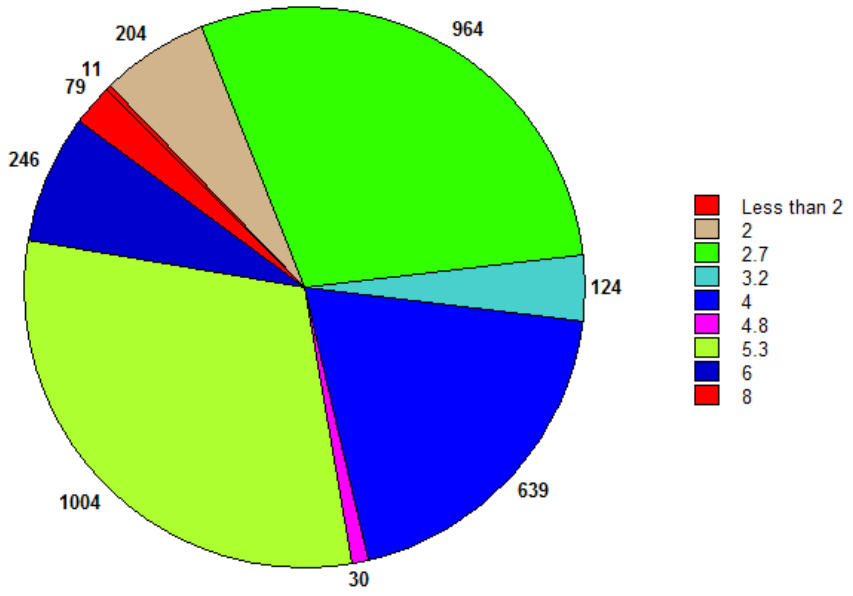


b)

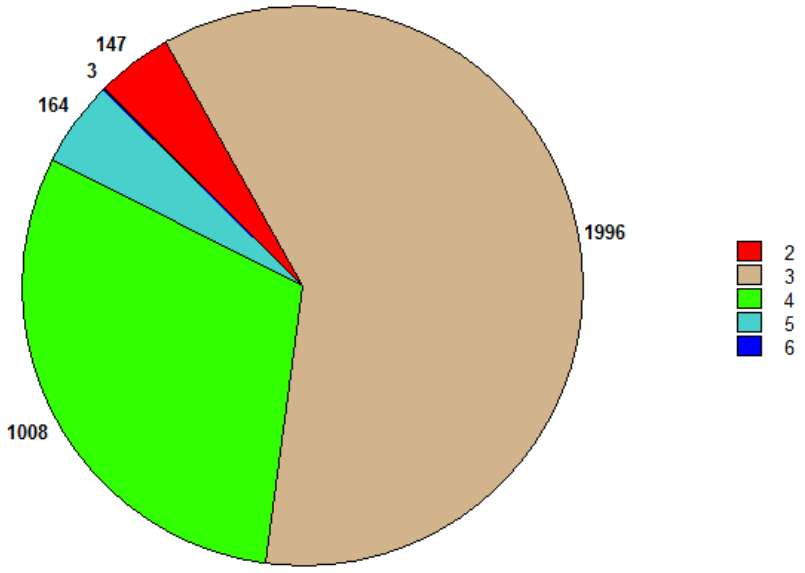


**Figure 4.7** Distribution of a) *m/z* spaces and b) charge states between light and heavy species of all PSMs in cPILOT experiment.

we observe that only half of HCD-$MS^3$ spectra result in reporter ions when the cysteine is within three positions relative to the N-terminus. Also, it appears that the enrichment efficiency of cysteinyl- peptides is lower for cPILOT (88.5% PSMs) compared to CysDML (98.3%). However, because we are reporting efficiency after derivatization of thiols with iodoTMT or IAM, it is possible that the labeling efficiency of cysteines with iodoTMT is also less. Detection of lower numbers of cysteinyl-peptides with cPILOT could be attributed to sample loss and lower $MS^3$ duty cycle. The latter occurred because excess iodoTMT reagent eluted throughout the course of the reversed-phase LC run and these contaminant ions were selected and fragmented numerous times. Finally, we noticed many instances whereby non-iodoTMT-tagged fragment ions were further selected for HCD-$MS^3$. As the most intense ions are selected for HCD-$MS^3$ this suggests that the instrument spent a great deal of time on ions that could not generate reporter ions. In the future we plan to remove these excess reagents as well as include these ions on a reject list and develop potentially more selective ion[53] or incorporate multinotch $MS^3$ [299] approaches. After application of stringent criteria, eleven proteins have statistically significant differential expression in liver from AD mice relative to WT from cysteine-selective cPILOT (Table 4.3).

### *4.3.5 Comparison of CysDML and cPILOT*

Both the CysDML and cPILOT approaches described herein, are novel methods to quantify cysteinyl-proteins in multiple samples simultaneously. The CysDML, duplex experiment, resulted in 2.5× more identified and quantified proteins in comparison to the cPILOT, 12-plex experiment. Although similar amounts of starting material where used for each experiment, the number of sample handling and sample cleanup and wash steps is substantially greater in the cPILOT approach. From the proteins identified with each method, 156 overlap and 1929 and 174 are unique

**Table 4.3** Differentially expressed proteins quantified from cPILOT experiment.

| Acc.no.[a] | Protein name | AD/WT[b] | $S_d$[c] | *p*-value[d] |
|---|---|---|---|---|
| A2A848 | Acyl-coenzyme A oxidase (Fragment) | 1.57 | 0.47 | 0.0006 |
| P05202 | Aspartate aminotransferase, mitochondrial | 0.71 | 0.24 | 0.0011 |
| H3BLB8 | Paraoxonase 1, isoform CRA_c | 0.70 | 0.27 | 0.0136 |
| Q9DBJ1 | Phosphoglycerate mutase 1 | 0.68 | 0.18 | 0.0005 |
| Q91Y97 | Fructose-bisphosphate aldolase B | 0.68 | 0.24 | 0.0001 |
| L7N451 | Interferon-induced very large GTPase 1 | 0.68 | 0.23 | 0.0140 |
| G3UX44 | Estradiol 17-beta-dehydrogenase 8 (Fragment) | 0.66 | 0.31 | 0.0439 |
| P15105 | Glutamine synthetase | 0.65 | 0.19 | 0.0009 |
| G3UYR8 | Alpha-aminoadipic semialdehyde dehydrogenase | 0.63 | 0.19 | 0.0001 |
| P99029-2 | Isoform cytoplasmic+peroxisomal of peroxiredoxin-5, mitochondrial | 0.52 | 0.18 | 0.0001 |
| J3QPZ9 | Enolase (Fragment) | 0.40 | 0.14 | 0.0001 |

[a]Accession number provided from the Uniprot mouse database (05/21/2014, 51344 sequences). [b]Average ratio of AD/WT. [c]Standard deviation. [d]*p*-value calculated from permutation test.

to the CysDML and cPILOT experiments, respectively. Thus there is good agreement in the proteins identified from both methods, however each approach can give new information not reported in the other method. Also, CysDML is more advantageous for deeper proteome coverage compared to cPILOT. Six CysDML experiments were completed compared to a single cPILOT experiment. However, if one is interested in generating a short list of starting candidates in a quick analysis, the cPILOT approach would be more beneficial.

Next, we compared the correlation in AD/WT ratios from CysDML and cPILOT experiments for all proteins quantified in six biological replicates regardless of *p*-values from statistical testing (Table 4.4) to better assess the performance of each method. In a majority of the cases, the AD/WT ratios are in good agreement (e.g., within ~20% error) between CysDML and cPILOT experiments. However, based on the results of statistical testing some proteins may not be considered as differentially-expressed in one or both methods. Furthermore, there exists a handful of proteins in which the AD/WT ratios are different between the CysDML and cPILOT experiments. In these cases, there are high standard deviation (>0.5) values across peptide ratios, differences in peptides detected and number of PSMs used for quantitation, and errors associated with variations in selection of peaks for MS/MS and HCD-$MS^3$ during data-dependent acquisition.

There are other considerations for sample multiplexing with CysDML or cPILOT. First, the number of necessary sample channels is important for determining if it is appropriate for a researcher to perform multiple duplex experiments or a single 12(or higher)-plex experiment. It could become rather cumbersome and time consuming to perform multiple combinatorial experiments to compare differences from more than two sample types with the CysDML approach. Whereas, with the cPILOT experiment every sample can be analyzed simultaneously with the noted tradeoff in breadth of proteome coverage. Incorporation of additional separation steps and

**Table 4.4** Proteins quantified in both experiments.

| Acc. No.[a] | Protein Name | CysDML | | | cPILOT | | |
|---|---|---|---|---|---|---|---|
| | | AD/WT[b] | $S_d$[c] | *p*-value[d] | AD/WT[b] | $S_d$[c] | *p*-value[d] |
| A2A848 | Acyl-coenzyme A oxidase (Fragment) | 1.46 | 1.04 | 0.4223 | 1.57 | 0.47 | 0.0006 |
| D3YZ54 | 2-hydroxyacyl-CoA lyase 1 | 1.09 | 0.23 | 0.4181 | 1.14 | 0.27 | 0.2848 |
| D3Z041 | Long-chain-fatty-acid--CoA ligase 1 | 1.04 | 0.15 | 0.7297 | 1.00 | 0.24 | 0.7662 |
| E9Q484 | 5-oxoprolinase (Fragment) | 0.90 | 0.13 | 0.1184 | 1.66 | 0.93 | 0.0146 |
| F8WIT2 | Annexin | 0.71 | 0.13 | 0.0001 | 0.85 | 0.24 | 0.1311 |
| G3UX44 | Estradiol 17-beta-dehydrogenase 8 (Fragment) | 1.00 | 0.28 | 0.7931 | 0.66 | 0.31 | 0.0439 |
| G3UYR8 | Alpha-aminoadipic semialdehyde dehydrogenase | 0.90 | 0.13 | 0.1251 | 0.63 | 0.19 | 0.0001 |
| H3BJI7 | Protein Mettl7a2Higd1c | 0.88 | 0.13 | 0.0494 | 0.81 | 0.18 | 0.0130 |
| O09173 | Homogentisate 1,2-dioxygenase | 1.02 | 0.14 | 0.8964 | 1.62 | 1.35 | 0.4210 |
| O35490 | Betaine--homocysteine S-methyltransferase 1 | 0.90 | 0.28 | 0.3071 | 0.72 | 0.22 | 0.0003 |
| O88844 | Isocitrate dehydrogenase [NADP] cytoplasmic | 1.04 | 0.14 | 0.5231 | 1.08 | 0.27 | 0.6399 |
| P05202 | Aspartate aminotransferase, mitochondrial | 1.29 | 0.56 | 0.2907 | 0.71 | 0.24 | 0.0011 |
| P07724 | Serum albumin | 0.84 | 0.15 | 0.0136 | 2.02 | 1.78 | 0.0448 |
| P08228 | Superoxide dismutase [Cu-Zn] | 0.72 | 0.18 | 0.0120 | 1.10 | 1.26 | 0.4258 |
| P08249 | Malate dehydrogenase, mitochondrial | 1.08 | 0.34 | 0.9507 | 0.84 | 0.16 | 0.0601 |
| P15105 | Glutamine synthetase | 0.82 | 0.33 | 0.1204 | 0.65 | 0.19 | 0.0009 |
| P24549 | Retinal dehydrogenase 1 | 1.12 | 0.30 | 0.4699 | 0.97 | 0.34 | 0.6036 |
| P26443 | Glutamate dehydrogenase 1, mitochondrial | 1.18 | 0.12 | 0.0001 | 0.86 | 0.23 | 0.1965 |
| P28474 | Alcohol dehydrogenase class-3 | 1.03 | 0.18 | 0.7972 | 0.75 | 0.18 | 0.0134 |
| P55264-2 | Isoform short of adenosine kinase | 1.27 | 0.52 | 0.2909 | 0.81 | 0.30 | 0.1686 |
| P63038 | 60 kDa heat shock protein, mitochondrial | 1.03 | 0.48 | 0.7183 | 0.88 | 0.24 | 0.2474 |
| P68368 | Tubulin alpha-4A chain | 1.09 | 0.30 | 0.6392 | 0.75 | 0.23 | 0.0136 |
| P97872 | Dimethylaniline monooxygenase [N-oxide-forming] 5 | 1.13 | 0.37 | 0.6649 | 0.81 | 0.26 | 0.1176 |
| P99028 | Cytochrome b-c1 complex subunit 6, mitochondrial | 1.11 | 0.69 | 0.7878 | 0.98 | 0.37 | 0.6367 |
| P99029-2 | Isoform cytoplasmic+peroxisomal of peroxiredoxin-5, mitochondrial | 0.92 | 0.22 | 0.3163 | 0.52 | 0.18 | 0.0001 |
| Q01853 | Transitional endoplasmic reticulum ATPase | 1.04 | 0.15 | 0.5979 | 0.80 | 0.35 | 0.0492 |
| Q3V0K6 | Kynurenine 3-monooxygenase | 3.67 | 6.01 | 0.2498 | 0.83 | 0.18 | 0.0414 |

*Continued on Page 100*

**Table 4.4** Proteins quantified in both experiments.

| Acc. No.[a] | Protein Name | CysDML | | | cPILOT | | |
|---|---|---|---|---|---|---|---|
| | | AD/WT[b] | $S_d$[c] | *p*-value[d] | AD/WT[b] | $S_d$[c] | *p*-value[d] |
| Q63880-2 | Isoform 2 of carboxylesterase 3A | 1.27 | 0.47 | 0.2585 | 0.80 | 0.23 | 0.0509 |
| Q6P3A8-2 | Isoform 2 of 2-oxoisovalerate dehydrogenase subunit beta, mitochondrial | 1.59 | 0.63 | 0.0473 | 1.04 | 0.43 | 0.8616 |
| Q6XVG2 | Cytochrome P450 2C54 | 1.18 | 0.57 | 0.5609 | 0.85 | 0.25 | 0.1228 |
| Q8BGT5 | Alanine aminotransferase 2 | 1.30 | 0.55 | 0.2580 | 1.18 | 0.45 | 0.5155 |
| Q8BH00 | Aldehyde dehydrogenase family 8 member A1 | 1.19 | 0.23 | 0.1230 | 0.80 | 0.18 | 0.0132 |
| Q8BMS1 | Trifunctional enzyme subunit alpha, mitochondrial | 1.01 | 0.18 | 0.9541 | 0.82 | 0.14 | 0.0001 |
| Q8C196 | Carbamoyl-phosphate synthase [ammonia], mitochondrial | 0.90 | 0.14 | 0.0842 | 0.81 | 0.21 | 0.0151 |
| Q8QZR5 | Alanine aminotransferase 1 | 1.66 | 1.19 | 0.0117 | 0.93 | 0.30 | 0.4005 |
| Q8VBW8 | Tetratricopeptide repeat protein 36 | 1.36 | 0.41 | 0.0766 | 0.75 | 0.29 | 0.0001 |
| Q8VCH0 | 3-ketoacyl-CoA thiolase B, peroxisomal | 1.25 | 0.28 | 0.0581 | 1.21 | 0.32 | 0.1415 |
| Q91X91 | Nicotinate-nucleotide pyrophosphorylase [carboxylating] | 1.07 | 0.44 | 0.9982 | 1.13 | 0.36 | 0.6188 |
| Q91XD4 | Formimidoyltransferase-cyclodeaminase | 1.06 | 0.35 | 0.9856 | 0.73 | 0.15 | 0.0001 |
| Q91Y97 | Fructose-bisphosphate aldolase B | 1.52 | 1.12 | 0.3734 | 0.68 | 0.24 | 0.0001 |
| Q922D8 | C-1-tetrahydrofolate synthase, cytoplasmic | 1.09 | 0.22 | 0.3899 | 1.17 | 0.30 | 0.2486 |
| Q93092 | Transaldolase | 1.00 | 0.15 | 0.8608 | 0.86 | 0.15 | 0.0543 |
| Q99KI0 | Aconitate hydratase, mitochondrial | 1.03 | 0.14 | 0.6775 | 0.77 | 0.17 | 0.0110 |
| Q99LB7 | Sarcosine dehydrogenase, mitochondrial | 1.03 | 0.15 | 0.6957 | 0.74 | 0.24 | 0.0006 |
| Q9CZ13 | Cytochrome b-c1 complex subunit 1, mitochondrial | 1.29 | 0.92 | 0.9196 | 1.06 | 0.39 | 0.9881 |
| Q9D8E6 | 60S ribosomal protein L4 | 1.01 | 0.18 | 0.9990 | 1.19 | 0.64 | 0.9857 |
| Q9DB77 | Cytochrome b-c1 complex subunit 2, mitochondrial | 1.03 | 0.32 | 0.9991 | 0.75 | 0.14 | 0.0003 |
| Q9DBJ1 | Phosphoglycerate mutase 1 | 0.99 | 0.29 | 0.7038 | 0.68 | 0.18 | 0.0005 |
| Q9DBM2 | Peroxisomal bifunctional enzyme | 1.18 | 0.21 | 0.0522 | 0.72 | 0.14 | 0.0001 |
| Q9DCW4 | Electron transfer flavoprotein subunit beta | 1.28 | 0.54 | 0.4343 | 0.67 | 0.38 | 0.0780 |
| Q9EQ20 | Methylmalonate-semialdehyde dehydrogenase [acylating], mitochondrial | 1.11 | 0.27 | 0.4578 | 0.77 | 0.21 | 0.0120 |
| Q9QXF8 | Glycine N-methyltransferase | 1.23 | 0.27 | 0.0568 | 0.93 | 0.10 | 0.1363 |

[a]Accession number provided from the Uniprot mouse database (05/21/2014, 51344 sequences). [b]Average ratio of AD/WT from six biological replicates. [c]Standard deviation. [d]*p*-value calculated from permutation test.

improvements to the cPILOT workflow to reduce sample handling steps and minimize sample loss, could significantly improve the proteome breadth of this approach. CysDML is a fairly inexpensive approach compared to cPILOT which involves the purchase of commercial isobaric tagging reagents. We maximized commercial reagents by using each iodoTMT[6] reagent vial to label two samples (75 µg for light and 75 µg for heavy dimethyl peptides). The use of isobaric reagents that could be synthesized in-house such as DiLEU tags[50,274] could help to reduce the cost of a cPILOT experiment while maintaining enhanced sample multiplexing capability. The CysDML sample preparation steps can be carried out in less than 24 hours while the cPILOTapproach can take up to two or three days. Overall, the cPILOT approach ends up taking less total experiment time as there is only one sample used for fractionation and smaller numbers of samples for MS acquisition. A major drawback to the CysDML approach is the limited amount of multiplexing capability that it has even with recent reports of five sample multiplexing with dimethyl labeling[40]. Currently we have demonstrated 12-plex analyses with cPILOT however note that further multiplexing is possible with the use of iTRAQ[8] reagents or TMT[10 286] reagents and additional stable-isotope precursors. The errors that arise from independent LC-MS/MS experiments in CysDML experiments are not present in cPILOT experiments, where all twelve samples are subject to the same exact MS conditions.

It must be noted that the enrichment of cysteine-containing peptides introduces additional sample handling steps that can increase variation in the workflow. In control CysDML experiments (Figure 4.3), accurate quantitation was obtained. Care was taken to ensure samples were treated similarly prior to the pooling steps. Normalization[55] of reporter ion signals was performed to help account for errors introduced from sample handling.

In both experiments, analysis of only cysteinyl-peptides dramatically simplifies precursor MS spectra relative to global dimethylation and cPILOT experiments. This simplification affords less spectral interference from closely-spaced precursors that are likely to be co-isolated and fragmented in global assays.

Shi et al. have identified one thousand proteins from mouse liver proteome in a single-run LC Orbitrap MS analysis[300]. Our analyses of liver tissue without enrichment generate similar results (data not shown). While enrichment of cysteine-containing peptides should allow for the same depth of proteome coverage, lower numbers of proteins are identified[140,264]. This could be attributed to several factors including minimal number of cysteine-containing peptides after enrichment for a given protein, peptides not being selected during a DDA experiment, and sample loss that can occur during the sample preparation steps as additional clean-up is necessary.

### *4.3.6 Differentially-Expressed Proteins in the Liver Proteome of an AD Mouse Model*

Herein CysDML and cPILOT methods identified 65 differentially-expressed proteins in liver tissue from an AD mouse model relative to WT controls. AD is a progressive neurodegenerative disorder and the most common form of dementia. Little is reported about changes in the liver proteome of AD patients or animal models. However, it is suggested that liver may be a major contributor to amyloid-β accumulation in the brain[301]. Liver has a wide range of functions including metabolism, biosynthesis of proteins and small molecules, as well as detoxification, however below the most interesting changes we have observed revolve around metabolism.

Several proteins have similar trends in differential-expression in AD in liver as compared to previously reported studies in AD brain and plasma: alpha-2-macroglobulin[302] and

hydroxymethylglutyaryl-CoA synthase[303] are higher in AD whereas ATP synthase subunit gamma[304,305], 14-3-3 zeta/delta[305,306], sodium/potassium-transporting ATPase subunit beta-1 ($Na^+/K^+$-ATPase)[304,305,307], phosphoglycerate mutase 1, enolase, and fructose-bisphosphate aldolase B[304,306,307] are lower in AD. One protein, superoxide dismutase [Cu-Zn] changes differently in liver tissue compared to brain for AD subjects. In liver, superoxide dismutase is lower in AD whereas in brain it has higher levels in AD[304,308]. Superoxide dismutase is a major protein targeted under oxidative stress in AD, and the Cys146 residue is irreversibly oxidized to cysteic acid[309]. In CysDML experiments, we detected a tryptic peptide containing Cys146 however it was unmodified. Oxidized cysteine residues are likely to be lost during the enrichment steps. Thus, while we observe lower levels of the unmodified peptide in AD mice, it is possible that our ratios would be different with detection of the oxidized version of the peptide.

The reactome pathway database[310] was used to provide biological processes related to the differentially-expressed proteins and here we focus on a few key aspects of metabolism.

First, carbohydrate metabolism appears to be altered in AD mouse liver. Phosphorylase, a protein involved in glycogenolysis is higher in AD mice relative to WT. Enzymes involved in glycolysis: fructose biphosphate aldolase, phosphoglycerate mutase, and enolase are lower in AD mice relative to WT. In the liver, glycogen synthesis and degradation regulate blood glucose levels. Higher phosphorylase suggests that high levels of glucose are generated in the liver, however, altered glycolysis implies that the glucose is not being utilized efficiently in this tissue. Hyperglycemia is a major risk factor for vascular injury associated with AD [311] and diabetes is also a risk factor for AD[312], and it is well known that lower glucose metabolism occurs in the brains of AD patients[166].

Second, our data suggest that lipid metabolism is augmented in AD mice. For instance, methylmalonyl-CoA mutase and acyl-CoA oxidase, enzymes involved degradation of long-chain fatty acids, are higher in AD mice. Changes in this pathway are consistent with other studies in our laboratory that have utilized global cPILOT methods to compare liver tissues in AD[54]. Another interesting finding is the increased level of ketogenesis. In AD brain, higher levels of ketone bodies were observed with the decrease of brain glucose uptake[313]. We observed higher levels of hydroxymethylglutaryl-CoA synthase in AD mice. This enzyme catalyzes the synthesis of acetoacetate, a major ketone bodies produced in ketogenesis. Ketone bodies migrate from the liver and enter the circulatory system. Ketone bodies have been suggested as alternative fuel for AD brain[166] and as a possible therapeutic approach of AD[314].

Finally, it appears that higher levels of ammonia that occur in the blood and brain of AD patients[315,316] may be linked to our observation of decreased consumption of ammonia by key enzymes in the liver. Aspartate aminotransferase and glutamine synthetase, involved in ammonia regulation, have lower levels in AD mice relative to WT. These lower levels suggest that ammonia is not being consumed by the liver and thus correlates well with reported higher levels of ammonia in blood and brain of AD subjects[315,316]. Hyperammonemia in the liver links to cognitive impairment in a model animal study[317].

## 4.4 CONCLUSIONS

Two novel cysteine-selective quantitative proteomics approaches were presented in this work: CysDML and cPILOT. These are two approaches that allow moderate and high levels of sample multiplexing in proteomics workflows. Based on our results, CysDML allows higher proteome coverage as compared to cysteine-selective cPILOT. However, cysteine-selective

cPILOT offers a more high-throughput approach to study many samples simultaneously. There are direct advantages and limitations to perform multiple duplex experiments or single 12-plex experiments, as we have thoroughly discussed. It is up to the researchers to design which approach is most suitable for their given research questions. Our application of both CysDML and cPILOT to the liver proteome from an AD mouse model resulted in identification of more than 2200 proteins, in which 65 were differentially-expressed in the AD model relative to WT controls. These are the first studies to report on changes in the liver proteome for this AD mouse model and AD in general. Many interesting findings, especially involved in metabolism occur in the liver of AD mice. A potential advantage of cysteine-selective proteomic approach is that it can couple with different thiol blocking and reducing techniques to study cysteine reversible modifications in complex samples. Cysteine is widely involved in many types of biological activities by forming different types of reversible modifications endogenously as described in **Chapter 2**. Characterization of the cysteine redox status using proteomic tools will benefit our understanding of neurodegenerative diseases, especially discovering the dysregulated molecular mechanisms involved. In **Chapters 5** and **6**, novel redox proteomics methods were developed based on the demonstrated CysDML and cPILOT methodologies. These methods provide quantitative information about cysteine reversible modifications in an AD mouse model.

# 5.0 A SIMPLE ISOTOPIC LABELING METHOD TO STUDY CYSTEINE OXIDATION IN ALZHEIMER'S DISEASE: OXIDIZED CYSTEINE-SELECTIVE DIMETHYLATION (OXCYSDML)

(Note that information in this chapter is written based on a published research paper[39], Gu, L.; Robinson, R. A. S. *Analytical and Bioanalytical Chemistry* **2016**, *408*, 2993-3004.)

## 5.1 INTRODUCTION

Proteins can be oxidized into a variety of post-translational modifications (PTMs)[318] and these oxidative PTMs have important biological relevance in both physiological and pathological conditions[68,74], which have been extensively reviewed in **Chapter 2**. Cysteine is one of the most susceptible amino acids and is subject to various oxidative PTMs[96]. These PTMs are involved in various cellular activities[64,319] and help maintain homeostasis under conditions of oxidative stress[320-322] as described in **Chapter 2**. Cysteine PTMs are of importance for fully understanding the physiological role of these cysteine in aging and disease[96].

Alzheimer's disease (AD) is a neurodegenerative disorder characterized by neurofibrillary tangles, senile plaques, and loss of synapses[185]. It has been widely accepted that oxidative stress plays an important role in AD pathogenesis[323]. Proteomic methods coupled with 2D gel electrophoresis and affinity enrichment have identified brain proteins that are significantly S-glutathionylated[169] or S-nitrosylated[123,171,176] in AD patients or transgenic mouse models relative to controls (more details about these studies were reviewed in **Chapter 2**). These modifications are likely due to elevated oxidative stress and are involved in various cellular pathways, such as glycolysis, calcium homeostasis and vesicle transport[169,171,176]. More recently, Cys113 oxidation of proline isomerase, Pin1, in postmortem AD brain has been associated with catalytic inactivity[178].

Gel-based and gel-free proteomic approaches have been applied in cysteine oxidative PTM characterization (**Chapter 2**)[324]. Briefly, due to some inherent limitations of gel-based approaches, gel-free approaches such as ICAT[32,101,138], iodoTMT[43,113,118] and resin-assisted mass tagging[99,100,119] are increasingly popular and can isolate and quantify cysteine PTMs from various biological samples with enhanced sensitivity.

On the other hand, multiplexing analysis of cysteine oxidation heavily relies on expensive isotope-coded reagents such as ICAT, TMT, and iodoTMT, which have been commercialized recently for the enrichment and detection of S-nitrosylation (SNO) from complex samples[43]. Because there are limited isotopic reagents that can be economically synthesized[274], there is still a demand to develop novel proteomic workflows to isolate, label, and quantify oxidized cysteines efficiently and cost-effectively. In this chapter we describe a new redox proteomic approach, oxidized cysteine-selective dimethylation (OxcysDML), an extension of our previous reported cysteine-selective dimethylation (CysDML) method in **Chapter 4**[38], to quantify cysteine oxidative modification levels from complex proteome samples. By using the CysDML method, 54 out of 2085 identified proteins exhibit significant alterations in AD liver tissue, and suggest dysregulated metabolic processes occur in AD, especially in carbohydrate metabolism, lipid metabolism, amino acid metabolism and ammonia regulation[38]. OxcysDML employs differential thiol labeling followed by thiol-affinity resin enrichment of cysteinyl peptides and on-resin stable-isotope dimethyl labeling. The thiol-affinity resin approach has superior enriching efficiency over biotin[107] or iodoTMT[113] techniques (>98% by spectral counts[38]), while solid-phase dimethyl labeling makes the workflow inexpensive and easy to perform[25]. To demonstrate its applicability to disease studies, we applied this method to quantify cysteine oxidation status in liver proteins from an AD mouse model and wild-type (WT) controls. Specifically, our approach first blocked unmodified cysteine

thiols with N-ethylmaleimide. After that proteins were treated to reduce total reversible cysteine modifications, which could be further captured by the thiol-affinity resin after tryptic digestion. Because a strong reducing reagent dithiothreitol is used prior to enrichment, all types of cysteine reversible modifications, e.g., S-nitrosylation (SNO), S-glutathionylation (SSG), S-palmitoylation, sulfenic acid and disulfide bonds are reduced to free thiols followed by resin capture. Irreversible modifications, including sulfinic and sulfonic acid, should not be enriched by this method. The on-resin isotopic dimethyl labeling enabled the relative quantification of site-specific cysteine modifications between WT and AD samples. The quantified ratios were normalized to protein expression abundances from our previously reported CysDML experiment (**Chapter 4**)[38]. After normalization, this method identified 828 *in vivo* oxidized cysteine residues from 527 liver proteins. Among them nineteen cysteine sites from seventeen proteins had significantly different cysteine oxidation levels in AD compared to WT. To the best of our knowledge, this is the first report of dimethylation-based methods to quantify cysteine oxidation from complex protein samples, and the first study to globally assess cysteine redox status in a peripheral organ system related to AD.

## 5.2 MATERIALS AND METHODS

### *5.2.1 Animals, Materials and Reagents*

Liver tissues from fourteen-month old amyloid precursor protein/presenilin-1 (APP/PS-1) double transgenic mice (AD) and wild type controls (WT) ($N$ = 6 for each genotype) were used in this study (see [38] for more details). Animal protocols were approved by the Institutional Animal Care and Use Committee at the University of Pittsburgh. Sodium cyanoborohydride ($NaBH_3CN$), formaldehyde (HCHO), formaldehyde - $^{13}C$, $^{2}H_2$ ($^{13}C^{2}H_2O$), N-ethylmaleimide (NEM), Thiopropyl Sepharose 6B resin, nitro blue tetrazolium chloride (NBT), trypsin from bovine

pancreas, anti-rabbit IgG alkaline phosphatase secondary antibody and formic acid were purchased from Sigma-Aldrich (St. Louis, MO). Iodoacetamide was purchased from Acros (Morris Plains, NJ). Sodium cyanoborodeuteride ($NaB^2H_3CN$) was obtained from Santa Cruz Biotechnology (Dallas, TX). Dithiothreitol (DTT) was purchased from Fisher Scientific (Fair Lawn, NJ). 5-bromo-4-chloro-3-indolyl phosphate (BCIP), spin column and BCA assay kit were purchased from Pierce Thermo (Rockford, IL). Deionized water was produced by a nanopure water system from Thermo (Rockford, IL). Protein carbonylation (PCO) measurement kit was from Millipore (Temecula, CA). All other chemicals were of analytical reagent grade.

### *5.2.2 Tissue Homogenization, Protein Digestion and Stable-isotope Dimethyl Labeling*

Liver tissues were homogenized in an ice-cold phosphate buffer saline (PBS, pH = 7.2) solution containing 8 M urea and 5 mM NEM. After BCA determination of protein concentration, each sample (100 µg protein) was diluted to a final concentration of 1 µg/µL with PBS (pH = 7.2) containing 8 M urea, 1% SDS and 50 mM NEM. Samples were incubated for two hours at room temperature in the dark. Excess reagents were depleted by acetone precipitation. The following procedures are similar to previous studies[38]. Briefly, proteins were dissolved in 50 mM Tris buffer with 8 M urea (pH = 8.2), reduced by 10 mM DTT for one hour at 37°C, and digested by adding 4% trypsin with overnight incubation at 37°C. After cleanup by Waters Oasis HLB $C_{18}$ cartridges, samples were lyophilized and enriched by Thiopropyl Sepharose 6B resin with one hour incubation at room temperature. Next, 11.2 µL of 4% $CH_2O/^{13}C^2H_2O$ and 11.2 µL of 0.6 M $NaBH_3CN/NaB^2H_3CN$ were added to WT and AD samples for light and heavy dimethylation labeling, respectively. After one hour incubation, 0.2% (v/v) concentration of ammonia was added to quench the reaction. 20 mM DTT was used to elute peptides, and 80 mM IAM was added to

alkylate sulfhydryl groups. Isotopically labeled WT and AD samples were randomly combined, and desalted using $C_{18}$ cartridges for LC-MS/MS analysis.

### *5.2.3 LC-MS/MS Analysis*

Online desalting and reversed-phase chromatography was performed with a Nano-LC system equipped with an autosampler (Eksigent; Dublin, CA). Mobile phases A and B were 3% (v/v) acetonitrile with 0.1% formic acid and 100% (v/v) acetonitrile with 0.1% formic acid, respectively. Sample (5 µL) was loaded onto a trapping column (100 µm i.d. × 2 cm), which was packed in-house with $C_{18}$ 200 Å 5 µm stationary phase material (Michrom Bioresource Inc.; Auburn, CA) at 3 µL/min in 3% mobile phase B for 3 min. The sample was loaded onto an analytical column (75 µm i.d. × 13.2 cm), which was packed in-house with $C_{18}$ 100 Å 5 µm stationary phase material (Michrom Bioresource Inc.; Auburn, CA). The following gradient was used: 0-5 min, 10% mobile phase B; 5-40 min, 10-15% B; 40-90 min, 15-25% B; 90-115 min, 25-30% B; 115-130 min, 30-60% B; 130-135 min, 60-80% B; 135-145 min, 80% B; 145-150 min, 80-10%B; 150-180 min, 10%B. The LC eluent was analyzed with positive ion nanoflow electrospray using a LTQ-Orbitrap Velos mass spectrometer (Thermo-Fisher Scientific; Waltham, MA).

OxcysDML samples were analyzed by employing gas phase fractionation (GPF). Specifically, each sample was injected six times and subjected to different mass spectrometry (MS) scans: the first to third injection) precursor scan over the *m/z* range 400-1700, fourth to sixth injections) *m/z* 400-777, *m/z* 762-902 and *m/z* 887-1700, respectively. The following data-dependent acquisition (DDA) parameters were used in each injection: the MS survey scan in the Orbitrap was 60 000 resolution; the top 15 most intense peaks in the MS survey scan were isolated

and fragmented with CID at an isolation width of 3 *m/z*; CID was performed in the ion trap with normalized collision energy 35%.

### *5.2.4 Data Analysis and Statistics*

RAW files were analyzed using the SEQUEST HT search engine with Proteome Discoverer 1.4 software (Thermo-Fisher Scientific; Waltham, MA) and searched against the Uniprot mouse database (Jan 7, 2015; 52639 sequences). SEQUEST HT search parameters of OxcysDML data are as follows: precursor mass tolerance 15 ppm; fragment mass tolerance 1 Da; static modifications light dimethyl/+28.031 Da (Lys) or heavy dimethyl/+36.076 Da (Lys); dynamic modifications light dimethyl/+28.031 Da (N-terminal) or heavy dimethyl/+36.076 Da (N-terminal), carbamidomethyl modification/+57.021 Da (Cys), N-ethylmaleimide/+125.048 Da (Cys), oxidation/+15.995 Da (Met). Decoy database searching was employed to generate medium ($p < 0.05$) and high ($p < 0.01$) confidence peptide lists. Only peptides containing cysteine residues with medium and high confidence were used further. Proteome Discoverer 1.4 provided peak area information for light and heavy labeled peptides and peptide ratio calculations. Peptide ratios were normalized based on the peptide median ratio in each biological replicate experiment. The resulting AD/WT cysteinyl peptide ratios were further normalized using the protein expression ratios [325] measured in an independent cysDML experiment[38]. The final peptide ratios were $\log_2$ transformed and subjected to permutation in MATLAB R2014a[38] to calculate the *p*-values. In addition to *p*-values, the average $\log_2$ ratios and the $\log_2$ standard deviations were calculated by EXCEL 2013 for each quantified peptide. Peptides measured in at least three biological replicates were further processed. From an independent experiment, we evaluated error of this method using an equimolar 1:1 light and heavy dimethylated liver tissue sample and analyzed by a single LC-MS/MS run. Based on these measurements, the overall CV of fold-change ratios (heavy/light) is

~ 30% (standard deviation = 0.38 on $\log_2$ scale, see Figure 5.1). This standard deviation level was used to perform FDR by generating a series of normal random numbers. First a stringent *p*-value of less than 0.01 was set as the *p*-value cutoff for the simulated peptides with different biological replicates (*N*). The calculated FDRs were 18%, 8%, 8% and 2% for *N* = 3, 4, 5 and 6, respectively. By adding criteria that also includes a $\log_2$ ratio cutoff of 0.38, the FDRs were 5%, 1%, 1% and 0.3% for *N* = 3, 4, 5 and 6, respectively. By increasing the $\log_2$ ratio cutoff from 0.38 to 0.50, the FDR is lowered to 1% for *N* = 3. For the analysis of AD liver tissue, we fixed the FDR to 1%, so that the ratio cutoff was 0.50 (for *N* = 3), 0.38 (for *N* = 4, 5 and 6), and a *p*-value cutoff (0.01) was required to determine redox-sensitive peptides. In addition, a standard deviation cutoff (0.70) was applied to filter out measurements with extreme variances as most of the standard deviations from repeated measurements do not exceed 0.70 from the simulation data (Table 5.1).

### *5.2.5 Oxidative Stress Measurement*

For protein carbonylation (PCO) measurement, five µL of each liver protein sample from WT (*N* = 6) and AD (*N* = 6) mice was incubated with 12% SDS and 20 mM 2,4-Dinitrophenylhydrazine (DNPH) solution for 20 min at room temperature. A neutralization solution was added to stop the reaction. Derivatized proteins (250 ng) were loaded onto a nitrocellulose membrane with a slot blot apparatus. The membranes were blocked with 3% (w/v) BSA solution overnight at 4℃ and incubated with a 1:2000 dilution of anti-DNP antibody for 2 hours. After rinsing the membrane, anti-rabbit IgG alkaline phosphatase secondary antibody was added with the dilution factor 1:5000 and incubated with the membrane for 1 hour. The membrane was washed in wash blot and developed using 5-bromo-4-chloro-3-indolyl phosphate (BCIP)/nitro blue tetrazolium chloride (NBT) colorimetric development. The blot was dried, scanned and slot

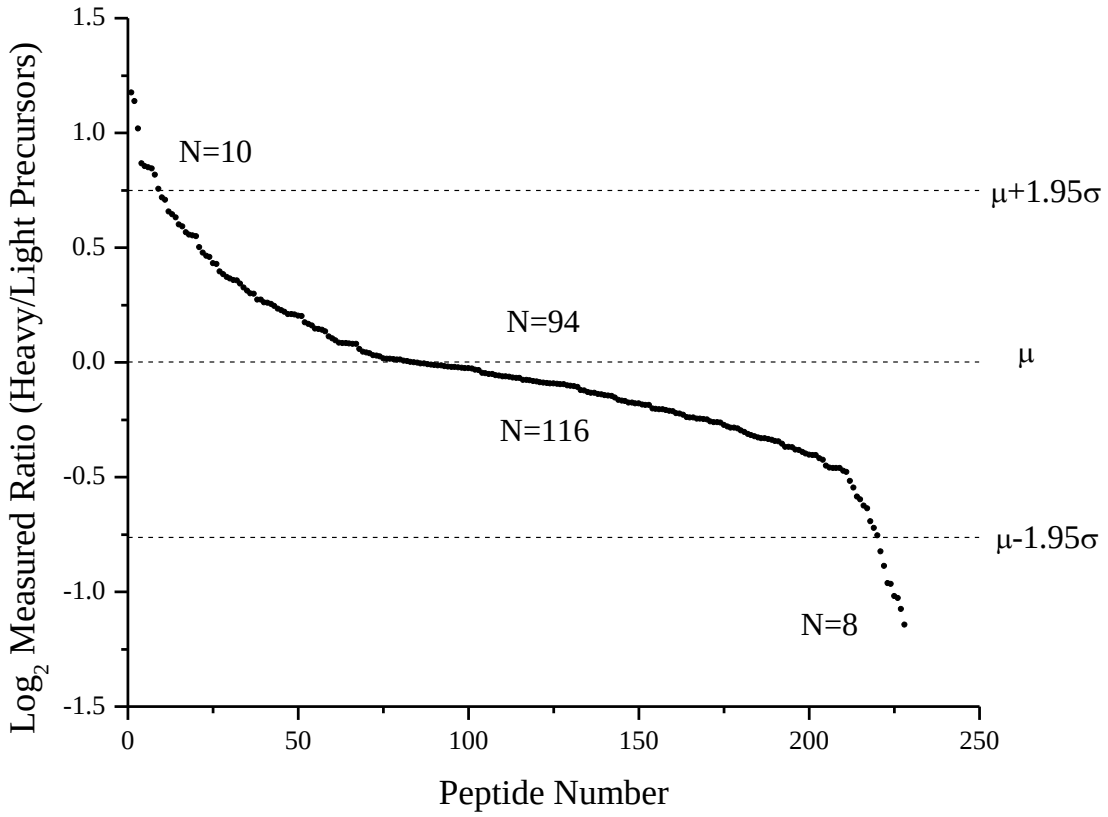


**Figure 5.1** Scatter plot of log2 peptide ratios measured in OxcysDML 1:1 experiment. Three horizontal lines represent average+1.95×standard deviation (upper 95% c.i.), average, and average-1.95×standard deviation (lower 95% c.i.), respectively. The quantified peptides within each region is labeled.

**Table 5.1** Summary of *p*-value, ratio and standard deviation (S.D.) cutoff used to determine redox-sensitive peptides.

| ***N*(Replicates)[a]** | **3** | **4** | **5** | **6** |
|---|---|---|---|---|
| FDR ($p$<0.01 & w/o ratio cutoff)[b] | 18% | 8% | 8% | 2% |
| Average $\log_2$ ratio cutoff[c] | >0.50 or <-0.50 | >0.38 or <-0.38 | >0.38 or <-0.38 | >0.38 or <-0.38 |
| $\text{Log}_2$ S.D. cutoff[d] | <0.7 | | | |
| FDR ($p$<0.01 & ratio cutoff)[e] | 1% | 1% | 1% | 0.3% |

[a]Replicates of simulation performed to mimic peptides quantified in different number of biological replicates. [b]FDR if only $p < 0.01$ filter is applied. [c]Ratio cutoff that is used. [d]Standard deviation cutoff based on the maximal standard deviation from the simulation data. [e]FDR if both $p < 0.01$ and ratio cutoff are applied.

profiles quantified using Scion Image. Statistical testing (student's t-test) was performed in Origin 8.0. The entire experiment was repeated twice.

## 5.3 RESULTS AND DISCUSSION

### *5.3.1 OxcysDML Methodology*

The three major steps in OxcysDML are reduction, isolation and dimethylation, as shown in Figure 5.2. Mouse liver tissues ($N$ = 6 for WT and AD) were homogenized in the presence of NEM (5 mM) to briefly block free thiols and minimize possible exchange between free thiols and oxidized thiols during protein extraction[326]. Next, a high dose of NEM (50 mM) was applied to each sample to further block all free thiols (buffer pH 7.2) and to minimize side reactions. Excess reagent was removed and proteins were treated with DTT to reduce any cysteine reversible modifications, such as disulfide bonds, S-sulfenylation, SNO, SSG and sulfenic acid. Here we applied a strong reducing reagent (i.e., DTT) to help capture multiple cysteine reversible modifications in order to gain global insight into cysteine oxidation status in AD. By using other reduction conditions, specific types of cysteine modifications (e.g., SNO, SSG) can be analyzed with OxcysDML[119]. Next proteins were digested with trypsin and the peptides containing newly-formed sulfhydryl groups were enriched by Thiopropyl Sepharose 6B resin and dimethylated[38]. WT and AD samples were labeled with light ($-C_2H_6$) or heavy ($-^{13}C_2{}^2H_6$) dimethyl tags, respectively. Peptides were eluted from the resin by DTT and alkylated by IAM. WT and AD samples were mixed and six samples were analyzed by LC-MS/MS. To improve proteome coverage with limited sample amount (estimated as ~24 µg in total), we used gas phase fractionation (GPF)[38,291]. In the dimethylation step, only two sample channels are labeled, which could be expanded to incorporate more samples by using sodium cyanoborohydride and

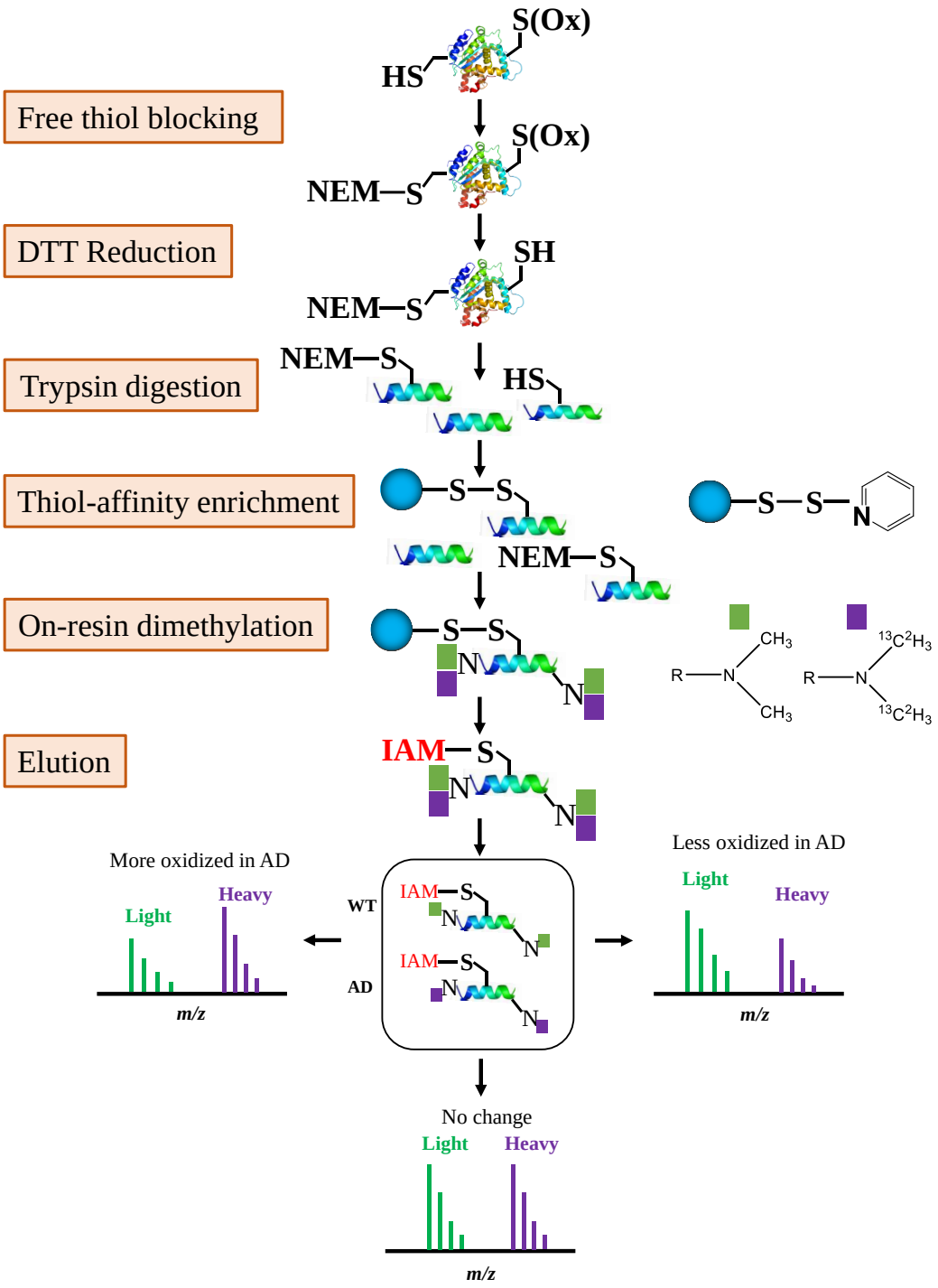


**Figure 5.2** Schematic representation of the oxidized cysteine-selective dimethylation (OxcysDML) redox proteomics workflow. Mouse liver proteins are treated with 50 mM NEM to block free sulfhydryl groups, then reduced with 10 mM DTT and digested. Reduced peptides containing newly-formed sulfhydryl groups are enriched by a thiol-affinity resin. WT and AD samples are labeled with light (-$C_2H_6$) and heavy (-$^{13}C_2{}^2H_6$) dimethyl tags respectively on the affinity resin. Peptides are eluted from the resin with 20 mM DTT and free cysteines are alkylated by iodoacetamide. WT and AD samples are combined, desalted and analyzed by LC-MS/MS.

formaldehyde containing different heavy atoms[40] or isobaric tagging methods[119].

The overall tagging efficiency and enrichment efficiency of OxcysDML is 97% and 99% (calculated by PSM), respectively. The flow through after enrichment consists of the cysteine-containing peptides that were NEM tagged (98.5% by PSM). The integration of the dimethylation reaction with peptide enrichment on the solid phase resin results in shortened sample handing time[109] and minimal sample loss. We have previously shown that our dimethylation labeling condition is sufficient for labeling all cysteinyl peptides isolated from 200 µg protein digest[38]. It is estimated that ~15% of total thiols are oxidized *in vivo*[64], therefore ~150 µg of oxidized cysteine-containing proteins can be isolated from 1 mg of tissue and tagged by OxcysDML. OxcysDML also has significant cost savings (<$1 US) due to the use of inexpensive isotopic reagents ($^{13}C^{2}H_2O$ and $NaB^{2}H_3CN$).

### *5.3.2 Application of OxcysDML to an AD Mouse Model*

To demonstrate the capability of cysteine redox quantification by OxcysDML method, we applied it to the liver proteome of an AD mouse model to gain insights into redox chemistry in AD. Based on cysteine occurrence (~14% of all *in silico* tryptic peptides) in the mouse proteome, it is estimated that only ~2% of tryptic peptides (~4 µg for each sample) are enriched and analyzed in OxcysDML.

Figure 5.3 displays some examples of MS and MS/MS spectra. The top panel shows a full scan of a triply charged peptide pair (light *m/z* = 818.754, heavy *m/z* = 821.435) that upon isolation of each peak and generated fragment ions is assigned to the sequence S(dimethyl)TEPC(IAM)AHLLVSSIGVVGTAEQNR from D-dopachrome decarboxylase. Independent MS/MS spectra of the light (black) and heavy (red) peaks are overlaid on the same

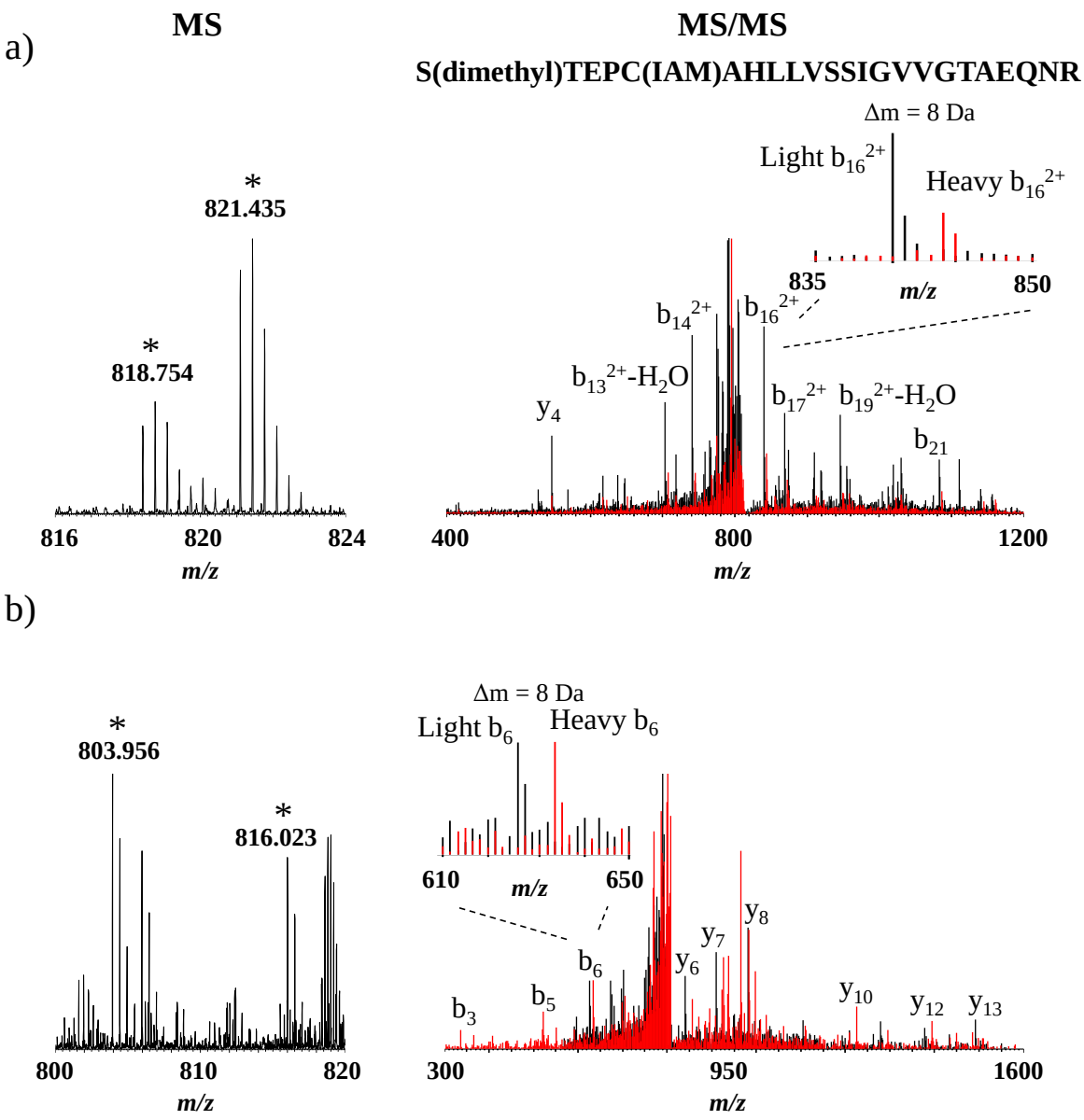


**Figure 5.3** Example OxcysDML MS and MS/MS spectra for: (a) pair of light (*m/z* = 818.754) and heavy (*m/z* = 821.435) peaks assigned to the triply charged peptide S(dimethyl)TEPC(IAM)AHLLVSSIGVVVGT AEQNR from D-dopachrome decarboxylase. MS/MS spectra of light (black) and heavy (red) peaks are overlaid. A zoomed-in spectra shows a mass shift of 8 Da for the $b_{16}^{2+}$ peaks representing the isotopic dimethylation on the N-terminus; (b) pair of light (*m/z* = 803.956) and heavy (*m/z* = 816.023) peaks assigned to the doubly charged peptide S(dimethyl)LVANLAAANC(IAM)YK(dimethyl)K(dimethyl) from isoform short of adenosine kinase. A zoomed-in spectra shows a mass shift of 8 Da for the $b_6$ peaks, representing isotopic dimethylation on the N-terminus.

spectrum. The isotopic dimethylation of the peptide N-terminus is indicated by an 8 Da mass shift between the pair. The cysteine residue labeled with IAM (Cys57) is reversibly oxidized *in vivo*. In order to determine if oxidation status changes with disease or external stimuli, it is required that the oxidative cysteine PTMs are normalized to total protein abundance levels. Our previously reported CysDML analysis of AD liver proteome (**Chapter 4**) was used to determine total protein abundance in WT and AD liver by focusing on cysteine-containing peptides (Appendix C Table 5.1)[38]. For the example shown in Figure 5.3a, peptide ratio data indicated no significant change of this modification in AD ($\log_2$(AD/WT) = 0.11, $p$ = 0.1785). However after normalization by the total protein abundance ratio, a significant increase is observed ($\log_2$(AD/WT) = 0.41, $p$ = 0.0001). Another peptide, S(dimethyl)LVANLAAANC(IAM)YK(dimethyl)K(dimethyl) from isoform short of adenosine kinase (Figure 5.3b), was quantified as not significant in AD liver tissue ($\log_2$(AD/WT) = -0.22, $p$ = 0.0139), and this significance was enhanced after normalizing to the total protein ratio ($\log_2$(AD/WT) = -0.47, $p$ = 0.0006). It must be noted that individual cysteine sites exhibit different oxidation status depending on sequence structure, solvent exposure, enzymatic function and cellular environment. This difference can be discriminated by quantifying cysteine oxidation at the peptide level, as most peptides contain only one cysteine residue.

In total, 808 peptides containing 828 reversibly oxidized cysteine residues from 527 proteins were identified in this work and they are listed in Appendix C Table 5.2. The most abundant oxidized cysteine site is Cys591 of serum albumin, a disulfide bond site identified by 638 MS/MS spectral counts. A large portion of proteins (192 out of 527) are identified by only one peptide (one spectral count), 211 one peptide (at least two spectral counts), and 124 two or more peptides, respectively (see Appendix C Table 5.2), which are consistent with other cysteine-redox proteomic studies[107,109]. Without using multi-dimensional separation techniques,

OxcysDML has comparable proteome coverage compared to ICAT[101] and iTRAQ-based methods[109] that used biotin as an enriching reagent and significantly higher proteome coverage in comparison to iodoTMT-based methods[113,118].

Quantitative analysis of the entire dataset involved a total of 323 peptides. These peptides were quantified by at least three biological replicates and were also measured with CysDML (see **Chapter 4**)[38], allowing us to obtain total protein abundance information (Appendix C Table 5.1). A major limitation of this work is that the relative quantification is mostly based on a single peptide for most proteins[109,116,118] whereas other applications have multiple peptides[38,54]. Because OxcysDML is evaluating low abundant *in vivo* oxidized cysteine modifications, it is critical to ensure that suitable criterion are employed to manage over interpretation of biologically insignificant results. So we applied the following stringent criteria to control the quality of the data: 1) we assessed the overall error of this method by an independent experiment, and the error was taken into consideration for determining appropriate ratio cutoff; 2) a strict *p*-value cutoff was applied; 3) FDR after using the above statistical criteria was verified using mathematical simulation; 4) six biological replicates were employed, and each peptide in Table 6.1 has at least four biological replicates and ten spectral identifications from multiple technical replicates; 5) protein ratios were used to normalize peptide ratios for unbiased quantification. This resulted in seventeen redox-sensitive peptides that have statistically significant ($p < 0.01$) different cysteine oxidation levels in AD mice compared to WT by at least 30% (Table 5.2 and Figure 5.4). A subset of these peptides have very small *p*-values ($p < 0.0001$) (Figure 5.4). Permutation test is an ideal statistical test for quantitative proteomic data to provide p-values without further adjustment[327]. However the *p*-value only indicates the mathematical probability of the null hypothesis ($H_0$: $\mu = 0$, no significant change), regardless of the degree of change. In an independent experiment, we

**Table 5.2** Redox-sensitive cysteine identified in AD and WT mouse liver tissues.

| Sequence[a] | Acc. No.[b] | Protein Name | # PSM[g] | $Log_2$ (AD/WT)[c] | S.D.[d] | *p*-val[e] | N[f] | Modification[h] |
|---|---|---|---|---|---|---|---|---|
| SLVANLAAANC$_{(159)}$YKK | P55264-2 | Isoform Short of Adenosine kinase | 102 | -0.47 | 0.26 | 0.0006 | 6 | |
| LC$_{(119)}$EAIC$_{(123)}$PAQAITIEAEPR | Q8K3J1 | NADH dehydrogenase [ubiquinone] iron-sulfur protein 8, mitochondrial | 67 | -0.80 | 0.45 | 0.0001 | 6 | Metal binding; Iron-sulfur 1 (Cys119) & 2 (Cys123) |
| AIAQSSVIFNPC$_{(254)}$LFGR | Q8VCC2 | Liver carboxylesterase 1 | 53 | 0.53 | 0.35 | 0.0001 | 6 | |
| LLQLAC$_{(168)}$PGTGEADAR | Q8K1B3 | Gltpd2 protein | 35 | -1.26 | 0.58 | 0.0003 | 6 | |
| ADHQPLTEASYVNLPTIALC$_{(148)}$NTDSPLR | P14206 | 40S ribosomal protein SA | 31 | 0.39 | 0.23 | 0.0010 | 6 | |
| STEPC$_{(57)}$AHLLVSSIGVVGTAEQNR | O35215 | D-dopachrome decarboxylase | 29 | 0.41 | 0.21 | 0.0001 | 6 | |
| TLTQC$_{(85)}$SWLLDGFPR | Q9WTP7 | GTP:AMP phosphotransferase AK3, mitochondrial | 28 | 0.39 | 0.24 | 0.0002 | 6 | |
| MTNGFSGADLTEIC$_{(691)}$QR | Q01853 | Transitional endoplasmic reticulum ATPase | 26 | -0.41 | 0.25 | 0.0001 | 5 | |
| NQEAMGAFQEFPQVEAC$_{(107)}$R | D3YZ54 | 2-hydroxyacyl-CoA lyase 1 | 22 | 0.54 | 0.49 | 0.0001 | 5 | |
| SAFEYGGQKC$_{(347)}$SAC$_{(350)}$SR | Q8CHT0 | Delta-1-pyrroline-5-carboxylate dehydrogenase, mitochondrial | 22 | -0.52 | 0.55 | 0.0001 | 5 | Active site; Nucleophile (Cys347) |
| GALVTVGQLSC$_{(180)}$YDQAK | Q9QZD8 | Mitochondrial dicarboxylate carrier | 17 | -1.46 | 0.17 | 0.0001 | 4 | |
| NNPAIVVIGNNGQINYDHQNDGATQALA SC$_{(182)}$QR | D3Z5B9 | Protein ERGIC-53 (Fragment) | 16 | -0.84 | 0.49 | 0.0001 | 6 | Disulfide |
| NILGGTVFREPIIC$_{(154)}$K | P54071 | Isocitrate dehydrogenase [NADP], mitochondrial | 16 | 0.66 | 0.30 | 0.0011 | 4 | |
| LC$_{(88)}$LTGQWEAAQELQHR | E9Q1R2 | 4-hydroxy-2-oxoglutarate aldolase, mitochondrial | 14 | 1.59 | 0.38 | 0.0001 | 6 | |
| DC$_{(177)}$LIPMGITSENVAER | Q8VCH0 | 3-ketoacyl-CoA thiolase B, peroxisomal | 10 | 0.58 | 0.51 | 0.0078 | 4 | |
| LADIGAC$_{(171)}$AQIVHK | Q8VCN5 | Cystathionine gamma-lyase | 10 | -0.67 | 0.13 | 0.0001 | 4 | |
| TAC$_{(377)}$YGHFGRSEFPWEVPK | Q91X83 | S-adenosylmethionine synthase isoform type-1 | 10 | 0.55 | 0.28 | 0.0001 | 4 | |

[a]Peptides are grouped by sequence. [b]Accession number provided from the Uniprot mouse database (Jan 7, 2015; 52639 sequences). [c]Average AD/WT ratior on log2 scale. [d]Standard deviation of log2(AD/WT). [e]*p*-value calculated from permutation test. [f]Number of biological replicates quantified. [g]Number of peptide spectra matchings. [h]Modification information is obtained from Uniprot database.

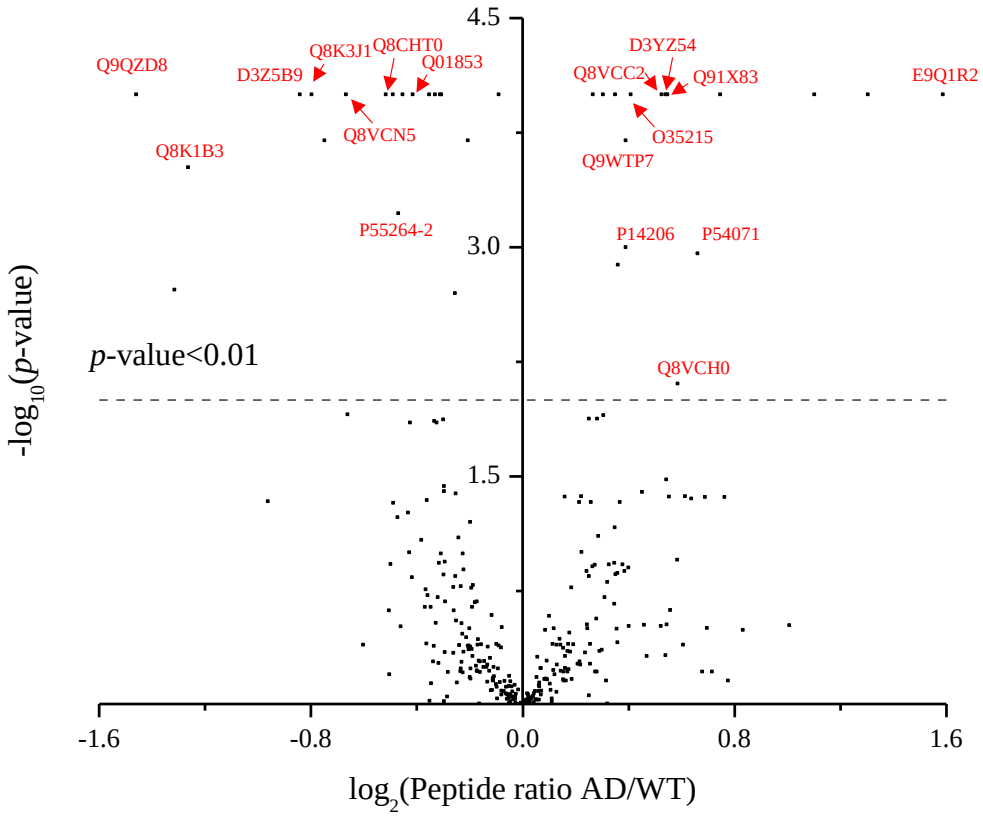


**Figure 5.4** Volcano plot displaying the difference in the levels of peptides containing oxidized cysteine between AD and WT liver. $Log_2$ peptide ratios are plotted against negative $log_{10}$ *p*-values. The accession numbers of proteins containing redox-sensitive cysteine are labeled. Because permutation operation was repeated 10000 times in the statistical algorithm, all probabilities less than 1/10000 would not be discriminated, and the *p*-value of them would be 0.0001, resulting in a horizontal line in the volcano plot.

evaluated the error of this method using an equimolar 1:1 light and heavy dimethylated liver tissue sample and analyzed by a single LC-MS/MS run. Based on this measurement, the overall CV of fold-change values was ~30%, which is slightly larger than most quantitative proteomic approaches (~20 - 25%)[297]. We believe this larger variation is a result of OxcysDML quantification on single peptides in most cases, instead of many peptides as in global protein analyses. We found that using 30% change as the ratio cutoff is sufficient for peptides quantified by four, five and six biological replicates to determine biological significance (FDR ≤ 1%). However a higher ratio cutoff is needed for peptides with three biological replicates (Table 5.1) in order to keep the FDR ≤ 1%. This restriction resulted in no redox-sensitive peptides with statistically significant differences in oxidization level being reported for $N = 3$ (Table 5.2). By using the combination of *p*-value and ratio cutoff, the FDR is no more than 1% for all peptides (Table 5.1). The seventeen redox-sensitive peptides with statistical significance are listed in Table 5.2, in which nine peptides have higher levels of oxidized cysteine in AD mice, whereas the other eight peptides have lower levels of oxidized cysteine in AD mice relative to WT. In comparison with other cysteine-redox proteomic studies[101,109], the number of redox-sensitive peptides obtained by OxcysDML are fewer, this is because: 1) no oxidizing reagent (e.g. hydrogen peroxide) is used for enhancing protein oxidation; 2) stringent criterion is utilized to determine redox-sensitive peptides. The most abundant redox-sensitive peptide in the list is SLVANLAAANC$_{(159)}$YKK from isoform short of adenosine kinase, and it was observed and quantified in all six biological replicates. The least abundant redox-sensitive peptides are DC$_{(177)}$LIPMGITSENVAER from 3-ketoacyl-CoA thiolase B, LADIGAC$_{(171)}$AQIVHK from Cystathionine gamma-lyase and TAC$_{(377)}$YGHFGRSEFPWEV PK from S-adenosylmethionine synthase isoform type-1, in which we detected ten PSMs for each across four biological replicates. This data indicates that we measured redox-sensitive peptides

with a dynamic range of abundance over ~ two orders of magnitude. This result is also consistent with our previous investigation of the dynamic range in cysDML approach[38], however experiments to measure the dynamic range in OxcysDML would be necessary. On the other hand, the highest and lowest $\log_2$ ratios in Table 6.1 are 1.59 and -1.46 (3.01 and 0.36 on normal scale, respectively), indicating the capability of measuring changes up to 3-fold in *in vivo* AD tissues.

The REACTOME database was employed to categorize the identified proteins with regard to biological pathways (Figure 5.5). Approximately 39% of the identified proteins belong to the metabolic pathway (139 out of 358, see Figure 5.5a), a proportion that is consistent with the mouse liver proteome[300]. A redox proteomic study of mouse liver mitochondria under Cadmium exposure indicates the broad involvement of cysteine redox chemistries in liver enzymatic pathways[328], which is consistent with our finding that metabolism is the most prominent pathway associated with cysteine reversible modifications in mouse liver. Proteins belonging to metabolism are further categorized (Figure 5.5b), in which energy-related metabolic pathways, including metabolism of amino acid and derivatives, metabolism of carbohydrates, metabolism of lipids and lipoproteins, the citric acid cycle and respiratory electron transport as well as biological oxidation are the predominant pathways (Appendix C Table 5.3). Network analysis using STRING (version 10) also shows that the identified proteins cover several basic molecular pathways in liver, e.g. amino acid metabolism, pyruvate metabolism, citrate cycle, glycolysis/gluconeogenesis and fatty acid degradation ($p < 0.05$, $n > 5$) (Figure 5.6). Redox-sensitive proteins in AD (Table 5.2) classify to metabolic pathways of amino acid, carbohydrates and lipids (Figure 5.5b) indicating the potential alteration of energy production and utilization in AD mouse liver tissue. This is consistent with: 1) dysregulated metabolic processes such as β-oxidation, pyruvate metabolism and glucose regulation in AD liver[54]; 2) alterations in carbohydrate metabolism, lipid metabolism and amino

a)

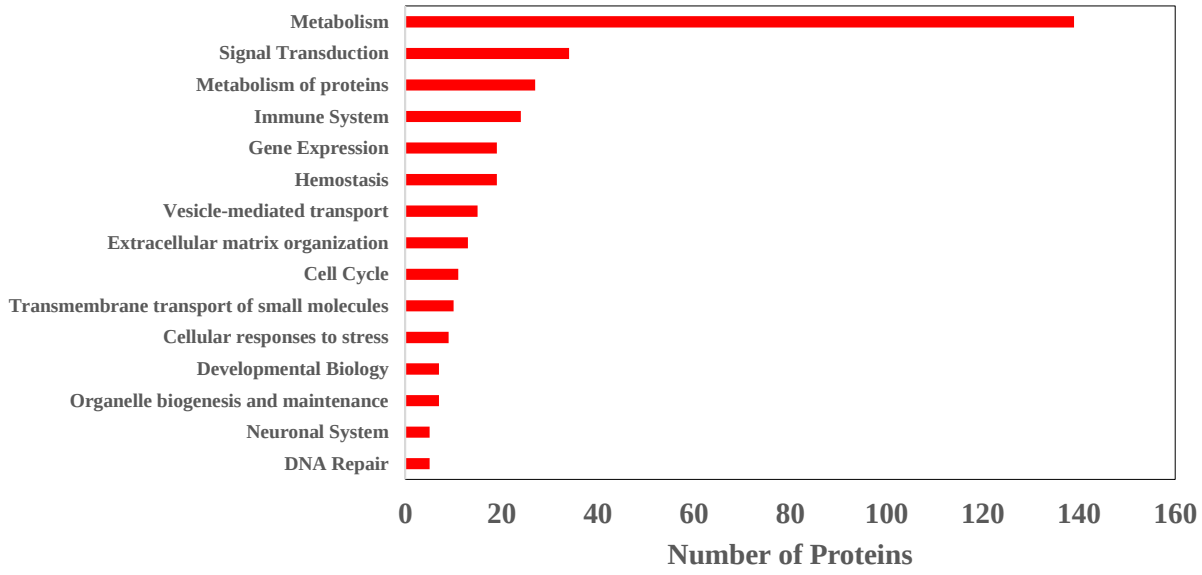


b)

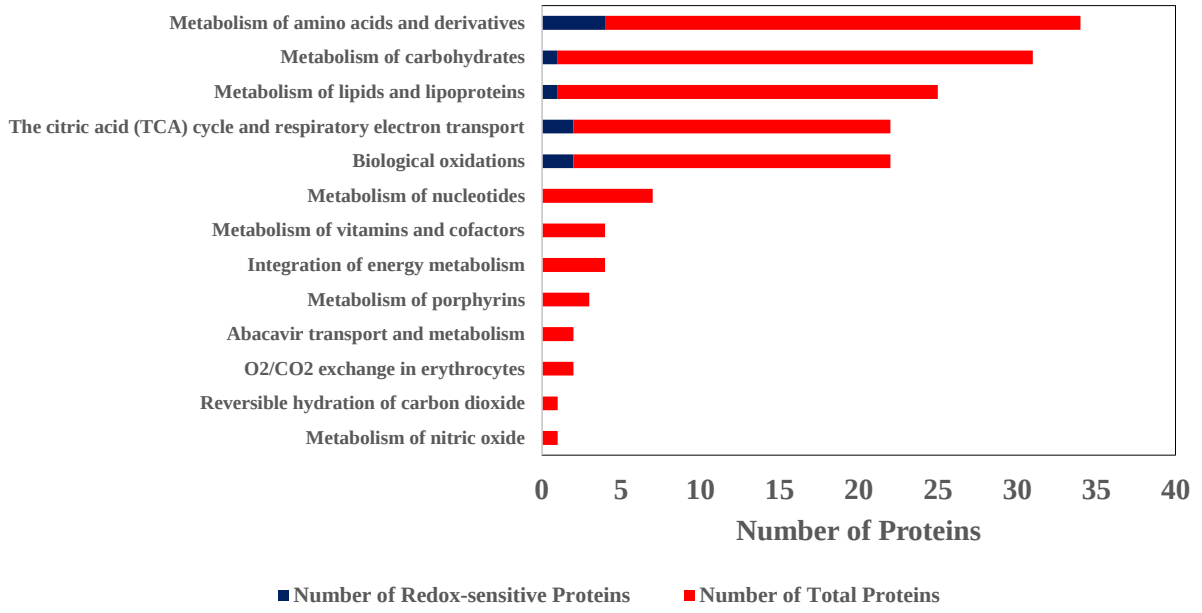


**Figure 5.5** Histogram plot of a) biological pathways and b) metabolism pathways associated with identified proteins ($N$ = 827) obtained from the REACTOME database. Redox-sensitive protein levels are indicated in b) with blue color.

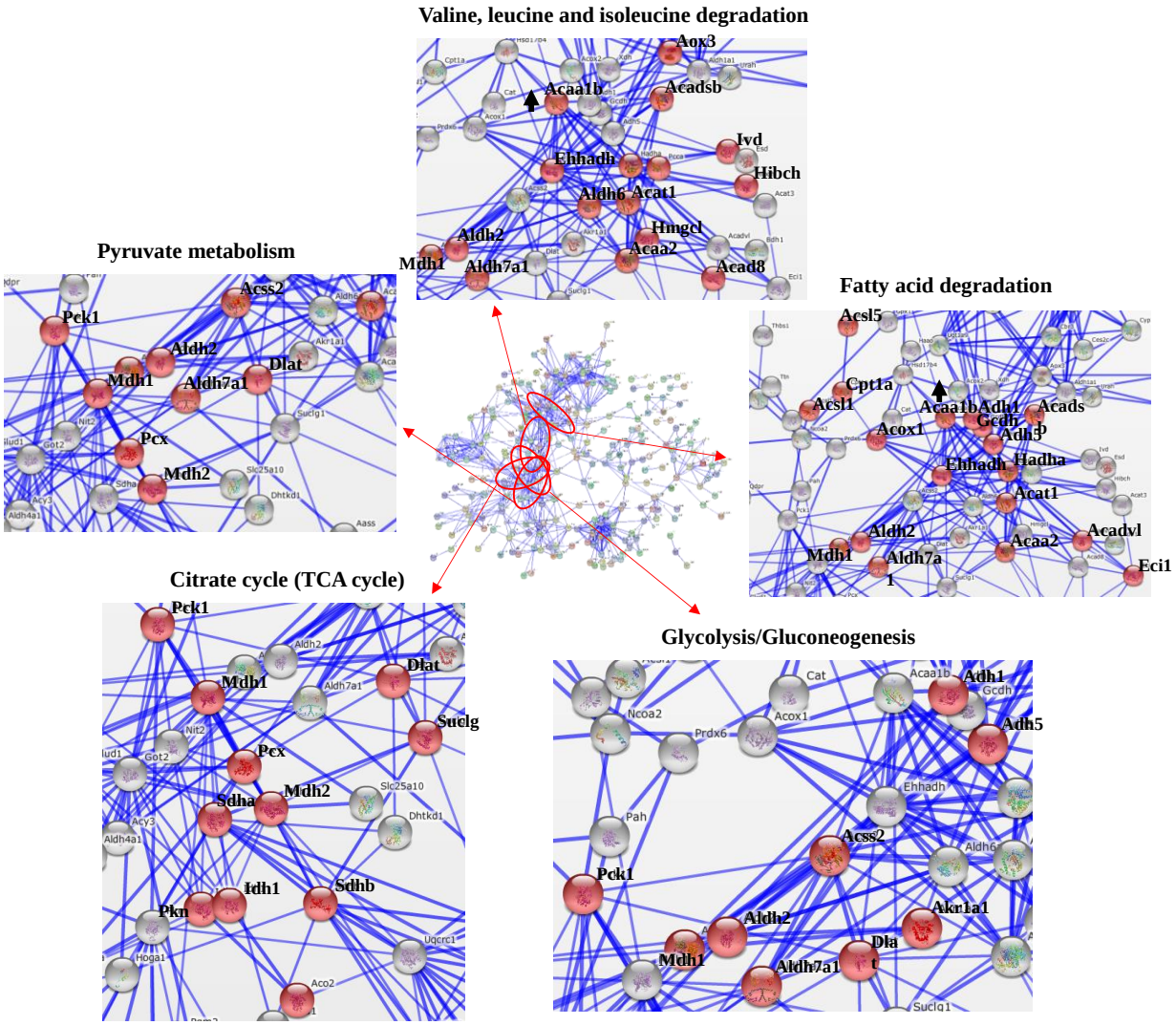


**Figure 5.6** Interaction network of identified Mus Musculus liver proteins containing modified cysteine in vivo by OxcysDML approach. Zoom-in details represent example pathways significantly enriched in the dataset (*p*-value < 0.05, n > 5). Red dots indicate the identified proteins by OxcysDML. Uniprot accession numbers were uploaded to STRING (version 10) and returned as gene symbols. Network analysis was performed using STRING (version 10) with confidence view and confidence score of 0.700, no text mining was used. Examples of proteins containing redox-sensitive cysteine as well as the direction of change in AD are highlighted.

acid metabolism[38]; and 3) differential SNO of proteins involved in energy metabolism and oxidative phosphorylation[176]. Further examination of redox-sensitive cysteine residues in Uniprot[329] was used to help with biological interpretation of changes in cysteine status. For example, Cys347 of delta-1-pyrroline-5-carboxylate dehydrogenase is an active site for catalysis[330], Cys119 and Cys123 of NADH dehydrogenase [ubiquinone] iron-sulfur protein 8 are sites for iron metal binding to form two 4Fe-4S clusters [55]) (Table 5.2). A rare situation is that a single peptide may contain multiple modified cysteine sites, in which the OxcysDML method is not able to differentiate their individual redox status, e.g., modified Cys119 and Cys123 of NADH dehydrogenase [ubiquinone] iron-sulfur protein 8 are identified from the same peptide. In this case we assigned the potentially oxidized cysteine sites based on MS/MS sequencing data individually, and we treat the peptide as a whole for quantitative analysis[176].

### *5.3.3 Proteins Containing Redox-sensitive Cysteine in AD Mouse Liver Tissue*

AD is a progressive neurodegenerative disorder and the most common form of dementia[331]. Our previous studies of peripheral organs and cells in an AD mouse model indicated dysregulated metabolic pathways in liver tissue[38,54] and elevated oxidative stress in T cells[189]. Although oxidative stress-induced cysteine PTMs (e.g. SNO, SSG) in AD have been reported, most of these studies were focused on brain tissue and used gel-based methods[123,124,147,176,324,332]. The role of peripheral organs involved in AD is still not clear. Liver is an organ with known metabolic, biosynthetic and detoxification functions and some studies have linked the liver to AD pathogenesis. For example, the neuroprotective fatty acid docosahexaenoic acid (DHA), is synthesized in liver and is helpful for decreasing amyloid beta (Aβ) deposition[333]. Liver may involve the clearance of Aβ deposition by expressing liver low-density lipoprotein receptor-related protein (LRP)[334]. Characterization of cysteine reversible oxidations in liver proteins facilitates

understanding of global processes involving cysteine redox switching, and the role that oxidative stress plays systemically in AD.

Interestingly, half of the proteins (eight out of seventeen) listed in Table 6.1 belong to metabolism, which is consistent with our previous work of liver proteome quantification using CysDML and cPILOT (**Chapter 4**)[38,54]. Among various metabolic processes, lipid metabolism, including ketone bodies synthesis and β-oxidation, is considered as a major source of reactive oxygen species (ROS). Two proteins involved in lipid metabolism, including peroxisomal 3-ketoacyl-CoA thiolase B and 2-hydroxyacyl-CoA lyase 1, are found to be in a more oxidized state in AD, which may be due to the overwhelmed oxidative stress associated with lipid metabolism. To further explore this, we measured the relative abundance of protein carbonylation (PCO) levels in liver proteins from WT and AD mice. PCO is a widely used biomarker for protein oxidative stress (**Chapter 2**). Our data (Figure 5.7) indicates there is a significantly elevated PCO level in AD mouse liver compared with WT ($p < 0.01$). Oxidative stress plays an important role in the AD pathogenesis as it has been demonstrated in brain[186], plasma[187], heart[188] and the immune system[188,189]. The liver is an organ that is susceptible to oxidative stress due to its high nature of metabolic activities[335]. The dysregulated metabolic processes, such as β-oxidation as we identified before[54], may contribute to the increased oxidative stress in AD liver. This is especially true for the β-oxidation occurred in peroxisomes, in which high-potential electrons generated by oxidative reaction are transferred to oxygen molecules and result in hydrogen peroxide[336]. Hydrogen peroxide is a well-known ROS species in cellular environment. 3-ketoacyl-CoA thiolase B is a peroxisomal enzyme catalyzing the fourth step of β-oxidation to cleave β-ketoacyl CoA and shorten the carbon chain. Our data indicates that Cys177 of 3-ketoacyl-CoA thiolase B has an ~ 50% elevated oxidation in AD liver compared with WT, which may suggest that a dysregulated

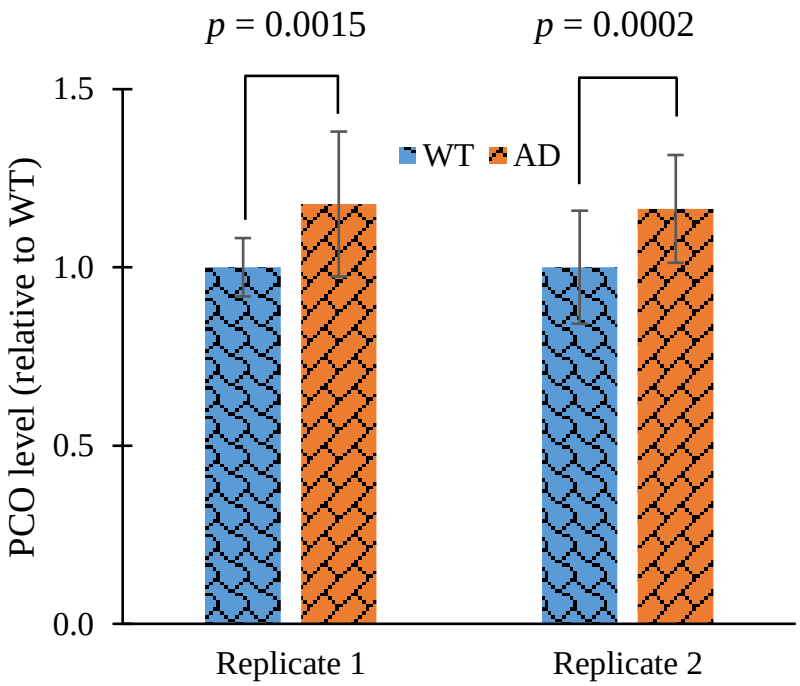


**Figure 5.7** Histogram plot of protein carbonylation (PCO) levels in liver proteins isolated from WT (*N* = 6) and AD (*N* = 6) mice. Intensities are normalized to WT. Error bar: ±standard deviation. *P*-values are provided. Replicates 1 and 2 are technical replicates.

lipid metabolism in AD liver is accompanied by oxidative stress.

## 5.4 CONCLUSIONS

This work described the OxcysDML method, which uses on-resin enrichment and isotopic dimethylation labeling. We demonstrated this method using liver from an AD mouse model, however it can be applied to many other biological samples (e.g. cell lysates, serum, brain etc.). The simple, efficient, and inexpensive nature of the OxcysDML method makes it amenable for studies involving comparisons of two conditions. The sample processing steps involved in the OxcysDML method, include reduction and dimethylation, and can be modified to accommodate the investigation of specific types of oxidative cysteine PTMs by varying the reducing reagent. Oxidized cysteinyl peptide ratios were corrected with global protein expression changes using independent cysDML data. Redox-sensitive proteins in the AD liver proteome widely participate in metabolic processes of glucose, lipids and amino acids, which provides additional evidence for dysfunctional metabolism in AD. The contributions of these changes in the liver to AD pathogenesis requires further investigation. Future directions include the incorporation of additional isotopic channels into the OxcysDML workflow to obtain oxidation level and total abundance data in a single run and comparing stoichiometries of cysteine status across modification types. In addition, it would be more helpful to isolate and quantify a specific type of cysteine modification from tissue samples. For example, SNO is an important cysteine PTM in redox signaling and shows both neuroprotective and neurodestructive effects in AD. In **Chapter 6** an enhanced multiplexing approach to characterize endogenous SNO from AD model mouse is discussed.

# 6.0 HIGH-THROUGHPUT ENDOGENEOUS MEASUREMENT OF S-NITROSYLATION IN ALZHEIMER'S DISEASE USING OXIDIZED CYSTEINE-SELECTIVE CPILOT

(Note that information in this chapter is written based on a published research paper[141], Gu, L.; Robinson, R. A. S. *Analyst* **2016**, DOI: 10.1039/c6an00417b)

## 6.1 INTRODUCTION

Cysteine is an important amino acid in biology as it can be endogenously oxidized into a number of oxidative post-translational modifications (PTMs) and these modifications are widely involved in biological activities such as cellular redox status, signaling and enzymatic catalysis[64,68,83,96,320] (see **Chapter 2**). Among them, S-nitrosylation (SNO) is key to cellular signaling processes similar to other majors PTMs such as phosphorylation[337,338] and can influence protein conformation, activity, protein-protein interactions, transcription, autophagy, apoptosis and DNA repair[339,340]. As opposed to some oxidative modifications that may occur sporadically to proteins, SNO is believed to be highly regulated and occur at specific cysteine sites[76]. SNO is critical in disease pathogenesis[339], especially in the context of neurodegenerative diseases[63,340]. SNO has been linked to protein aggregation and misfolding, mitochondrial dysfunction, synaptic injury, neuronal loss, impaired metabolism and autophagy in Alzheimer's disease (AD)[63]. While these are detrimental consequences of SNO that likely occur with high concentrations of NO derived from environmental toxins, this PTM can be neuroprotective AD and has been used as a therapeutic target[341]. Many proteins have been S-nitrosylated in tissues of AD patients or models, including: cyclin-dependent-like kinase 5 (Cdk5), apolipoprotein E (ApoE), tubulin, glyceraldehyde-3-phosphate dehydrogenase (GAPDH), voltage-dependent anion-selective

channel protein (VDAC), superoxide dismutase [Mn] (SOD2) and heat shock protein HSP 90 (HSP90)[63].

There are noted challenges to studying SNO on a global scale, which include its reversible nature as it can be denitrosylated/transnitrosylated enzymatically, its low abundance, and its potential occurrence at multiple cysteine sites in a protein[96,342]. Redox proteomics however, provides tools with which SNO can be studied for individual proteins or globally in an entire proteome. Several approaches, which use different techniques of affinity purification, chemical derivatization and mass spectrometry (MS)[43,98,100,113,116,118,123,126,137], been developed and have been recently reviewed[74,82,83,96,343] (see **Chapter 2** for more details). Among all available methods, isobaric tagging such as iodoTMT, TMT, or the inclusion of iTRAQ[100] allow greater sample multiplexing capabilities (i.e., up to eight samples can be analyzed simultaneously). In **Chapter 5**, we developed a simple, straightforward, and robust approach to measure oxidized cysteine in global proteome experiments, through coupling on-resin capture of cysteines and isotopic dimethylation reactions[39]. This approach, called OxcysDML, could be readily modified to study SNO by exchanging the dithiothreitol reducing agent with ascorbate. Ours and other methods[118,138] however, require additional experiments in order to normalize the SNO modification levels to total protein abundance and have limited sample throughput (i.e., can only multiplex two to six samples).

In order to help improve the sample multiplexing capability of measuring SNO in a global fashion and the sensitivity to measure endogenous levels of SNO in biological tissues, we developed an oxidized cysteine-selective combined precursor isotopic labeling and isobaric tagging (OxcyscPILOT) strategy. OxcyscPILOT, is based on global cPILOT for quantifying proteomes[36,54] and total cysteine proteome (**Chapter 4**)[38] detection. While we use TMT$^6$ reagents to multiplex 12 samples in a single analysis, the method is amenable to 20 samples by using

TMT[10]-plex reagents[286]. A primary advantage of having enhanced multiplexing is the ability to analyze several biological replicates which minimizes false-positive detection of biologically relevant SNO modifications and methodological error. Additionally, because there are 12 channels available for measurement, total cysteine abundance levels can be obtained alongside SNO modification levels. As a biologically relevant demonstration of OxcyscPILOT, the strategy was applied to brain homogenates from an APP/PS-1 transgenic mouse model[54,344] of AD. SNO modification in AD has been reported in the literature[63,123,171,176] including, specific SNO-modification sites and proteins. In a single analysis, OxcyscPILOT allows unbiased quantification of SNO-modified protein levels in wild-type and APP/PS-1 mice across biological replicates. Also, SNO levels for specific cysteine sites and the relative amount of SNO compared to total cysteine levels are obtained. Among 520 identified proteins, 135 are SNO-modified proteins, and are mainly involved in metabolism and signal transduction pathways. After conservative criteria were applied, eleven SNO sites were statistically different in expression levels in the AD mice. OxcyscPILOT is a versatile and flexible redox proteomics method, and can be applied to study other oxidative PTMs of cysteine in addition to SNO.

## 6.2 EXPERIMENTAL

### *6.2.1 Animal Husbandry*

Fourteen-month old APP/PS-1 male mice [B6.Cg-Tg(APPswe,PSEN1dE9)85Dbo/Mmjax, stock number 005864, genetic background C57BL/6J express the chimeric mouse/human (Mo/Hu) APP695swe (i.e., K595N and M596L) and a mutant human PS1-dE9] and the genetically heterogeneous wild type (WT) (stock number 000664, genetic background C57BL/6J) were purchased from Jackson Laboratory. Mice were housed in the Division of Laboratory Animal

Resources at the University of Pittsburgh and fed standard Purina rodent laboratory chow *ad libitum* on a 12 hour light/dark cycle. APP/PS-1 (hereafter referred to as AD) and WT mice (*N* = 4 for each genotype) were euthanized using $CO_2$. Brain tissues were harvested immediately and stored at -80°C until further experiments. Animal protocols were approved by the Institutional Animal Care and Use Committee at the University of Pittsburgh.

### *6.2.2 Brain Homogenization and Protein Digestion*

Brain tissues were homogenized in an ice-cold phosphate buffer saline (PBS) solution containing 8 M urea with 100 passes of a Wheaton homogenizer for total cysteine enrichment. For SNO cysteine enrichment, the same homogenization procedure was utilized except 5 mM N-ethylmaleimide (NEM) and 5 mM EDTA were added into the buffer. Homogenate solution was collected, sonicated, and centrifuged at 13000 rpm for 10 minutes (4°C) to collect supernatant. For total cysteine samples, WT or AD proteins (100 µg, two aliquots for each genotype) containing equimolar mixing of four biological replicates were digested according to previously reported procedures (**Chapter 4**)[38]. Briefly, proteins were denatured and reduced in 50 mM Tris buffer (pH = 8.2), 8 M urea, and 10 mM dithiothreitol (DTT) for 1 hour at 37°C. The resulting protein mixture was diluted 10-fold with 20 mM Tris buffer (pH = 8.2). TPCK-treated trypsin from bovine pancreas (Sigma) was added to each sample in a 4% w/w enzyme/protein ratio and incubated at 37°C overnight. For SNO samples, WT or AD proteins (four biological replicates for each genotype) were incubated with 50 mM NEM for two hours at room temperature in the dark followed by acetone precipitation. After BCA determination of protein concentrations, each sample (1 mg) was digested by adding 4% trypsin in 20 mM Tris buffer (pH = 8.2). Digests were acidified with 0.5% formic acid, cleaned using Waters Oasis HLB $C_{18}$ cartridges, and lyophilized.

### *6.2.3 SNO Measurement by Slot Blot*

Brain tissues from WT ($N$ = 4) and AD ($N$ = 4) mice were homogenized with the presence of NEM and incubated with 5% SDS for 0.5 h at room temperature. BCA assay was used to determine protein concentrations. An aliquot of 250 µL PBS containing 0.5 µg protein was loaded onto a nitrocellulose membrane with a slot blot apparatus (Bio-Rad). The membranes were blocked with 3% (w/v) BSA solution and 5 mM NEM overnight at 4℃ and incubated with a 1:2500 dilution of anti-SNO antibody produced by mouse (Sigma) for 2 hours. After rinsing the membrane, anti-mouse IgG alkaline phosphatase secondary antibody (Sigma) was added with the dilution factor 1:5000 and incubated with the membrane for 1 hour. The membrane was washed in wash blot (PBS with 0.1% Tween 20) and developed using 5-bromo-4-chloro-3-indolyl phosphate (BCIP) (Thermo Fisher)/nitro blue tetrazolium chloride (NBT) (Sigma) colorimetric development. The blot was dried, scanned and slot profiles quantified using Scion Image. Statistical testing (student's t-test) was performed in Origin 8.0. The entire experiment was repeated twice.

### *6.2.4 Total Cysteine and SNO-cysteine Enrichment*

Enrichment of total cysteine-containing peptides were performed as previously described (**Chapter 4**)[38]. Briefly, tryptic digests were reduced with 5 mM DTT for 1 hour at 37°C, after which the samples were diluted five-fold to lower the concentration of DTT. After dilution, resin was largely in excess, and the concentration of DTT (< 1 mM) was lower than the minimum level required for efficient reduction of disulfide bonds[345]. Any remaining DTT, did not appear to significantly affect the resin's enriching capacity, based on no observable changes to the resin's physical properties after enrichment[295] and previous experiments by our laboratory[38]. For SNO-cysteine enrichment, tryptic mixtures were reconstituted by HEPES buffer (pH = 7.7) and 20 mM

sodium ascorbate was added to selectively reduce SNO. All samples were immediately mixed with pretreated 35 mg Thiopropyl Sepharose 6B thiol-affinity resin (Sigma) for 1.5 h incubation at room temperature. Unbound portion was removed by centrifugation, and the resin was washed by Tris buffer (pH = 8.0), 2 M NaCl, 80% acetonitrile/0.1% TFA and 1% acetic acid (pH = 2.5).

### *6.2.5 On-Resin Low pH Stable-Isotope Dimethyl Labeling*

Extensively washed resin was mixed with 100 µL of 1% acetic acid solution. After that 8 µL of 4% $CH_2O$/$^{13}C^2H_2O$ (98% $^2H$ and 99% $^{13}C$) and 8 µL of 0.6 M $NaBH_3CN$/$NaB^2H_3CN$ (96% $^2H$) were added to the sample for light and heavy labeling. The following samples were subject to light (i.e., $(-CH_3)_2$) dimethylation: one total cysteine sample from WT, one total cysteine sample from AD, two SNO samples from WT, and two SNO samples from AD. The remaining samples were subject to heavy dimethylation (i.e., $(-^{13}C^2H_3)_2$). Samples were incubated for 10 min while mixing, and terminated by adding ammonia to a final 0.2% (v/v) concentration. After centrifugation, the resin was washed by tetraethylammonium bromide (TEAB).

### *6.2.6 On-Resin High pH TMT Tagging*

Purified resin was mixed with 75 µL TEAB, and tagged with TMT$^6$ reagents (Thermo Scientific) individually according to the manufacturer's protocol. TMT reagents 126 and 127 were used to tag total cysteine samples from WT and AD, respectively. SNO samples from WT were tagged with TMT$^6$ reagents 128 and 130, and SNO samples from AD were tagged with TMT$^6$ reagents 129 and 131. Tagging reactions were quenched by 1% hydroxylamine, and the resin washed by Tris buffer (pH = 8.0).

### *6.2.7 Elution, Alkylation and Strong Cation Exchange Fractionation*

The captured and labeled cysteinyl-peptides were released by incubating the resin with 20 mM DTT. Each elution was reacted with 80 mM iodoacetamide for 1 hour at room temperature in the dark. Samples were pooled into a single mixture, purified by HLB $C_{18}$ cartridges, dried and dissolved by SCX reconstitution buffer. The pooled peptide sample was separated by a SCX spin tip (Protea Biosciences) according to manufacturer's instruction. Four fractions were collected by eluting the sample using buffers containing 40 mM, 80 mM, 150 mM and 500 mM ammonia acetate (10% ACN, pH = 3). Each fraction was dried by speed-vac and reconstituted in 0.1% formic acid solution.

### *6.2.8 LC-MS/MS Analysis*

Online desalting and reversed-phase chromatography was performed with a Nano-LC system equipped with an autosampler (Eksigent). Mobile phases A and B were 3% (v/v) acetonitrile with 0.1% formic acid and 100% (v/v) acetonitrile with 0.1% formic acid, respectively. Sample (5 µL) was loaded onto a trapping column (100 µm i.d. × 2 cm), which was packed in-house with $C_{18}$ 200 Å 5 µm stationary phase material (Michrom Bioresource Inc) at 3 µL/min in 3% mobile phase B for 3 min. The sample was loaded onto an analytical column (75 µm i.d. × 13.2 cm), which was packed in-house with $C_{18}$ 100 Å 5 µm stationary phase material (Michrom Bioresource Inc.; Auburn, CA). The following gradient was used: 0-5 min, 10% mobile phase B; 5-40 min, 10-15% B; 40-90 min, 15-25% B; 90-115 min, 25-30% B; 115-130 min, 30-60% B; 130-135 min, 60-80% B; 135-145 min, 80% B; 145-150 min, 80-10%B; 150-180 min, 10%B. The LC eluent was analyzed with positive ion nanoflow electrospray using a LTQ-Orbitrap Velos mass spectrometer (Thermo Fisher).

Each SCX fraction was injected two times. The MS survey scan in the Orbitrap was 60 000 resolution over *m/z* 400-1700. The top seven ions were selected for each DDA cycle. DDA parameters were as follows: precursor ions were isolated with a width of 2.8 *m/z* and normalized collision energy of 35%, the most intense CID fragment ion over the *m/z* range 400-1300 was selected for HCD-$MS^3$. The HCD fragment-ion isolation width was set to 3 *m/z*, the normalized collision energy was 60%, and HCD resolution was 7500 in the Orbitrap. The maximum fill time for MS, MS/MS and $MS^3$ is 500 ms, 50 ms and 250 ms, respectively. The total duty cycle timing is ~4 sec.

### *6.2.9 Database Searching and Data Analysis*

RAW files were analyzed using the SEQUEST HT search engine with Proteome Discoverer 1.4 software (Thermo Fisher) and searched against the Uniprot mouse database. SEQUEST HT search parameters are as follows: precursor mass tolerance 15 ppm; fragment mass tolerance 1 Da; dynamic modifications light dimethyl/+28.031 Da (N-terminal) or heavy dimethyl/+36.076 Da (N-terminal), dynamic carbamidomethyl modification/+57.021 Da (Cys), dynamic ethylmaleimide/+125.048 Da (Cys), dynamic oxidation/+15.995 Da (Met) and dynamic TMT-6plex/+229.163 Da (Lys). Decoy database searching was employed to calculate false discovery rate and the cutoff was set to 5% to ensure high level of confidence while maintaining high proteome coverage[287]. The reporter ions (i.e., *m/z* 126-131) were identified with the following parameters: centroid with smallest delta mass, 30 ppm for reporter ion mass tolerance. Only peptide spectral matchings (PSMs) containing reporter ions of 126 and 127 were used for quantification. The median value across an individual reporter ion channel was calculated from all extracted PSMs, and used for normalization. SNO channels with missing signal were replaced by a minimal signal, and the ratios were calculated based on the summed reporter ion intensities. SNO

site occupancy was calculated based on reporter ion intensities of SNO to total cysteine in WT or AD (e.g. 128/126, 130/126 for WT and 129/127, 131/127 for AD, see formulas 1 and 2). Protein level ratios were used to correct SNO ratios between AD and WT. SNO ratios were then log(2) transformed for statistical analysis. For SNO peptides quantified by three or four biological replicates, permutation tests were used to calculate *p*-values. For SNO peptides quantified by two biological replicates, relative standard deviation (RSD) was calculated. *P*-value cutoff and RSD cutoff were 0.05 and 30%, respectively. Finally, a fold change cutoff of 25% ($\log_2$ (AD/WT) > 0.3 or < -0.3) was also applied. This cutoff was determined based on the relative error of TMT reporter ion signals (Figure 6.1).

$$SNO\ site\ occupancy\ in\ WT\ \% = \frac{I_{128}}{I_{126} \times 10} \times 100\%\ or\ \frac{I_{130}}{I_{126} \times 10} \times 100\% \qquad (1)$$

$$SNO\ site\ occupancy\ in\ AD\ \% = \frac{I_{129}}{I_{127} \times 10} \times 100\%\ or\ \frac{I_{131}}{I_{127} \times 10} \times 100\% \qquad (2)$$

## 6.3 RESULTS AND DISCUSSION

SNO is a notable PTM in AD and contributes to both neuroprotective[346] and neurodestructive processes[347]. In the APP/PS-1 mouse model of AD used in this work, SNO is detectable in brain tissue homogenates by immunoblot detection (Figure 6.2). While there is a trend towards higher expression levels of SNO in AD animals, there was no statistically significant difference based on a student's *t*-test ($p < 0.05$). A moderate number of animals were used ($N = 4$) for this analysis and that SNO is a highly dynamic modification would contribute to this observation. Because the immunoblot detection represents changes across many proteins, assessment of the individual differences in SNO levels of proteins requires more specific detection methods such as immunoprecipitation or MS.

a)

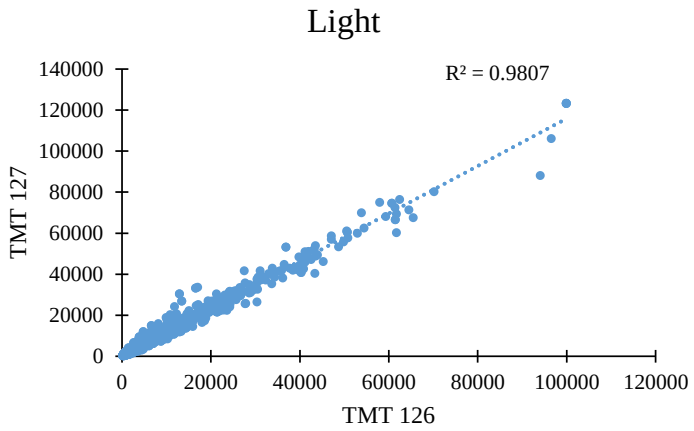


b)

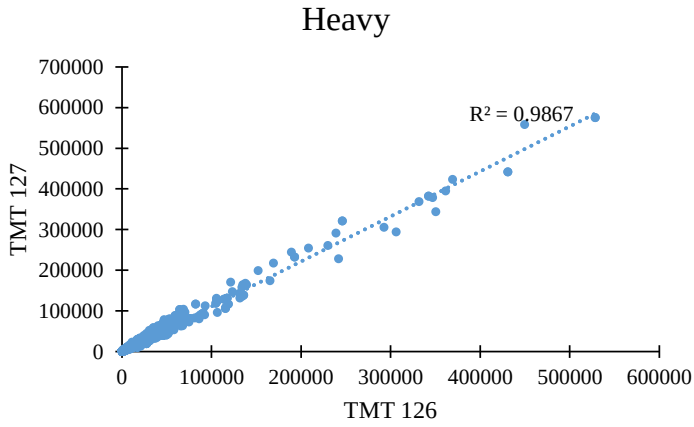


c)

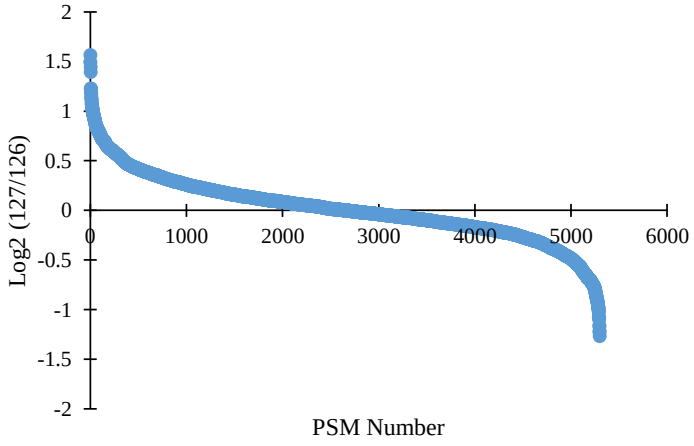


**Figure 6.1** Correlation of reporter ions of TMT 126 and 127 tags in a) light and b) heavy channels. The linearity is indicated by $R^2$ value. The distribution of TMT 126 and 127 ratios is shown in c) with a calculated error of 25%.

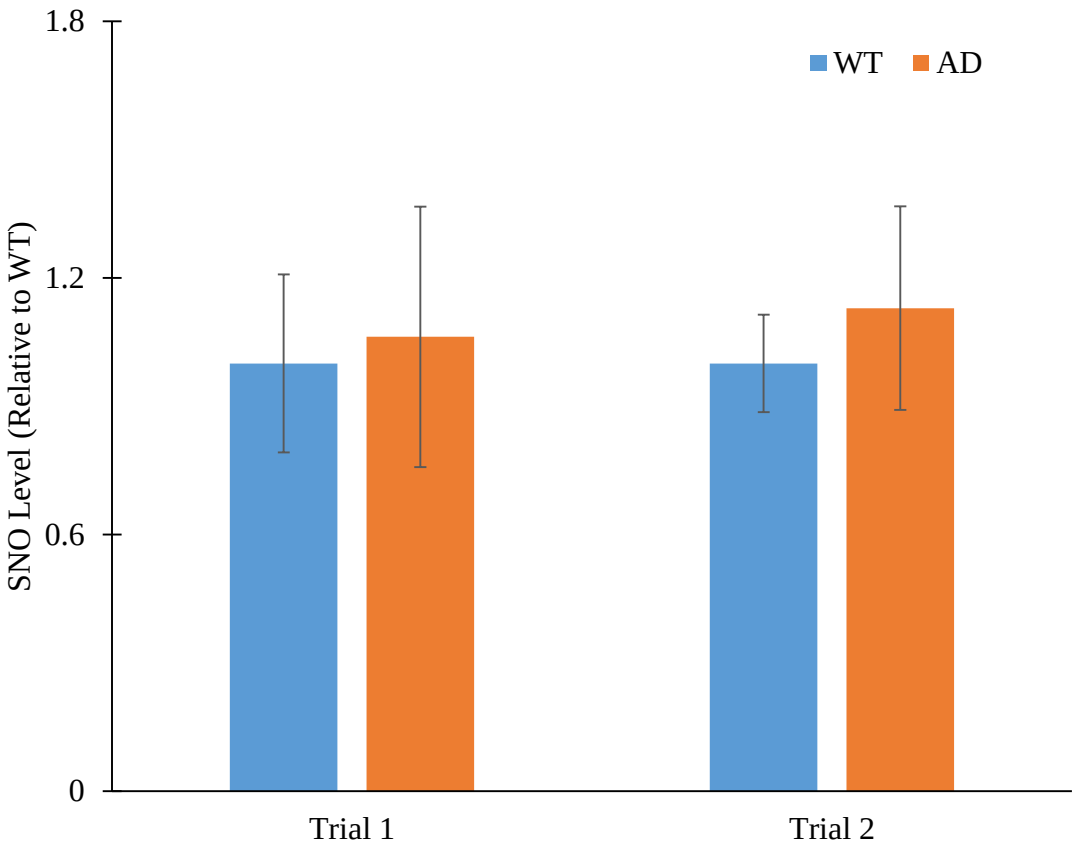


**Figure 6.2** Histogram plot of protein S-nitrosylation (SNO) levels in brain proteins isolated from WT (*N* = 4) and AD (*N* = 4) mice. Intensities are normalized to WT. Error bar: ±standard deviation. *P*-values are 0.57 and 0.10 for trial one and trial two, respectively.

Here we developed an enhanced multiplexing approach "OxcyscPILOT" to detect SNO-proteins and quantify their levels across multiple biological replicates in a single analysis (Figure 6.3). This approach is an extension to our cPILOT methodologies[36,38,54] and allows more specificity and multiplexing than the previously reported OxcysDML approach (**Chapter 5**) [39]. Oxidative modifications to cysteine are several and overall occur at low abundance levels estimated to be ~1-2% across all tryptic peptides[64]; and SNO-modified peptides are estimated to be even lower. Enrichment methods are extremely valuable for increasing the detection of these modifications in complex tissues, such as brain homogenate. Realizing this large difference in concentration levels of cysteine-containing peptides and those peptides modified with SNO, we varied the amount of protein starting material used to detect total cysteine levels in comparison to SNO modifications on peptides. Additionally, to enable normalization of the protein SNO levels to the protein abundance, a pooled sample (0.1 mg) of either wild-type or AD tissues across the four biological replicates was generated. Pooled samples were subject to DTT (10 mM) in order to reduce all thiols, trypsin digestion, and then were enriched using a Thiol Sepharose 6B resin. Digested samples were dimethylated (either isotopically labeled light or heavy versions) at low pH conditions to tag N-termini and then labeled with TMT reagents 126 or 127 on lysine amines, for WT and AD samples respectively. Brain homogenate samples (1 mg) from each individual animal were subject to NEM (50 mM) in order to label any free thiols. Next proteins were digested and subject to ascorbate to specifically reduce SNO sites. In this manner, the peptides are enriched with the thiol resin however we note that SNO-modifications are not directly detected in the mass spectrum. These previously SNO-modified peptides were dimethylated (light or heavy) and tagged with TMT reagents 128 to 131. This on-resin dual tagging strategy allows 12 samples to be multiplexed in a single analysis that enables direct normalization of SNO levels to total protein

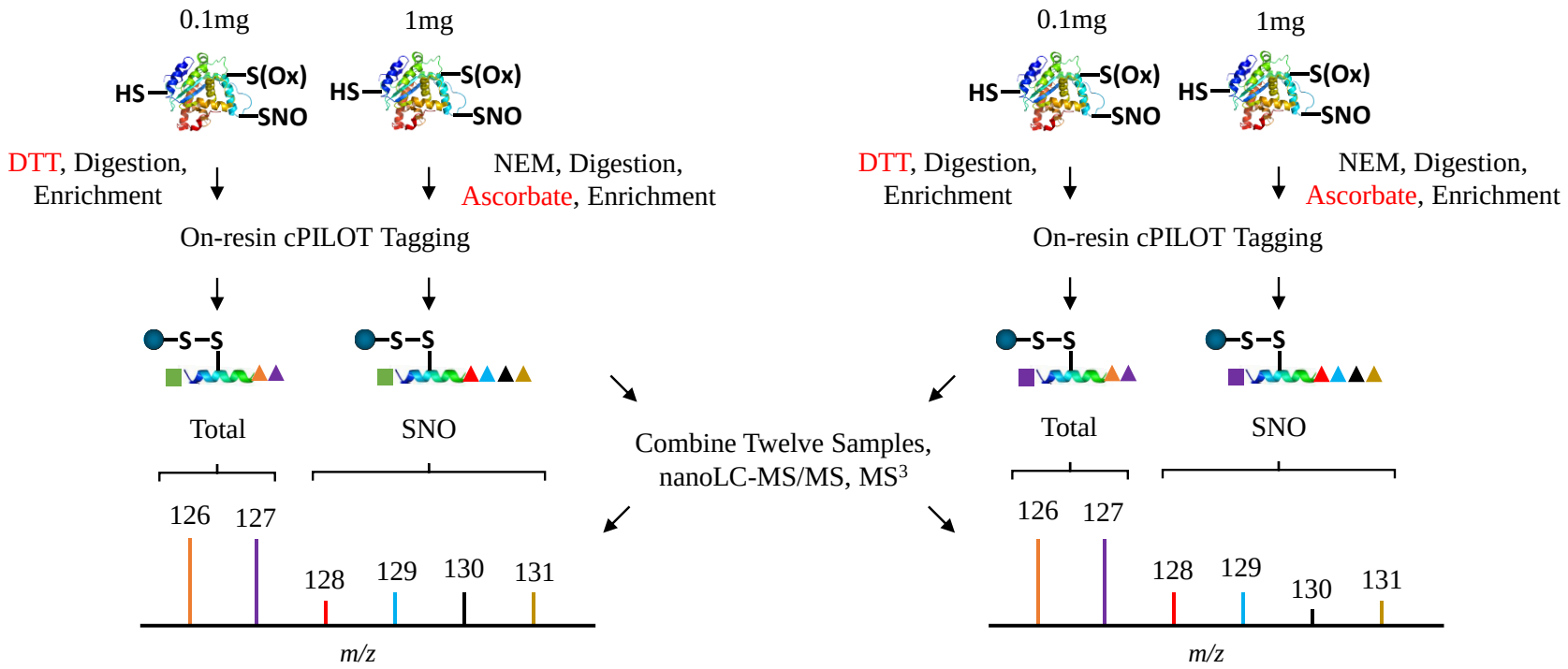


**Figure 6.3** Schematic representation of the oxidized cysteine-selective cPILOT (OxcyscPILOT) redox proteomics workflow. For protein level quantification, a pooled sample of 0.1 mg of brain total protein containing an equimolar mixture proteins from four biological replicates of WT or AD mouse is made. Proteins are reduced by DTT and digested by trypsin. Cysteine-containing peptides are enriched by a thiol-affinity resin followed by on-resin low pH dimethylation using light (-$C_2H_6$) or heavy (-$^{13}C_2{}^2H_6$) tags. After buffer exchange, resin-linked peptides are labeled with TMT 126 and 127 reagents for WT and AD, respectively. For S-nitrosylation quantification, 1 mg brain proteins from individual WT or AD mice are treated with NEM to block free sulfhydryl groups. After tryptic digestion, ascorbate is added to the peptide mixture to selectively reduce SNO. Reduced peptides containing newly-formed sulfhydryl groups are enriched by the thiol-affinity resin and subject to similar tagging procedures as the total cysteine samples, except TMT 128, TMT 129, TMT 130 and TMT 131 are used for WT and AD samples from different animals, respectively. Enriched and tagged peptide samples are eluted from the resin and alkylated by iodoacetamide. The twelve samples are combined to a single mixture. This mixture is fractionated by SCX and analyzed using nanoLC-MS/$MS^3$. Protein level ratios, SNO site occupancy in WT or AD, and SNO ratios between WT and AD can be calculated by using corresponding reporter ion intensities.

abundance and allows comparison across several biological replicates. Strong cation exchange fractionation coupled with reversed-phase nanoLC-MS/MS and $MS^3$ in the HCD of the LTQ Orbitrap Velos was used for separation and mass analysis.

The efficiencies of the enrichment, dimethylation, and TMT tagging are higher than 98%, 97% and 96% based on peptide spectral matches (PSMs), respectively, and are consistent with previous reports by our laboratory[38,39], which allows us to examine a large number of cysteine-containing proteins and get quantitative information. The total number of cysteine-containing peptides identified in this experiment is 661 (520 proteins) and we detected 138 SNO peptides (135 SNO-proteins) (Table 6.1). Compared with the previously demonstrated cysteine-selective cPILOT[38], OxcyscPILOT identified 170% more cysteinyl peptides with experimental conditions that employed half the number of SCX fractions and 2/3 less instrument acquisition time. The number of SNO-modified proteins is comparable to several iodoTMT[43,113,118] or label-free[176] based quantitative studies, and higher than gel-based approaches[123]. In terms of quantitation, ~ 36% of the identified peptide spectra did not have quantitative information via HCD $MS^3$. This is mostly due to the tryptic peptides with Arg on C-terminus which lack a TMT tag. In a previous study performed by our laboratory whereby trypsin and Lys-C were evaluated. Trypsin resulted in better proteome coverage compared with Lys-C[36]. Trypsin can also generate peptides with missed cleavage sites, and these peptides (up to two miscleavages) are included in the quantification for individual proteins. In addition, not all peptides modified by TMT can release reporter ions in $MS^3$. One reason is the selection of a *b*-type ion in MS/MS spectra that is fragmented by HCD and resulting in no reporter ions. The other reason is the very low abundance of SNO modifications present in the samples and the MS3 acquisition is accompanied with significant loss of signal intensities. A dramatic increase in SNO-modifications will be possible with instrumentation such

**Table 6.1** Summary of OxcyscPILOT results in WT and AD brain tissues.

| | |
|---|---|
| Total Proteins Identified | 520 |
| Total Cysteinyl Peptides Identified | 661 |
| Light PSMs | 6574 |
| Heavy PSMs | 8557 |
| WT SNO Proteins | 115 |
| AD SNO Proteins | 113 |
| Total SNO Proteins | 135 |
| Total SNO Peptides | 138 |
| Quantified SNO-modified Peptides ($N$ = 4) | 43 (6)[a] |
| Quantified SNO-modified Peptides ($N$ = 3) | 14 (2)[a] |
| Quantified SNO-modified Peptides ($N$ = 2) | 41 (4)[b] |
| Quantified SNO-modified Peptides ($N$ = 1) | 40 |

[a]Number in bracket indicates the significantly changed SNO-modified peptides in AD compared with WT. A $p$-value cutoff (<0.05) and fold change cutoff (>25%) is applied.

[b]Number in bracket indicates the significantly changed SNO-modified peptides in AD compared with WT. A RSD cutoff (<30%) and fold change cutoff (>25%) is applied.

as the Orbitrap Fusion mass spectrometer equipped with faster $MS^3$ acquisition and synchronous precursor selection technology, which takes multiple fragment ions from the MS/MS for HCD-$MS^3$ and results in enhanced sensitivity of reporter ions[348].

In this particular experiment, it is important to note that not all cysteine-containing peptides will generate SNO-related reporter ion signals. For example, the precursor peaks at *m/z* 617.673 and 620.354 correspond to the triply-charged peptide G(dimethyl)VLFGVPGAFTPGC(IAM) SK($TMT^6$) of peroxiredoxin-5 (Figure 6.4a). Upon isolation and fragmentation of the $y_5$ fragments, the $MS^3$ spectrum shows only reporter ion signal at *m/z* 126 and 127, for the total WT and AD pooled samples. No measurable signal is detected for SNO of this peptide which is consistent with likely sulfenic acid modification of Cysteine 96 on this protein[349]. Because OxcyscPILOT is only selective to SNO modification, sulfenic acid modifications are not expected to be reduced, enriched and detected. The peptide with Cys96 of peroxiredoxin-5 only shows detectable signals in TMT channels 126 and 127. In WT and AD brain tissues, the lack of TMT signals in this peptide suggest that Cys96 is not SNO-modified in our experiments, or is at such low concentration and not detectable in our experiments, resulting in missing signals in TMT channels 128-131 for this peptide. There are several sample preparation steps (i.e., reduction, enrichment, digestion, chemical labeling, etc.) in OxcyscPILOT that present opportunities for the introduction of experimental error. The intensities of the reporter ions for the WT and AD pooled samples shown in Figure 6.4a, are very similar across the light and heavy dimethylated samples. Total TMT signals from all peptides detected in the WT or AD pooled samples are heavily correlated in the light ($R^2$ = 0.9807) and heavy dimethylation samples ($R^2$ = 0.9867) (Figure 6.1). This indicates the robustness of this approach and lends to an overall error of ~25%.

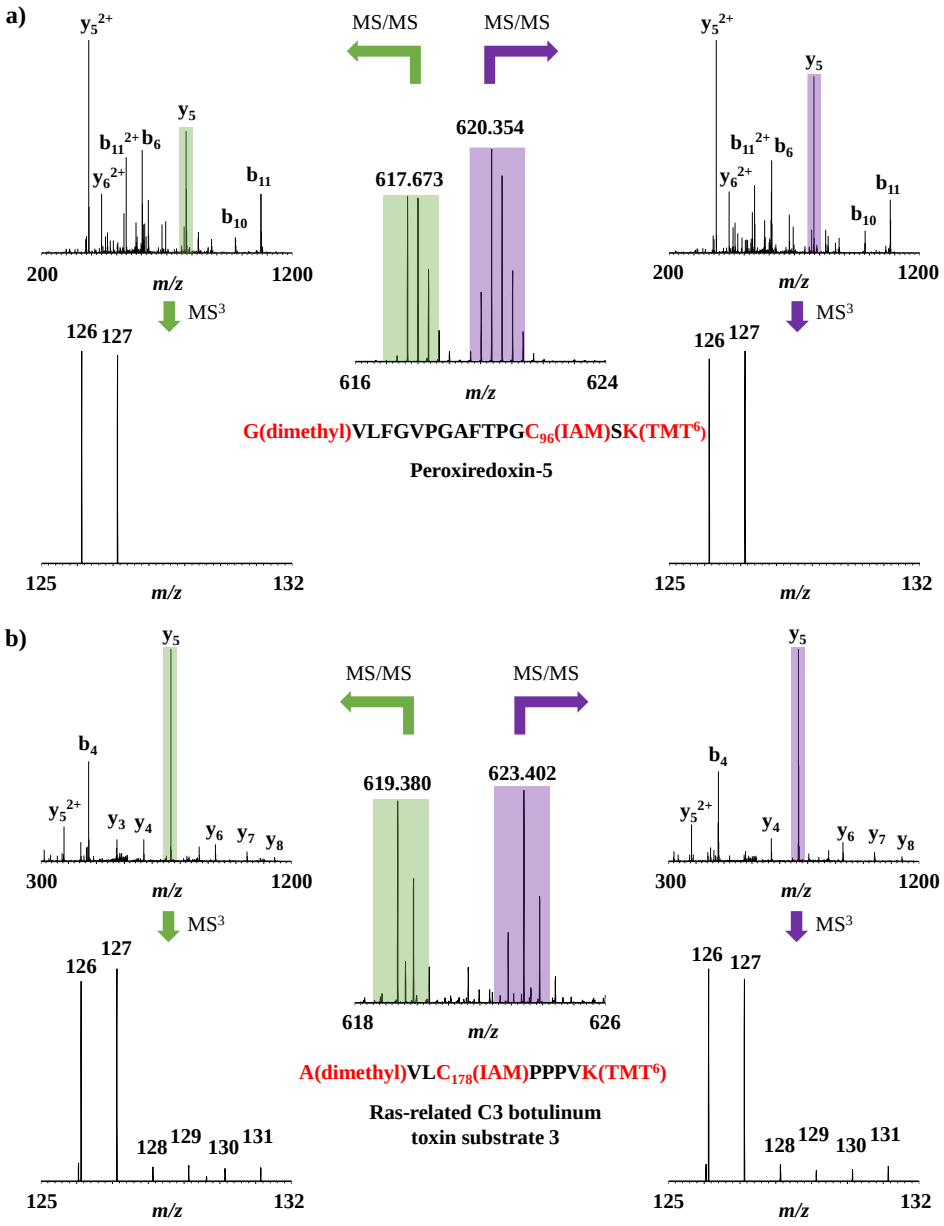


**Figure 6.4** Example OxcyscPILOT MS spectra. a) Pair of triply charged precursor peaks with *m/z* = 617.673 and *m/z* = 620.354. Both peaks are isolated and fragmented by CID to generate tandem mass spectra to sequence the peptide, which is G(dimethyl)VLFGVPGAFTPGC$_{96}$(IAM)SK(TMT$^6$) of peroxiredoxin-5. The most intense peaks within the *m/z* range of 400-1300 in CID spectra ($y_5$) are further selected and fragmented to give the HCD MS$^3$ spectra, which are zoomed-in over the reporter ion region. Reporter ions of 126 and 127 represent the level of total cysteine, and the absence of reporter ion 128, 129, 130 and 131 indicate this site is not modified by SNO. b) Pair of doubly charged precursor peaks with *m/z* = 619.380 and *m/z* = 623.402. Both peaks are isolated and fragmented by CID to generate tandem mass spectra to sequence the peptide, which is A(dimethyl)VLC$_{178}$(IAM)PPPVK(TMT$^6$) of ras-related C3 botulinum toxin substrate 3. The most intense peaks within the *m/z* range of 400-1300 in CID spectra ($y_5$) are further selected and fragmented to give the HCD MS$^3$ spectra, which are zoomed-in over the reporter ion region. Reporter ions of 126 and 127 represent the level of total cysteine, and the signals of 128, 129, 130 and 131 indicate the presence of SNO on this site.

Several situations arise in this dataset where the detection of SNO may only exist in peptides detected for a single biological replicate ($N$ = 40) or in as many as all four biological replicates ($N$ = 43) of WT and AD animals (see Table 6.1 and Appendix D Tables 6.2 and 6.3). Stringent criteria were applied and only those peptides that were detected in any two biological replicates were considered for further analysis. Ideally, all peptides that are SNO-modified would be detected in reporter ion channels 128-131 in both light and heavy dimethylated samples. An example of this is shown in Figure 6.4b, for the doubly-charged precursor pair at *m/z* 619.380 and 623.402 identified as A(dimethyl)VLC(IAM)PPPVK(TMT$^6$) of the ras-related C3 botulinum toxin substrate 3 protein. The MS$^3$ spectra for both light and heavy $y_5$ fragments show low intensity of detectable ion signals across reporter ions for all four biological replicates.

A total of 115 SNO-modified proteins were identified in WT mice and 113 SNO-modified proteins were identified in AD mice (Appendix D Table 6.1). Ninety-three proteins had detectable SNO-modified peptides in both WT and AD samples, while 22 and 20 SNO- modified proteins are exclusive for WT and AD, respectively. A total of 135 SNO-modified proteins are involved in a range of biological pathways such as cell cycle, immune system, homeostasis, neuronal system, and vesicle-mediated transport (Figure 6.5). A majority of SNO-modified proteins are involved in metabolism (32 proteins) or signal transduction (29 proteins). An interesting example is L-lactate dehydrogenase, which is only present in WT but not in AD (Appendix D Table 6.1). The SNO modification of L-lactate dehydrogenase in WT tissue has been reported for normal enzymatic function in metabolism[350]. The absence of this modification in AD brain may be indicative of dysregulated energy metabolism in disease. These results indicate that SNO is a very dynamic modification, and are highly consistent with other reports in the literature[123,176]. A total of 56 SNO-modified proteins (Appendix D Table 6.1) were also frequently reported in previous

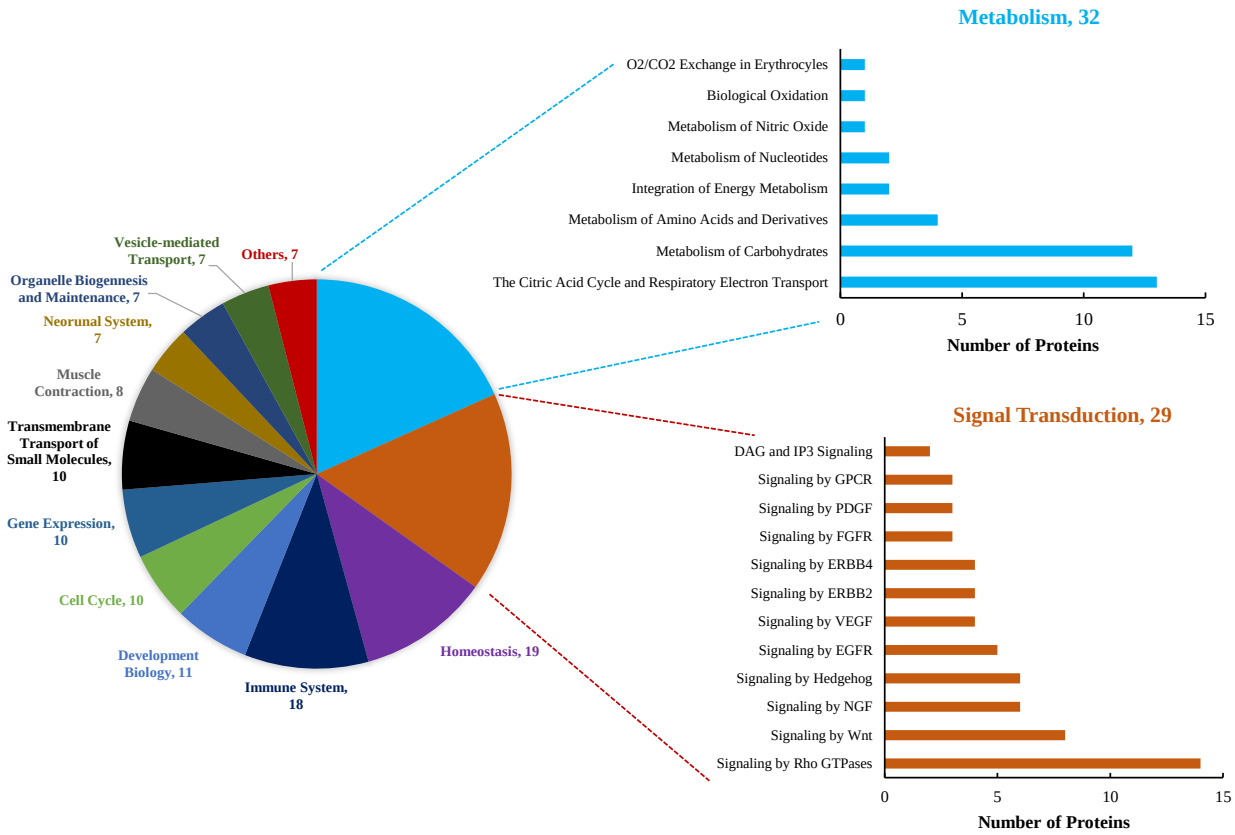


**Figure 6.5** Pathway analysis of 135 SNO-proteins identified in WT and AD mouse brain tissues using Reactome database (http://www.reactome.org/). The pie chart shows primary pathways that SNO-proteins are involved and the number of proteins in each pathway. SNO-proteins involved in metabolism and signal transduction are further broken down into categories as shown in histogram plots.

AD studies, such as glial fibrillary acidic protein[123,171,176], heat shock cognate 71 kDa protein[123,176], elongation factor 2[176], sarcoplasmic/endoplasmic reticulum calcium ATPase 2[176], glyceraldehyde-3-phosphate dehydrogenase[123,176], triosephosphate isomerase[123,171,176], fructose-bisphosphate aldolase A[123,176], dynamin-1-like protein[351], 2',3'-cyclic-nucleotide 3'-phosphodiesterase[176,352], ras-related C3 botulinum substrate 3[176,353] and ADP/ATP translocase 1[176,353]. In addition 79 SNO-modified proteins (Appendix D Table 6.1) were identified for the first time in this work. It is important to observe the number of cellular signaling pathways, such as Pho GTPases, Wnt, NGF that SNO contributes to which suggests this oxidation status of cysteine is critical for normal cellular signaling (Figure 6.5). Network analysis of 135 SNO-modified proteins in WT and AD brains using STRING (version 10) shows that the modified proteins are enriched in some basic molecular pathways such as citrate cycle, 2-oxocarboxylic acid metabolism, oxidative phosphorylation, glycolysis/gluconeogenesis, Huntington's disease and axon guidance (Figure 6.6). These pathways are zoomed-in to show the differences of the network patterns of SNO-modified proteins in WT and AD. Although most of SNO-modified proteins widely participate in both WT and AD, some pathways containing abnormal SNO are observed. For example in the pathway of glycolysis/gluconeogenesis, triosephosphate isomerase (Tpi1), glucose-6-phosphate isomerase (GM1840) and alcohol dehydrogenase 1 (Adha) have SNO modifications in WT but not AD. A lower *p*-value (3.29E-8 v.s. 2.01E-4) and a higher gene number (8 v.s. 5) indicates that SNO is more enriched in WT than AD in glycolysis/gluconeogenesis pathway. The different SNO involvement in carbohydrate metabolism in AD mice brain was also reported in a previous study[176], and is consistent with the finding of altered glucose tolerance and metabolic changes in PET analyses of AD patients[354]. While previous studies mainly focused on proteins with only SNO modification in AD[123,176], our data also suggests the absence of SNO modification may be

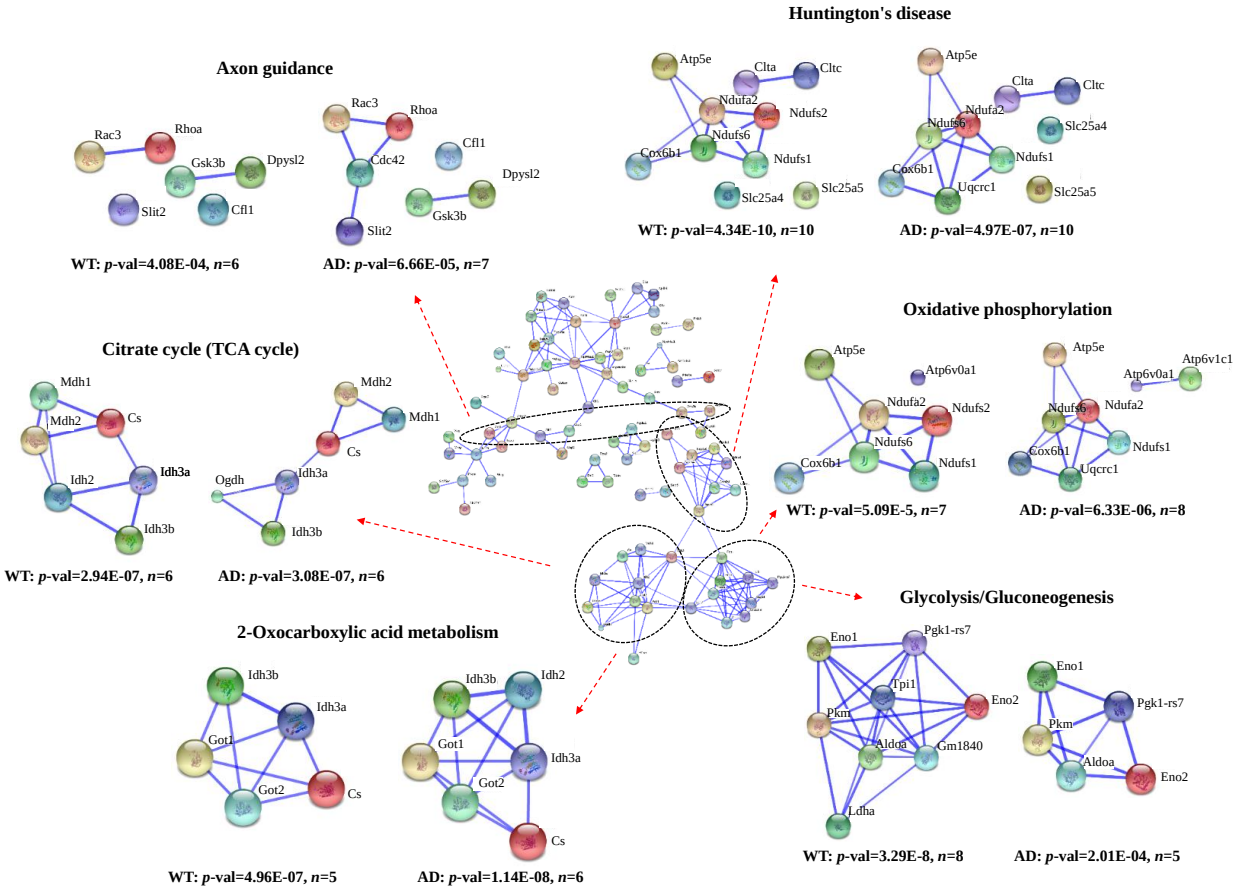


**Figure 6.6** Interaction network of 135 SNO-modified proteins identified in WT and AD mouse brain tissues. Some example KEGG pathways are circled by dished ovals and zoomed-in to show the differences of the network patterns between WT and AD. The *p*-value and number of proteins in each pathway are provided. Network analysis was performed using STRING (version 10) with confidence view and confidence score of 0.700. No text mining was used. Uniprot accession numbers are uploaded to STRING and return as gene symbols.

important for disease pathogenesis in AD. Generally SNO-modified proteins in this study have a trend of increased levels in AD compared to WT (Figure 6.1 and Table 6.2).

There are several challenges for quantifying SNO-modified proteins in disease. One is cysteine PTM levels can be affected by protein expression changes. In order to take this into consideration, multiple experiments must be performed. For example, in a redox proteomic study using duplex ICAT reagents, because there are no more channels available for protein quantification, a separate experiment using isotopic dimethyl labeling is employed to provide protein abundance data[101]. Even in our OxcysDML approach, two experiments were performed to obtain total cysteine oxidation levels and protein abundance information based on cysteine-containing peptides[39]. Two, there is a large difference (roughly two to three orders of magnitude[65]) between total peptide and SNO-modified peptide abundance. This means non-cysteinyl peptides can cause significant matrix effects and suppress the detection of SNO-modified peptides, thus decreasing sensitivity. Solutions are to use the total cysteinyl peptides to represent the protein for protein abundance information, and to increase the sample starting material of SNO-modified samples by a factor of 10. The latter helps facilitate reducing the abundance differences, so that both total cysteinyl and SNO-modified peptides can be detected in a single experiment. This design was successfully been utilized with iodoTMT[118]. The throughput of iodoTMT is greater than ICAT or OxcysDML methods but still requires multiple experiments to measure across biological replicates[118]. Due to the enhanced multiplexing ability of OxcyscPILOT, the total cysteinyl peptides which represent the protein abundance in each genotype and also SNO levels from four biological replicates of each genotype can be detected in a single run. After proteins were filtered based on having SNO-modifications detectable in at least two biological replicates, the SNO levels were normalized to the total protein abundance level (see Experimental). Following normalization,

**Table 6.2** Quantified SNO sites with significant changes in levels between WT and AD.

| Protein Name | Uniprot Acc. No. | Peptide Sequence | Modified Site | Protein Level AD/WT | Relative SNO Site Occupancy in WT[a] | Relative SNO Site Occupancy in AD[a] | SNO log(2) Fold Change AD/WT in Each Biological Replicate | | | | Average SNO log(2) Fold Change AD/WT[b] | Statistics | | *N*[e] |
|---|---|---|---|---|---|---|---|---|---|---|---|---|---|---|
| | | | | | | | 1 | 2 | 3 | 4 | | | | |
| Septin-5 | Q9Z2Q6 | ADCLVPSEIRK | C193 | 0.895 | 0.18% | 0.30% | 1.868 | 0.528 | 0.576 | 0.246 | 0.804 | | 0.0001 | 4 |
| ADP/ATP translocase 1 | P48962 | EFNGLGDCLTK | C160 | 0.850 | 0.73% | 1.05% | 0.410 | 0.330 | 0.176 | 1.325 | 0.560 | | 0.0001 | 4 |
| Myc box-dependent-interacting protein 1 | O08539 | AAPQWCQGK | C186 | 0.906 | 0.35% | 0.47% | 0.979 | 0.045 | 0.415 | 0.341 | 0.445 | | 0.0050 | 4 |
| Isocitrate dehydrogenase [NAD] subunit | Q91VA7 | GVIECLK | C184 | 0.936 | 0.29% | 0.38% | 0.657 | 0.123 | 0.644 | 0.092 | 0.379 | *p*-value[c] | 0.0112 | 4 |
| Ras-related C3 botulinum toxin substrate 3 | P60764 | AVLCPPPVK | C178 | 0.929 | 0.48% | 0.60% | 1.073 | 0.006 | 0.020 | 0.362 | 0.365 | | 0.0099 | 4 |
| 14-3-3 protein gamma | P61982 | NCSETQYESK | C112 | 1.152 | 7.18% | 5.00% | -0.626 | -0.023 | -0.967 | -0.549 | -0.541 | | 0.0001 | 4 |
| Glutamine synthetase | P15105 | TLDCEPK | C49 | 0.911 | 0.22% | 0.29% | 0.200 | 0.742 | 0.520 | N.A. | 0.487 | | 0.0001 | 3 |
| Myelin proteolipid protein | P60202 | VCGSNLLSICK | C220 | 1.099 | 2.29% | 0.89% | -2.385 | -2.091 | -0.826 | N.A. | -1.767 | | 0.0001 | 3 |
| Citrate synthase, mitochondrial | Q9CZU6 | FRGYSIPECQK | C101 | 0.988 | 0.07% | 0.42% | 2.658 | 2.434 | N.A. | N.A. | 2.546 | | 0.1097 | 2 |
| 14-3-3 protein zeta/delta | P63101 | ACSLAK | C188 | 0.515 | 27.86% | 54.41% | 0.868 | 1.072 | N.A. | N.A. | 0.970 | | 0.0998 | 2 |
| 2',3'-cyclic-nucleotide 3'-phosphodiesterase | P16330 | TAWRLDCAQLK | C157 | 1.149 | 0.45% | 0.66% | 0.515 | 0.581 | N.A. | N.A. | 0.548 | RSD[d] | 0.0326 | 2 |
| Citrate synthase, mitochondrial | Q9CZU6 | GYSIPECQK | C101 | 0.933 | 0.21% | 0.30% | 0.310 | 0.731 | N.A. | N.A. | 0.520 | | 0.2045 | 2 |

[a]Relative SNO site occupancy percentage is calculated based on normalized reporter ion intensities of SNO to total cysteine in WT or AD (e.g. 128/126, 130/126 for WT and 129/127, 131/127 for AD, see formulas 1 and 2).

[b]SNO fold changes are corrected by protein level abundance change. A fold change of at least 25% is applied to determine significance ($\log_2$(AD/WT)>0.3 or <-0.30).

[c]*P*-value cutoff (<0.05) is applied for group of $N = 4$ and 3.

[d]RSD cutoff (<30%) is applied for group of $N = 2$ .

[e]Number of biological replicates quantified.

permutation testing[38,327] was done in order to determine which SNO-modified peptides were statistically different between WT and AD samples. Table 6.2 provides a list of 11 proteins that were statistically different in SNO modification level in AD compared to WT mice. Most of these proteins have SNO site occupancy below 1%, except for 14-3-3 proteins. The high SNO-modification levels (28-54%) of 14-3-3 proteins may be linked to the binding nature of 14-3-3 proteins to microtubule-associated protein tau, whose hyperphosphorylation results in the formation of amyloid plaques and neurofibrillary tangles in AD[355]. The low SNO site occupancy percentage data in Table 6.2 suggests the room for further improvement. In the sample preparation we used a 10-fold higher sample amount for SNO enrichment. However, if the tissue amounts permit, our data suggests a 100-fold SNO loading amount would be a better choice. SNO levels are variable amongst mice of the same genetic background, leading to differences in the AD/WT ratios detected. For some peptides, the measured SNO ratios are highly diverse. We mainly attribute this to the dynamic nature of SNO modification across different animals, and used permutation testing for statistical analysis. Permutation testing is an ideal statistical test for proteomic data to calculate *p*-values without further adjustment[327]. However the *p*-value only indicates the mathematical probability of the null hypothesis ($H_0$: $\mu = 0$, no significant change), regardless of the degree of change. Thus we also applied a 25% SNO ratio cutoff to look for the peptides with the significant changes of SNO modification. As we can see from Table 6.2, most of them have increased SNO levels in AD, which is consistent with previous studies[123,176]. A few of these proteins have been previously identified as SNO-modified in AD: ADP/ATP translocase 1[176,353], ras-related C3 botulinum toxin substrate 3[176,353], 14-3-3 protein zeta/delta[123], glutamine synthetase[123,176], myelin proteolipid protein[176], citrate synthase[176] and 2',3'-cyclic-nucleotide 3'-phosphodiesterase[176]. Furthermore, specific modification sites such as C160 for ADP/ATP

translocase 1 and C178 for ras-related C3 botulinum toxin substrate 3 have been quantified as significantly SNO-modified in AD mouse brain tissue over WT, which are consistent with a relevant proteomic study[176]. These two proteins have been linked with AD and reviewed in detail[356,357]. It must be noted that the whole brain tissue is used in this study. This is unlike some other studies using specific cell types or brain regions. For example, one report studied the SNO-modified proteins in different AD brain regions (hippocampus, substantia nigra and cortex)[123], and another study focused on the synaptosome of APP mouse[176]. Brain is a highly heterogeneous organ and different portions exhibit various changes in AD. Using the entire homogenate of the brain may cause misrepresentation of the changes in specific regions or cells in AD. Because there is some literature precedence for SNO-modified proteins in brain homogenate[123,176], we chose this sample to benchmark our novel method. A total of 50 SNO-modified proteins identified by this work were also reported in these two studies[123,176] (Appendix D Table 6.1). It would be interesting to study SNO-modified proteins at the level of different cells (e.g., microglia, neurons) or brain regions (e.g., cortex, striatum) and compare to entire homogenate.

Characterization of specific cysteine reversible modification (e.g., SNO) from complex samples is challenging due to its low abundance and labile nature. We believe a desirable redox proteomic strategy to study cysteine PTM should be site-specific, sensitive, versatile, unbiased and highly multiplexed. OxcyscPILOT is one such strategy. First, unlike gel-based approach, in which the site information of cysteine PTM is generally unavailable, OxcyscPILOT is able to localize cysteine PTM on the protein primary sequence, and link this information to protein structure and function for biological interpretation. This is a limitation however when multiple cysteinse are present on the same peptide and it is not possible to determine which site was initially modified. Because NEM blocking was employed prior to reduction and enrichment, peptides observed with

multiple cysteines (e.g. ACNCLLLK, Appendix D Table 6.2) should have multiple SNO sites. Second, OxcyscPILOT has desirable sensitivity in terms of its proteome coverage and its ability for isolation and $MS^3$ quantification of SNO-modified peptides with ~1% abundance. We attribute this to the efficient enriching ability of the thiol-affinity resin, and the integration of all chemical labeling steps on the resin. Although many sample preparation steps are involved in the OxcyscPILOT workflow, repeated sample extraction and cleanup steps are not needed. This can potentially minimize sample loss and improve sensitivity. Third, we used SNO here to demonstrate the application of OxcyscPILOT methodology. In fact this method is versatile to follow other SNO modifications. For example, by simply changing the selective reduction reagent, different types of cysteine reversible modifications, such as S-glutathionylation or sulfenic acid, can be characterized in the same method. Fourth, the number of multiplexing channels can also be expanded by utilizing triplex dimethylation or ten-plex TMT reagents. Fifth, OxcyscPILOT is an unbiased proteomic approach because protein ratios are simultaneously determined and used for SNO-peptide normalization. Sixth, the relative site occupancy of site-specific SNO can be calculated, which is helpful to screen the proteins that are susceptible to nitric oxide attack, e.g., 14-3-3 proteins in this study.

## 6.4 CONCLUSIONS

A novel quantitative proteomics approach to quantify endogenous SNO from multiple complex samples, OxcyscPILOT, is presented in this work. Endogenous levels of SNO are very low abundant and require high sample starting amounts or very sensitive detection methods in combination with enrichment strategies. This enhanced multiplexing technique for cysteine PTM quantification enables enrichment and tagging of twelve samples for unbiased detection of SNO-modified proteins. This was extremely useful for measuring changes across multiple biological

replicates and for measuring total protein abundance levels for data normalization. Because all chemical reactions are coupled with affinity purification on the solid phase resin, the entire workflow exhibits desirable efficiency in terms of cysteinyl proteome coverage and cysteine PTM isolation. We demonstrate this method to study SNO using brain tissues from an AD mouse model, and much of the biological changes are consistent with previous findings in AD. In particular, SNO-modified proteins are heavily involved in normal cellular signaling processes and metabolism, amongst other functions such as axon guidance, vesicle-transport and immune system response. We believe this technique can be directly applied to investigate other types of cysteine oxidative modifications by simply changing the sample preparation conditions. Furthermore, the sensitivity can be improved by employing SPS $MS^3$ acquisition, and the multiplexing capabilities can be enhanced to 20 or 24 samples using TMT10-plex or DiLeu isobaric tagging reagents.

# 7.0 CONCLUDING REMARKS AND FUTURE DIRECTIONS

## 7.1 SUMMARY

This dissertation presented mass spectrometry (MS)-based studies of protein oxidative modifications. The following is a brief summary for each chapter.

**Chapter 2** reviewed protein post-translational modifications (PTMs) induced by oxidative stress, such as cysteine reversible modifications and protein carbonylation. More emphasis was on the biological significance of cysteine oxidative PTMs and current proteomic tools for investigation, including the widely used enrichment and isotopic labeling techniques. Oxidative stress plays important roles in aging and neurodegenerative diseases, and the relevant applications of redox proteomics in disease studies were discussed.

**Chapter 3** presented a study of mapping protein oxidative modifications through MS techniques. A model protein was oxidized by metal-catalyzed oxidation, and combined top-down and bottom-up MS methods were developed and utilized to localize different types of oxidative modifications, such as hydroxylation, carbonylation, deamidation and decarboxylation.

**Chapter 4** demonstrated novel multiplexing approaches to isolate and quantify the cysteinyl proteome. Because most proteins contain cysteine, cysteine-selective proteomics methods can quantify protein expression and also simply the samples. Two different approaches were developed in this chapter, cysteine-selective dimethylation (CysDML), a duplex method using inexpensive dimethylation and cysteine-selective combined precursor isotopic labeling and isobaric tagging (CyscPILOT), a 12-plex technique using combined dimethylation and iodoTMT tagging. To facilitate sample processing, dimethylation reactions were performed on the solid phase resin. CysDML was accurate over a dynamic range of one order of magnitude with RSD ~

20%. Both methods were used to study the liver proteome of APP/PS-1 mice, an Alzheimer's disease (AD) model mouse. CysDML and CyscPILOT delivered consistent quantitative data, and in total more than 2000 proteins were identified. Differentially-expressed proteins in AD liver are involved in carbohydrate and lipid metabolism, which correlates well with other AD studies.

Cysteine-selective proteomics methods provide the ability to study cysteine PTMs due to the enriching capability. **Chapter 5** demonstrated such one example using oxidized CysDML (OxcysDML). OxcysDML was an accurate but inexpensive method for cysteine redox proteomics, and was applied to characterize the redox status of liver proteome of APP/PS-1 mice in AD. This work discovered dysregulated lipid metabolism in AD liver tissue associated with elevated oxidative stress.

**Chapter 6** further developed and optimized the demonstrated CyscPILOT approach (**Chapter 4**) and achieved quantification of S-nitrosylation (SNO) in tissues (e.g., OxcyscPILOT). OxcyscPILOT employed ascorbate reduction to capture SNO peptides, and solid-phase TMT tagging to improve proteome coverage. By a single run, OxcyscPILOT was able to quantify endogenous SNO from four biological replicates. OxcyscPILOT was applied to the brain proteome of the APP/PS-1 mice to study the expression of protein SNO in AD. A 24-hour LC-MS/$MS^3$ run identified 135 SNO-modified proteins, which mostly participated in metabolism and signal transduction. OxcyscPILOT had eight times higher efficiency compared with CyscPILOT method (based on the number of identified peptides by the same instrumental time) and had sensitivity to isolate endogenous SNO. OxcyscPILOT successfully expanded sample throughput in cysteine PTM quantification.

In summary, novel methods for studying oxidative modifications were presented in this dissertation. The utilization of protein enrichment and tagging chemistry created diverse

workflows for quantification of total cysteine, oxidized cysteine and specific cysteine PTM by multiplexing either two or twelve samples in one experiment. These workflows were built based on simple chemical reactions and commercially available reagents, and could be adapted in any laboratory to save costs of isotopic materials or instrument time for studying cysteinyl proteome and oxidative modifications in different biological systems.

## 7.2 FUTURE DIRECTIONS

### *7.2.1 Improve the OxcyscPILOT Methodology: Sample Preparation and Data Acquisition*

A typical 12-plex OxcyscPILOT experiment in **Chapter 6** requires ~7 days for sample preparation. Multiple reaction steps were performed in spin column for each sample. Repeated resin washes by flash centrifugation were required before and after reactions to minimize non-specific binding, which was time-consuming and labor-intensive. It would be even more challenging if more samples are multiplexed using TMT 10-plex or DiLeu 12-plex reagents[41,286,358]. This means optimized sample preparation should focus on improving automation and shortening sample preparation time. One potential solution is to design a specialized well plate to handle samples in a multiplexing manner. This type of well plate has not been commercially available. The ideal well plate should contain a top cover and a bottom cover (similar to the spin column's top and bottom cap), so the plate can switch between incubation and washing modes. A collection system with different volume capacity under the plate is also needed so flow through can be easily collected after centrifugation by a plate spinner (Figure 7.1). This system will provide the ability to perform multiple chemical reactions and resin washes without manual handling, incorporating more samples in one experiment, and ultimately decreasing sample's variance and improving data's quality.

a) Current Sample Preparation

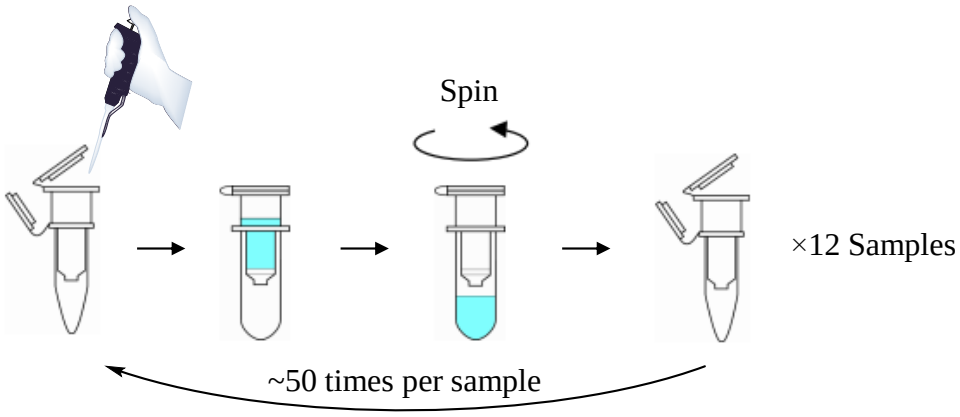


b) Proposed Sample Preparation Using Well Plate

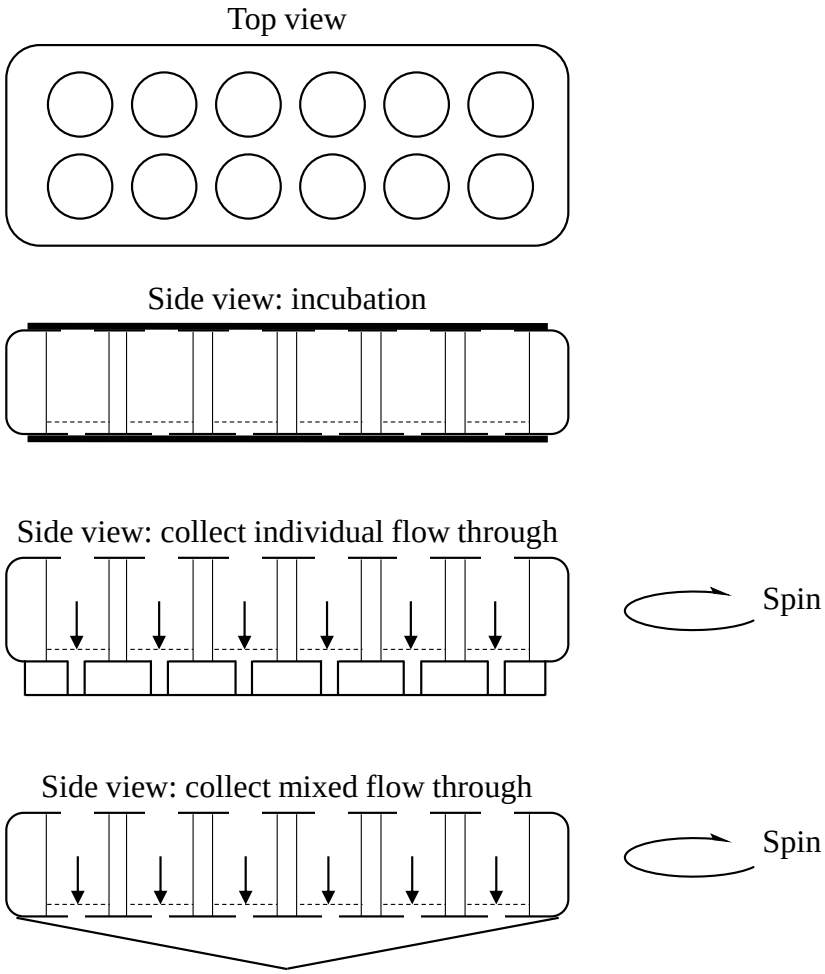


**Figure 7.1** Optimization of OxcyscPILOT sample preparation. a) Current sample preparation used in **Chapter 6**. b) Sample preparation can be improved by using well plate.

OxcyscPILOT presented in **Chapter 6** utilized $MS^3$ for quantification. In a typical DDA scan the most intense ion of MS/MS spectra within an *m/z* range was isolated and fragmented by HCD $MS^3$ to release reporter ions. $MS^3$ was important for better accuracy however with some tradeoffs. First, the cPILOT methodology required that TMT tag was only attached to lysine residue on peptide C-terminus. This means $MS^3$ spectra may not contain reporter ion signals if it was *b*-type ion that was isolated and fragmented instead of *y*-type ion. Second, $MS^3$ scan had lower reporter ion sensitivity and higher likelihood of missing channels compared to MS/MS. In addition, SNO was naturally present at very low abundance (< 1% on peptide level). As a result, a large number of empty SNO channels were observed in $MS^3$ spectra. These limitations could be potentially solved by employing MultiNotch $MS^3$ method, in which multiple MS/MS fragment ions are co-isolated and co-fragmented[299]. This technique can significantly increase sensitivity, dynamic range and ultimately generate more high-quality quantitative data (Figure 7.2). This technique is renamed as synchronous precursor selection (SPS) and is equipped on Thermo's recent Orbitrap Fusion Tribrid MS and allows isolation of up to 20 precursor ions for $MS^n$ scan[348]. Moreover, compared with Orbitrap Velos MS, Orbitrap Fusion increases solving power and scan rate by 5-fold and 20-fold, respectively[359]. All of these can benefit the high-throughput quantification of low abundant PTMs using cPILOT methodology.

### *7.2.2 Use OxcyscPILOT to Enrich and Quantify Other Types of PTMs*

**Chapter 6** demonstrated OxcyscPILOT, an enhanced approach to quantify SNO from tissue samples. This methodology is expected to expand its utility in targeting a broad range of PTMs by employing different chemistry.

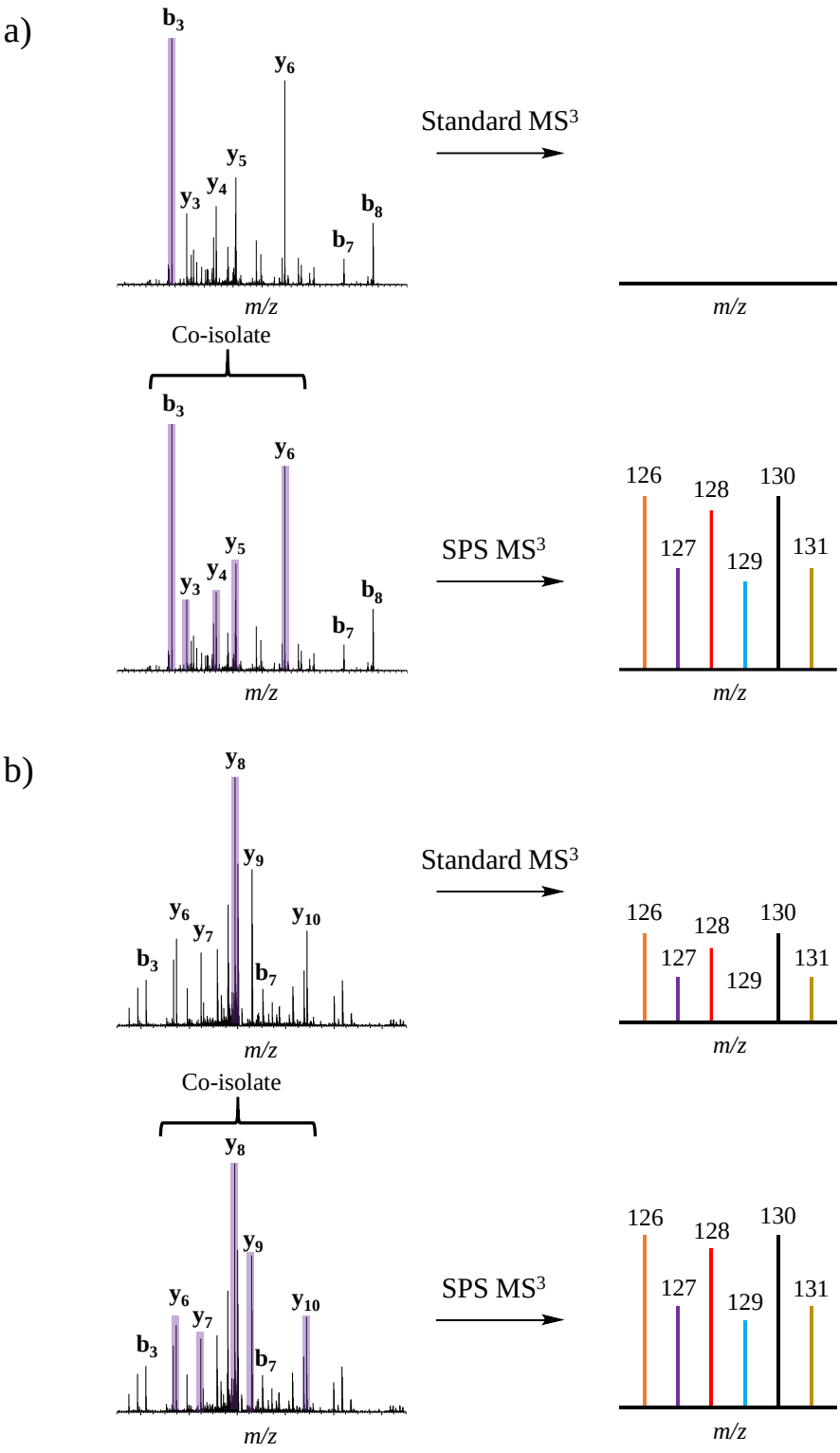


**Figure 7.2** Improvement of HCD $MS^3$ data quality by using SPS technique. Compared with standard $MS^3$ method used in **Chapter 6**, SPS technique can generate a) more spectra containing reporter ions and b) spectra with enhanced reporter ion intensities.

As reviewed in **Chapter 2**, cysteine is subjected to a number of reversible modifications, and the modification of interest can be isolated by selective reductions. OxcyscPILOT provides the ability to multiplex many samples in a single run, which makes it ideal to investigate several cysteine reversible modifications simultaneously. For example, by using TMT 10-plex reagent, OxcyscPILOT method is able to quantify four different cysteine PTMs (total cysteine oxidation, S-nitrosylation, S-glutathionylation and sulfenic acid) between two biological conditions (e.g., WT v.s. AD) (Figure 7.3). Similar to **Chapter 6**, the enrichment of total cysteinyl peptides enables the correction of PTM ratios to protein abundance changes, and more biological replicates can be incorporated due to the cPILOT tagging methodology. This study can benefit our understanding of the redox status of each cysteine residue in physiological and pathological conditions, and allow one to explore the interplay between different cysteine modifications.

In addition to targeting various cysteine oxidations, OxcyscPILOT can be adapted in quantifying some other types of PTMs, such as carbonylation, phosphorylation, and glycosylation. As reviewed in **Chapter 2**, carbonylation is a desirable biomarker of protein oxidative damage, and has implicated in various diseases[61]. Phosphorylation is attachment of a phosphoryl group ($PO_3^{2-}$) on serine or threonine (in most cases) and important for cell signaling[360]. Glycosylation, on the other hand, is a covalent linkage of glycan to protein asparagine, serine or threonine residues. Glycoproteins are involved in many physiological functions and potentially important biomarkers of disease and therapeutic targets[361]. Studying these PTMs on the proteome scale by MS has been challenging mostly due to the low natural occurrence rate. Although current MS techniques can detect biomolecules as low as high-femtomole/low-picomole levels, the complex matrices significantly suppress the PTM signals and severely limit the actual sensitivity[362]. Towards this end, many enriching techniques were developed, including biotin hydrazide[363], immobilized metal

| Channel | 126 | 127a, 127b | 128a, 128b | 129a, 129b | 130a, 130b | 131 |
|---|---|---|---|---|---|---|
| **Genotype** | WT | WT, AD | WT, AD | WT, AD | WT, AD | AD |
| **Selectivity** | Total Cysteine | Total Oxidized Cysteine | S-nitrosylation | S-glutathionylation | Sulfenic Acid | Total Cysteine |
| **Thiol Blocking** | N.A. | NEM | NEM | NEM | NEM | N.A. |
| **Reductant** | DTT | DTT | Ascorbate | Glutaredoxin | Arsenite | DTT |

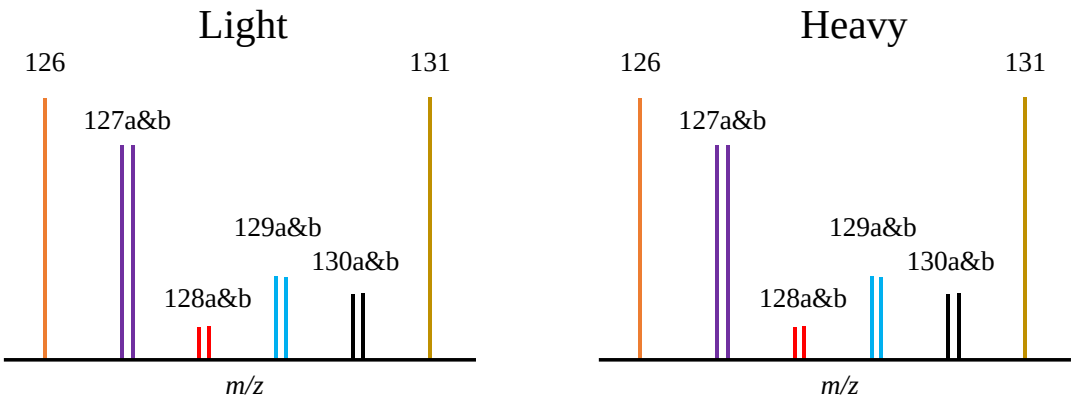


**Figure 7.3** Analysis of various types of cysteine modifications using OxcyscPILOT methodology.

affinity chromatography (IMAC)[360] and solid hydrazide[361] for isolation of protein carbonylation, phosphorylation and glycosylation, respectively. These techniques have been coupled with stable isotopic labeling techniques (e.g., SILAC, dimethylation, TMT, iTRAQ, see **Chapters 1** and **2**) to quantitatively analyze PTMs on the whole proteome[293,325,364,365]. The cPILOT methodology requires peptide tagging by both isotopic and isobaric tags for enhanced multiplexing, and can be utilized for studying protein carbonylation, phosphorylation and glycosylation. The general strategies are listed in Table 7.1. Due to the diverse chemical natures of PTMs, there will be some differences in sample preparations. For example, carbonylated proteins requires being derivatized by biotin tag at the beginning of sample preparations. Also oxidation of glycosylated peptides is required before affinity capture. It must be noted that solid phase hydrazide is compatible with dimethylation reaction[293]. This implies that the cPILOT tagging of glycosylated peptides may be performed on the solid phase. In **Chapter 6** the values of performing solid phase peptide reactions have been highlighted. We suggest further testing the possibilities of solid phase tagging in isolation and quantification of protein carbonylation, phosphorylation and glycosylation.

### *7.2.3 Alzheimer's Disease and Protein Oxidative Modifications*

**Chapters 4 - 6** characterized cysteine and oxidative PTMs in liver and brain tissues in APP/PS-1 mouse model and demonstrated the utility of the novel proteomics methods in disease study. To summarize, the liver proteome study in **Chapters 4** and **5** presented novel findings of cysteinyl proteome in the peripheral organ in AD. The dysregulated energy metabolic pathways in AD liver result in lowered glucose metabolism and elevated lipid metabolism. Elevated lipid metabolism generates more ketone bodies in liver, which enter into the blood, pass the blood-brain barrier (BBB) and serve as an alternative energy source for brain in AD. As a result, more radical oxygen species (ROS) are produced by β-oxidation of fatty acid molecules and elevated oxidative

**Table 7.1** General procedures of studying some other PTMs using cPILOT methodology.

| | **Carbonylation** | **Phosphorylation** | **Glycosylation** |
|---|---|---|---|
| 1. Pre-derivatization | Biotin Hydrazide | N.A. | N.A. |
| 2. Proteolysis | Trypsin | Trypsin | Trypsin |
| 3. Isotopic Labeling | Dimethylation | Dimethylation | Dimethylation |
| 4. Isobaric Tagging | TMT | TMT | TMT |
| 4. Post-derivatization | N.A. | N.A. | Oxidation |
| 5. Affinity Capture | Avidin Chromatography | IMAC | Solid Phase Hydrazide |

stress as well as more oxidized proteins in AD liver are observed. In **Chapter 6**, novel proteins containing differential SNO in AD brain were identified. Therefore, the future directions can focus on the following three aspects.

First, integrate proteomics data with metabolomics data to investigate the larger cellular networks in AD. Enzymatic proteins regulate biological processes through the biotransformation of specific substrates to products. The incorporation of metabolome data may provide another layer of information and provide insights into AD. Gonzalez-Dominguez *et. al.* have conducted such a metabolomics study of liver tissue[366] using APP/PS-1 mouse so a deep data analysis is necessary to correlate the findings of multi "omics". For example, the decreased levels of hypotaurine and taurine by metabolomics study suggested the lowered level of antioxidants in AD liver tissue, which fits well with the following results in **Chapters 4** and **5**: 1) the level of superoxide dismutase in AD was significantly decreased; 2) the overall oxidative stress was elevated in AD liver tissue; 3) some proteins involved in lipid metabolism were significantly oxidized in AD. These consistent conclusions indicate the important roles of oxidative stress in the liver of AD. Also metabolomics discovered differential expression of many energy metabolites, which agree with the changes of proteins involved in carbohydrate and lipid metabolism.

Another direction is the determination of the chemical structures that exhibited differential cysteine oxidation in **Chapter 5**. Redox proteomics method (OxycsDML) in **Chapter 5** provided the ability to screen cysteine oxidations with significant changes in AD liver tissue, however the tradeoff was the loss of structural information of cysteine PTM. This problem can be potentially solved by applying immunoprecipitation of proteins followed by non-reducing digestion and MS identification[249,367,368]. For example, the peptides containing disulfide bonds can generate *b*- and *y*-type ions with characteristic mass shifts in MS/MS[369]. Further validations can also be done by

measuring the enzyme activities before and after oxidation to access the effects of cysteine oxidations[61,107]. A series of biophysical characterizations, such as light scattering, circular dichroism and surface plasmon resonance are also suggested to examine the potential changes of protein structures due to cysteine oxidation[370]. Protein modeling and simulating programs, which predict the oxidation-susceptible cysteine, may be utilized with experiments to identify possible oxidation sites[371]. Cysteine is involved into a number of bioactivities through formation of PTMs (reviewed in **Chapter 2**). Understanding the cysteine biochemical reactions in AD liver may help discover the potential redox biomarkers for diagnostics, and identify the novel cellular signaling in AD.

Third, based on the above findings, novel therapeutic treatments of AD may be developed by targeting proteins with significant changes of redox status. Due to the important roles of oxidative stress in AD, antioxidant such as N-acetylcysteine had been explored as an AD treatment, which can increase glutathione levels and scavenge free radicals[372]. Proteomics studies can identify proteins associated with a disease and suggest target therapies for lower side effects and higher treating efficiency[373]. **Chapter 6** identified more than 100 SNO-modified proteins in AD brain. Some SNO-modified proteins have well demonstrated biological effects in AD. For example, SNO of dynamin-1-like proteins and glyceraldehyde-3-phosphate dehydrogenase are related to synaptic damage and neuronal cell death, respectively[192]. These protein targets can be used as a start to explore novel treatments. For example the 3D protein structures can provide information so a specially designed small molecule can fit the SNO-modified site and inhibit its oxidation[374]. Also biopharmaceutical drugs (e.g., antibody-drug conjugate) can be explored for targeting proteins of interest[375]. Large-scale screening of target proteins as well as drug candidates is the essential.

## APPENDIX A

## APPENDIX B

## APPENDIX C

**Appendix C Table 5.1** Protein ratios used as the normalization factors for OxcysDML data.……...…....Attached CD

**Appendix C Table 5.2** Peptides identified in OxcysDML experiment…...…....…… Attached CD

**Appendix C Table 5.3** List of pathways that identified proteins are involved.…….... Attached CD

## APPENDIX D

## REFERENCES


(1) Gohlke, R. S. *Anal Chem* **1959**, *31*, 535.

(2) Bensimon, A.; Heck, A. J.; Aebersold, R. *Annu Rev Biochem* **2012**, *81*, 379.

(3) Fenn, J. B.; Mann, M.; Meng, C. K.; Wong, S. F.; Whitehouse, C. M. *Science* **1989**, *246*, 64.

(4) Karas, M.; Hillenkamp, F. *Anal Chem* **1988**, *60*, 2299.

(5) Makarov, A. *Anal Chem* **2000**, *72*, 1156.

(6) Domon, B.; Aebersold, R. *Science* **2006**, *312*, 212.

(7) Aebersold, R.; Mann, M. *Nature* **2003**, *422*, 198.

(8) Olsen, J. V.; Schwartz, J. C.; Griep-Raming, J.; Nielsen, M. L.; Damoc, E.; Denisov, E.; Lange, O.; Remes, P.; Taylor, D.; Splendore, M.; Wouters, E. R.; Senko, M.; Makarov, A.; Mann, M.; Horning, S. *Mol Cell Proteomics* **2009**, *8*, 2759.

(9) Han, X.; Jin, M.; Breuker, K.; McLafferty, F. W. *Science* **2006**, *314*, 109.

(10) Shen, Y.; Tolic, N.; Xie, F.; Zhao, R.; Purvine, S. O.; Schepmoes, A. A.; Moore, R. J.; Anderson, G. A.; Smith, R. D. *J Proteome Res* **2011**, *10*, 3929.

(11) Swaney, D. L.; McAlister, G. C.; Coon, J. J. *Nat Methods* **2008**, *5*, 959.

(12) Cook, S. L.; Zimmermann, C. M.; Singer, D.; Fedorova, M.; Hoffmann, R.; Jackson, G. P. *Journal of Mass Spectrometry* **2012**, *47*, 786.

(13) Yang, Y. H.; Lee, K.; Jang, K. S.; Kim, Y. G.; Park, S. H.; Lee, C. S.; Kim, B. G. *Anal Biochem* **2009**, *387*, 133.

(14) Nagaraj, N.; D'Souza, R. C.; Cox, J.; Olsen, J. V.; Mann, M. *J Proteome Res* **2010**, *9*, 6786.

(15) Eng, J. K.; McCormack, A. L.; Yates, J. R. *J Am Soc Mass Spectrom* **1994**, *5*, 976.

(16) Elias, J. E.; Gygi, S. P. *Methods Mol Biol* **2010**, *604*, 55.

(17) Siuti, N.; Kelleher, N. L. *Nat Methods* **2007**, *4*, 817.

(18) Smith, L. M.; Kelleher, N. L.; Consortium for Top Down, P. *Nat Methods* **2013**, *10*, 186.

(19) Catherman, A. D.; Skinner, O. S.; Kelleher, N. L. *Biochem Biophys Res Commun* **2014**, *445*, 683.

(20) Durbin, K. R.; Fornelli, L.; Fellers, R. T.; Doubleday, P. F.; Narita, M.; Kelleher, N. L. *J Proteome Res* **2016**, *15*, 976.

(21) Tran, J. C.; Zamdborg, L.; Ahlf, D. R.; Lee, J. E.; Catherman, A. D.; Durbin, K. R.; Tipton, J. D.; Vellaichamy, A.; Kellie, J. F.; Li, M.; Wu, C.; Sweet, S. M.; Early, B. P.; Siuti, N.; LeDuc, R. D.; Compton, P. D.; Thomas, P. M.; Kelleher, N. L. *Nature* **2011**, *480*, 254.

(22) Han, X.; Aslanian, A.; Yates, J. R., 3rd *Curr Opin Chem Biol* **2008**, *12*, 483.

(23) Washburn, M. P.; Wolters, D.; Yates, J. R., 3rd *Nat Biotechnol* **2001**, *19*, 242.

(24) Bantscheff, M.; Schirle, M.; Sweetman, G.; Rick, J.; Kuster, B. *Anal Bioanal Chem* **2007**, *389*, 1017.

(25) Bantscheff, M.; Lemeer, S.; Savitski, M. M.; Kuster, B. *Anal Bioanal Chem* **2012**, *404*, 939.

(26) Chahrour, O.; Cobice, D.; Malone, J. *J Pharm Biomed Anal* **2015**, *113*, 2.

(27) Wong, J. W.; Cagney, G. *Methods Mol Biol* **2010**, *604*, 273.

(28) Ong, S. E.; Blagoev, B.; Kratchmarova, I.; Kristensen, D. B.; Steen, H.; Pandey, A.; Mann, M. *Mol Cell Proteomics* **2002**, *1*, 376.

(29) Hsu, J. L.; Huang, S. Y.; Chow, N. H.; Chen, S. H. *Anal Chem* **2003**, *75*, 6843.

(30) Evans, A. R.; Miriyala, S.; St Clair, D. K.; Butterfield, D. A.; Robinson, R. A. *J Proteome Res* **2012**, *11*, 1054.

(31) Mertins, P.; Udeshi, N. D.; Clauser, K. R.; Mani, D. R.; Patel, J.; Ong, S. E.; Jaffe, J. D.; Carr, S. A. *Mol Cell Proteomics* **2012**, *11*, M111 014423.

(32) Gygi, S. P.; Rist, B.; Gerber, S. A.; Turecek, F.; Gelb, M. H.; Aebersold, R. *Nat Biotechnol* **1999**, *17*, 994.

(33) Yao, X.; Freas, A.; Ramirez, J.; Demirev, P. A.; Fenselau, C. *Anal Chem* **2001**, *73*, 2836.

(34) Qin, H.; Wang, F.; Zhang, Y.; Hu, Z.; Song, C.; Wu, R.; Ye, M.; Zou, H. *Chem Commun (Camb)* **2012**, *48*, 6265.

(35) Koehler, C. J.; Arntzen, M. O.; de Souza, G. A.; Thiede, B. *Anal Chem* **2013**, *85*, 2478.

(36) Evans, A. R.; Robinson, R. A. *Proteomics* **2013**, *13*, 3267.

(37) Boersema, P. J.; Aye, T. T.; van Veen, T. A.; Heck, A. J.; Mohammed, S. *Proteomics* **2008**, *8*, 4624.

(38) Gu, L.; Evans, A. R.; Robinson, R. A. *J Am Soc Mass Spectrom* **2015**, *26*, 615.

(39) Gu, L.; Robinson, R. A. *Anal Bioanal Chem* **2016**, *408*, 2993.

(40) Wu, Y.; Wang, F.; Liu, Z.; Qin, H.; Song, C.; Huang, J.; Bian, Y.; Wei, X.; Dong, J.; Zou, H. *Chem Commun (Camb)* **2014**, *50*, 1708.

(41) Frost, D. C.; Greer, T.; Li, L. *Anal Chem* **2015**, *87*, 1646.

(42) Thompson, A.; Schafer, J.; Kuhn, K.; Kienle, S.; Schwarz, J.; Schmidt, G.; Neumann, T.; Johnstone, R.; Mohammed, A. K.; Hamon, C. *Anal Chem* **2003**, *75*, 1895.

(43) Pan, K. T.; Chen, Y. Y.; Pu, T. H.; Chao, Y. S.; Yang, C. Y.; Bomgarden, R. D.; Rogers, J. C.; Meng, T. C.; Khoo, K. H. *Antioxid Redox Signal* **2014**, *20*, 1365.

(44) Hahne, H.; Neubert, P.; Kuhn, K.; Etienne, C.; Bomgarden, R.; Rogers, J. C.; Kuster, B. *Anal Chem* **2012**, *84*, 3716.

(45) Ross, P. L.; Huang, Y. L. N.; Marchese, J. N.; Williamson, B.; Parker, K.; Hattan, S.; Khainovski, N.; Pillai, S.; Dey, S.; Daniels, S.; Purkayastha, S.; Juhasz, P.; Martin, S.; Bartlet-Jones, M.; He, F.; Jacobson, A.; Pappin, D. J. *Molecular & Cellular Proteomics* **2004**, *3*, 1154.

(46) Ramsubramaniam, N.; Tao, F.; Li, S.; Marten, M. R. *J Mass Spectrom* **2013**, *48*, 1032.

(47) Xiang, F.; Ye, H.; Chen, R. B.; Fu, Q.; Li, L. J. *Anal Chem* **2010**, *82*, 2817.

(48) Frost, D. C.; Greer, T.; Xiang, F.; Liang, Z.; Li, L. *Rapid Commun Mass Spectrom* **2015**, *29*, 1115.

(49) Savitski, M. M.; Mathieson, T.; Zinn, N.; Sweetman, G.; Doce, C.; Becher, I.; Pachl, F.; Kuster, B.; Bantscheff, M. *Journal of Proteome Research* **2013**, *12*, 3586.

(50) Sturm, R. M.; Lietz, C. B.; Li, L. *Rapid Commun Mass Spectrom* **2014**, *28*, 1051.

(51) Wenger, C. D.; Lee, M. V.; Hebert, A. S.; McAlister, G. C.; Phanstiel, D. H.; Westphall, M. S.; Coon, J. J. *Nat Methods* **2011**, *8*, 933.

(52) Ting, L.; Rad, R.; Gygi, S. P.; Haas, W. *Nat Methods* **2011**, *8*, 937.

(53) Robinson, R. A.; Evans, A. R. *Anal Chem* **2012**, *84*, 4677.

(54) Evans, A. R.; Gu, L.; Guerrero, R., Jr.; Robinson, R. A. *Proteomics Clin Appl* **2015**, *9*, 872.

(55) Dephoure, N.; Gygi, S. P. *Sci Signal* **2012**, *5*, rs2.

(56) Everley, R. A.; Kunz, R. C.; McAllister, F. E.; Gygi, S. P. *Anal Chem* **2013**, *85*, 5340.

(57) Hebert, A. S.; Merrill, A. E.; Stefely, J. A.; Bailey, D. J.; Wenger, C. D.; Westphall, M. S.; Pagliarini, D. J.; Coon, J. J. *Mol Cell Proteomics* **2013**, *12*, 3360.

(58) Potts, G. K.; Voigt, E. A.; Bailey, D. J.; Rose, C. M.; Westphall, M. S.; Hebert, A. S.; Yin, J.; Coon, J. J. *Anal Chem* **2016**, *88*, 3295.

(59) Witze, E. S.; Old, W. M.; Resing, K. A.; Ahn, N. G. *Nat Methods* **2007**, *4*, 798.

(60) Duan, G.; Walther, D. *PLoS Comput Biol* **2015**, *11*, e1004049.

(61) Butterfield, D. A.; Gu, L.; Di Domenico, F.; Robinson, R. A. *Mass Spectrom Rev* **2014**, *33*, 277.

(62) Finkel, T.; Holbrook, N. J. In *Nature*; 2000/11/23 ed. 2000; Vol. 408, p 239.

(63) Zhao, Q. F.; Yu, J. T.; Tan, L. *Mol Neurobiol* **2015**, *51*, 268.

(64) Garcia-Santamarina, S.; Boronat, S.; Hidalgo, E. *Biochemistry* **2014**, *53*, 2560.

(65) Giron, P.; Dayon, L.; Sanchez, J. C. *Mass Spectrom Rev* **2011**, *30*, 366.

(66) Cominetti, O.; Nunez Galindo, A.; Corthesy, J.; Oller Moreno, S.; Irincheeva, I.; Valsesia, A.; Astrup, A.; Saris, W. H.; Hager, J.; Kussmann, M.; Dayon, L. *J Proteome Res* **2016**, *15*, 389.

(67) Gu, L.; Robinson, R. A. *Proteomics Clin Appl* **2016**, *Manuscript in Preparation*.

(68) Verrastro, I.; Pasha, S.; Jensen, K. T.; Pitt, A. R.; Spickett, C. M. *Biomolecules* **2015**, *5*, 378.

(69) Wang, Y.; Yang, J.; Yi, J. *Antioxid Redox Signal* **2012**, *16*, 649.

(70) Ratnayake, S.; Dias, I. H.; Lattman, E.; Griffiths, H. R. *J Proteomics* **2013**, *92*, 160.

(71) Mossner, E.; Iwai, H.; Glockshuber, R. *FEBS Lett* **2000**, *477*, 21.

(72) Chung, H. S.; Wang, S. B.; Venkatraman, V.; Murray, C. I.; Van Eyk, J. E. *Circ Res* **2013**, *112*, 382.

(73) Couvertier, S. M.; Zhou, Y.; Weerapana, E. *Biochim Biophys Acta* **2014**.

(74) Boronat, S.; Garcia-Santamarina, S.; Hidalgo, E. *Free Radic Res* **2015**, *49*, 494.

(75) Gupta, V.; Carroll, K. S. *Biochim Biophys Acta* **2014**, *1840*, 847.

(76) Foster, M. W.; Hess, D. T.; Stamler, J. S. *Trends in Molecular Medicine* **2009**, *15*, 391.

(77) Mieyal, J. J.; Gallogly, M. M.; Qanungo, S.; Sabens, E. A.; Shelton, M. D. *Antioxid Redox Signal* **2008**, *10*, 1941.

(78) Aicart-Ramos, C.; Valero, R. A.; Rodriguez-Crespo, I. *Biochim Biophys Acta* **2011**, *1808*, 2981.

(79) Hogg, P. J. *Trends in Biochemical Sciences* **2003**, *28*, 210.

(80) Carbone, D. L.; Doorn, J. A.; Kiebler, Z.; Petersen, D. R. *Chem Res Toxicol* **2005**, *18*, 1324.

(81) Cai, Z.; Yan, L. J. *J Biochem Pharmacol Res* **2013**, *1*, 15.

(82) Butterfield, D. A.; Dalle-Donne, I. *Mass Spectrom Rev* **2014**, *33*, 1.

(83) Lennicke, C.; Rahn, J.; Heimer, N.; Lichtenfels, R.; Wessjohann, L. A.; Seliger, B. *Proteomics* **2016**, *16*, 197.

(84) Charles, R.; Jayawardhana, T.; Eaton, P. *Biochim Biophys Acta* **2014**, *1840*, 830.

(85) Held, J. M.; Gibson, B. W. *Mol Cell Proteomics* **2012**, *11*, R111 013037.

(86) Seeley, W. W.; Crawford, R. K.; Zhou, J.; Miller, B. L.; Greicius, M. D. *Neuron* **2009**, *62*, 42.

(87) Beal, M. F. *Ann Neurol* **1995**, *38*, 357.

(88) Butterfield, D. A.; Stadtman, E. R. *Adv Cell Aging Gerontol* **1997**, *2*, 161.

(89) Stadtman, E. R.; Levine, R. L. *Amino Acids* **2003**, *25*, 207.

(90) Berlett, B. S.; Stadtman, E. R. *J Biol Chem* **1997**, *272*, 20313.

(91) Butterfield, D. A.; Lauderback, C. M. *Free Radic Biol Med* **2002**, *32*, 1050.

(92) Liang, X.; Kaya, A.; Zhang, Y.; Le, D. T.; Hua, D.; Gladyshev, V. N. *BMC Biochem* **2012**, *13*, 21.

(93) Levine, R. L.; Stadtman, E. R. In *Exp Gerontol*; 2001/08/30 ed. 2001; Vol. 36, p 1495.

(94) Zhang, Y.; Fonslow, B. R.; Shan, B.; Baek, M. C.; Yates, J. R., 3rd *Chemical Reviews* **2013**, *113*, 2343.

(95) Leonard, S. E.; Carroll, K. S. *Curr Opin Chem Biol* **2011**, *15*, 88.

(96) Couvertier, S. M.; Zhou, Y.; Weerapana, E. *Biochimica Et Biophysica Acta-Proteins and Proteomics* **2014**, *1844*, 2315.

(97) Wojdyla, K.; Rogowska-Wrzesinska, A. *Redox Biol* **2015**, *6*, 240.

(98) Forrester, M. T.; Foster, M. W.; Benhar, M.; Stamler, J. S. *Free Radic Biol Med* **2009**, *46*, 119.

(99) Forrester, M. T.; Hess, D. T.; Thompson, J. W.; Hultman, R.; Moseley, M. A.; Stamler, J. S.; Casey, P. J. *J Lipid Res* **2011**, *52*, 393.

(100) Forrester, M. T.; Thompson, J. W.; Foster, M. W.; Nogueira, L.; Moseley, M. A.; Stamler, J. S. *Nat Biotechnol* **2009**, *27*, 557.

(101) Garcia-Santamarina, S.; Boronat, S.; Espadas, G.; Ayte, J.; Molina, H.; Hidalgo, E. *J Proteomics* **2011**, *74*, 2476.

(102) Greco, T. M.; Hodara, R.; Parastatidis, I.; Heijnen, H. F.; Dennehy, M. K.; Liebler, D. C.; Ischiropoulos, H. *Proc Natl Acad Sci U S A* **2006**, *103*, 7420.

(103) Hao, G.; Derakhshan, B.; Shi, L.; Campagne, F.; Gross, S. S. *Proc Natl Acad Sci U S A* **2006**, *103*, 1012.

(104) Held, J. M.; Danielson, S. R.; Behring, J. B.; Atsriku, C.; Britton, D. J.; Puckett, R. L.; Schilling, B.; Campisi, J.; Benz, C. C.; Gibson, B. W. *Molecular & Cellular Proteomics* **2010**, *9*, 1400.

(105) Jaffrey, S. R.; Erdjument-Bromage, H.; Ferris, C. D.; Tempst, P.; Snyder, S. H. *Nat Cell Biol* **2001**, *3*, 193.

(106) Krishnan, N.; Fu, C.; Pappin, D. J.; Tonks, N. K. *Sci Signal* **2011**, *4*, ra86.

(107) Li, R.; Huang, J. Q.; Kast, J. *Journal of Proteome Research* **2015**, *14*, 2026.

(108) Lind, C.; Gerdes, R.; Hamnell, Y.; Schuppe-Koistinen, I.; von Lowenhielm, H. B.; Holmgren, A.; Cotgreave, I. A. *Arch Biochem Biophys* **2002**, *406*, 229.

(109) Liu, P.; Zhang, H.; Wang, H.; Xia, Y. *Proteomics* **2014**, *14*, 750.

(110) Lu, X. M.; Lu, M.; Tompkins, R. G.; Fischman, A. J. *J Mass Spectrom* **2005**, *40*, 1140.

(111) Murray, C. I.; Uhrigshardt, H.; O'Meally, R. N.; Cole, R. N.; Van Eyk, J. E. *Mol Cell Proteomics* **2012**, *11*, M111 013441.

(112) Parker, J.; Balmant, K.; Zhu, F.; Zhu, N.; Chen, S. *Mol Cell Proteomics* **2014**, *14*, 237.

(113) Qu, Z.; Meng, F.; Bomgarden, R. D.; Viner, R. I.; Li, J.; Rogers, J. C.; Cheng, J.; Greenlief, C. M.; Cui, J.; Lubahn, D. B.; Sun, G. Y.; Gu, Z. *J Proteome Res* **2014**, *13*, 3200.

(114) Saurin, A. T.; Neubert, H.; Brennan, J. P.; Eaton, P. *Proc Natl Acad Sci U S A* **2004**, *101*, 17982.

(115) Su, D.; Gaffrey, M. J.; Guo, J.; Hatchell, K. E.; Chu, R. K.; Clauss, T. R.; Aldrich, J. T.; Wu, S.; Purvine, S.; Camp, D. G.; Smith, R. D.; Thrall, B. D.; Qian, W. J. *Free Radic Biol Med* **2013**.

(116) Su, D.; Shukla, A. K.; Chen, B.; Kim, J. S.; Nakayasu, E.; Qu, Y.; Aryal, U.; Weitz, K.; Clauss, T. R.; Monroe, M. E.; Camp, D. G., 2nd; Bigelow, D. J.; Smith, R. D.; Kulkarni, R. N.; Qian, W. J. *Free Radic Biol Med* **2013**, *57*, 68.

(117) Wan, J.; Roth, A. F.; Bailey, A. O.; Davis, N. G. *Nat Protoc* **2007**, *2*, 1573.

(118) Wojdyla, K.; Williamson, J.; Roepstorff, P.; Rogowska-Wrzesinska, A. *J Proteomics* **2015**, *113*, 415.

(119) Guo, J.; Gaffrey, M. J.; Su, D.; Liu, T.; Camp, D. G., 2nd; Smith, R. D.; Qian, W. J. *Nat Protoc* **2014**, *9*, 64.

(120) Sultana, R.; Perluigi, M.; Newman, S. F.; Pierce, W. M.; Cini, C.; Coccia, R.; Butterfield, D. A. *Antioxid Redox Signal* **2010**, *12*, 327.

(121) Robinson, R. A.; Lange, M. B.; Sultana, R.; Galvan, V.; Fombonne, J.; Gorostiza, O.; Zhang, J.; Warrier, G.; Cai, J.; Pierce, W. M.; Bredesen, D. E.; Butterfield, D. A. *Neuroscience* **2011**, *177*, 207.

(122) Reed, T. T.; Pierce, W. M.; Markesbery, W. R.; Butterfield, D. A. *Brain Res* **2009**, *1274*, 66.

(123) Zahid, S.; Khan, R.; Oellerich, M.; Ahmed, N.; Asif, A. R. *Neuroscience* **2014**, *256*, 126.

(124) Di Domenico, F.; Cenini, G.; Sultana, R.; Perluigi, M.; Uberti, D.; Memo, M.; Butterfield, D. A. *Neurochem Res* **2009**, *34*, 727.

(125) Hurd, T. R.; Prime, T. A.; Harbour, M. E.; Lilley, K. S.; Murphy, M. P. *J Biol Chem* **2007**, *282*, 22040.

(126) Chouchani, E. T.; Hurd, T. R.; Nadtochiy, S. M.; Brookes, P. S.; Fearnley, I. M.; Lilley, K. S.; Smith, R. A.; Murphy, M. P. *Biochemical Journal* **2010**, *430*, 49.

(127) Sinha, V.; Wijewickrama, G. T.; Chandrasena, R. E.; Xu, H.; Edirisinghe, P. D.; Schiefer, I. T.; Thatcher, G. R. *ACS Chem Biol* **2010**, *5*, 667.

(128) Wang, Y. T.; Piyankarage, S. C.; Williams, D. L.; Thatcher, G. R. *ACS Chem Biol* **2014**, *9*, 821.

(129) Martinez-Acedo, P.; Nunez, E.; Gomez, F. J.; Moreno, M.; Ramos, E.; Izquierdo-Alvarez, A.; Miro-Casas, E.; Mesa, R.; Rodriguez, P.; Martinez-Ruiz, A.; Dorado, D. G.; Lamas, S.; Vazquez, J. *Mol Cell Proteomics* **2012**, *11*, 800.

(130) Leichert, L. I.; Gehrke, F.; Gudiseva, H. V.; Blackwell, T.; Ilbert, M.; Walker, A. K.; Strahler, J. R.; Andrews, P. C.; Jakob, U. *Proc Natl Acad Sci U S A* **2008**, *105*, 8197.

(131) Kumsta, C.; Thamsen, M.; Jakob, U. *Antioxid Redox Signal* **2011**, *14*, 1023.

(132) Knoefler, D.; Thamsen, M.; Koniczek, M.; Niemuth, N. J.; Diederich, A. K.; Jakob, U. *Mol Cell* **2012**, *47*, 767.

(133) Brandes, N.; Reichmann, D.; Tienson, H.; Leichere, L. I.; Jakob, U. *Journal of Biological Chemistry* **2011**, *286*, 41893.

(134) Fares, A.; Rossignol, M.; Peltier, J. B. *Biochem Biophys Res Commun* **2011**, *416*, 331.

(135) Fares, A.; Nespoulous, C.; Rossignol, M.; Peltier, J. B. *Methods Mol Biol* **2014**, *1072*, 609.

(136) Wu, C.; Parrott, A. M.; Liu, T.; Beuve, A.; Li, H. *Methods* **2013**, *62*, 151.

(137) Wu, C.; Parrott, A. M.; Liu, T.; Jain, M. R.; Yang, Y.; Sadoshima, J.; Li, H. *J Proteomics* **2011**, *74*, 2498.

(138) Garcia-Santamarina, S.; Boronat, S.; Domenech, A.; Ayte, J.; Molina, H.; Hidalgo, E. *Nat Protoc* **2014**, *9*, 1131.

(139) Liu, T.; Qian, W. J.; Strittmatter, E. F.; Camp, D. G., 2nd; Anderson, G. A.; Thrall, B. D.; Smith, R. D. *Anal Chem* **2004**, *76*, 5345.

(140) Liu, T.; Qian, W. J.; Chen, W. N.; Jacobs, J. M.; Moore, R. J.; Anderson, D. J.; Gritsenko, M. A.; Monroe, M. E.; Thrall, B. D.; Camp, D. G., 2nd; Smith, R. D. *Proteomics* **2005**, *5*, 1263.

(141) Gu, L.; Robinson, R. A. *Analyst* **2016**. DOI: 10.1039/c6an00417b

(142) Guo, J.; Nguyen, A. Y.; Dai, Z.; Su, D.; Gaffrey, M. J.; Moore, R. J.; Jacobs, J. M.; Monroe, M. E.; Smith, R. D.; Koppenaal, D. W.; Pakrasi, H. B.; Qian, W. J. *Mol Cell Proteomics* **2014**, *13*, 3270.

(143) Kohr, M. J.; Aponte, A. M.; Sun, J.; Wang, G.; Murphy, E.; Gucek, M.; Steenbergen, C. *Am J Physiol Heart Circ Physiol* **2011**, *300*, H1327.

(144) Kohr, M. J.; Sun, J.; Aponte, A.; Wang, G.; Gucek, M.; Murphy, E.; Steenbergen, C. *Circ Res* **2011**, *108*, 418.

(145) Paulech, J.; Solis, N.; Edwards, A. V.; Puckeridge, M.; White, M. Y.; Cordwell, S. J. *Anal Chem* **2013**, *85*, 3774.

(146) Yan, L. J.; Forster, M. J. *J Chromatogr B Analyt Technol Biomed Life Sci* **2011**, *879*, 1308.

(147) Butterfield, D. A.; Perluigi, M.; Reed, T.; Muharib, T.; Hughes, C. P.; Robinson, R. A.; Sultana, R. *Antioxid Redox Signal* **2012**, *17*, 1610.

(148) Linares, M. a.; Marín-García, P.; Méndez, D. o.; Puyet, A.; Diez, A.; Bautista, J. M. *Journal of Proteome Research* **2011**, *10*, 1719.

(149) Irazusta, V.; Moreno-Cermeno, A.; Cabiscol, E.; Tamarit, J.; Ros, J. *Curr Protein Pept Sci* **2010**, *11*, 652.

(150) Sheehan, D.; McDonagh, B.; Barcena, J. A. *Expert Rev Proteomics* **2010**, *7*, 1.

(151) Dalle-Donne, I.; Carini, M.; Orioli, M.; Vistoli, G.; Regazzoni, L.; Colombo, G.; Rossi, R.; Milzani, A.; Aldini, G. *Free Radic Biol Med* **2009**, *46*, 1411.

(152) Oh-Ishi, M.; Ueno, T.; Maeda, T. *Free Radic Biol Med* **2003**, *34*, 11.

(153) Yoo, B. S.; Regnier, F. E. *Electrophoresis* **2004**, *25*, 1334.

(154) Korolainen, M. A.; Pirttila, T. *Acta Neurol Scand* **2009**, *119*, 32.

(155) Butterfield, D. A.; Perluigi, M.; Reed, T.; Muharib, T.; Hughes, C. P.; Robinson, R. A.; Sultana, R. *Antioxid Redox Signal* **2012**.

(156) Madian, A. G.; Regnier, F. E. In *J Proteome Res*; 2010/06/05 ed. 2010; Vol. 9, p 3766.

(157) Madian, A. G.; Regnier, F. E. *J Proteome Res* **2010**, *9*, 1330.

(158) Madian, A. G.; Myracle, A. D.; Diaz-Maldonado, N.; Rochelle, N. S.; Janle, E. M.; Regnier, F. E. *Journal of Proteome Research* **2011**, *10*, 3959.

(159) Madian, A. G.; Diaz-Maldonado, N.; Gao, Q.; Regnier, F. E. *J Proteomics* **2011**, *74*, 2396.

(160) Mirzaei, H.; Baena, B.; Barbas, C.; Regnier, F. *Proteomics* **2008**, *8*, 1516.

(161) Mirzaei, H.; Regnier, F. *Anal Chem* **2005**, *77*, 2386.

(162) Slade, P. G.; Williams, M. V.; Brahmbhatt, V.; Dash, A.; Wishnok, J. S.; Tannenbaum, S. R. *Chem Res Toxicol* **2010**, *23*, 557.

(163) Chavez, J. D.; Bisson, W. H.; Maier, C. S. *Anal Bioanal Chem* **2010**, *398*, 2905.

(164) Chavez, J.; Wu, J.; Han, B.; Chung, W. G.; Maier, C. S. *Anal Chem* **2006**, *78*, 6847.

(165) Slade, P. G.; Williams, M. V.; Chiang, A.; Iffrig, E.; Tannenbaum, S. R.; Wishnok, J. S. *Mol Cell Proteomics* **2011**, *10*, M111 007658.

(166) Cunnane, S.; Nugent, S.; Roy, M.; Courchesne-Loyer, A.; Croteau, E.; Tremblay, S.; Castellano, A.; Pifferi, F.; Bocti, C.; Paquet, N.; Begdouri, H.; Bentourkia, M.; Turcotte, E.; Allard, M.; Barberger-Gateau, P.; Fulop, T.; Rapoport, S. I. *Nutrition* **2011**, *27*, 3.

(167) Floyd, R. A.; Hensley, K. *Neurobiol Aging* **2002**, *23*, 795.

(168) Choi, J.; Levey, A. I.; Weintraub, S. T.; Rees, H. D.; Gearing, M.; Chin, L. S.; Li, L. *J Biol Chem* **2004**, *279*, 13256.

(169) Newman, S. F.; Sultana, R.; Perluigi, M.; Coccia, R.; Cai, J.; Pierce, W. M.; Klein, J. B.; Turner, D. M.; Butterfield, D. A. *J Neurosci Res* **2007**, *85*, 1506.

(170) Hains, P. G.; Truscott, R. J. *Biochim Biophys Acta* **2008**, *1784*, 1959.

(171) Riederer, I. M.; Schiffrin, M.; Kovari, E.; Bouras, C.; Riederer, B. M. *Brain Res Bull* **2009**, *80*, 233.

(172) Perez, V. I.; Pierce, A.; de Waal, E. M.; Ward, W. F.; Bokov, A.; Chaudhuri, A.; Richardson, A. *Methods Enzymol* **2010**, *473*, 161.

(173) Wang, S.; Circu, M. L.; Zhou, H.; Figeys, D.; Aw, T. Y.; Feng, J. *J Chromatogr A* **2011**, *1218*, 6756.

(174) Wang, S. Y.; Njoroge, S. K.; Battle, K.; Zhang, C.; Hollins, B. C.; Soper, S. A.; Feng, J. *Lab Chip* **2012**, *12*, 3362.

(175) Zhang, C.; Kuo, C. C.; Chiu, A. W. L.; Feng, J. *Journal of Alzheimers Disease* **2012**, *30*, 919.

(176) Zareba-Koziol, M.; Szwajda, A.; Dadlez, M.; Wyslouch-Cieszynska, A.; Lalowski, M. *Mol Cell Proteomics* **2014**, *13*, 2288.

(177) McDonagh, B.; Sakellariou, G. K.; Smith, N. T.; Brownridge, P.; Jackson, M. J. *J Proteome Res* **2014**, *13*, 5008.

(178) Chen, C. H.; Li, W.; Sultana, R.; You, M. H.; Kondo, A.; Shahpasand, K.; Kim, B. M.; Luo, M. L.; Nechama, M.; Lin, Y. M.; Yao, Y.; Lee, T. H.; Zhou, X. Z.; Swomley, A. M.; Allan Butterfield, D.; Zhang, Y.; Lu, K. P. *Neurobiol Dis* **2015**, *76*, 13.

(179) Innes, B. T.; Sowole, M. A.; Gyenis, L.; Dubinsky, M.; Konermann, L.; Litchfield, D. W.; Brandl, C. J.; Shilton, B. H. *Biochim Biophys Acta* **2015**, *1852*, 905.

(180) Chen, L. N.; Shi, Q.; Zhang, B. Y.; Zhang, X. M.; Wang, J.; Xiao, K.; Lv, Y.; Sun, J.; Yang, X. D.; Chen, C.; Zhou, W.; Han, J.; Dong, X. P. *Mol Neurobiol* **2015**.

(181) Correani, V.; Di Francesco, L.; Cera, I.; Mignogna, G.; Giorgi, A.; Mazzanti, M.; Fumagalli, L.; Fabrizi, C.; Maras, B.; Schinina, M. E. *Mol Biosyst* **2015**, *11*, 1584.

(182) Menger, K. E.; James, A. M.; Cocheme, H. M.; Harbour, M. E.; Chouchani, E. T.; Ding, S.; Fearnley, I. M.; Partridge, L.; Murphy, M. P. *Cell Rep* **2015**, *11*, 1856.

(183) Fan, X.; Zhou, S.; Wang, B.; Hom, G.; Guo, M.; Li, B.; Yang, J.; Vaysburg, D.; Monnier, V. M. *Mol Cell Proteomics* **2015**.

(184) Truscott, R. J. *Exp Eye Res* **2005**, *80*, 709.

(185) Blennow, K.; de Leon, M. J.; Zetterberg, H. *Lancet* **2006**, *368*, 387.

(186) Abdul, H. M.; Sultana, R.; Clair, D. K. S.; Markesbery, W. R.; Butterfield, D. A. *Free Radical Biology and Medicine* **2008**, *45*, 1420.

(187) Sinclair, A. J.; Bayer, A. J.; Johnston, J.; Warner, C.; Maxwell, S. R. J. *International Journal of Geriatric Psychiatry* **1998**, *13*, 840.

(188) Smith, M. A.; Rottkamp, C. A.; Nunomura, A.; Raina, A. K.; Perry, G. *Biochim Biophys Acta* **2000**, *1502*, 139.

(189) Robinson, R. A.; Cao, Z.; Williams, C. *J Alzheimers Dis* **2013**, *37*, 661.

(190) Nathan, C.; Xie, Q. W. *Cell* **1994**, *78*, 915.

(191) Choi, Y. B.; Tenneti, L.; Le, D. A.; Ortiz, J.; Bai, G.; Chen, H. S.; Lipton, S. A. *Nat Neurosci* **2000**, *3*, 15.

(192) Nakamura, T.; Lipton, S. A. *Trends Pharmacol Sci* **2016**, *37*, 73.

(193) Johnson, W. M.; Wilson-Delfosse, A. L.; Mieyal, J. J. *Nutrients* **2012**, *4*, 1399.

(194) Sultana, R.; Boyd-Kimball, D.; Poon, H. F.; Cai, J.; Pierce, W. M.; Klein, J. B.; Markesbery, W. R.; Zhou, X. Z.; Lu, K. P.; Butterfield, D. A. *Neurobiol Aging* **2006**, *27*, 918.

(195) Furdui, C. M.; Poole, L. B. *Mass Spectrom Rev* **2014**, *33*, 126.

(196) Dawson, T. M.; Dawson, V. L. *Science* **2003**, *302*, 819.

(197) Haltia, M. *Ann Med* **2000**, *32*, 493.

(198) Butterfield, D. A.; Abdul, H. M.; Newman, S.; Reed, T. *NeuroRx* **2006**, *3*, 344.

(199) Di Domenico, F.; Coccia, R.; Butterfield, D. A.; Perluigi, M. *Biochim Biophys Acta* **2011**, *1814*, 1785.

(200) Castegna, A.; Aksenov, M.; Aksenova, M.; Thongboonkerd, V.; Klein, J. B.; Pierce, W. M.; Booze, R.; Markesbery, W. R.; Butterfield, D. A. *Free Radic Biol Med* **2002**, *33*, 562.

(201) Castegna, A.; Aksenov, M.; Thongboonkerd, V.; Klein, J. B.; Pierce, W. M.; Booze, R.; Markesbery, W. R.; Butterfield, D. A. *J Neurochem* **2002**, *82*, 1524.

(202) Sultana, R.; Boyd-Kimball, D.; Poon, H. F.; Cai, J.; Pierce, W. M.; Klein, J. B.; Merchant, M.; Markesbery, W. R.; Butterfield, D. A. *Neurobiol Aging* **2006**, *27*, 1564.

(203) Selkoe, D. J. *Science* **2002**, *298*, 789.

(204) Korolainen, M. A.; Goldsteins, G.; Nyman, T. A.; Alafuzoff, I.; Koistinaho, J.; Pirttila, T. *Neurobiol Aging* **2006**, *27*, 42.

(205) Korolainen, M. A.; Nyman, T. A.; Nyyssonen, P.; Hartikainen, E. S.; Pirttila, T. *Clin Chem* **2007**, *53*, 657.

(206) Yu, H. L.; Chertkow, H. M.; Bergman, H.; Schipper, H. M. *Proteomics* **2003**, *3*, 2240.

(207) Choi, J.; Malakowsky, C. A.; Talent, J. M.; Conrad, C. C.; Gracy, R. W. *Biochem Biophys Res Commun* **2002**, *293*, 1566.

(208) Cocciolo, A.; Di Domenico, F.; Coccia, R.; Fiorini, A.; Cai, J.; Pierce, W. M.; Mecocci, P.; Butterfield, D. A.; Perluigi, M. *Free Radic Biol Med* **2012**.

(209) Boyd-Kimball, D.; Castegna, A.; Sultana, R.; Poon, H. F.; Petroze, R.; Lynn, B. C.; Klein, J. B.; Butterfield, D. A. *Brain Res* **2005**, *1044*, 206.

(210) Boyd-Kimball, D.; Sultana, R.; Poon, H. F.; Lynn, B. C.; Casamenti, F.; Pepeu, G.; Klein, J. B.; Butterfield, D. A. *Neuroscience* **2005**, *132*, 313.

(211) Boyd-Kimball, D.; Poon, H. F.; Lynn, B. C.; Cai, J.; Pierce, W. M., Jr.; Klein, J. B.; Ferguson, J.; Link, C. D.; Butterfield, D. A. *Neurobiol Aging* **2006**, *27*, 1239.

(212) Yagi, H.; Katoh, S.; Akiguchi, I.; Takeda, T. *Brain Res* **1988**, *474*, 86.

(213) Poon, H. F.; Castegna, A.; Farr, S. A.; Thongboonkerd, V.; Lynn, B. C.; Banks, W. A.; Morley, J. E.; Klein, J. B.; Butterfield, D. A. *Neuroscience* **2004**, *126*, 915.

(214) Gu, L.; Robinson, R. A. *PLoS One* **2015**, *10*, e0116606.

(215) Moller, I. M.; Rogowska-Wrzesinska, A.; Rao, R. S. *J Proteomics* **2011**, *74*, 2228.

(216) Stadtman, E. R.; Berlett, B. S. In *Chem Res Toxicol*; 1997/05/01 ed. 1997; Vol. 10, p 485.

(217) Ntai, I.; Kim, K.; Fellers, R. T.; Skinner, O. S.; Smith, A. D. t.; Early, B. P.; Savaryn, J. P.; LeDuc, R. D.; Thomas, P. M.; Kelleher, N. L. *Anal Chem* **2014**, *86*, 4961.

(218) Yuan, Z. F.; Arnaudo, A. M.; Garcia, B. A. *Annu Rev Anal Chem (Palo Alto Calif)* **2014**, *7*, 113.

(219) Peng, Y.; Gregorich, Z. R.; Valeja, S. G.; Zhang, H.; Cai, W.; Chen, Y. C.; Guner, H.; Chen, A. J.; Schwahn, D. J.; Hacker, T. A.; Liu, X.; Ge, Y. *Mol Cell Proteomics* **2014**.

(220) Li, H.; Wongkongkathep, P.; Van Orden, S. L.; Ogorzalek Loo, R. R.; Loo, J. A. *J Am Soc Mass Spectrom* **2014**.

(221) Wells, J. M.; McLuckey, S. A. *Methods Enzymol* **2005**, *402*, 148.

(222) Brodbelt, J. S.; Wilson, J. J. *Mass Spectrom Rev* **2009**, *28*, 390.

(223) Bakhtiar, R.; Guan, Z. *Biochem Biophys Res Commun* **2005**, *334*, 1.

(224) Wiesner, J.; Premsler, T.; Sickmann, A. *Proteomics* **2008**, *8*, 4466.

(225) Catherman, A. D.; Durbin, K. R.; Ahlf, D. R.; Early, B. P.; Fellers, R. T.; Tran, J. C.; Thomas, P. M.; Kelleher, N. L. *Molecular & Cellular Proteomics* **2013**, *12*, 3465.

(226) Gregorich, Z. R.; Ge, Y. *Proteomics* **2014**, *14*, 1195.

(227) Dekker, L.; Wu, S.; Vanduijn, M.; Tolic, N.; Stingl, C.; Zhao, R.; Luider, T.; Pasa-Tolic, L. *Proteomics* **2014**, *14*, 1239.

(228) Moradian, A.; Kalli, A.; Sweredoski, M. J.; Hess, S. *Proteomics* **2014**, *14*, 489.

(229) Deterding, L. J.; Bhattacharjee, S.; Ramirez, D. C.; Mason, R. P.; Tomer, K. B. In *Anal Chem*; American Chemical Society: 2007; Vol. 79, p 6236.

(230) Ge, Y.; Lawhorn, B. G.; ElNaggar, M.; Sze, S. K.; Begley, T. P.; McLafferty, F. W. *Protein Science* **2003**, *12*, 2320.

(231) Lourette, N.; Smallwood, H.; Wu, S.; Robinson, E.; Squier, T.; Smith, R.; Paša-Tolić, L. *J Am Soc Mass Spectrom* **2010**, *21*, 930.

(232) Rogowska-Wrzesinska, A.; Wojdyla, K.; Nedic, O.; Baron, C. P.; Griffiths, H. *Free Radic Res* **2014**, 1.

(233) Fedorova, M.; Bollineni, R. C.; Hoffmann, R. *Mass Spectrom Rev* **2014**, *33*, 79.

(234) Ciechanover, A.; Orian, A.; Schwartz, A. L. *J Cell Biochem Suppl* **2000**, *34*, 40.

(235) Shang, F.; Taylor, A. *Free Radic Biol Med* **2011**, *51*, 5.

(236) Kastle, M.; Grune, T. *Current Pharmaceutical Design* **2011**, *17*, 4007.

(237) Hershko, A.; Ciechanover, A. *Annu Rev Biochem* **1998**, *67*, 425.

(238) Sharp, J. S.; Becker, J. M.; Hettich, R. L. *Anal Biochem* **2003**, *313*, 216.

(239) Stadtman, E. R.; Oliver, C. N. *J Biol Chem* **1991**, *266*, 2005.

(240) Yi, D.; Perkins, P. D. *J Biomol Tech* **2005**, *16*, 364.

(241) Downard, K. M.; Maleknia, S. D.; Akashi, S. *Rapid Commun Mass Spectrom* **2012**, *26*, 226.

(242) McClintock, C.; Kertesz, V.; Hettich, R. L. *Anal Chem* **2008**, *80*, 3304.

(243) Aye, T. T.; Low, T. Y.; Sze, S. K. *Anal Chem* **2005**, *77*, 5814.

(244) Shi, H.; Gu, L.; Clemmer, D. E.; Robinson, R. A. *J Phys Chem B* **2013**, *117*, 164.

(245) Swaney, D. L.; Wenger, C. D.; Coon, J. J. *Journal of Proteome Research* **2010**, *9*, 1323.

(246) Xu, G. H.; Chance, M. R. *Chemical Reviews* **2007**, *107*, 3514.

(247) Chalkley, R. J.; Hansen, K. C.; Baldwin, M. A. *Methods Enzymol* **2005**, *402*, 289.

(248) Borazjani, A.; Edelmann, M. J.; Hardin, K. L.; Herring, K. L.; Allen Crow, J.; Ross, M. K. *Chem Biol Interact* **2011**, *194*, 1.

(249) Wang, L.; Cvetkov, T. L.; Chance, M. R.; Moiseenkova-Bell, V. Y. *J Biol Chem* **2012**, *287*, 6169.

(250) Liu, H.; Lei, Q. P.; Washabaugh, M. *ASMS Annual Conference* **2014**.

(251) Hartmer, R. G.; Kaplan, D. A.; Stoermer, C.; Lubeck, M.; Park, M. A. *Rapid Commun Mass Spectrom* **2009**, *23*, 2273.

(252) Mikesh, L. M.; Ueberheide, B.; Chi, A.; Coon, J. J.; Syka, J. E.; Shabanowitz, J.; Hunt, D. F. *Biochim Biophys Acta* **2006**, *1764*, 1811.

(253) Sze, S. K.; Ge, Y.; Oh, H.; McLafferty, F. W. In *Proc Natl Acad Sci U S A*; 2002/02/14 ed. 2002; Vol. 99, p 1774.

(254) Sze, S. K.; Ge, Y.; Oh, H.; McLafferty, F. W. *Anal Chem* **2003**, *75*, 1599.

(255) Madian, A. G.; Hindupur, J.; Hulleman, J. D.; Diaz-Maldonado, N.; Mishra, V. R.; Guigard, E.; Kay, C. M.; Rochet, J. C.; Regnier, F. E. *Mol Cell Proteomics* **2012**, *11*, M111 010892.

(256) Zhao, C.; Sethuraman, M.; Clavreul, N.; Kaur, P.; Cohen, R. A.; O'Connor, P. B. *Anal Chem* **2006**, *78*, 5134.

(257) Bacarese-Hamilton, A. J.; Adrian, T. E.; Chohan, P.; Antony, T.; Bloom, S. R. *Peptides* **1985**, *6*, 17.

(258) Hayes, C. S.; Illades-Aguiar, B.; Casillas-Martinez, L.; Setlow, P. *J Bacteriol* **1998**, *180*, 2694.

(259) Maskos, Z.; Rush, J. D.; Koppenol, W. H. *Arch Biochem Biophys* **1992**, *296*, 521.

(260) Solar, S. *Radiation Physics and Chemistry* **1985**, *26*, 103.

(261) Maleknia, S. D.; Brenowitz, M.; Chance, M. R. *Anal Chem* **1999**, *71*, 3965.

(262) Wu, L.; Han, D. K. *Expert Rev Proteomics* **2006**, *3*, 611.

(263) Bachi, A.; Dalle-Donne, I.; Scaloni, A. *Chemical Reviews* **2013**, *113*, 596.

(264) Wang, H.; Qian, W. J.; Chin, M. H.; Petyuk, V. A.; Barry, R. C.; Liu, T.; Gritsenko, M. A.; Mottaz, H. M.; Moore, R. J.; Camp Ii, D. G.; Khan, A. H.; Smith, D. J.; Smith, R. D. *J Proteome Res* **2006**, *5*, 361.

(265) Liu, M.; Hou, J.; Huang, L.; Huang, X.; Heibeck, T. H.; Zhao, R.; Pasa-Tolic, L.; Smith, R. D.; Li, Y.; Fu, K.; Zhang, Z.; Hinrichs, S. H.; Ding, S. J. *Anal Chem* **2010**, *82*, 7160.

(266) Palani, A.; Lee, J. S.; Huh, J.; Kim, M.; Lee, Y. J.; Chang, J. H.; Lee, K.; Lee, S. W. *J Proteome Res* **2008**, *7*, 3591.

(267) Xu, Y.; Cao, Q.; Svec, F.; Frechet, J. M. *Anal Chem* **2010**, *82*, 3352.

(268) Raftery, M. J. *Anal Chem* **2008**, *80*, 3334.

(269) Giron, P.; Dayon, L.; David, F.; Sanchez, J. C.; Rose, K. *J Proteomics* **2009**, *71*, 647.

(270) Dai, J.; Wang, J.; Zhang, Y.; Lu, Z.; Yang, B.; Li, X.; Cai, Y.; Qian, X. *Anal Chem* **2005**, *77*, 7594.

(271) Giron, P.; Dayon, L.; Mihala, N.; Sanchez, J. C.; Rose, K. *Rapid Commun Mass Spectrom* **2009**, *23*, 3377.

(272) Jaffrey, S. R.; Snyder, S. H. *Sci STKE* **2001**, *2001*, pl1.

(273) Lin, D.; Li, J.; Slebos, R. J.; Liebler, D. C. *J Proteome Res* **2010**, *9*, 5461.

(274) Xiang, F.; Ye, H.; Chen, R.; Fu, Q.; Li, L. *Anal Chem* **2010**, *82*, 2817.

(275) Shi, Y.; Xiang, R.; Crawford, J. K.; Colangelo, C. M.; Horvath, C.; Wilkins, J. A. *J Proteome Res* **2004**, *3*, 104.

(276) Zhou, H.; Ranish, J. A.; Watts, J. D.; Aebersold, R. *Nat Biotechnol* **2002**, *20*, 512.

(277) Guo, M.; Galan, J.; Tao, W. A. *Chem Commun (Camb)* **2007**, 1251.

(278) Ahrends, R.; Pieper, S.; Kuhn, A.; Weisshoff, H.; Hamester, M.; Lindemann, T.; Scheler, C.; Lehmann, K.; Taubner, K.; Linscheid, M. W. *Mol Cell Proteomics* **2007**, *6*, 1907.

(279) Zhang, L.; Guo, Y. L.; Liu, H. Q. *J Mass Spectrom* **2004**, *39*, 447.

(280) Olsen, J. V.; Andersen, J. R.; Nielsen, P. A.; Nielsen, M. L.; Figeys, D.; Mann, M.; Wisniewski, J. R. *Mol Cell Proteomics* **2004**, *3*, 82.

(281) Qiu, Y.; Sousa, E. A.; Hewick, R. M.; Wang, J. H. *Anal Chem* **2002**, *74*, 4969.

(282) Shen, M.; Guo, L.; Wallace, A.; Fitzner, J.; Eisenman, J.; Jacobson, E.; Johnson, R. S. *Mol Cell Proteomics* **2003**, *2*, 315.

(283) Giron, P.; Dayon, L.; Turck, N.; Hoogland, C.; Sanchez, J. C. *J Proteome Res* **2011**, *10*, 249.

(284) Su, D.; Gaffrey, M. J.; Guo, J.; Hatchell, K. E.; Chu, R. K.; Clauss, T. R. W.; Aldrich, J. T.; Wu, S.; Purvine, S.; Camp, D. G.; Smith, R. D.; Thrall, B. D.; Qian, W. J. *Free Radic Biol Med* **2014**, *67*, 460.

(285) Guo, J.; Nguyen, A. Y.; Dai, Z.; Su, D.; Gaffrey, M. J.; Moore, R. J.; Jacobs, J. M.; Monroe, M. E.; Smith, R. D.; Koppenaal, D. W.; Pakrasi, H. B.; Qian, W. J. *Mol Cell Proteomics* **2014**.

(286) McAlister, G. C.; Huttlin, E. L.; Haas, W.; Ting, L.; Jedrychowski, M. P.; Rogers, J. C.; Kuhn, K.; Pike, I.; Grothe, R. A.; Blethrow, J. D.; Gygi, S. P. *Anal Chem* **2012**, *84*, 7469.

(287) Qian, W. J.; Liu, T.; Monroe, M. E.; Strittmatter, E. F.; Jacobs, J. M.; Kangas, L. J.; Petritis, K.; Camp, D. G., 2nd; Smith, R. D. *J Proteome Res* **2005**, *4*, 53.

(288) Chen, D.; Shah, A.; Nguyen, H.; Loo, D.; Inder, K. L.; Hill, M. M. *J Proteome Res* **2014**.

(289) Ludbrook, J.; Dudley, H. *American Statistician* **1998**, *52*, 127.

(290) Musunuri, S.; Wetterhall, M.; Ingelsson, M.; Lannfelt, L.; Artemenko, K.; Bergquist, J.; Kultima, K.; Shevchenko, G. *Journal of Proteome Research* **2014**, *13*, 2056.

(291) Dayon, L.; Sonderegger, B.; Kussmann, M. *J Proteome Res* **2012**, *11*, 5081.

(292) Boersema, P. J.; Raijmakers, R.; Lemeer, S.; Mohammed, S.; Heck, A. J. *Nat Protoc* **2009**, *4*, 484.

(293) Sun, Z.; Qin, H.; Wang, F.; Cheng, K.; Dong, M.; Ye, M.; Zou, H. *Anal Chem* **2012**, *84*, 8452.

(294) Jentoft, N.; Dearborn, D. G. *Journal of Biological Chemistry* **1979**, *254*, 4359.

(295) Liu, T.; Qian, W. J.; Camp, D. G., 2nd; Smith, R. D. *Methods Mol Biol* **2007**, *359*, 107.

(296) Carr, S. A.; Abbatiello, S. E.; Ackermann, B. L.; Borchers, C.; Domon, B.; Deutsch, E. W.; Grant, R. P.; Hoofnagle, A. N.; Huttenhain, R.; Koomen, J. M.; Liebler, D. C.; Liu, T.; MacLean, B.; Mani, D.; Mansfield, E.; Neubert, H.; Paulovich, A. G.; Reiter, L.; Vitek, O.; Aebersold, R.; Anderson, L.; Bethem, R.; Blonder, J.; Boja, E.; Botelho, J.; Boyne, M.; Bradshaw, R. A.; Burlingame, A. L.; Chan, D.; Keshishian, H.; Kuhn, E.; Kinsinger, C.; Lee, J. S. H.; Lee, S. W.; Moritz, R.; Oses-Prieto, J.; Rifai, N.; Ritchie, J.; Rodriguez, H.; Srinivas, P. R.; Townsend, R. R.; Van Eyk, J.; Whiteley, G.; Wiita, A.; Weintraub, S. *Molecular & Cellular Proteomics* **2014**, *13*, 907.

(297) Lau, H. T.; Suh, H. W.; Golkowski, M.; Ong, S. E. *J Proteome Res* **2014**, *13*, 4164.

(298) El-Khatib, A. H.; Esteban-Fernandez, D.; Linscheid, M. W. *Anal Bioanal Chem* **2012**, *403*, 2255.

(299) McAlister, G. C.; Nusinow, D. P.; Jedrychowski, M. P.; Wuhr, M.; Huttlin, E. L.; Erickson, B. K.; Rad, R.; Haas, W.; Gygi, S. P. *Anal Chem* **2014**, *86*, 7150.

(300) Shi, R.; Kumar, C.; Zougman, A.; Zhang, Y.; Podtelejnikov, A.; Cox, J.; Wisniewski, J. R.; Mann, M. *Journal of Proteome Research* **2007**, *6*, 2963.

(301) Sutcliffe, J. G.; Hedlund, P. B.; Thomas, E. A.; Bloom, F. E.; Hilbush, B. S. *J Neurosci Res* **2011**, *89*, 808.

(302) Hye, A.; Lynham, S.; Thambisetty, M.; Causevic, M.; Campbell, J.; Byers, H. L.; Hooper, C.; Rijsdijk, F.; Tabrizi, S. J.; Banner, S.; Shaw, C. E.; Foy, C.; Poppe, M.; Archer, N.; Hamilton, G.; Powell, J.; Brown, R. G.; Sham, P.; Ward, M.; Lovestone, S. *Brain* **2006**, *129*, 3042.

(303) VanItallie, T. B.; Nufert, T. H. *Nutrition Reviews* **2003**, *61*, 327.

(304) Martin, B.; Brenneman, R.; Becker, K. G.; Gucek, M.; Cole, R. N.; Maudsley, S. *PLoS One* **2008**, *3*, e2750.

(305) Shevchenko, G.; Wetterhall, M.; Bergquist, J.; Hoglund, K.; Andersson, L. I.; Kultima, K. *J Proteome Res* **2012**, *11*, 6159.

(306) Musunuri, S.; Wetterhall, M.; Ingelsson, M.; Lannfelt, L.; Artemenko, K.; Bergquist, J.; Kultima, K.; Shevchenko, G. *Journal of Proteome Research* **2014**.

(307) Andreev, V. P.; Petyuk, V. A.; Brewer, H. M.; Karpievitch, Y. V.; Xie, F.; Clarke, J.; Camp, D.; Smith, R. D.; Lieberman, A. P.; Albin, R. L.; Nawaz, Z.; El Hokayem, J.; Myers, A. J. *J Proteome Res* **2012**, *11*, 3053.

(308) Schonberger, S. J.; Edgar, P. F.; Kydd, R.; Faull, R. L.; Cooper, G. J. *Proteomics* **2001**, *1*, 1519.

(309) Choi, J.; Rees, H. D.; Weintraub, S. T.; Levey, A. I.; Chin, L. S.; Li, L. *Journal of Biological Chemistry* **2005**, *280*, 11648.

(310) Croft, D.; Mundo, A. F.; Haw, R.; Milacic, M.; Weiser, J.; Wu, G. M.; Caudy, M.; Garapati, P.; Gillespie, M.; Kamdar, M. R.; Jassal, B.; Jupe, S.; Matthews, L.; May, B.; Palatnik, S.; Rothfels, K.; Shamovsky, V.; Song, H.; Williams, M.; Birney, E.; Hermjakob, H.; Stein, L.; D'Eustachio, P. *Nucleic Acids Research* **2014**, *42*, D472.

(311) Carvalho, C.; Katz, P. S.; Dutta, S.; Katakam, P. V.; Moreira, P. I.; Busija, D. W. *J Alzheimers Dis* **2014**, *38*, 75.

(312) Vignini, A.; Giulietti, A.; Nanetti, L.; Raffaelli, F.; Giusti, L.; Mazzanti, L.; Provinciali, L. *Curr Diabetes Rev* **2013**, *9*, 218.

(313) Ding, F.; Yao, J.; Rettberg, J. R.; Chen, S.; Brinton, R. D. *PLoS One* **2013**, *8*, e79977.

(314) Henderson, S. T. *Neurotherapeutics* **2008**, *5*, 470.

(315) Branconnier, R. J.; Dessain, E. C.; Mcniff, M. E.; Cole, J. O. *American Journal of Psychiatry* **1986**, *143*, 1313.

(316) Hoyer, S.; Nitsch, R.; Oesterreich, K. *Neuroscience Letters* **1990**, *117*, 358.

(317) Rodrigo, R.; Cauli, O.; Gomez-Pinedo, U.; Agusti, A.; Hernandez-Rabaza, V.; Garcia-Verdugo, J. M.; Felipo, V. *Gastroenterology* **2010**, *139*, 675.

(318) Tornvall, U. *Analytical Methods* **2010**, *2*, 1638.

(319) Klomsiri, C.; Karplus, P. A.; Poole, L. B. *Antioxid Redox Signal* **2011**, *14*, 1065.

(320) Baez, N. O. D.; Reisz, J. A.; Furdui, C. M. *Free Radical Biology and Medicine* **2015**, *80*, 191.

(321) Biteau, B.; Labarre, J.; Toledano, M. B. *Nature* **2003**, *425*, 980.

(322) Chang, T. S.; Jeong, W.; Woo, H. A.; Lee, S. M.; Park, S.; Rhee, S. G. *Journal of Biological Chemistry* **2004**, *279*, 50994.

(323) Rosales-Corral, S.; Tan, D. X.; Manchester, L.; Reiter, R. J. *Oxid Med Cell Longev* **2015**, *2015*, 985845.

(324) Butterfield, D. A.; Gu, L.; Domenico, F. D.; Robinson, R. A. *Mass Spectrom Rev* **2013**, *33*, 277.

(325) Wu, R.; Dephoure, N.; Haas, W.; Huttlin, E. L.; Zhai, B.; Sowa, M. E.; Gygi, S. P. *Mol Cell Proteomics* **2011**, *10*, M111 009654.

(326) Kumar, V.; Kleffmann, T.; Hampton, M. B.; Cannell, M. B.; Winterbourn, C. C. *Free Radical Biology and Medicine* **2013**, *58*, 109.

(327) Chen, D.; Shah, A.; Nguyen, H.; Loo, D.; Inder, K. L.; Hill, M. M. *J Proteome Res* **2014**, *13*, 4184.

(328) Go, Y. M.; Roede, J. R.; Orr, M.; Liang, Y.; Jones, D. P. *Toxicol Sci* **2014**, *139*, 59.

(329) Bairoch, A.; Apweiler, R.; Wu, C. H.; Barker, W. C.; Boeckmann, B.; Ferro, S.; Gasteiger, E.; Huang, H.; Lopez, R.; Magrane, M.; Martin, M. J.; Natale, D. A.; O'Donovan, C.; Redaschi, N.; Yeh, L. S. *Nucleic Acids Research* **2005**, *33*, D154.

(330) Pace, N. J.; Weerapana, E. *Biomolecules* **2014**, *4*, 419.

(331) Morris, J. K.; Honea, R. A.; Vidoni, E. D.; Swerdlow, R. H.; Burns, J. M. *Biochimica Et Biophysica Acta-Molecular Basis of Disease* **2014**, *1842*, 1340.

(332) Swomley, A. M.; Forster, S.; Keeney, J. T.; Triplett, J.; Zhang, Z.; Sultana, R.; Butterfield, D. A. *Biochimica Et Biophysica Acta-Molecular Basis of Disease* **2014**, *1842*, 1248.

(333) Hooijmans, C. R.; Rutters, F.; Dederen, P. J.; Gambarota, G.; Veltien, A.; van Groen, T.; Broersen, L. M.; Lutjohann, D.; Heerschap, A.; Tanila, H.; Kiliaan, A. J. *Neurobiol Dis* **2007**, *28*, 16.

(334) Sagare, A.; Deane, R.; Bell, R. D.; Johnson, B.; Hamm, K.; Pendu, R.; Marky, A.; Lenting, P. J.; Wu, Z.; Zarcone, T.; Goate, A.; Mayo, K.; Perlmutter, D.; Coma, M.; Zhong, Z.; Zlokovic, B. V. *Nat Med* **2007**, *13*, 1029.

(335) Cichoz-Lach, H.; Michalak, A. *World Journal of Gastroenterology* **2014**, *20*, 8082.

(336) Fransen, M.; Nordgren, M.; Wang, B.; Apanasets, O. *Biochim Biophys Acta* **2012**, *1822*, 1363.

(337) Ruprecht, B.; Lemeer, S. *Expert Rev Proteomics* **2014**, *11*, 259.

(338) Hunter, T. *Cold Spring Harb Perspect Biol* **2014**, *6*, a020644.

(339) Lopez-Sanchez, L. M.; Lopez-Pedrera, C.; Rodriguez-Ariza, A. *Mass Spectrom Rev* **2014**, *33*, 7.

(340) Akhtar, M. W.; Sunico, C. R.; Nakamura, T.; Lipton, S. A. *Int J Cell Biol* **2012**, *2012*, 463756.

(341) Nakamura, T.; Lipton, S. A. *Cell Calcium* **2010**, *47*, 190.

(342) Torta, F.; Usuelli, V.; Malgaroli, A.; Bachi, A. *Proteomics* **2008**, *8*, 4484.

(343) Gu, L.; Robinson, R. A. S. *Proteomics Clin Appl* **2016**, *Manuscript in Preparation*.

(344) Jankowsky, J. L.; Fadale, D. J.; Anderson, J.; Xu, G. M.; Gonzales, V.; Jenkins, N. A.; Copeland, N. G.; Lee, M. K.; Younkin, L. H.; Wagner, S. L.; Younkin, S. G.; Borchelt, D. R. *Hum Mol Genet* **2004**, *13*, 159.

(345) Braakman, I.; Helenius, J.; Helenius, A. *EMBO J* **1992**, *11*, 1717.

(346) Nakamura, T.; Tu, S.; Akhtar, M. W.; Sunico, C. R.; Okamoto, S.; Lipton, S. A. *Neuron* **2013**, *78*, 596.

(347) Nakamura, T.; Lipton, S. A. *Antioxid Redox Signal* **2011**, *14*, 1479.

(348) Murphy, J. P.; Stepanova, E.; Everley, R. A.; Paulo, J. A.; Gygi, S. P. *Molecular & Cellular Proteomics* **2015**, *14*, 2454.

(349) Nelson, K. J.; Knutson, S. T.; Soito, L.; Klomsiri, C.; Poole, L. B.; Fetrow, J. S. *Proteins-Structure Function and Bioinformatics* **2011**, *79*, 947.

(350) Gould, N.; Doulias, P. T.; Tenopoulou, M.; Raju, K.; Ischiropoulos, H. *J Biol Chem* **2013**, *288*, 26473.

(351) Cho, D. H.; Nakamura, T.; Fang, J.; Cieplak, P.; Godzik, A.; Gu, Z.; Lipton, S. A. *Science* **2009**, *324*, 102.

(352) Doulias, P. T.; Tenopoulou, M.; Greene, J. L.; Raju, K.; Ischiropoulos, H. *Sci Signal* **2013**, *6*, rs1.

(353) Kohr, M. J.; Aponte, A. M.; Sun, J. H.; Wang, G. H.; Murphy, E.; Gucek, M.; Steenbergen, C. *American Journal of Physiology-Heart and Circulatory Physiology* **2011**, *300*, H1327.

(354) Kuntzelmann, A.; Guenther, T.; Haberkorn, U.; Essig, M.; Giesel, F.; Henze, R.; Schroeter, M. L.; Schroder, J.; Schonknecht, P. *Neuroscience Letters* **2013**, *534*, 12.

(355) Foote, M.; Zhou, Y. *Int J Biochem Mol Biol* **2012**, *3*, 152.

(356) Repalli, J. *Curr Aging Sci* **2014**, *7*, 168.

(357) Hooff, G. P.; Wood, W. G.; Muller, W. E.; Eckert, G. P. *Biochimica Et Biophysica Acta-Molecular and Cell Biology of Lipids* **2010**, *1801*, 896.

(358) Werner, T.; Becher, I.; Sweetman, G.; Doce, C.; Savitski, M. M.; Bantscheff, M. *Anal Chem* **2012**, *84*, 7188.

(359) Senko, M. W.; Remes, P. M.; Canterbury, J. D.; Mathur, R.; Song, Q.; Eliuk, S. M.; Mullen, C.; Earley, L.; Hardman, M.; Blethrow, J. D.; Bui, H.; Specht, A.; Lange, O.; Denisov, E.; Makarov, A.; Horning, S.; Zabrouskov, V. *Anal Chem* **2013**, *85*, 11710.

(360) Collins, M. O.; Yu, L.; Choudhary, J. S. *Proteomics* **2007**, *7*, 2751.

(361) Pan, S.; Chen, R.; Aebersold, R.; Brentnall, T. A. *Mol Cell Proteomics* **2011**, *10*, R110 003251.

(362) Kwon, S. J.; Choi, E. Y.; Choi, Y. J.; Ahn, J. H.; Park, O. K. *Journal of Experimental Botany* **2006**, *57*, 1547.

(363) Madian, A. G.; Regnier, F. E. *Journal of Proteome Research* **2010**, *9*, 3766.

(364) Lei, Z.; Beuerman, R. W.; Chew, A. P.; Koh, S. K.; Cafaro, T. A.; Urrets-Zavalia, E. A.; Urrets-Zavalia, J. A.; Li, S. F.; Serra, H. M. *J Proteome Res* **2009**, *8*, 1992.

(365) Feng, J.; Xie, H.; Meany, D. L.; Thompson, L. V.; Arriaga, E. A.; Griffin, T. J. *J Gerontol A Biol Sci Med Sci* **2008**, *63*, 1137.

(366) Gonzalez-Dominguez, R.; Garcia-Barrera, T.; Vitorica, J.; Gomez-Ariza, J. L. *Electrophoresis* **2015**.

(367) Nelson, K. J.; Klomsiri, C.; Codreanu, S. G.; Soito, L.; Liebler, D. C.; Rogers, L. C.; Daniel, L. W.; Poole, L. B. *Methods in Enzymology, Vol 473: Thiol Redox Transitions in Cell Signaling, Pt A: Chemistry and Biochemistry of Low Molecular Weight and Protein Thiols* **2010**, *473*, 95.

(368) Juschke, C.; Knoblich, J. A. *Methods Mol Biol* **2008**, *420*, 347.

(369) Tsai, P. L.; Chen, S. F.; Huang, S. Y. *Reviews in Analytical Chemistry* **2013**, *32*, 257.

(370) Eliezer, D. *Curr Opin Struct Biol* **2009**, *19*, 23.

(371) Sanchez, R.; Riddle, M.; Woo, J.; Momand, J. *Protein Science* **2008**, *17*, 473.

(372) Robinson, R. A.; Joshi, G.; Huang, Q.; Sultana, R.; Baker, A. S.; Cai, J.; Pierce, W.; St Clair, D. K.; Markesbery, W. R.; Butterfield, D. A. *Proteomics* **2011**, *11*, 4243.

(373) Walgren, J. L.; Thompson, D. C. *Toxicol Lett* **2004**, *149*, 377.

(374) Anderson, A. C. *Chem Biol* **2003**, *10*, 787.

(375) Zolot, R. S.; Basu, S.; Million, R. P. *Nat Rev Drug Discov* **2013**, *12*, 259.